The Design and Field Evaluation of a New Dual Pressure and Temperature Tapered Probe

by

Matthew G. Chartier

Bachelor of Science in Geology
New York State College at Oneonta, Oneonta, New York
(2000)

SUBMITTED TO THE DEPARTMENT OF CIVIL AND ENVIRONMENTAL ENGINEERING IN PARTIAL FULFILLMENT OF THE REQUIREMENTS FOR THE DEGREE OF

MASTER OF SCIENCE IN CIVIL AND ENVIRONMENTAL ENGINEERING
AT THE
MASSACHUSETTS INSTITUTE OF TECHNOLOGY

June 2005

Signature of Author _____
Department of Civil and Environmental Engineering
May 23, 2005

Certified by _____
John T. Germaine
Principal Research Associate of Civil and Environmental Engineering
Thesis Supervisor

Accepted by _____
Professor Andrew J. Whittle
Chairman, Department Committee for Graduate Studies

The Design and Field Evaluation of a New Dual Pressure and Temperature Tapered Probe

by

Matthew G. Chartier

Submitted to the Department of Civil and Environmental Engineering
on May 23, 2005 in partial fulfillment of the requirements for the degree of
Master of Science in Civil and Environmental Engineering

ABSTRACT

The T2P is a new penetration device that measures temperature at its tip and pore pressure at a point just above the tip and at a second location near the base of the probe shaft. The main purpose of the T2P, recently designed and fabricated at MIT, is to reduce the time required to accurately estimate in-situ pore pressures (u_o) of marine sediments. This goal will be accomplished by using the two-point matching method (Whittle et al., 1997; 2001) to compare measured partial T2P dissipation records with theoretical dissipation curves, derived using the Strain Path Method (Baligh, 1985) and total or effective stress soil models.

A four-day field program was conducted at a test site in Newbury, Massachusetts to evaluate the design and performance of the T2P. The field program was designed with the intention of performing a number of dissipation tests at a series of elevations within a deep deposit of Boston Blue Clay. Twenty-four hour operation of the data acquisition system allowed overnight dissipation data to be collected. Two boreholes were used to collect a total of eight pore pressure dissipation records, whose length ranged from 0.74 to 19.74 hours. It is not clear if any of the eight monitoring periods were of sufficient duration for full dissipation to occur; it is suspected that measurement periods longer than 20 hours are required to allow complete dissipation around the probe, which is in agreement with previous research (Varney, 1998).

The field test data was used to estimate u_o at various locations within the clay, using the inverse time extrapolation method and the two-point matching method. It was found that inverse time extrapolation could be used to approximate u_o within 10% accuracy from T2P tip data within an average monitoring time of 942 seconds; however, the two-point matching method consistently produced more accurate estimates of u_o than inverse time extrapolation at similar dissipation times. In addition, soil hydraulic conductivity (k) was interpreted by comparing the measured dissipation data with theoretical curves, using the T_{50} matching method. The calculated values of k closely matched values previously obtained through laboratory measurements. The T2P field test data is compared with piezoprobe and piezocone penetration and dissipation records, collected at a site in Saugus, Massauchusetts (Varney, 1998).

Recent modifications have been made to the T2P prototype since the 2004 field test, in preparation for an upcoming sea deployment. These modifications were based upon the field performance of the T2P prototype and design changes required for offshore operations.

Thesis Supervisor: Dr. John T. Germaine
Title: Principal Research Associate of Civil and Environmental Engineering

ACKNOWLEDGMENTS

I am forever indebted to my wife, Christina, for keeping me sane during my time at MIT and for constantly believing in me. I could not have made it without her.

Of course, I could never repay my parents for all the love and support that they've given me over the years. This thesis is not big enough to contain all the reasons that I have to be thankful to them.

Special thanks to Dr. Lucy Jen for having more faith in me that I ever did myself, and for pushing me to achieve things that I never considered possible. She has been a great friend and an inspiration to me.

I also have to thank my professors from my alma mater, SUNY Oneonta, especially Dr. P.J. Fleisher and Dr. Arnold Palmer. My experiences with them changed the way I look at the world and life in general.

I am also very thankful to have had the opportunity to work with Dr. Germaine at MIT, who is both a true professional and a great guy.

Finally, I'd like to give props to all my boys from New York for keeping it real.

DEDICATION:

To the Bronx.

Table of Contents

LIST OF TABLES

LIST OF FIGURES

1 INTRODUCTION

The in-situ temperature and pore water pressure of sub-seafloor sediments are of great interest to both the scientific community and the offshore oil and natural gas industries. Fluid pressure and temperature affect the solubility of gas in water and impact the permeability of marine sediments (Kvenvolden, 1993). The migration of pore fluids and dissolved gases is driven by the permeability of these sediments and in-situ pressure and temperature gradients. Excess pore pressures within continental slopes have been linked to marine slope failures (Dugan and Flemings, 2002). Direct measurements of in-situ pore pressures within sub-seafloor sediments have been limited by the time and cost required to collect this data. The Integrated Ocean Drilling Program (IODP), an international research program involved in the exploration of marine hydrogeology, has obtained high-quality direct sub-seafloor temperature and pressure measurements through the use of long-term, seafloor observatories installed in boreholes (i.e., Circulation Obviation Retrofit Kits or CORKS). However, the time and expense associated with the installation and maintenance of these observatories make this approach unrealistic for routine data collection.

IODP and the oil and gas industries have also used penetration devices to measure the in-situ pore pressure and permeability of marine sediments. The first modern penetration device was the electric cone (de Ruiter, 1970), which has both an axial load cell to measure tip resistance and a friction sleeve to calculate soil/steel interface resistance. Continuous measurements of tip and friction resistance collected during cone penetration are correlated with variations in soil properties, thus providing an efficient method to determine subsurface profiles. However, it was not until Senneset (1974) developed the piezocone by adding a pressure transducer to the electric cone, that a single tool could concurrently measure pore pressure, tip resistance, and frictional resistance in the same borehole (Varney, 1998). The combination of pore pressure and tip force measurements in a single device improved the accuracy of the modern penetrometer as a profiling tool.

Penetration devices, such as the piezocone, are also commonly used to measure pore pressure during penetration of sediments at the base of boreholes drilled into the

seafloor. The insertion of the tool creates a pressure pulse, the rate of which is controlled by the radius of the penetrometer and the permeability and compressibility of the surrounding sediments.

Traditionally, piezocones have been deployed in this manner by industry and the Davis-Villinger Temperature-Pressure Probe (DVTP-P) has been used by the IODP. However, the time required to reach full dissipation using either of these tools can exceed 24 hours (Whittle et al., 2001), which is a prohibitively long time for a drilling vessel to remain stationary on the ocean surface while pressure measurements are being recorded. In order to address this problem, Fugro-McClelland Marine Geosciences, Inc. (FMMG) developed the FMMG piezoprobe, which measures pore pressure near the tip of a 26.5 cm long, 0.64 cm wide, tapered extension piece that is attached to the end of a standard piezocone shaft. This design is intended to accelerate the dissipation of penetration-induced excess pore pressure, thus reducing the required time to reach the in-situ value.

The geometries of the piezoprobe and the DVTP-P devices differ dramatically, as shown in Figure 1.1. Each tool measures pressure through a porous element near its tip. However, the piezoprobe measures pressure at a point located 2.4 cm above its tip, while the DVTP-P's porous element is located 10 cm above its tip. It has been found that the geometry of the DVTP-P causes dissipation to occur more slowly than it does for the piezoprobe in soils with similar permeability and compressibility. In addition, the piezoprobe is significantly narrower then the DVTP-P; therefore, the magnitude of the pressure pulse induced by the DVTP-P is considerably greater than that caused by the piezoprobe. It is also suspected that DVTP-P penetration may cause formation failure, due to the relatively large size of this tool. Since a drilling vessel must remain stationary during the deployment of a penetration device, it is impractical for a tool to remain at the measurement location for longer than a few hours. The time required for full dissipation of excess pore pressure induced by either DVTP-P or piezoprobe penetration is considerably longer than this; therefore, these tools are impractical for routine measurements. Therefore, an important goal of the IODP has been to develop a device that can measure in-situ pressures in shorter time periods.

In an effort to infer in-situ pore pressures from incomplete dissipation records, the inverse time extrapolation method has traditionally been used. For this method, pressure is plotted versus inverse time on a natural scale. A tangent line is then extended from the final portion of the incomplete dissipation record, with the y-intercept assumed to be the in-situ pressure. Figure 1.2 illustrates how this construction is used on a partial dissipation record, in which the in-situ pore pressure is estimated at 166.7 and 500 seconds after the start of dissipation. As indicated in this figure, the accuracy of the estimate of in-situ pore pressure improves as the length of the dissipation increases. Because the dissipation data is non-linear at large time scales, this method typically overestimates in-situ pressures for both the piezoprobe and the DVTP-P (Whittle et al., 2001).

In order to improve the reliability of estimates of hydraulic conductivity from incomplete dissipation records, the MIT geotechnical group (Aubeny et al., 2000; Whittle, 1992; Whittle and Sutabutr, 1999, Whittle, 2001) used the Strain Path Method (SPM [Baligh, 1985]) in combination with effective stress soil models based on elasto-plasticity (MIT-E3 [Whittle et al, 1994]) to predict changes in stress during post-penetration consolidation. In this manner, a characteristic dissipation curve was derived for the penetrometer, based on specific input soil parameters. The dissipation of penetration-induced pore pressure is plotted versus a dimensionless time factor, from which hydraulic conductivity can be derived,

$$T = \frac{\sigma' kt}{\gamma_w R_2^2} \qquad \text{Equation 1.1}$$

where T is the model time factor, k is hydraulic conductivity, γ_w is the unit weight of water, R_2 is the radius of the larger-diameter shaft of the piezoprobe, σ' is the in-situ mean effective stress at the pore pressure measurement point, and t is the measured time. The T_{50} matching method can be used to calculate hydraulic conductivity from the measured and predicted curves by matching the model predicted time factor for 50% dissipation (T_{50}) with the measured time (t_{50}) required for 50% dissipation of excess pore pressures. Hydraulic conductivity can then be calculated in the following manner:

$$k = \frac{T_{50}\gamma_w R_2^2}{\sigma' t_{50}}$$ Equation 1.2

Figure 1.3 shows how this technique was used to estimate hydraulic conductivity from measured and predicted dissipation of excess pore pressure for the FMMG piezoprobe.

The MIT geotechnical group also introduced a novel method for predicting in-situ pore pressures from incomplete dissipation records using SPM in combination with either effective stress or total stress soil models. This technique, referred to as the two point matching method, was used to improve the piezoprobe design. Whittle et al. (1997; 2001) predicted that concurrent measurements of pore pressure at two locations on the surface of a tapered probe could be used to make reliable predictions of in-situ pressures and to provide a consistent approach for controlling the required dissipation measurement duration. Figure 1.4 illustrates the predicted dissipation behavior for a dual-pressure probe, in which pore pressures are measured at both the tip (radius = 0.6 cm) and shaft (radius = 3.6 cm). This figure shows that approximately 90% dissipation of excess pore pressure will occur at the tip of a tapered probe when the magnitudes of dissipated pore pressure (u_i-u) are identical at both the tip and shaft. Once this intersection point is reached, it is possible to predict the in-situ pore pressure from incomplete dissipation data. Therefore, this approach provides a practical method for controlling dissipation measurement duration (i.e., data must only be collected until the intersection point is reached). It has been estimated that the intersection point will occur in as little as 30 minutes after the onset of dissipation for a piezoprobe in sub-seafloor sediment at the Hydrate Ridge, located offshore from Oregon, USA (Flemings et al., 2003). It has also been found that the intersection point will occur at approximately 90% dissipation of excess pore pressure at the tip, regardless of soil properties or stress history. Hence, it is not necessary to measure the soil properties of the deposit of interest or to run additional numerical simulations before using this method. The MIT group has verified the validity of this technique by combining and analyzing piezocone and FMMG piezoprobe dissipation data that was collected at a site in Saugus, Massachusetts (Varney, 1998).

In summary, a piezoprobe that measures pore pressure at multiple locations will improve the estimation of in-situ pore pressures at deep-water sites in shorter times than was previously possible with existing penetration tools.

1.1 Purpose of this Project

This thesis describes the design and land-based field evaluation of a probe prototype (referred to as the T2P) that measures temperature at its tip and pore pressure at two monitoring points with different radii. The T2P field data are presented, interpreted, and compared with the results of a previous land-based field evaluation of several piezoprobes and piezocones that was performed by Varney (1998).

This thesis is part of a larger project funded by the National Science Foundation. The overall goal of this project is to produce a dual-pressure probe capable of offshore deployment by the IODP. Since the 2004 T2P field test, various modifications have been made to the T2P in preparation for an anticipated offshore deployment in June and July of 2005. These design changes are discussed in Chapter 7 and illustrated in Appendix C.

1.2 Organization of Thesis

Chapter 2 presents the results of several geotechnical investigations previously performed at the Newbury field test site in Massachusetts. A summary of the theoretical framework used to create the model predictions presented in this thesis is also included in this chapter.

Chapter 3 describes the geometry of the tool, design considerations, and the equipment used during the December 2004 T2P field test. The equipment discussed in this chapter includes the prototype T2P housing, transducers, electrical connections, data acquisition, and support equipment.

Chapter 4 discusses the manner in which the field test was conducted and the steps taken to ensure the collection of high-quality data. The field stability and resolution of the pore pressure measurements are also examined in this section.

Chapter 5 presents the T2P temperature and pressure data collected during the field test. The resulting penetration, dissipation, and extraction records are examined for the influence of electrical noise and other equipment problems. The T2P dissipation data

is compared with the piezoprobe and piezocone dissipation records, collected by Varney (1998).

Chapter 6 discusses the various methods used to interpret the T2P dissipation data. The values of in-situ pore pressure and permeability inferred from the T2P dissipation records are also presented in this chapter.

Chapter 7 summarizes the results and conclusions from the T2P field test and describes the advancements in the T2P design that have been implemented to date.

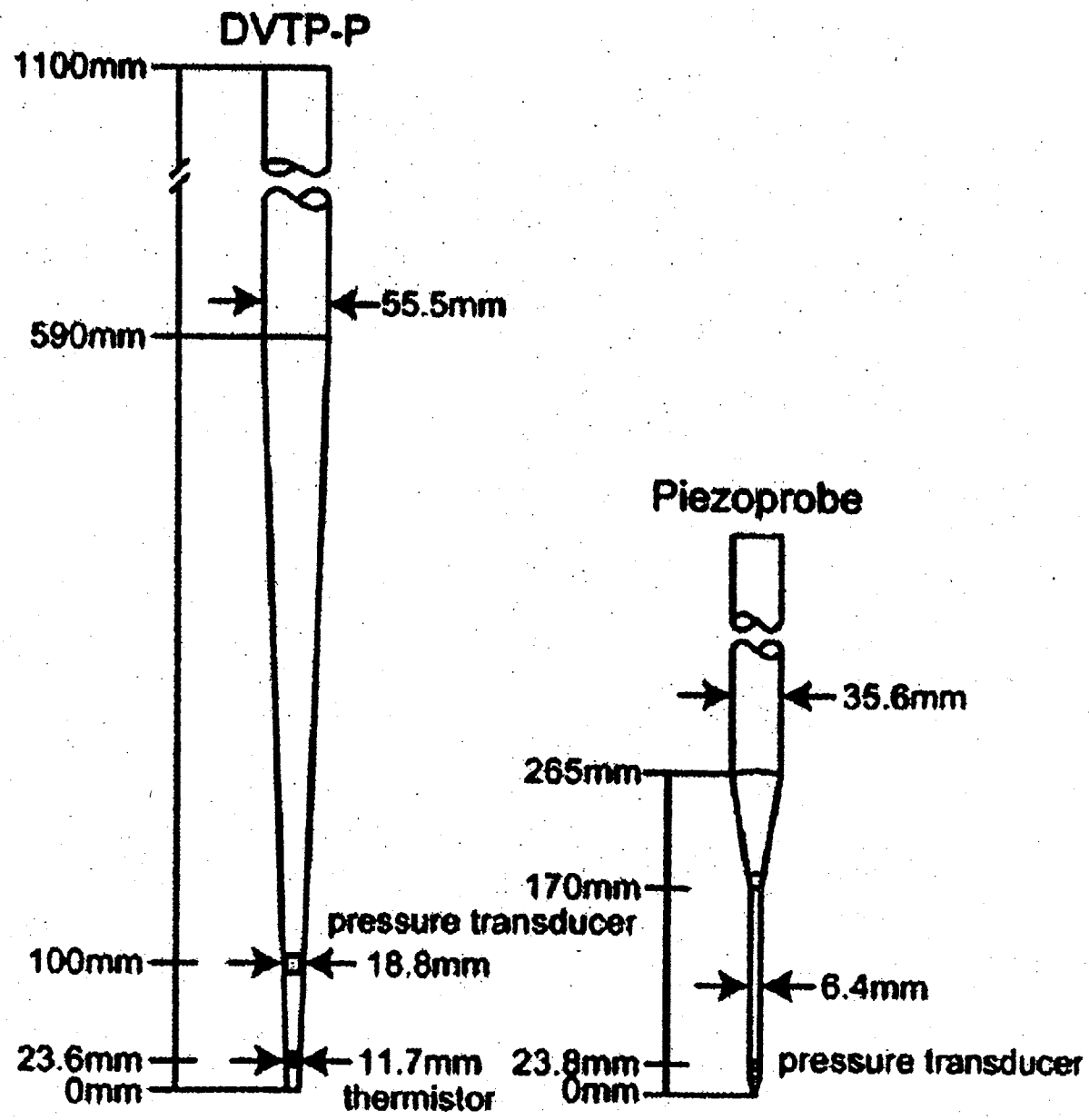

Figure 1.1 Geometry of the FMMG Piezoprobe (Ostermeier et al., 2001) and the DVTP-P (Schroeder, 2002)

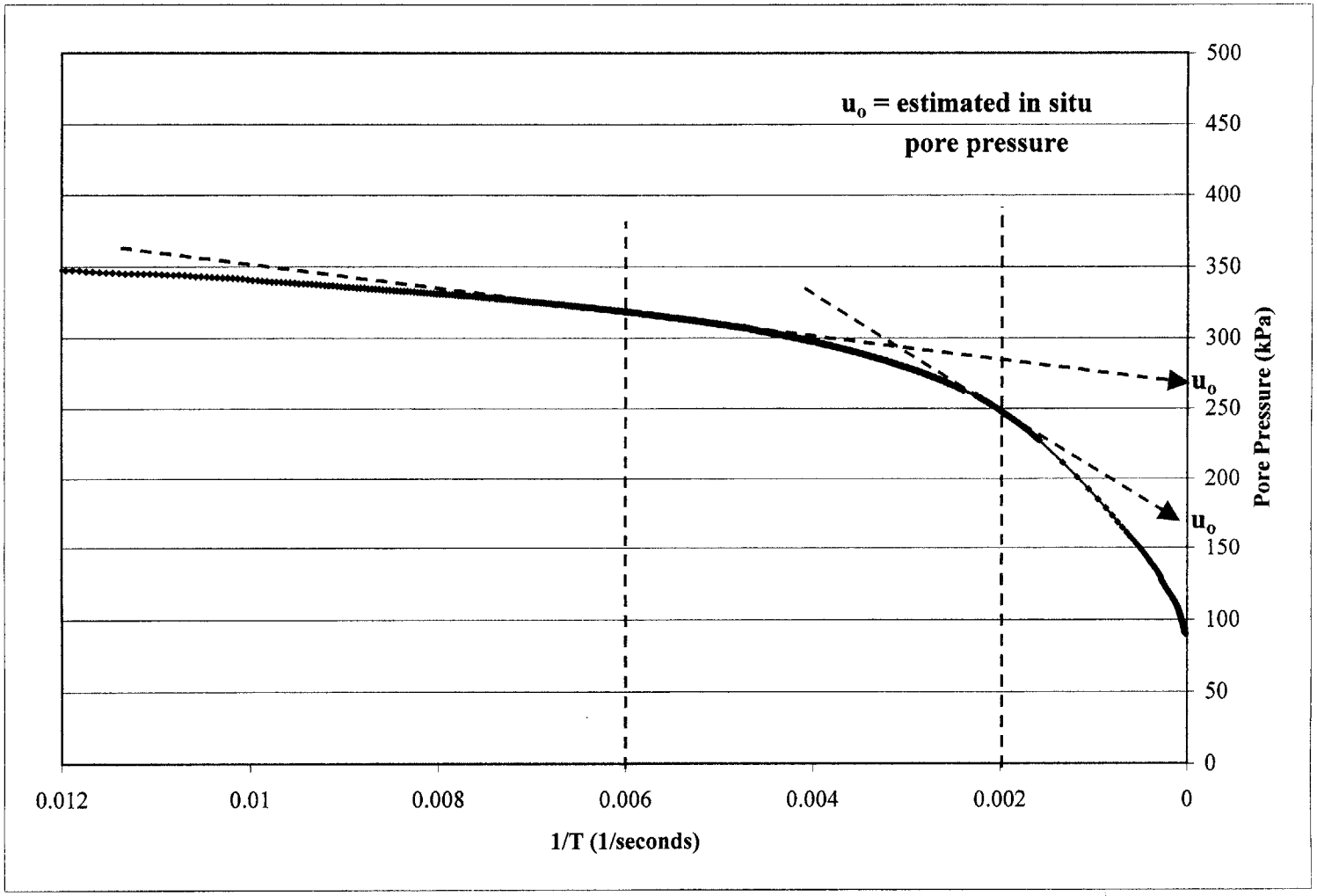

Figure 1.2 Example of Inverse Time Extrapolation Method to Estimate In-Situ Pore Pressure

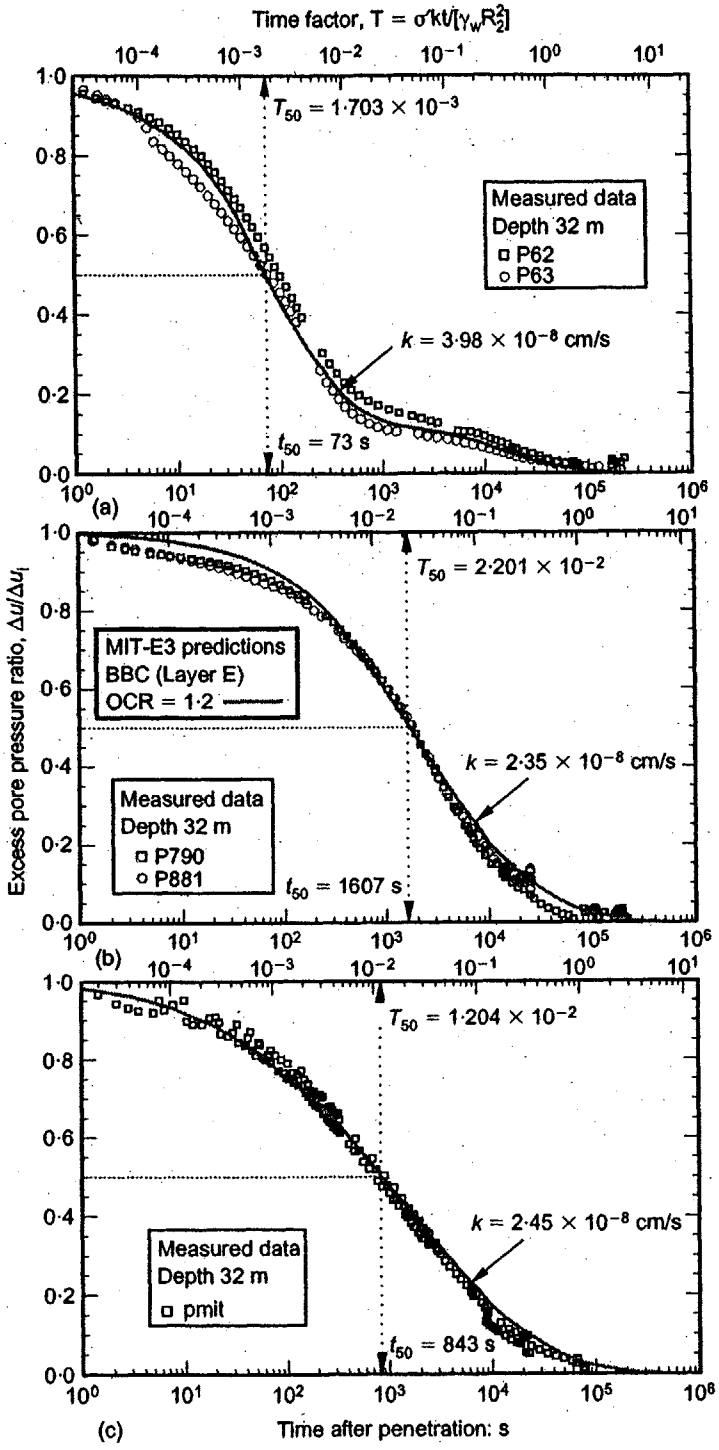

Figure 1.3 Calculation of Hydraulic Conductivity from Measured and Predicted Dissipation Behavior Using T_{50} Matching (Whittle et at., 2001)

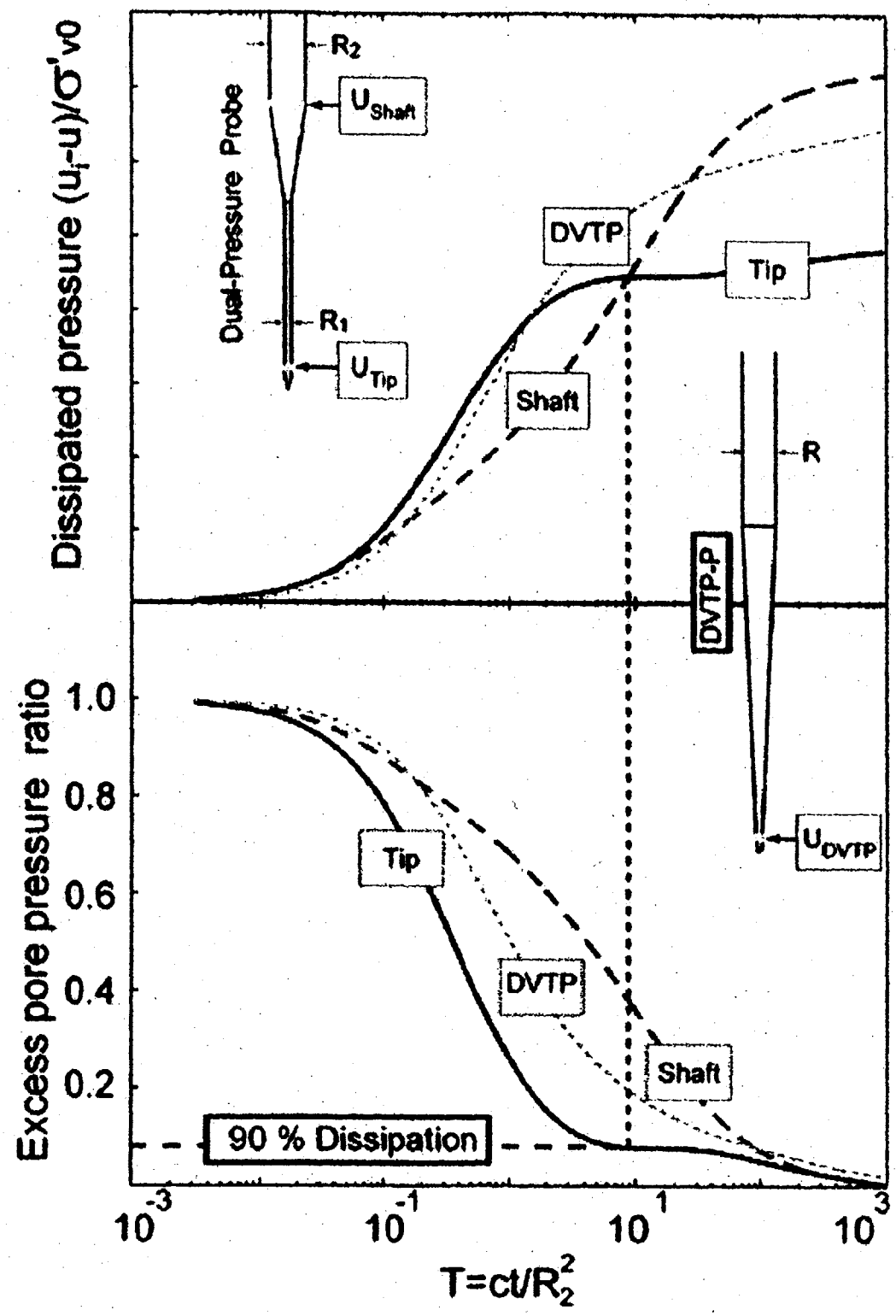

Figure 1.4 Modeled Dissipation Behavior of Dual-Pressure Probe as predicted with a Total Stress Soil Model

2 BACKGROUND

This chapter provides background information concerning the Newbury site used to perform the 2004 T2P field, a description of the scope of the field program, and a brief overview of the theoretical framework used to interpret the dissipation data. This chapter also includes background information for a site in Saugus, Massachusetts at which Varney (1998) evaluated the performance of several piezocones and piezoprobes. Penetration data collected at the Saugus site will be compared with T2P data in Chapters 5 and 6.

2.1 T2P Field Test Site

The field test site is located in Newbury, Massachusetts, next to the Newburyport Massachusetts Bay Transportation Authority (MBTA) train station. Refer to Figure 2.1 for the site location. The first subsurface studies at the site were conducted in the 1930's, for the construction of a foundation for a multi-span, concrete-reinforced bridge along Route 1 in Newbury (Paikowsky and Hart, 1998). This bridge, completed in 1935, was demolished in 1996. Additional geotechnical studies were performed at the site in the 1988 and throughout the 1990's for the construction of a replacement bridge. A total of 36 borings were completed at the site before the 2004 T2P field test (Paikowsky and Hart, 1998).

This site was chosen as the initial test location for the T2P because it contains a 9 to 12 meter-thick deposit of BBC, close to the ground surface. A detailed plan of the site is shown in Figure 2.2. The plan includes borings from previous research projects and the three borings created and used for the 2004 T2P field test (Borings TP1, TP2, and L1). The average ground elevation at the site is approximately 5.4 meters above mean sea level (DeGroot et al., 2004). The test site is bordered to the north by the MBTA station exit ramp, to the south by the foundation of the overlying Route 1 bridge, to the east by a utility road, and to the west by the MBTA commuter train tracks. Several piers supporting the bridge are located in the site area. The presence of the bridge over the site limits the available overhead clearance for drilling operations to approximately 8 meters.

2.1.1 Summary of Newbury Site Subsurface Conditions

The following description of the Newbury test site deposit was abstracted from Paikowsky and Hart (1998), and is based upon field and laboratory testing of soil samples, performed at the University of Massachusetts at Lowell. Figure 2.3 illustrates an average geological cross-section of the site. From the ground surface downward, the general soil profile consists of 2.4 meters of granular fill, consisting of very dense, brown sand and gravel, intermixed with concrete fragments, overlying approximately 0.3 meters of organic silt and peat. Below the organic layer is a 13.7-meter thick deposit of Boston Blue Clay (BBC), a marine clay deposited by glacial meltwater. The BBC is composed of approximately 2.7 meters of medium stiff to very stiff, overconsolidated clay, over 6.1 meters of very soft to soft, plastic, normally to slightly overconsolidated clay, and 4.9 meters of soft, plastic, normally consolidated clay. A 2.9-meter thick layer of interbedded silt, fine sand, and silty clay lies beneath the BBC. Below this interbedded deposit is a 2.4-meter thick stratum of silty sand. A second interbedded deposit of silt, fine sand, and silty clay, approximately 2.3 meters thick, underlies the silty sand. Beneath this interbedded deposit is 2.4 meters of medium dense to dense, fine to medium sand. Below the fine to medium sand is a dense glacial till, composed of medium dense to dense, fine to coarse sand and gravel, with traces of rock fragments and silt. Underlying the till is mylonitic, basalt bedrock.

Figure 2.4 plots water table elevation measurements made at the Newbury test site by Paikowsky and Hart (1998) between March 5 and September 4, 1996. Over this period, the depth of the water table generally ranged from 1.75 and 2.5 meters.

The index and engineering properties for the Newbury BBC deposit are listed in Table 2.1 and Figure 2.5 is a plasticity chart indicating the location of the Newbury site BBC. In the United Soil Classification System (USCS), the Newbury site BBC plots above the A-line and is designated CL, i.e., low-plasticity clay.

The stress history profile of the BBC is shown in Figure 2.6. The preconsolidation pressure is at a maximum at the top of the clay, decreases to a minimum at an approximate depth of 9 meters, and then increases linearly with depth. Figure 2.5

indicates that the overconsolidation ratio (OCR) of the deposit ranges from 4 to 7 at the top, decreases to 1 within the upper 7 meters, and then remains constant with depth.

Figure 2.7 presents the undrained strength profile of the clay, as measured with SHANSEP, DSS, UU, and UC laboratory tests. This figure indicates that the undrained shear strength approaches 100 kPa near the top of the deposit, and then ranges from 15 to 50 kPa below a depth of 5.5 meters. The trend in strength is similar to that of the preconsolidation pressure profile. It should be noted that the engineering properties for the Newbury BBC deposit have not been independently verified at MIT.

Data from several piezocone profiles perfomed at the Newbury site by Jacubowski (2004) are shown in Figure 2.8.

2.2 Saugus Field Test Site

Since the mid-1960's, MIT has conducted various field programs at a well-documented site in Saugus, Massachusetts, including a 1996 field evaluation of two FMMG piezoprobes, two standard piezocones, and one MIT piezocone (Varney, 1998). A detailed plan of this site, located approximately 10 miles from MIT, is shown in Figure 2.9. The plan shows the locations of boreholes used for both the 1996 field program and for previous research projects. For the 1996 field test, two borings (790PUSH and 881PUSH) were used to perform continuous piezocone penetration soundings, and five borings were installed to collect long-term dissipation data: one for each piezoprobes (PP62 and PP63), one for each piezocone (PC790 and PC881), and one for the MIT piezocone (MIT). Three borings (M206A, M206B, and M206C) were used to install piezometers and one borehole (B96) was installed to collect undisturbed soil samples. The pore pressure data from a continuous piezocone profile and piezoprobe penetration records collected by Varney are plotted versus depth and are shown in Figure 2.10. For additional information on the manner by which the 1996 field program was conducted, refer to Varney (1998).

2.2.1 Subsurface Conditions at the Saugus Site

The following description of subsurface conditions at the Saugus field test site was summarized from Varney (1998) and is based on data collected during the 1996 field

test and from previous research programs. The soil profile is listed in Table 2.2. From the surface downward, this profile consists of 1.2 to 1.8 meters of peat overlying 5 meters of sand. Below the sand is a 37-meter thick deposit of BBC, over glacial till. The upper 4 meters of the BBC (Zone A) are stiff and strongly interbedded with sand. The next 3 meters of the clay (Upper Clay Zone B) are also stiff, with numerous sand layers. Upper Clay Zone B is significantly desiccated, with large variations in piezocone penetration resistance. The next 6 meters (Upper Clay Zone C) are stiff and have thicker clay layers, with large disparities in penetration resistance. Below Upper Clay Zone C is a transition zone (Middle Clay Zone D), which exhibits a constant to decreasing penetration resistance with depth and is considerably more uniform than the clay above. The remaining 24 meters of BBC (Lower Clay Zone E) are softer and more uniform, with little sand.

The index properties and stress history for the Saugus site clay deposit are shown in Figure 2.11. The natural water content of the clay gradually increases from roughly 30% near the top to approximately 45% in the soft clay, then is constant throughout the rest of the deposit (Germaine, 1980). The plasticity index ranges from 15 to 30% and is generally lower and more variable in the upper 15 meters. The location of the Newbury site BBC. Like the Newbury BBC, the clay at the Saugus site is designated as CL (low-plasticity clay) in the USCS, and plots above the A-line in a plasticity chart, as shown in Figure 2.5.

Figure 2.11 indicates that the OCR of the clay is at a maximum of approximately 6 near the top of the deposit, and then decreases with depth. The scatter of calculated OCR values is larger in the upper layers. The BBC is normally consolidated below a depth of roughly 24 meters.

The undrained strength profile, as determined with a Geonor field vane, is presented in Figure 2.12. The undrained strength of the clay is larger and more scattered near the top of the deposit and then increases linearly with depth in Lower Clay Zone E.

Figure 2.13 presents laboratory measurements of the hydraulic conductivity of the clay. The values range from approximately $3x10^{-6}$ cm/s at the top of the deposit, to $3x10^{-8}$ cm/s within the normally consolidated zone.

2.3 Comparison between the Newbury and Saugus Clay Deposits

Both the Newbury and Saugus BBC deposits are overconsolidated near the top and normally consolidated at depth. The water contents of the normally consolidated sections of both deposits have similar ranges and average values; however the Newbury BBC has a lower liquid limit and plasticity index than the Saugus clay. In addition, the undrained shear strength of the normally consolidated section of the Saugus deposit, as measured with a field vane, is generally higher than the undrained strength of the normally consolidated portion of the Newbury deposit, as measured with a field vane.

2.4 Scope of 2004 T2P Field Program

The T2P field program had a number of goals: 1) evaluate the performance of the tool in a controlled environment and compare the quality of the T2P penetration and dissipation data with previously collected piezoprobe and piezocone data; 2) assess the robustness of the individual mechanical and electrical probe components; 3) determine the ease of T2P field assembly and disassembly; 4) collect and assess several long-term T2P dissipation records that would not be possible to obtain during a sea deployment; 5) evaluate the resulting dissipation records in an attempt to optimize the final T2P tip geometries; 6) examine the effectiveness of the two-point matching method in calculating in-situ pore pressures from T2P dissipation data; 7) collect and evaluate temperature measurements during penetration and dissipation in order to assess the responsiveness and accuracy of the T2P temperature sensor; 8) determine the success of the T50 matching method in calculating in-situ permeabilities from T2P dissipation records.

The 2004 T2P field test ran from Tuesday, December 14th to Monday, December 20th. Two boreholes (TP1 and TP2) were installed to collect penetration, dissipation, and extraction data. A third borehole, B104A, was installed to obtain samples of the BBC deposit; however, the collected samples have not yet been analyzed. The borehole locations were controlled by the geometry of the site and the presence of pre-existing boreholes.

A cargo van was brought to the site to house the data acquisition system, computers, power supply, and support equipment. The van also served as a shelter from

the elements for the personnel conducting the field test. As the site was not secure after dark, the van was locked with the field test equipment inside when the site was not manned. Power for the data acquisition system and accompanying computers was provided by the van's battery during the day and by an external battery at night. The van's engine was left running during the day to prevent the drainage of the vehicle's battery and to keep the field personnel warm. Power for the T2P's transducers was provided by an external battery at all times.

New Hampshire Boring, Inc. was subcontracted by Pennsylvania State University to install the boreholes, collect soil samples, and supply the drill rig and standard drilling and sampling equipment, the drilling operator, driller's apprentice, and drill rods.

2.4.1 Penetrations

Although dissipation measurements were a main focus of the field program, penetration data was also collected for several reasons. Recording temperature and pressure measurements during penetration at a fast sampling rate provides an opportunity to field-evaluate the response time of the temperature and pressure transducers. By examining the variation in excess pore pressure generated during each penetration, it is also possible to assess the intensity of layering within the soil deposit. Additionally, the penetration pore pressure records helped define the initial pressure (u_i) that is used in the dissipation analysis. The magnitudes of penetration-induced pore pressure can also be used to make comparisons between different sites and devices and to determine if normalized values of penetration pore pressure (u/σ'_v) relate to the OCR of the deposit.

2.4.2 Dissipations

A major goal of the field program was to measure excess pore pressure dissipation data with the T2P. Both short (approximately one hour or less) and long (overnight) dissipation records were collected. By recording several overnight dissipations, it was hoped that full dissipation of excess pore pressures would occur, in order to compare the in-situ pore pressures measured after full dissipation with the values calculated from partial dissipation records. However, the available time for dissipation measurements was limited during the field test and, as discussed in Chapter 6, it is

uncertain if full dissipation occurred during any of the records. A total of eight dissipations were recorded during the field test, and all took place at depths between 6.1 and 12.8 meters below ground surface (bgs), within the BBC deposit. Six of the dissipations (TP1_P3, TP1_P4, TP1_P5, TP1_P6, TP2_P1, andTP2_P2) occurred within the normally consolidated portion of the BBC. Figure 2.14 illustrates the locations within the soil deposit at which the eight dissipations took place.

2.5 Theoretical Framework for Predictions

This section presents a brief description of the theoretical analyses used to model the dissipation of excess pore pressures induced by penetration of BBC. The intention is to provide sufficient information to allow duplication of the theoretical results. Much of the following was summarized from Varney (1998), where a more complete discussion of the analytical details can be found. Additional information was provided by Hui Long, a PhD candidate at Pennsylvania State University, who performed the theoretical analyses for the T2P.

The analyses used to predict the consolidation of clay around the T2P were performed in two main phases:

1) Simulation of undrained penetration of clay by the T2P, using the Strain Path Method (SPM [Baligh, 1985]).
2) Finite element calculations of pore pressure dissipation.

These two phases are shown schematically in Figure 2.15. SPM is an analytical framework that predicts the distortion caused by deep, quasi-static penetration of homogeneous clay by a penetrometer. SPM assumes that the soil deformations are effectively independent of the shear strength of the soil. SPM was used to determine the strains that occur when the T2P penetrates in an undrained shearing mode.

To model the geometry of the probe, the "method of sources and sinks" (Weinstein, 1948; Rouse, 1959) was used. Since the T2P is axisymmetrical, its outer surface could be modeled using a series of line sources and sinks distributed along the centerline of the body. Levadoux and Baligh (1980) originally used this technique for 18° and 60° cone penetrometers. The T2P geometry was modeled by Long using 300

uniformly distributed source-sink combinations, although there are an infinite number of source-sink distributions that can match the probe geometry.

Once the probe geometry is accurately modeled and the penetration displacements determined by SPM, either a total stress soil model with uncoupled consolidation (T-U analysis) or an effective stress soil model with coupled consolidation (E-C analysis) could then be used to predict the soil response. E-C analyses of dissipation behavior utilize the time factor presented in Chapter 1,

$$T = \frac{\sigma' kt}{\gamma_w R_2^2} \qquad \text{Equation 1.1}$$

which involves soil permeability (k), in-situ mean effective stress (σ'), and the unit weight of water (γ_w). T-U analyses, which do not account for changes in effective stress that take place during consolidation, utilize a different time factor,

$$T = \frac{ct}{R_2^2} \qquad \text{Equation 2.1}$$

where c is a coefficient of consolidation (L^2/T) that controls the rate of pore pressure dissipation, t is the elapsed time from the end of penetration, and R_2 is the radius of the larger-diameter shaft of the piezoprobe. Both E-C and T-U analyses can provide realistic predictions of the dissipation behavior of penetrometers (Whittle et al., 2001). However, because T-U analyses do not involve hydraulic permeability, k cannot be determined using this method of analysis.

A T-U analysis was utilized for the analyses of the T2P field test results, i.e. a total stress soil model (MIT-T1 [Levadoux, 1980]) was used to simulate the pore pressure build-up and the dissipation was modeled as uncoupled consolidation using the ABAQUS™ finite element code. Table 2.3 lists the input soil parameters that were used in the analysis. Since no data were available for the Newbury site, model parameters for resedimented BBC were used in the model (for additional information regarding these parameters, refer to Levadoux, 1980). The finite element mesh used to model the T2P geometry consists of 3861 elements and 4000 nodes, and involves 4-node elements.

Figure 2.16 illustrates typical MIT-TI predictions of excess pore pressure dissipation in normally consolidated, resedimented BBC, as measured at the tip and shaft of the T2P. The top plot in this figure presents the results in terms of normalized dissipated excess pore pressures ($(u_i-u)/\sigma'_{vo}$) and the bottom plot in terms of the excess pore pressure ratio ($(u-u_o)/(u_i-u_o)$). As mentioned in Chapter 1, an intersection point occurs when the magnitudes of dissipated pore pressure (u_i-u) are identical at both the tip and shaft. For a particular soil type, stress level, and probe geometry, this intersection corresponds to a characteristic point on the normalized pore pressure ($(u-u_o)/(u_i-u_o)$) dissipation curve (Varney, 1998). Using the input soil parameters listed in Table 2.3, the theoretical results predict that the intersection point will occur at 92% dissipation of excess pore pressure at the T2P tip. Thus, by measuring u_i and the tip pore pressure at the time of intersection (u), the in-situ pressure can be calculated by setting $(u-u_{2pt})/(u_i-u_{2pt}) = 0.088$, where u_{2pt} is the in-situ pore pressure calculated using the two-point intersection method. Hence, once the intersection point has been reached, in-situ pore pressures can be determined from incomplete dissipation records, thus reducing the required duration for dissipation measurements.

The bottom plot of Figure 2.16 shows that normalized pore pressures measured at the tip exhibit an inflection point or "brake point" at which the rate of change of normalized pore pressures significantly decreases. It is believed that this brake point occurs as the pressure pulse generated by the penetration of the larger diameter cone begins to affect pressure measurements made at the tip. Varney (1998) reported that dissipation data from several Fugro-McClelland Marine Geosciences (FMMG) piezoprobes, used to penetrate normally consolidated BBC at the Saugus site, produced brake points at dissipated pore pressure ratios ranging from 10 to 20%. The geometries of the T2P and the FMMG piezoprobes are similar; both models have a 6 mm diameter tips that eventually expand to 3.6 cm diameter tubes. Both models also measure pore pressure at a location just above the tip. However, the thin shaft of the FMMG piezoprobe, leading to the tip, has a 0.6° taper, unlike the straight shaft of the T2P. Additionally, the conical section at the top of the T2P's shaft has a much sharper angle (20°) than that of the FMMG piezoprobe (9°).

Soil Properties		Overconsolidated Clay Layer	Soft Normally Consolidated Clay Layer	Normally Consolidated Clay Layer
Depth	(m)	2.72-5.49	5.49-11.58	11.58-16.46
	(ft)	(9-18)	(18-38)	(38-54)
Natural Water Content (%)		21-47	39-51	22-39
Atterburg Limit (%)	PL	20.0 - 29.1	22.0-27.3	17.5-26.4
	LL	37.0-48.8	37.0-45.2	26.6-44.0
Unit Weight	(pcf)	116-121	107-113.5	112-119
	(kN/m^3)	18.2-19.0	16.8-17.8	17.6-18.7
Shear Strength	UU Test	60-100 kPa 1253-2089 psf	15-50 kPa 313-1044 psf	15-25 kPa 313-522 psf
	UU Test	N/A	30 kPa 627 psf	N/A
	Torvane	40-210 kPa 835-4386 psf	20-25 kPa 418-522 psf	15 kPa 313 psf
	Pocket Penetrometer	130-375 kPa 2715-7832 psf	45-55 kPa 940-1149 psf	30 kPa 626 psf
Sensitivity	Field Vane Shear Test	N/A	6.87-9.4	9.3
	Lab, Vane Shear Test	N/A	1.1-1.6	2.3-4
Friction Angle (°)		34	N/A	N/A
Cohesion (psi / kPa)		3.58 / 24.7	N/A	N/A
Coefficient of Consolidation c_v (cm^2/min)		0.066	0.06	0.072
Coefficient of Permeability kv (cm/s)		5.5×10^{-9}	5.0×10^{-9}	7.0×10^{-9}
OCR		2-7	1-1.8	1

Table 2.1 Newbury Test Site Soil Properties (Paikowsky and Hart, 1998)

Description	depth (ft)	Characersitics
a layer of peat exists over this depth	4 - 8	q_c is low with small variability (Fig 4.11).
sand layer	8 - 17	sharp increase in q_c (Fig. 4.11)
transition zone starting with clean sand changing to sandy clay with interstatial sand lenses (referred to as upper clay- Zone A).	17 - 30	very clear decrease in mean value of q_c with high variability. u is very low at d=20 ft and increases thereafter with large variability in magnitude.
Upper clay- Zone B	30 - 40	u and q_c are essentially constant with some variability.
Upper clay- Zone C	40 - 60	Both u and q_c increase at approximately the same rate.
Middle clay- Zone D	60 - 75	Smaller rate of increase in both u and q_c compared to above.
Lower clay- Zone E	75 - 140	Both u and q_c increase at the same rate with small variability.
Glacial Till	140	Sharp increase in q_c and decrease in u.

Table 2.2 Geologic Profile of Saugus Site (Varney, 1998)

1. Elastic Shear Modulus

$G/\bar{\sigma}_{vc} = 182.479$

2. Initial Yield Surfaces (Spheres)

Yield Surface Number m	Center Location $\alpha_1^{(m)}/\bar{\sigma}_{vc}$	Radius $k^{(m)}/\bar{\sigma}_{vc}$	Elasto-Plastic Modulus $H_m/\bar{\sigma}_{vc}$
1	0.4874	0.0244	239.649
2	0.4429	0.0942	166.263
3	0.3999	0.1630	110.842
4	0.3625	0.2218	73.895
5	0.3338	0.2675	49.263
6	0.3087	0.3066	32.842
7	0.2895	0.3370	21.895
8	0.2726	0.3629	14.596
9	0.2595	0.3830	9.731
10	0.2480	0.3999	6.487
11	0.2388	0.4127	4.325
12	0.2304	0.4234	2.883
13	0.2237	0.4313	1.922
14	0.2177	0.4379	1.281
15	0.2129	0.4429	0.854
16	0.2088	0.4471	0.570
17	0.2056	0.4503	0.380
18	0.2030	0.4530	0.253
19	0.2010	0.4550	0.169
20	0.1995	0.4565	0.113
21	0.1987	0.4573	0.050
22	0.1980	0.4580	0.000

3. Change in Plastic Modulus (Eq. 6.13).

Rate of Decrease in Plastic Modulus $A_m = 25.0$

Limiting (Minimum) Plastic Modulus $H'^{\ell}_m/H'^{0}_m = 0.10$

$\Big\}\ m=1,2,\ldots,22$

4. Strain Softening; Post-Peak (Eq. 6.15)

Rate of Decrease in Radius $A_p = 10.55$

Initial Radius $k_o^{(p)}/\bar{\sigma}_{vc} = 0.458$

Limiting (Minimum) Radius $k_\ell^{(p)}/\bar{\sigma}_{vc} = 0.260$

Table 2.3 Numerical Values of the Model Parameters for Normally Consolidated BBC, with $K_o = 0.537$ (Levadoux, 1980)

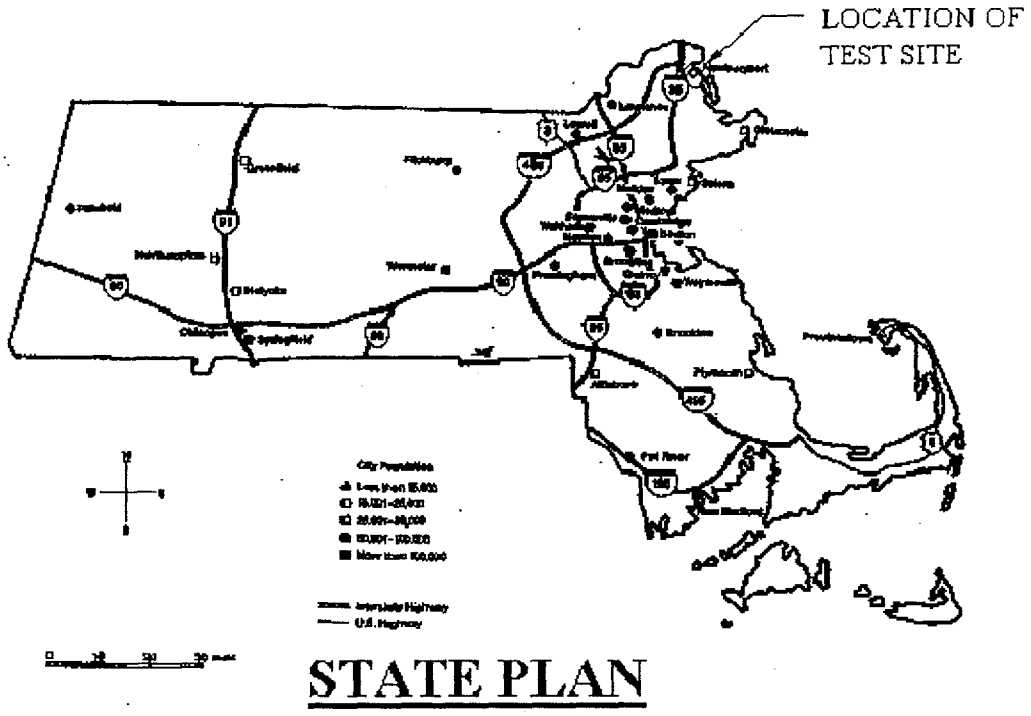

STATE PLAN

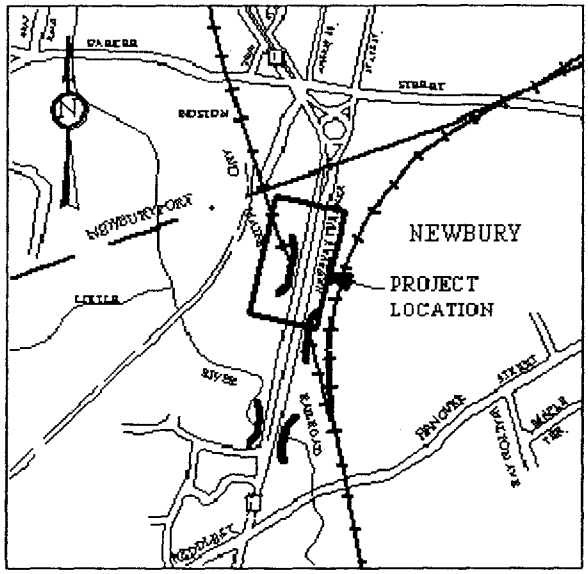

LOCATION PLAN

SCALE: 1" = 1400'

Figure 2.1 T2P Field Test Site Location (Paikowsky and Hart, 1998)

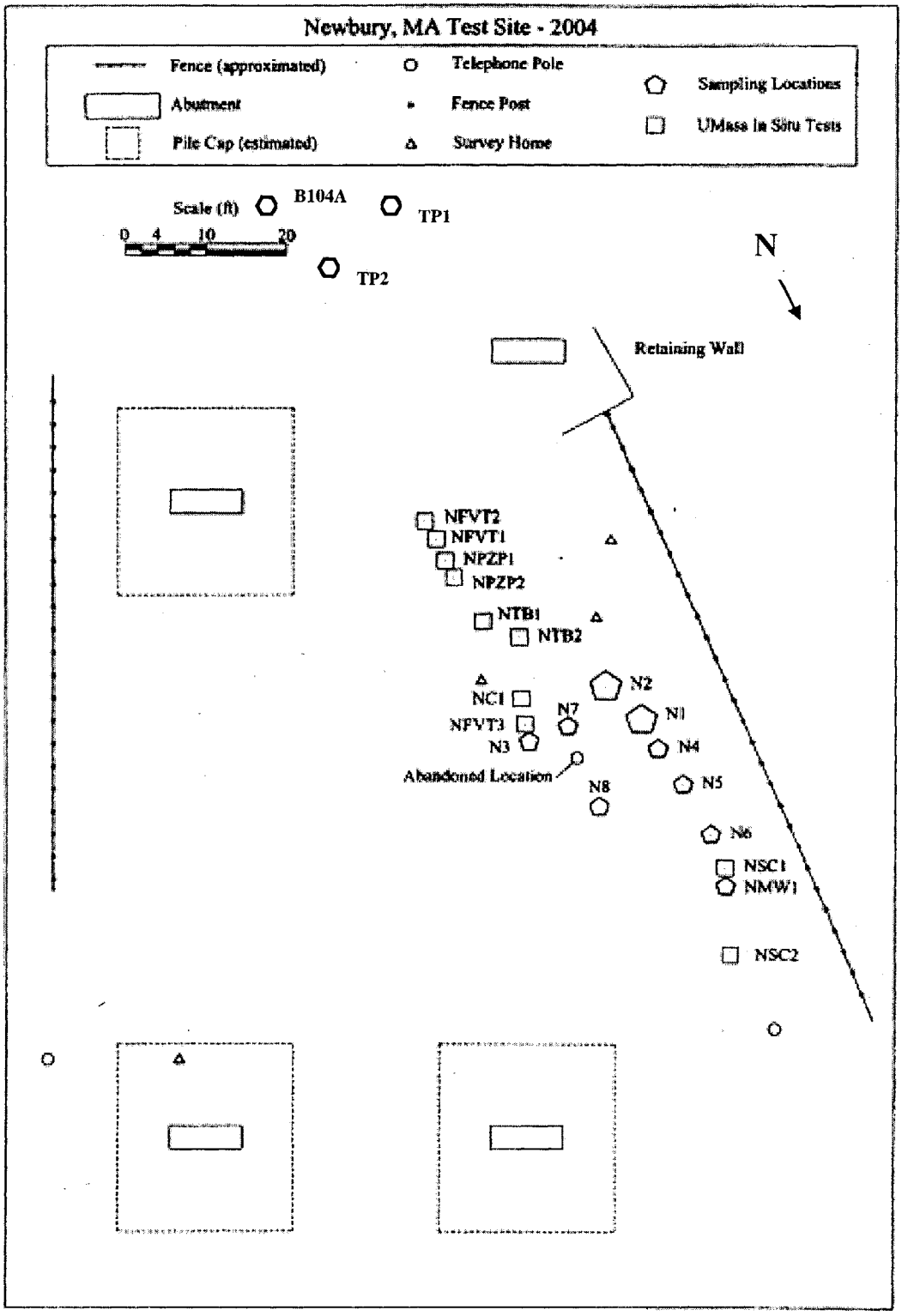

Figure 2.2 Newbury Field Test Site Plan with Boring Locations (based on figure from Degroot et al., 2004)

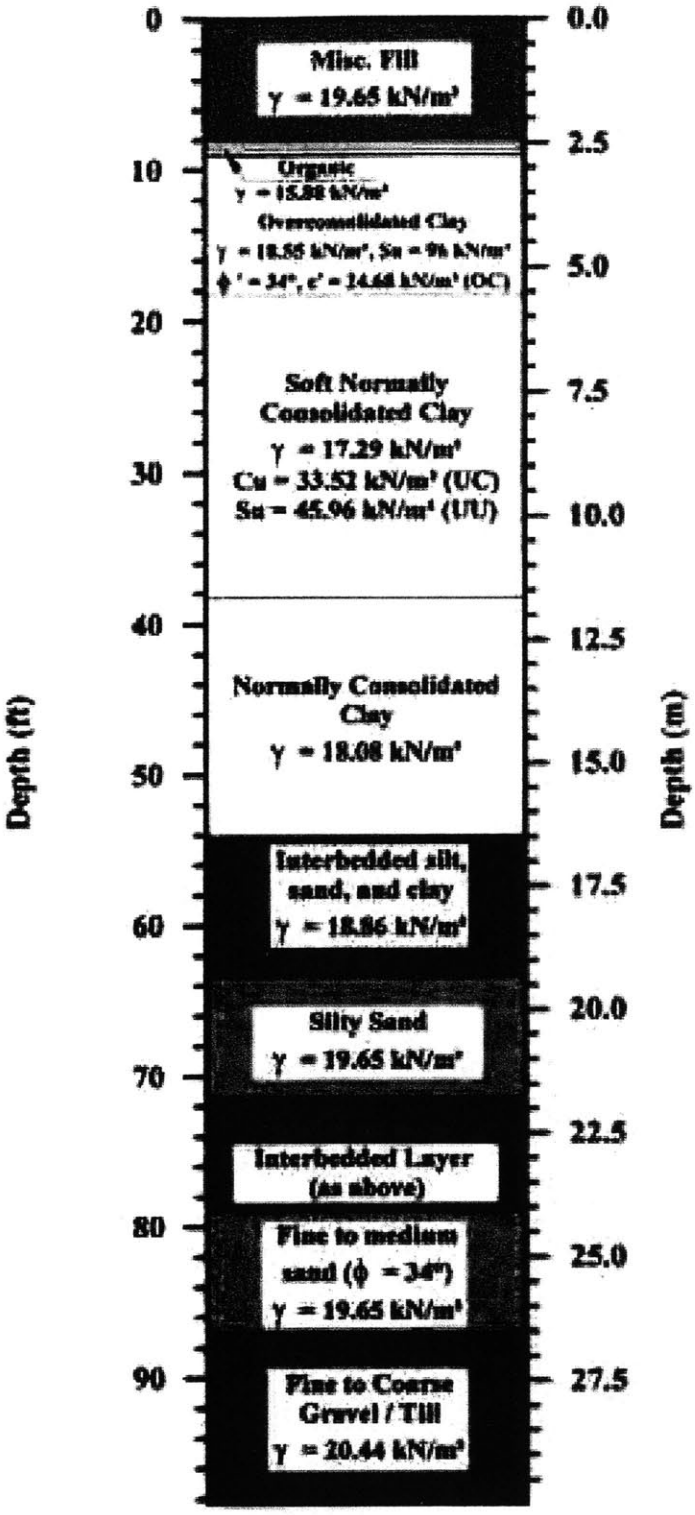

Figure 2.3 Newbury Test Site Soil Profile (Paikowsky and Hart, 1998)

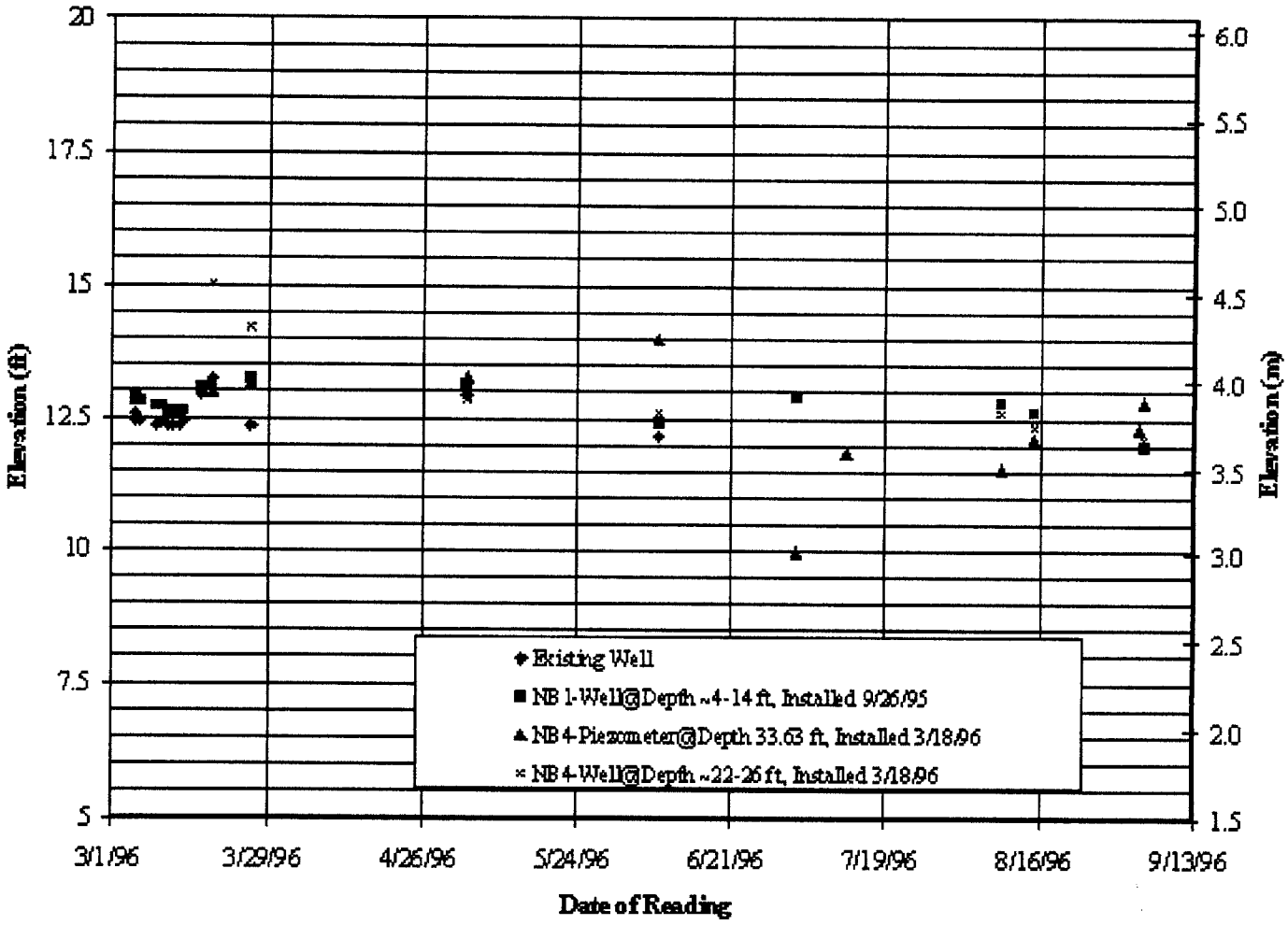

Figure 2.4 **Water Table Elevation Measurements from the Newbury Test Site (Paikowsky and Hart, 1998)**

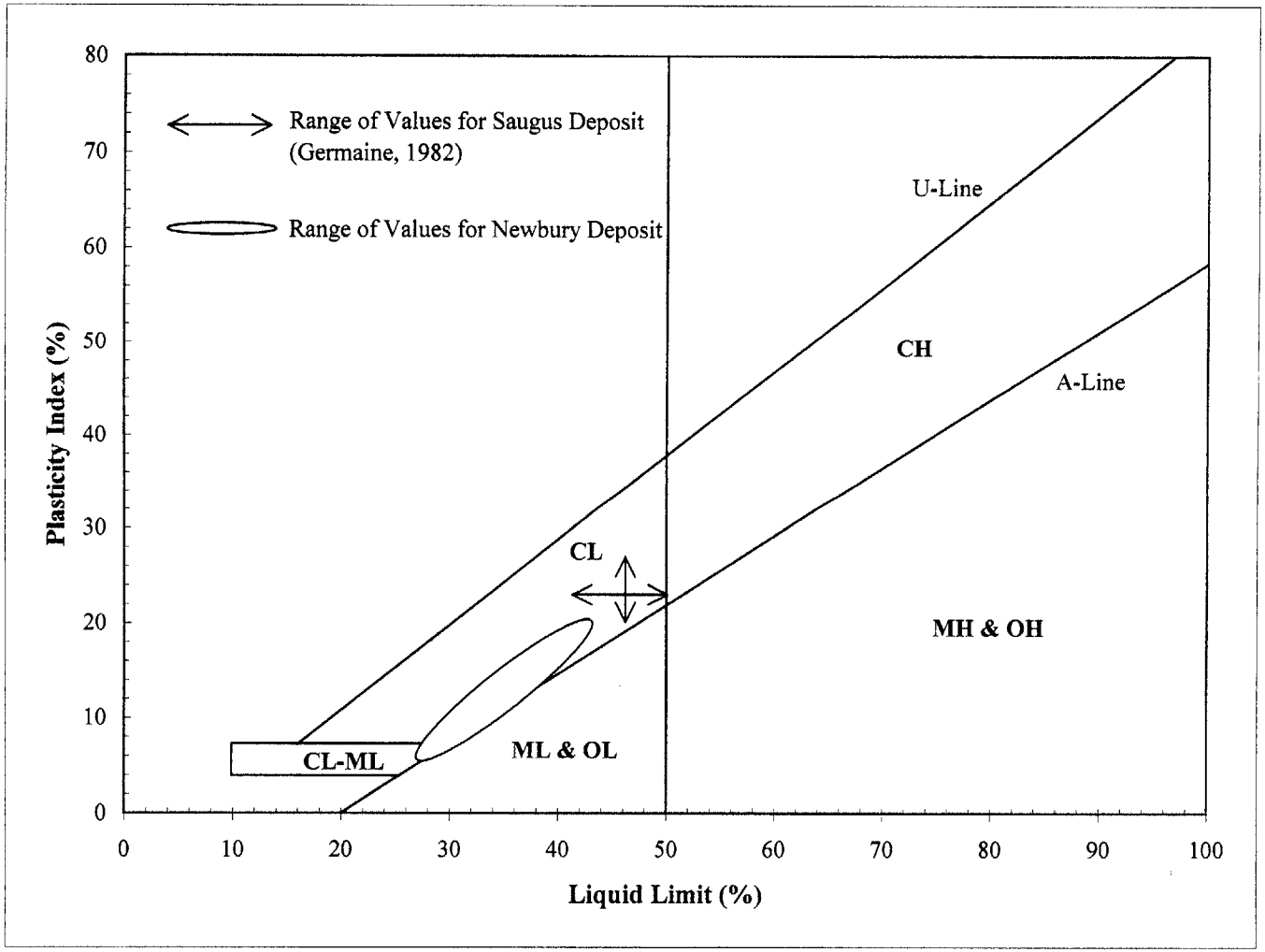

Figure 2.5 Plasticity Chart

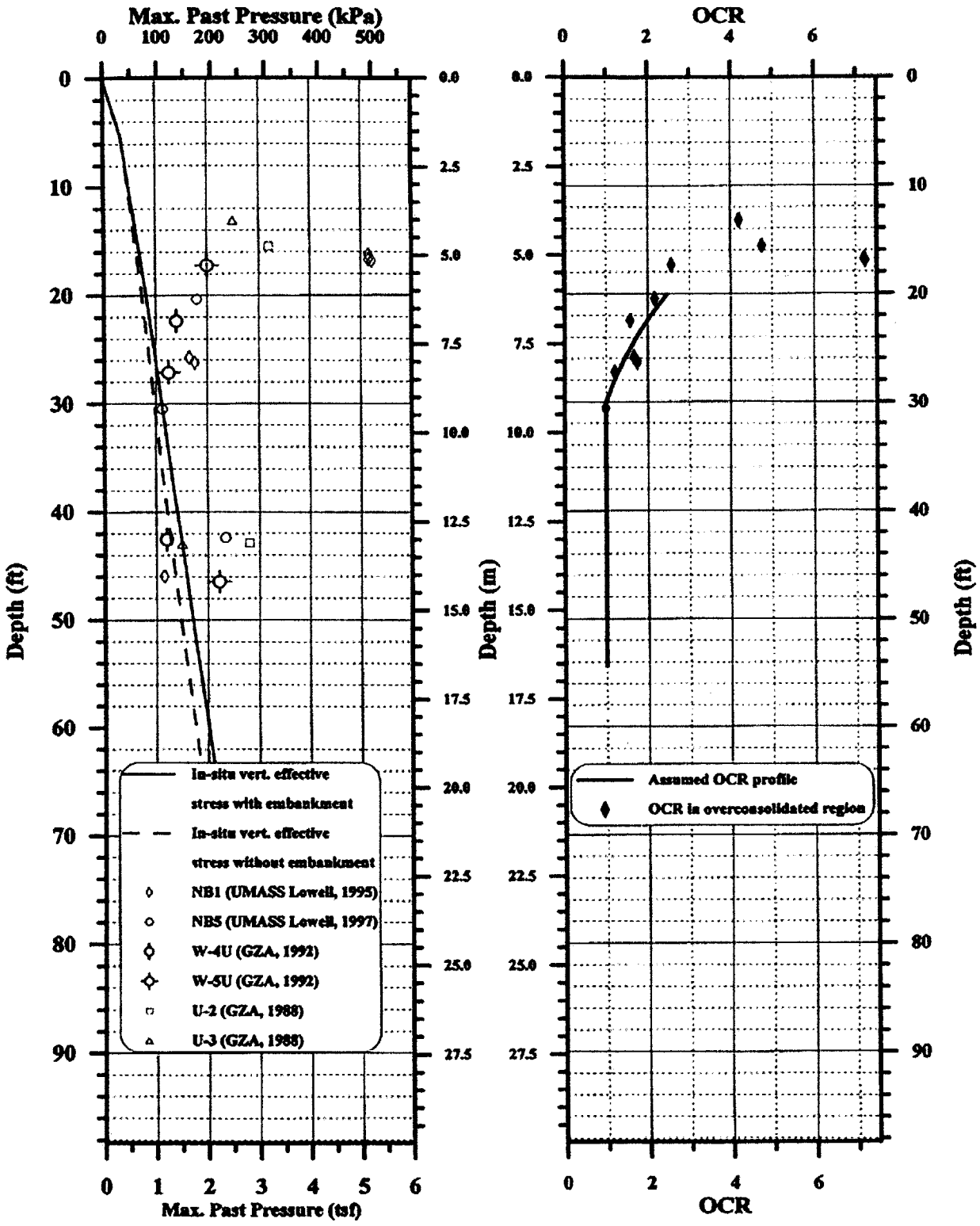

Figure 2.6 Stress History Profile for Newbury Site (Paikowsky and Hart, 1998)

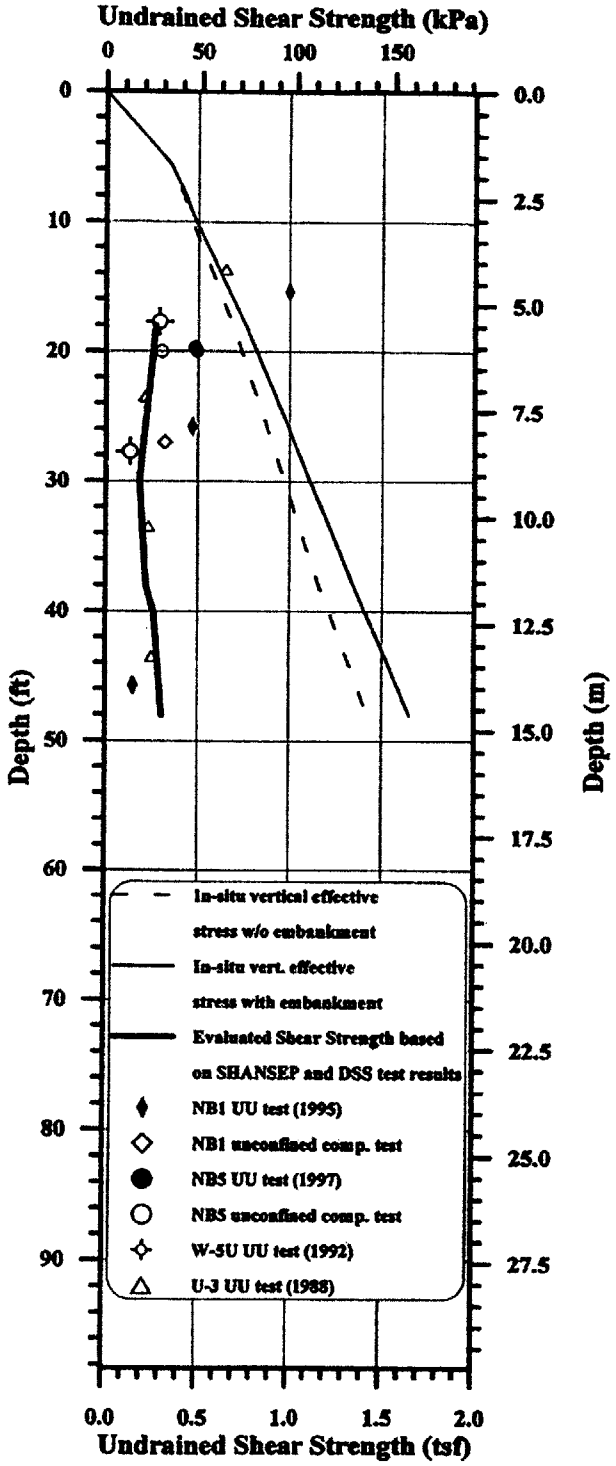

Figure 2.7 Calculated and Measured Undrained Shear Strength at the Newbury Test Site (Paikowsky and Hart, 1998)

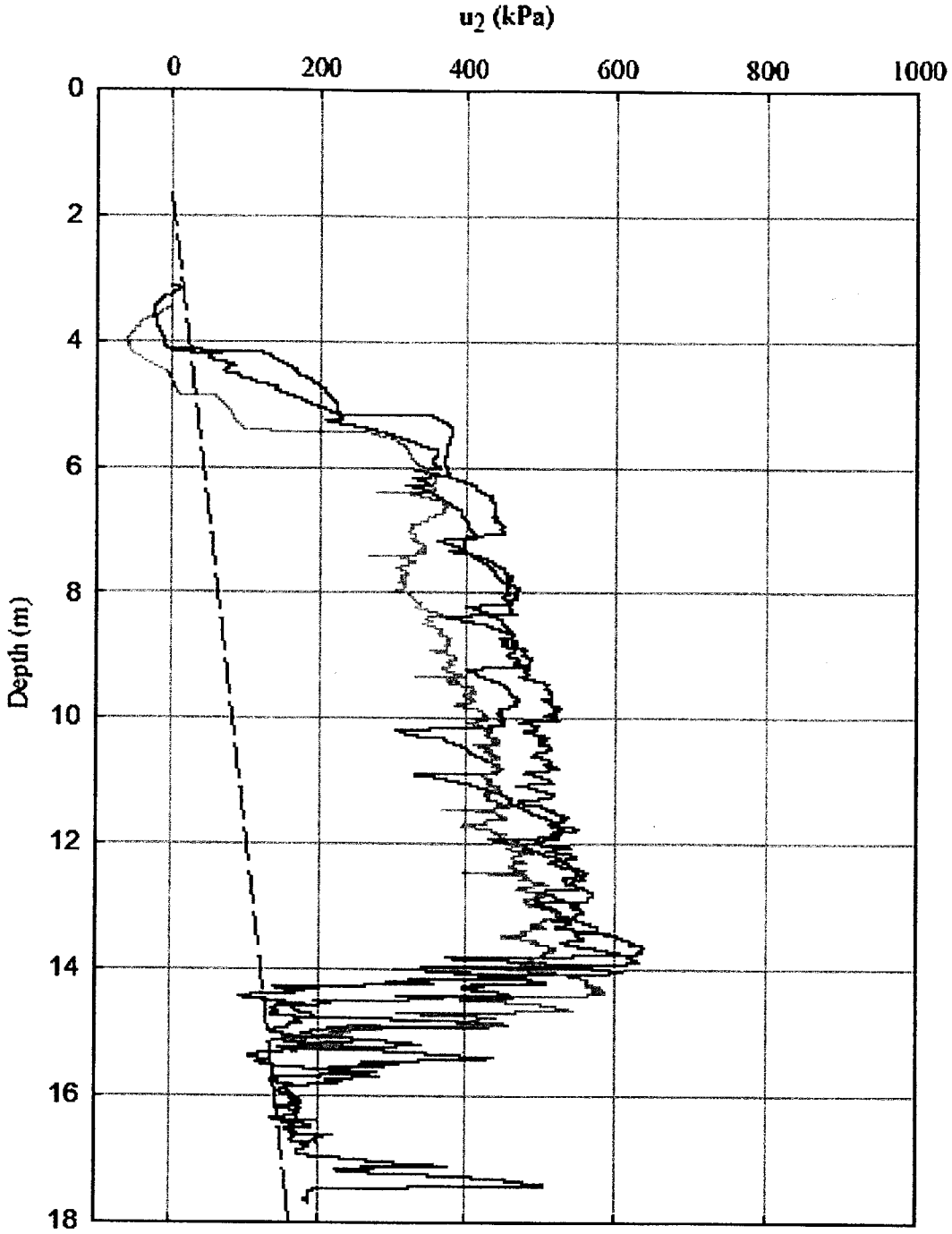

Figure 2.8 **Cone Penetrometer Data from Three Penetrations (DeGroot, 2005)**

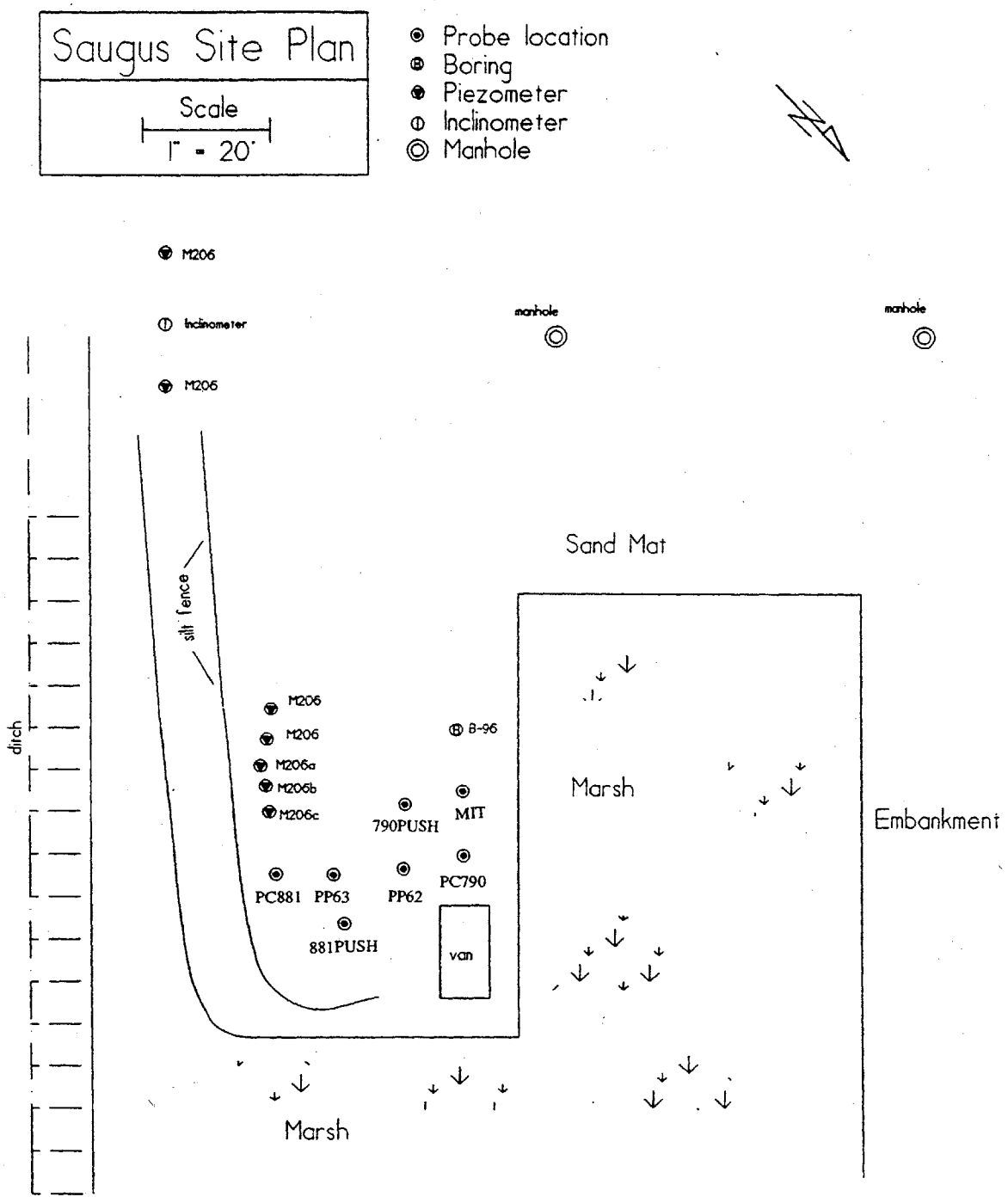

Figure 2.9 Saugus Site Plan (Varney, 1998)

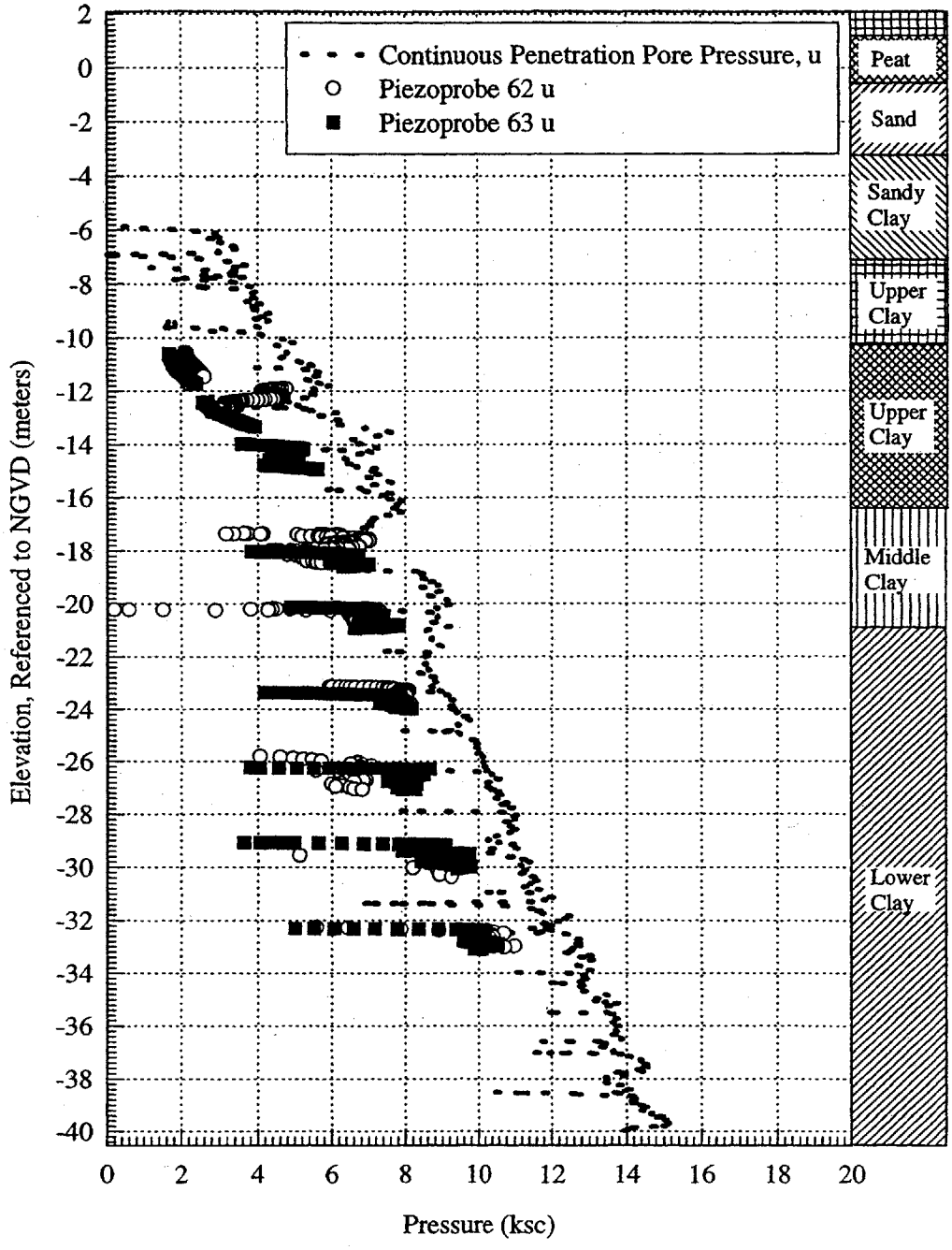

Figure 2.10 Comparison of Piezoprobe Piecewise Penetration Records with Continuous Piezocone Penetration Records at Saugus (Varney, 1998)

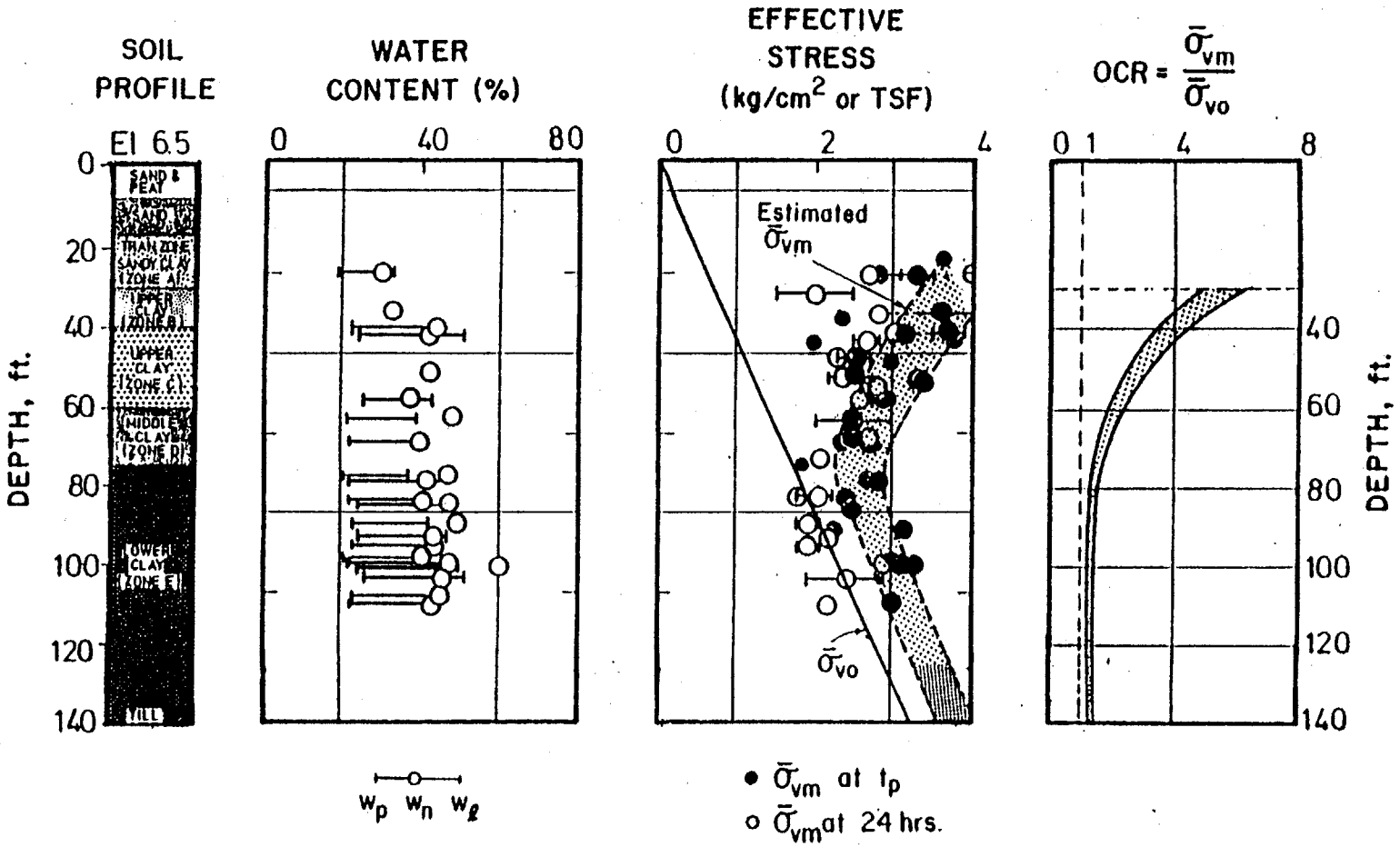

Figure 2.11 Index Properties and Stress History of BBC at the Saugus Site (Varney, 1998)

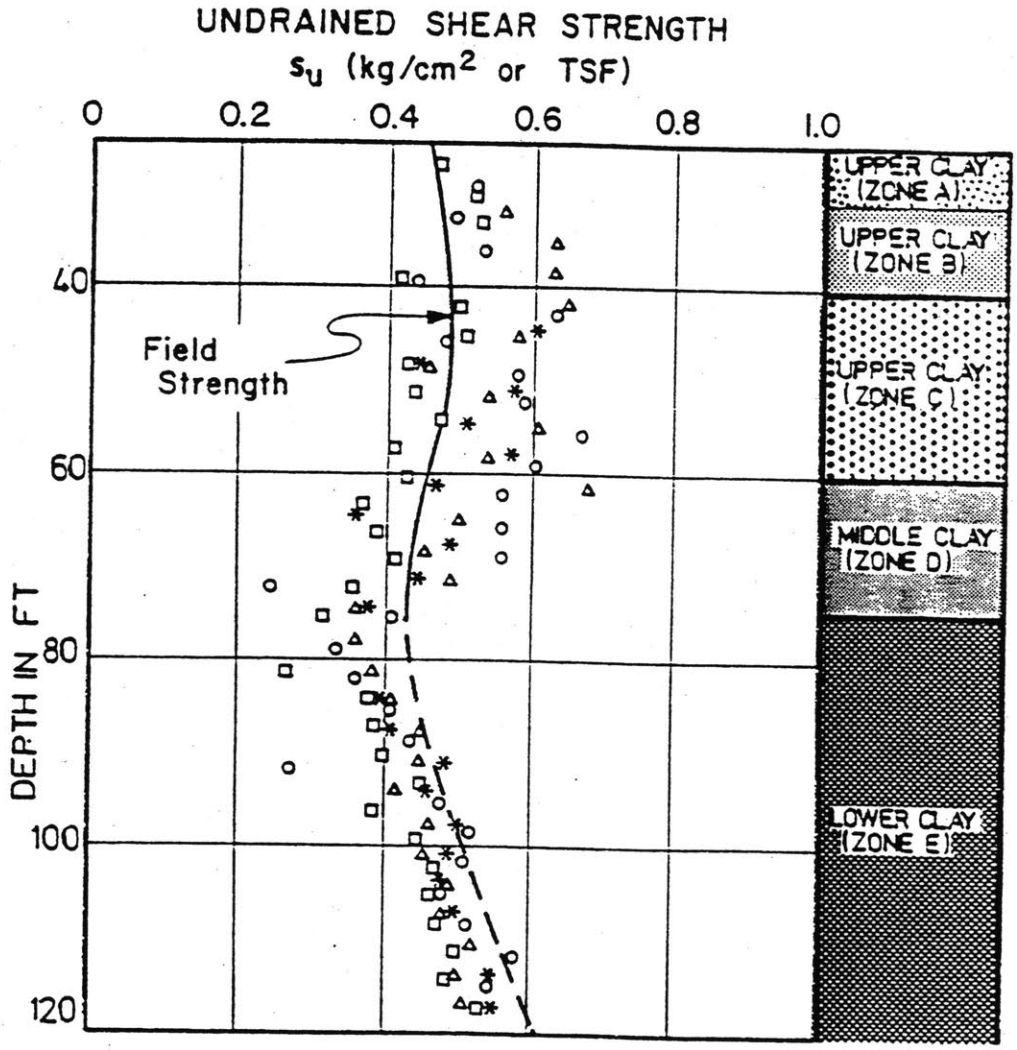

Figure 2.12 Field Vane Strength of BBC at the Saugus Site (Varney, 1998)

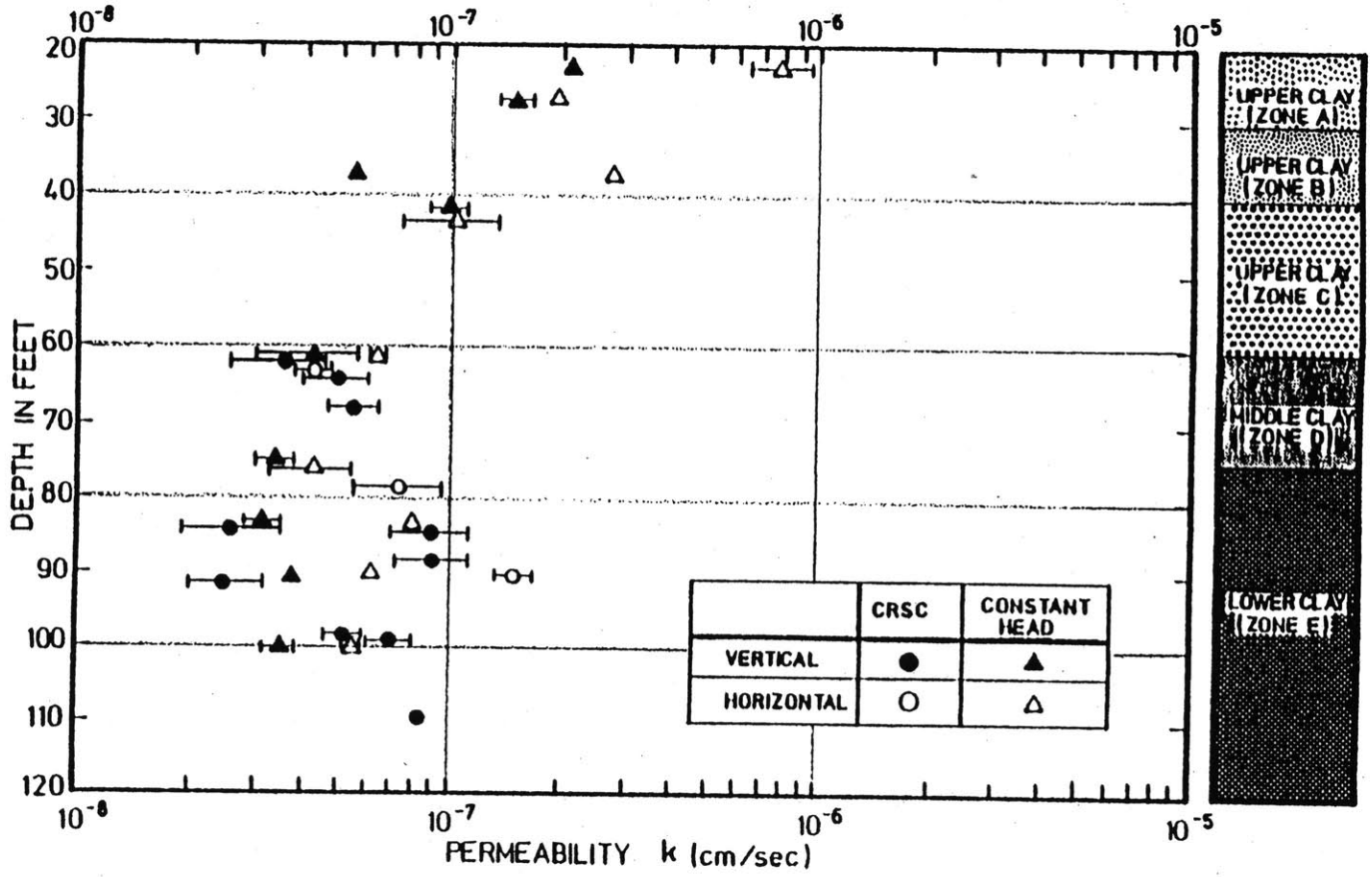

Figure 2.13 Laboratory Measurements of Soil Permeability at Saugus (Varney, 1998)

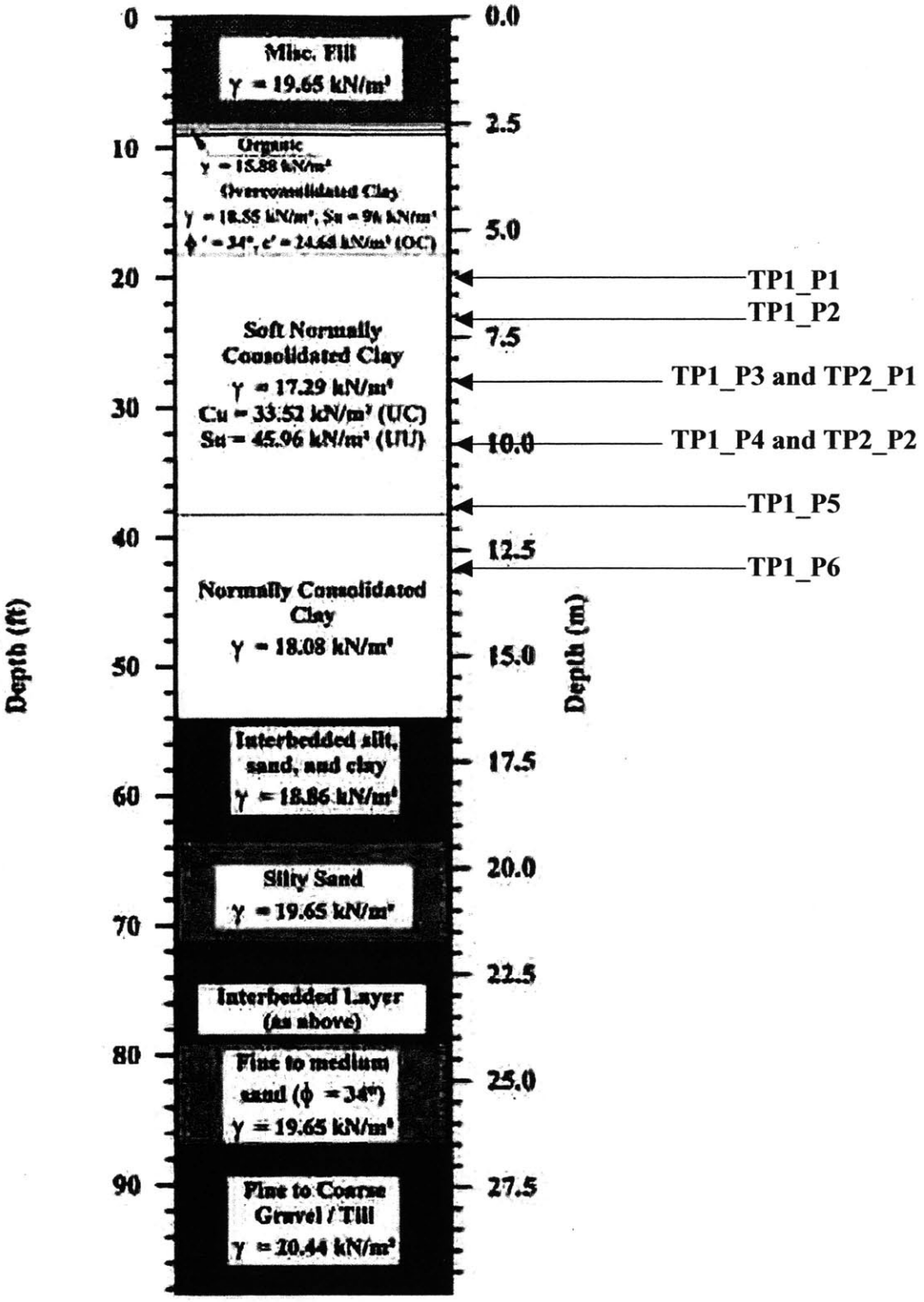

Figure 2.14 Newbury Test Site Soil Profile (Paikowsky and Hart, 1998) with Locations of T2P Tip Dissipation Measurements

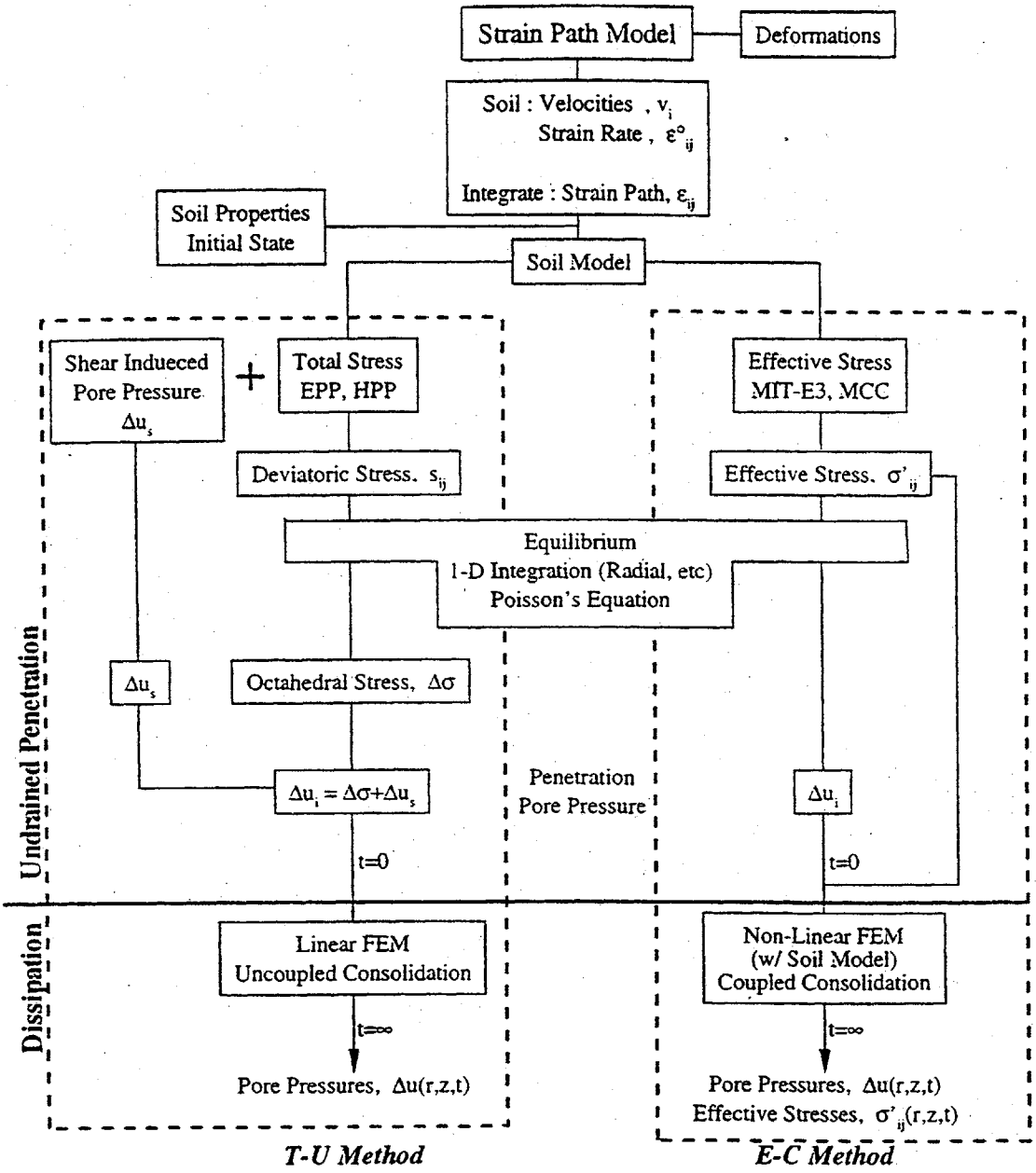

Figure 2.15 Schematic of the Method used to Calculate Strain, Stress, and Pore Pressure During Probe Penetration and Dissipation (Varney, 1998; Whittle et al., 1997)

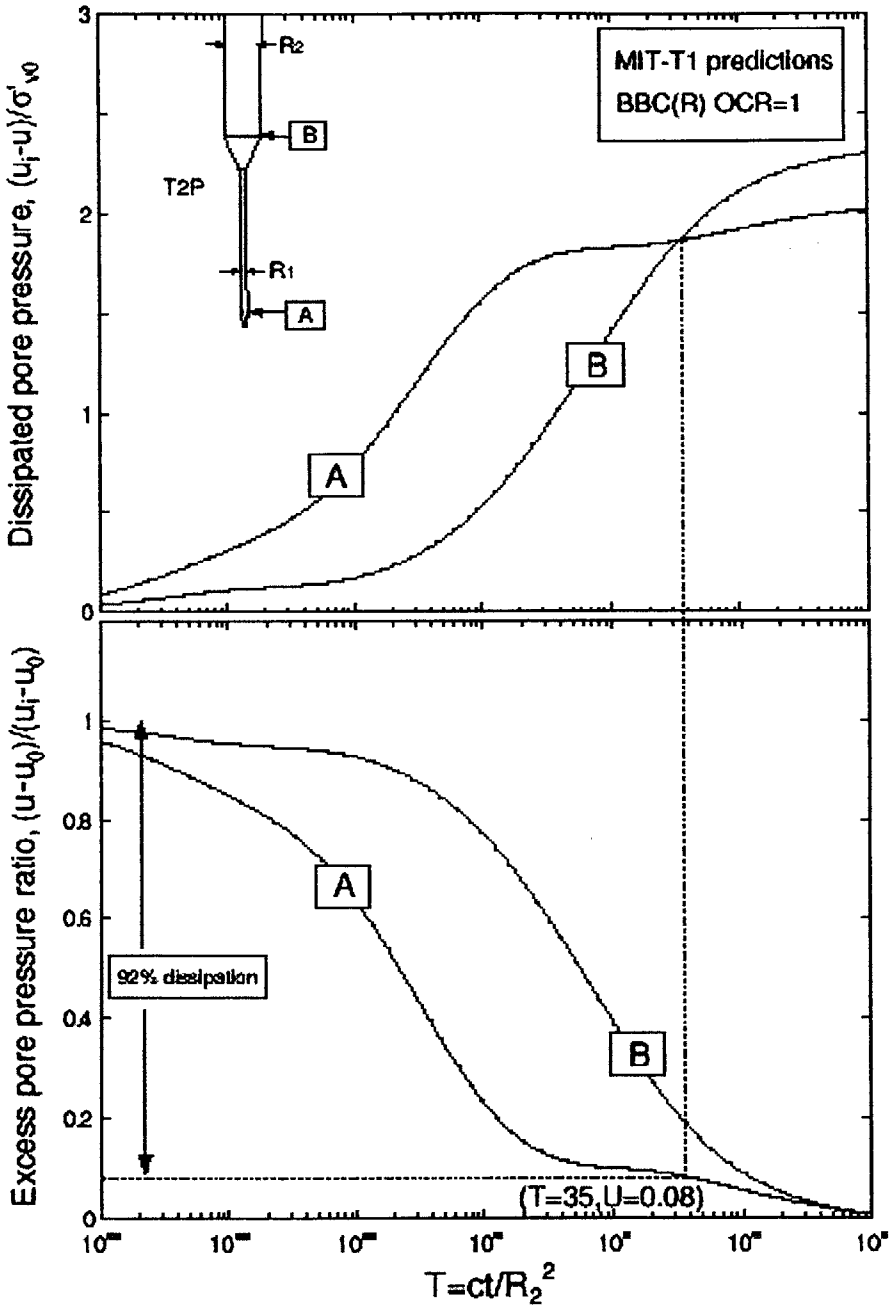

Figure 2.16 Modeled Results for T2P Dissipation (courtesy of Hui Long, personal communication)

3 EQUIPMENT

This chapter describes the prototype T2P tool, including the housing, transducers, electrical connections, data acquisition, and support equipment utilized for the December 2004 T2P field test in Newbury, Massachusetts. As previously mentioned, further development of the T2P and associated equipment has occurred in preparation for an anticipated ocean deployment in May 2005. Chapter 7 includes a discussion of the alterations made to the probe for this deployment and Appendix C contains drawings illustrating the details of the modified tool.

3.1 T2P Piezoprobe

The T2P was designed and constructed at MIT from January to December, 2004. As discussed in Chapter 1, the objective was to design a probe that can measure both pore pressure and temperature at a location near its tip, and can measure pore pressure at a second location on its larger diameter shaft. The probe must be easy to assemble in the field and has to be able to withstand the significant vibrations that will occur during deployments at sea. In addition, the required resolutions for temperature and pore pressure measurements were 0.02°C and 1 psi, respectively. The T2P was designed for a 1-meter penetration below the bottom of a borehole and the tip diameter was minimized to reduce the amount of time required for full dissipation. Although the T2P prototype, described below, was designed to connect to an AW rod for the land-based field test, the final version has been modified for attachment to IODP's colleted delivery system. Additionally, the data acquisition system and associated power source used for the field test has been replaced with a system that is contained within the T2P housing, thus requiring no interface with the surface during deployment.

3.1.1 Physical Configuration

The housing consists of seven sections: the tip, needle, transducer block, drive tube, drive tube nut, AW coupling, and spin collar. An image of the assembled probe is shown in Figure 3.1. All sections are composed of 17-4 PH stainless steel, with the exception of the drive shaft, which is made of 304 stainless steel. A total of seven o-ring

seals are used to prevent the inflow of water into the probe housing. The housing was checked for external collapsing pressure using an equation for the collapsing pressure of thick-walled cylinders (Avalone, 1996, pg. 5-45) and the axial load required to cause buckling of the needle was calculated with the Rankin formula (Timoshenko, 1961, chapter 4). The shear strength of all threaded sections was evaluated in both tension and compression with equations provided by Norton (2000, section 14-3).

The T2P has a threaded 60° tip, roughly 1.1 cm in length and 0.6 cm in diameter. A 32.8-cm long, stainless steel tube is epoxied to the tip. This tube contains the thermistor and associated wires, and has an outer diameter of 1.5 mm and an inner diameter of 1.3 mm. The tip and connected tube is shown in Figure 3.2.

The tip screws into female threads at the bottom of the needle. The needle (Figure 3.3) is a thin cylinder, approximately 16.5 cm long and 0.6 cm in diameter. The top of the needle tapers at a 20° angle to form an inverted cone with a 3.6-cm diameter base. The needle can withstand a maximum axial compressive force of approximately 600 lbs before bucking will occur.

The transducer block (Figure 3.4) screws into female threads at the top of the needle. The transducer block is a primarily solid, 3.6 cm diameter cylinder, approximately 8.1 cm long. The block has external threads at the top and bottom, and threaded insertion channels for the two pore pressure transducers.

The top of the transducer block screws into female threads at the base of the drive tube. The drive tube is 95.9 cm in length and has an outer diameter of 3.60 cm and an approximate inner diameter of 2.54 cm (the inner diameter is slightly enlarged at the top and bottom ends of the drive tube, where it is threaded). The drive tube can withstand an external water pressure of approximately 15,000 psi, and axial compressive and tensile forces of approximately 16,000 lbs.

The drive tube nut screws onto external threads at the top of the drive tube. This nut, with an outer diameter of 5.6 cm, is further secured to the drive tube with two set screws. An image of the drive tube and drive tube nut is shown in Figure 3.5.

The AW coupling (Figure 3.6), required only for the land-based field test, bears directly on the top of the drive tube nut, and provides the interface between the T2P and

the drill string. The coupling is approximately 17.8 cm long, and has a maximum outer diameter of 8.9 cm. The top of the coupling interfaces directly with the drill rods through a threaded connection, and is firmly attached to the drive tube and drive tube nut by the spin collar. The spin collar (Figure 3.7) fits snugly against the drive tube and drive tube nut, and screws onto the external threads at the base of the AW coupling.

Drawings of each component of the T2P are included in Appendix B.

3.1.2 Pore Pressure Measurement

The T2P measures pore pressure at two locations along the probe housing, the first (the tip filter) directly above the tip and the second (the shaft filter) at the base of the transducer block, just above the conical section of the needle. Figure 3.8 illustrates the locations at which pore pressures are measured (for one penetration during the field test, a second needle geometry was used, in which the lower filter was located 5.6 cm above the tip).

The tip pore pressure element is a porous 10-micron sintered stainless steel cylindrical filter, with an outer diameter of 0.6 cm, an inner diameter of 0.4 cm, and a length of 0.5 cm. The tip filter is held tightly in place between the needle and removable tip.

The shaft pore pressure element is a porous 20-micron sintered stainless steel cylindrical filter, with an outer diameter of 3.6 cm, an inner diameter of 3.0 cm, and a length of 0.5 cm. The shaft filter is held firmly in place between the transducer block and the conical section of the needle. Both the tip and shaft filters were manufactured by GKN Sinter Metals.

Each filter is hydraulically connected to a separate pressure transducer through internal conduits. Pore water from the shaft filter collects in an annulus directly behind the filter. This annulus is hydraulically connected with a pressure transducer by a single conduit, as shown in Figure 3.8. A groove cut through the threads behind the tip filter hydraulically connects this filter with a conduit, 2 mm in diameter, drilled through the centerline of the needle. Pore water can then flow upwards through an annulus bounded by the walls of this conduit and the exterior of a stainless steel tube, with a length of 32.8 cm, an outer diameter of 1.5 mm, and an inner diameter of 1.3 mm, that is epoxied into

the tip to protect the thermistor and associated wires. A second conduit, shown in Figure 3.8, links a pressure transducer to the channel drilled down the centerline of the needle. The pore pressure measurement system was designed to be stiff enough to prevent significant expansion of the system due to the anticipated increase in pore pressure during penetration.

Originally, Kulite absolute pressure transducers, with capacities of 1724 kPa and a maximum output voltages of 75 mV at 10 V excitation, were used for both tip and shaft pore pressure measurements. However, the original tip pore pressure transducer broke after the first penetration of the field test, and was replaced with a Kulite gauge pressure transducer with a capacity of 3447 kPa and a maximum output voltage of 75mV at 10 V excitation. Both pressure transducers are screwed into the top surface of the transducer blocks. O-ring seals are used to maintain the integrity of the hydraulic connections.

3.1.3 Temperature Measurement

Temperature is measured using a General Electric, glass encapsulated chip, 500 KOhm thermistor. The thermistor is epoxied at the base of a 32.8 cm long, stainless steel tube, with an outer diameter of 1.5 mm and an inner diameter of 1.3 mm. This thin tube, in turn, is epoxied into the base of the removable probe tip, as shown in Figure 3.2. Therefore, temperature is measured directly at the tip of the probe. The 1.5 mm diameter tube protects the thermistor and associated wires from the pore fluids flowing through the probe conduits.

The resistance of the thermistor to electrical current increases with a decrease in temperature. A 137 kOhm resistor is connected in series with the thermistor. The output voltage is measured across this fixed resistor to correlate the resistance of the thermistor with temperature. The relationship between thermistor resistance and temperature, as provided by the manufacturer, is listed in Table 3.1.

3.1.4 Electrical Connections

A circuit board, designed and constructed at MIT, is located within the drive tube. The power, ground, positive output, and negative output wires from each pressure tranducer are attached to this circuit board with removable Philmore dual row header

electrical connectors. The power and ground wires from the thermistor are also attached to this board with these connectors. One power wire and one return wire are connected in series to each of the pressure transducers and the thermistor. The fixed resistor associated with the thermistor is also located on this circuit board. The presence of the circuit board provides a convenient point to test the individual transducers and allows for a reduction in the number of wires connecting the T2P to the surface instrumentation.

A 12-pin Fisher locking plug is wired directly to the circuit board. This plug mechanically connects to a compatible 12-pin Fisher panel receptacle, mounted at the base of the AW coupling. A 120-foot long, shielded cable is wired permanently to the panel receptacle, providing an electrical connection to the power supply and data acquisition system at the surface. This cable contains 6 pairs of twisted #24 AWG copper wire conductors. Each of the pairs has an aluminum shield and an individual drain wire within the shields. The cable, itself, is protected from the elements by ½ inch diameter plastic tubing. A standard 3/8 inch Swagelok connector provides a water-tight seal between the plastic tubing and the interface section.

3.2 Depth Locator Box

A depth locator box, shown in Figure 3.9 and originally constructed and described by Varney (1998), was used to determine the displacement of the T2P from the bottom of the borehole. This piece of equipment consists of a spring-loaded spindle, whose rotational displacement is determined by a Claristat potentiometer. As the spindle turns, the potentiometer also rotates. Both the spindle and the potentiometer are cased to protect them from the elements. A string is wrapped around the spindle, with one end emerging from the box through a hole in the casing. To calculate probe displacement, the depth box is clamped to the drill string and one end of the string is attached to the borehole casing. When the drill rods are lowered into the borehole, the spindle recoils as the attached string slackens, causing rotation of the potentiometer. The outside circumference was designed to allow approximately five feet of displacement for ten rotations of the potentiometer.

3.3 Atmospheric Pressure Transducer

A Motorola MPX2200 pressure transducer was used to measure fluctuations in atmospheric pressure during the field test. This transducer has a capacity of 200 kPa and a maximum output voltage of 40 mV at 10 V excitation.

3.4 Response Chamber

A hydraulic response chamber (Figure 3.10) was designed and constructed at MIT to evaluate the response of the T2P's pore pressure measurement system in both the lab and the field. This chamber consists of a 47 cm long PVC tube, with an outside diameter of 5.5 cm and a wall thickness of approximately 0.5 cm. One end of the tube is permanently closed by a PVC cap, epoxied in place, and a drainage valve is located near the bottom of the chamber. A "witness" pressure transducer, located near the bottom of the tube, is hydraulically connected to the interior of the response chamber, and fitted with an o-ring seal. The witness transducer is a Data Instruments AB absolute pressure transducer, with a 1380 kPa range, and a maximum output of 100 mV at 5 V excitation. The inside surface near the top of the response chamber is fitted with an o-ring, specifically sized to fit the 3.6 cm diameter stainless steel housing of the T2P.

The chamber is filled with water while the witness transducer is attached. The witness transducer is then loosened to allow water to fill the conduit linking the response chamber to the transducer. Once this conduit has been filled, the witness is firmly screwed into place. The T2P is then inserted partway into the chamber with the drainage valve open to allow air to vacate the chamber. Once the T2P is partly within the chamber, with clearance between the tip and the base of the tube, the drainage valve is then closed, thereby sealing the response chamber.

The manner in which this setup is used to evaluate the response of the pore pressure measuring system will be described in Chapter 4.

3.5 Porous Element Saturation System

Two different methods were used to saturate the T2P's filters. Both methods were originally described by Varney (1998) and are summarized below.

The first method has been used since the 1970's at MIT to saturate porous elements and is shown schematically in Figures 3.11 and 3.12. For this method, the filters were first left in a 100°C overnight to remove trapped moisture. Upon removal from the oven, they were immediately placed in a sealed chamber, connected to a vacuum pump. The vacuum pump was then used to evacuate all air from the chamber, to approximately 200 mTorr. The filters remained in the chamber under vacuum for approximately 30 minutes.

Once all internal moisture and air was removed from the stones, they were saturated with distilled and deaired water. This was accomplished by opening a three-way valve connecting the chamber with a container of distilled and deaired water, thus flooding the chamber and saturating the stones. After 30 minutes, the vacuum was released and the filters were transferred to a sealed container, completely filled with deaired and distilled water. This container was used to transport the filters to the field.

The second method consisted on placing the filters in a container of boiling water for 20 minutes. The filters were then immediately transferred to an ultrasound bath for 45 minutes. Finally, the filters were transferred to a sealed container, completely filled with deaired and distilled water for transport to the field. Both of the methods described above provided adequate filter saturation.

3.6 Data Acquisition

An Iotech Personal Daq/56 data acquisition system was used for both lab and field testing of the T2P. This system uses a 22-bit analog to digital converter, accepts direct current voltage inputs ranging from -10 V to +20 V, and can record up to 10 differential voltage channels at one time. Both the sample rate and integration time can be input. The Iotech system interfaces directly with a Gateway Solo 1450 laptop computer through a USB connection. The data acquisition system was mounted on a wooden board, along with a junction box to distribute power to the various transducers.

Since the Iotech data acquisition system has a single A/D converter, each channel is read and recorded sequentially; therefore, the maximum sample rate is reduced as the number of recorded channels increases. Additionally, once a data collection routine has begun, the number and choice of recorded channels, sample rate, and integration time

cannot be changed without stopping the data collection and manually changing the channel configuration, which was inconvenient during the field test.

Seven different data acquisition configurations were used during the field test. Each configuration was designed to optimize the resolution by varying the integration time and utilizing the minimum number of channels possible. The manner in which each configuration was used during the field test, the specific channels recorded during each configuration, and the respective integration times and sampling rates, will be discussed in Chapter 4.

3.7 Power Supply

3.7.1 Power for Data Acquisition System and Laptop Computer

For the field test, a van was used to both transport the required equipment to the site and to provide a heated shelter to work in. During the day, the van engine was kept running and the laptop computer received power from the van's 12 V battery. A Targus Mobile 70 Auto Adapter with a DC/DC voltage regulator was used to provide a direct connection between the van's cigarette lighter receptacle and the laptop computer. The Iotech data acquisition system, in turn, received power from the laptop computer, through a USB connection.

After dark, the site was unattended; therefore, the van engine had to be turned off. During these hours, the laptop and data acquisition system were powered by a U.S. Battery 31 TMX 12 V deep cycle battery with 130 amp hours. A car lighter receptacle and attached positive and negative cables were used to connect the TMX battery to the Targus auto adapter. During the day, the TMX battery was recharged offsite.

3.7.2 Power for T2P and Support Equipment

During the field test, the two Kulite pore pressure transducers, the temperature sensor, the depth box, the atmospheric pressure transducer, and the witness pressure transducer were powered by a UB1270 12 V battery with 7 amp hours. #26 AWG solid steel conducters with PVC jackets were soldered to RadioShack Female Quick Disconnect terminals to provide an electrical connection between the battery and the

junction box mounted next to the data acquisition system. The depth box, atmospheric pressure transducer, and cable connecting the T2P to the surface were wired directly to the junction box, thus receiving 12 V power from the battery. A voltage loss of approximately 0.18 V occurred across the 120-foot long cable bringing power from the battery to the T2P transducers; therefore, this power loss had to be taken into account during the calibration of the thermistor and pressure transducers.

The witness pressure transducer has a maximum excitation rating of 6V. To prevent over-excitation of this transducer, a fixed resistor, with an identical resistance to the witness transducer, was placed in series between the junction box and the witness pressure transducer, thus reducing the applied power voltage to approximately 6 V.

Temperature (°C)	Resistance of Thermistor (kOhm)
0	1741.00
5	1336.35
10	1033.80
15	805.75
20	632.55
25	500.00
30	398.00
35	318.60
40	256.70
45	208.05
50	169.60
55	139.00
60	114.50
65	94.80
70	78.87
75	65.93
80	55.36
85	46.69
90	39.54
95	33.62
100	28.70

Table 3.1 Relationship between Thermistor Resistance and Temperature (provided by General Electric, Inc.)

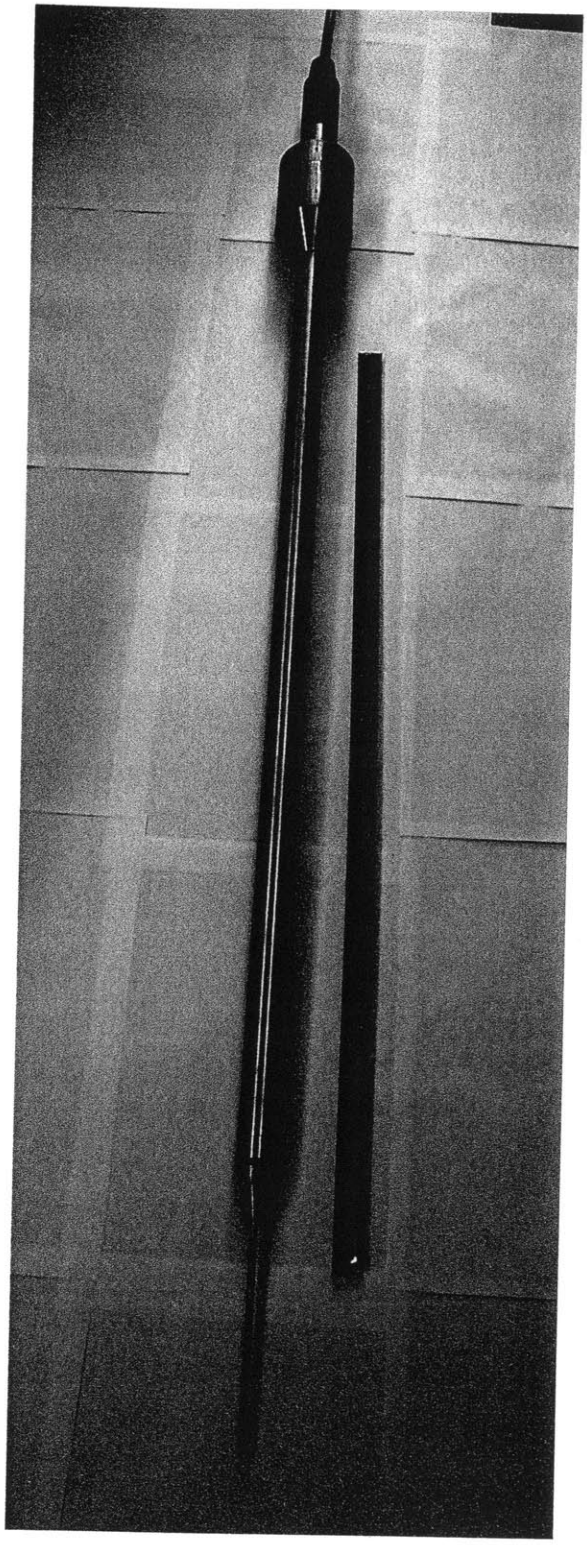

Figure 3.1 T2P Probe

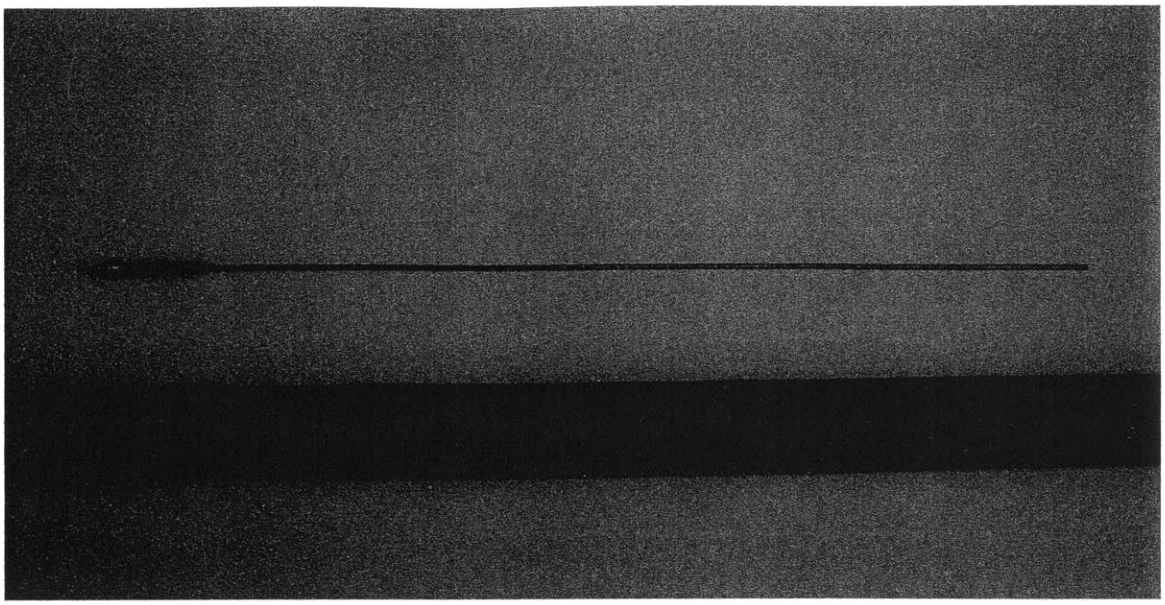

Figure 3.2 Tip with Attached Thermistor Tube

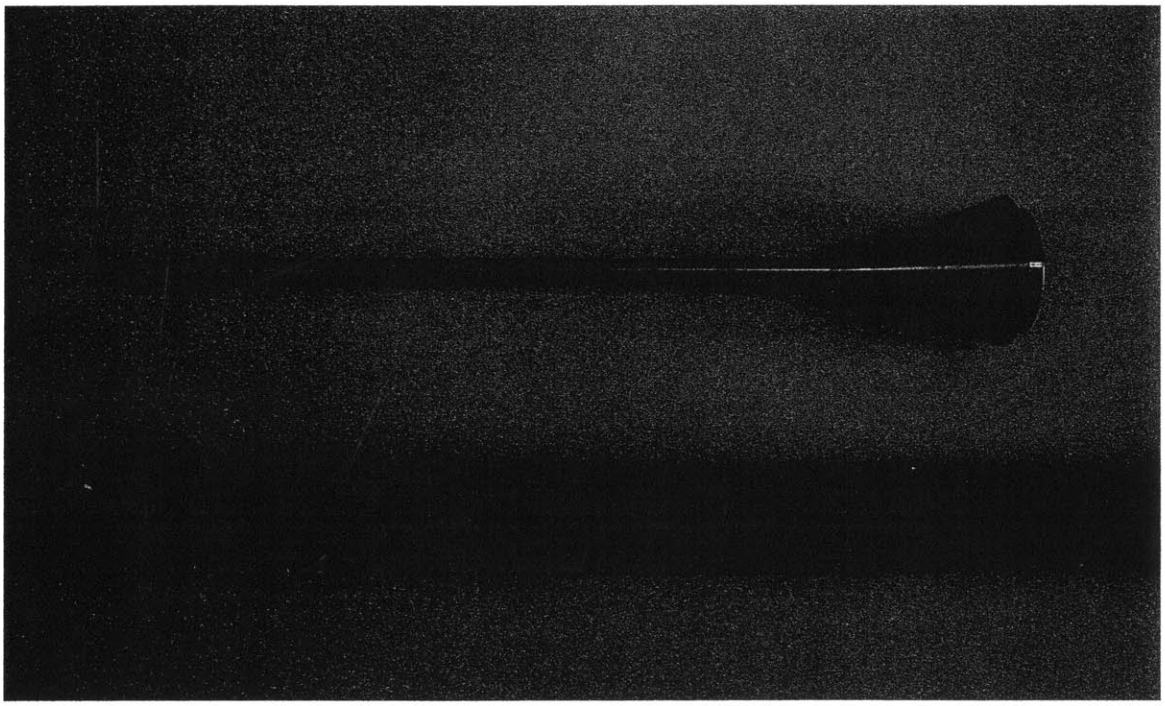

Figure 3.3 Needle

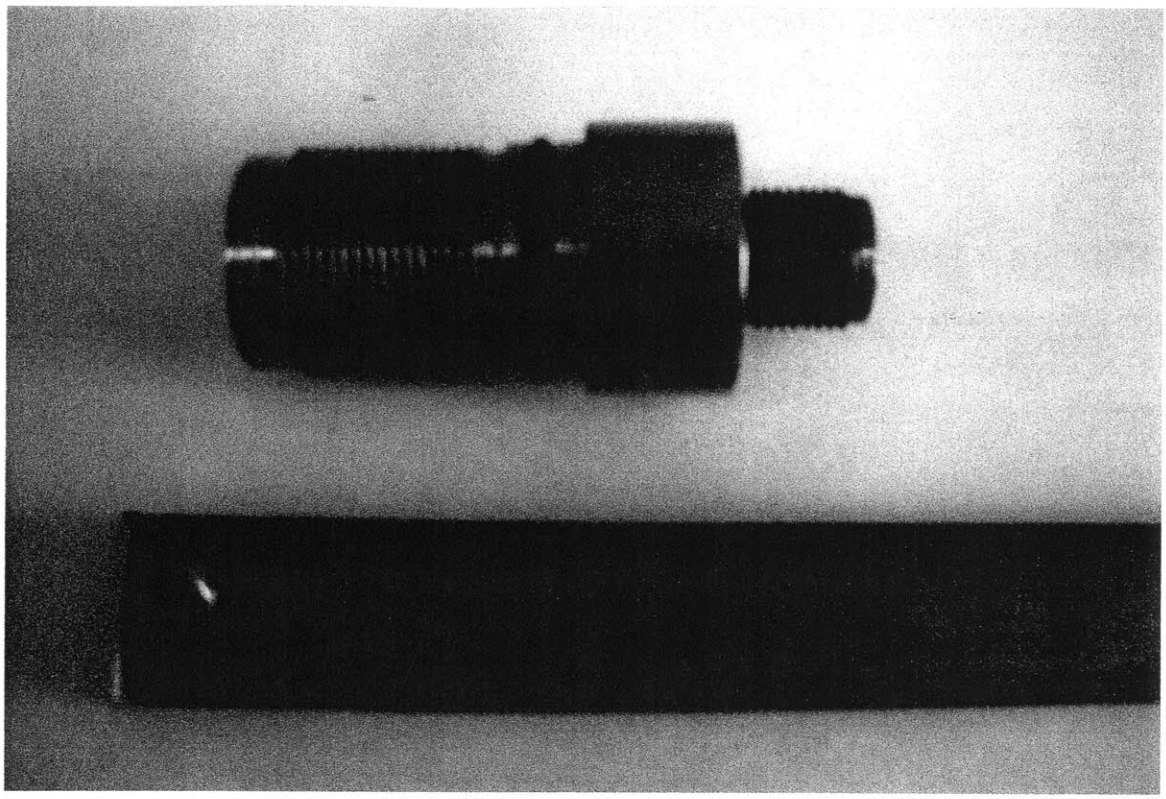

Figure 3.4 Transducer Block

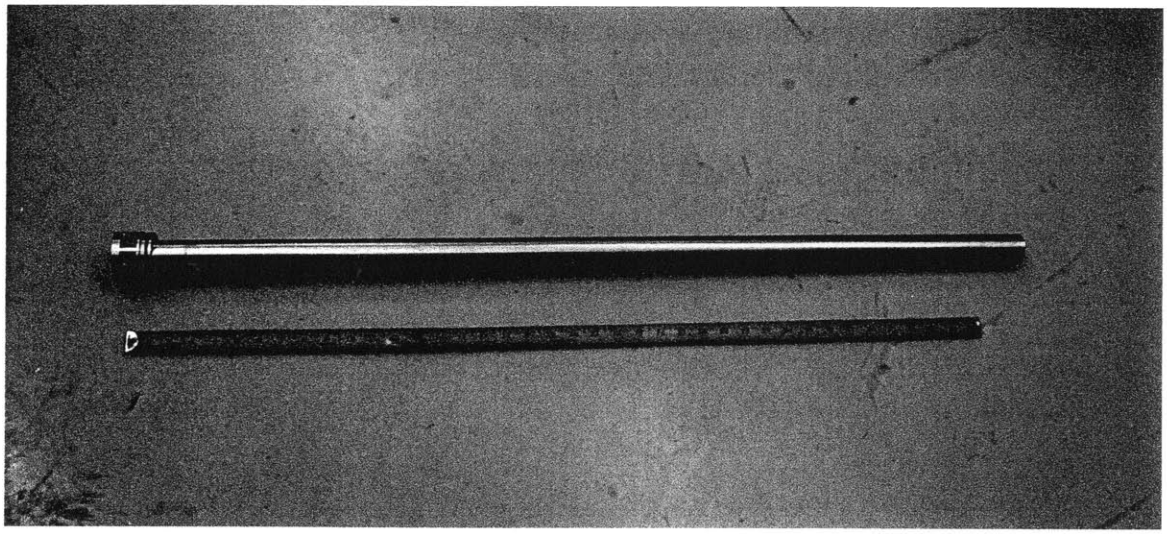

Figure 3.5 Drive Tube with Drive Tube Nut Attached

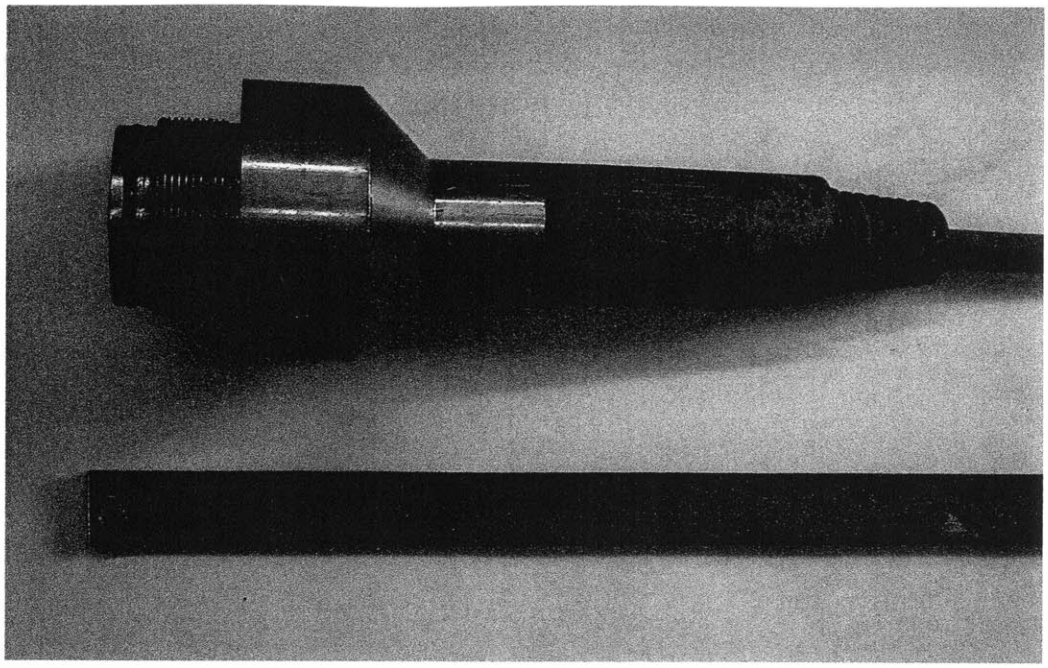

Figure 3.6 AW Coupling with Threaded AW Connection

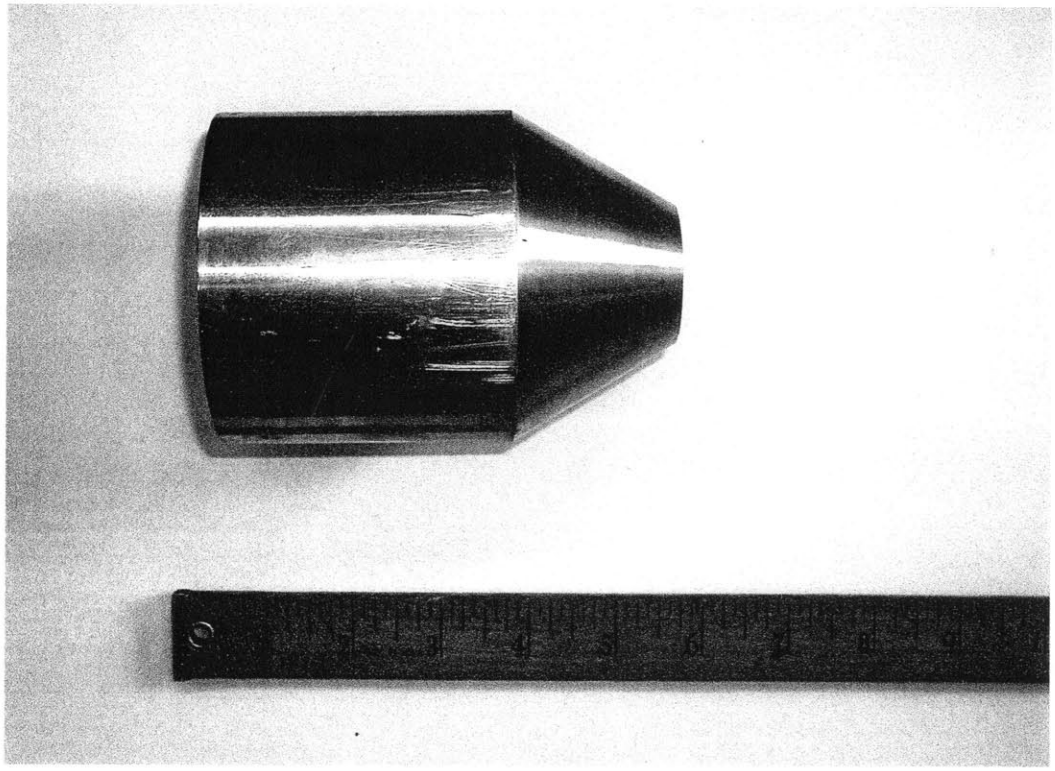

Figure 3.7 Spin Collar

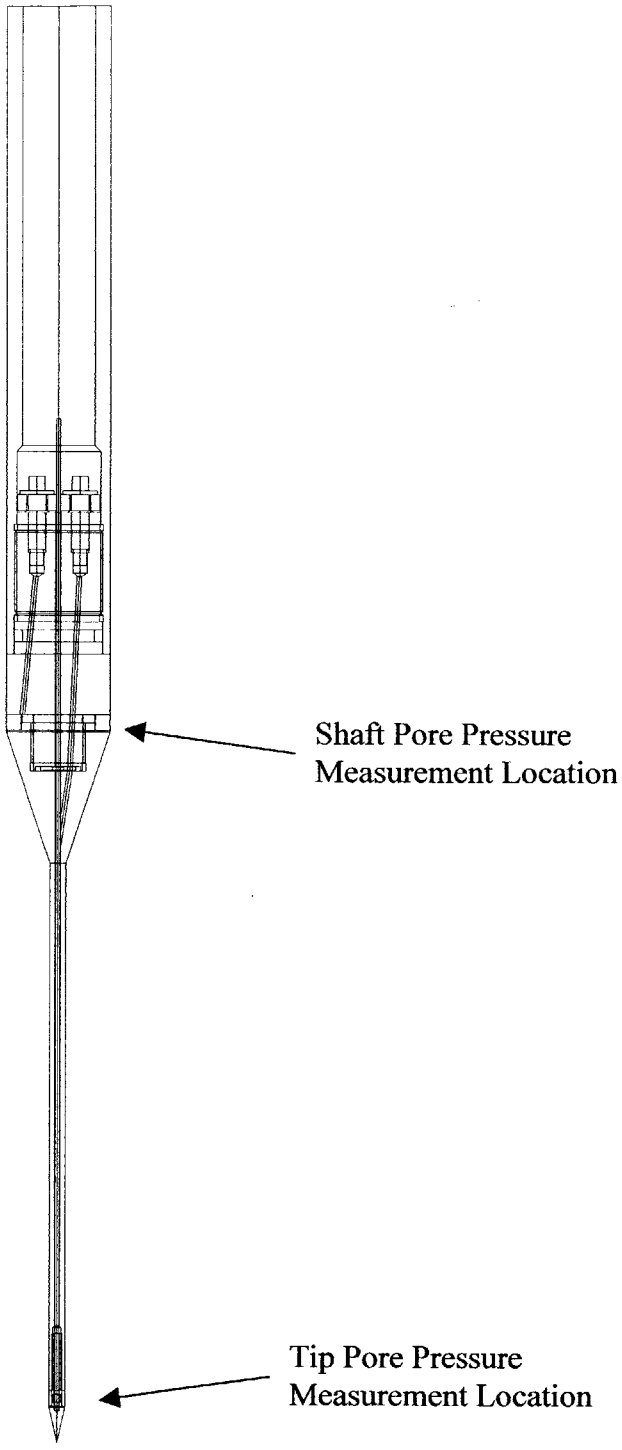

Figure 3.8 T2P Pore Pressure Measurement Locations

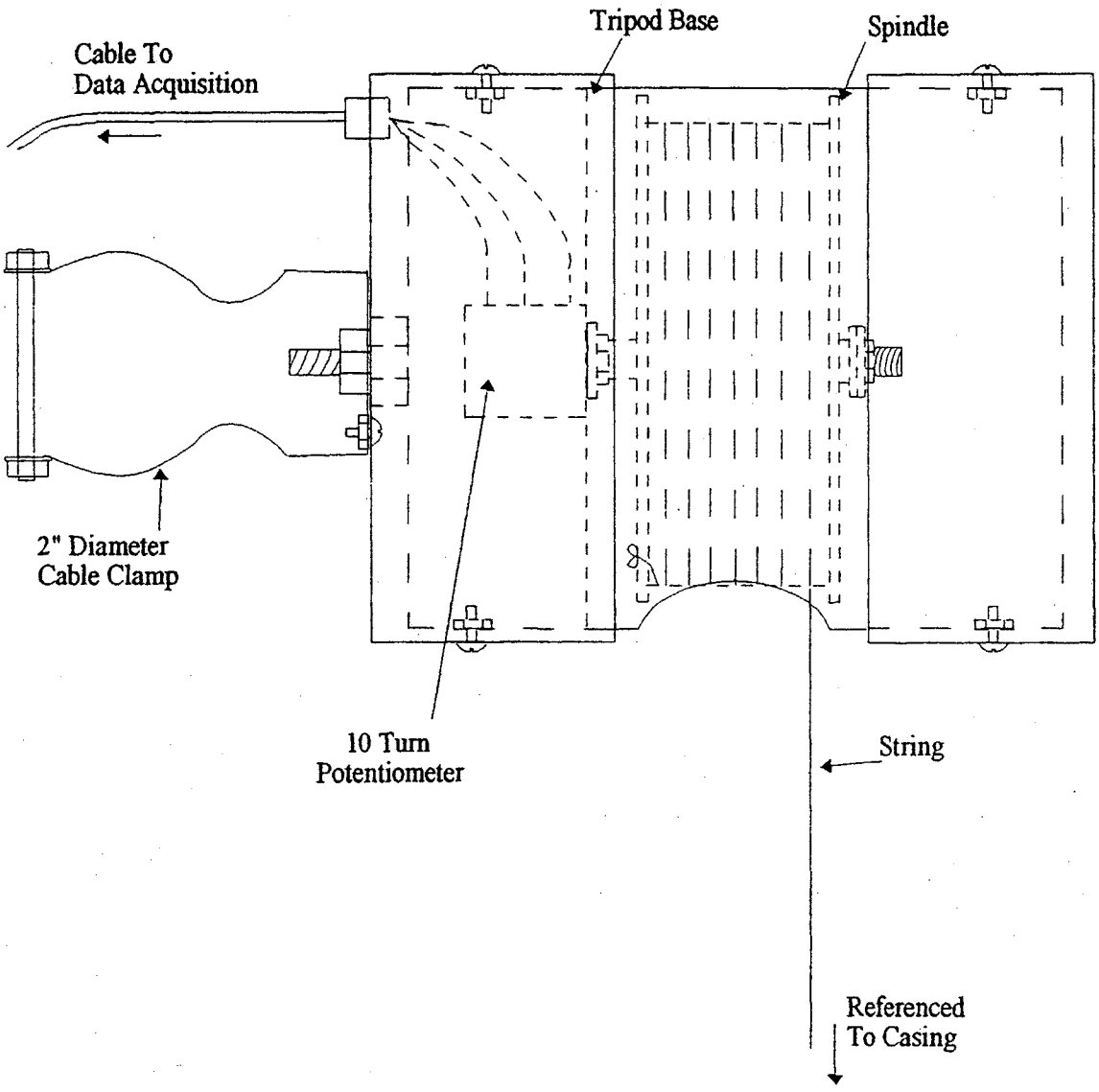

Figure 3.9 Depth Locator Box (Varney, 1998)

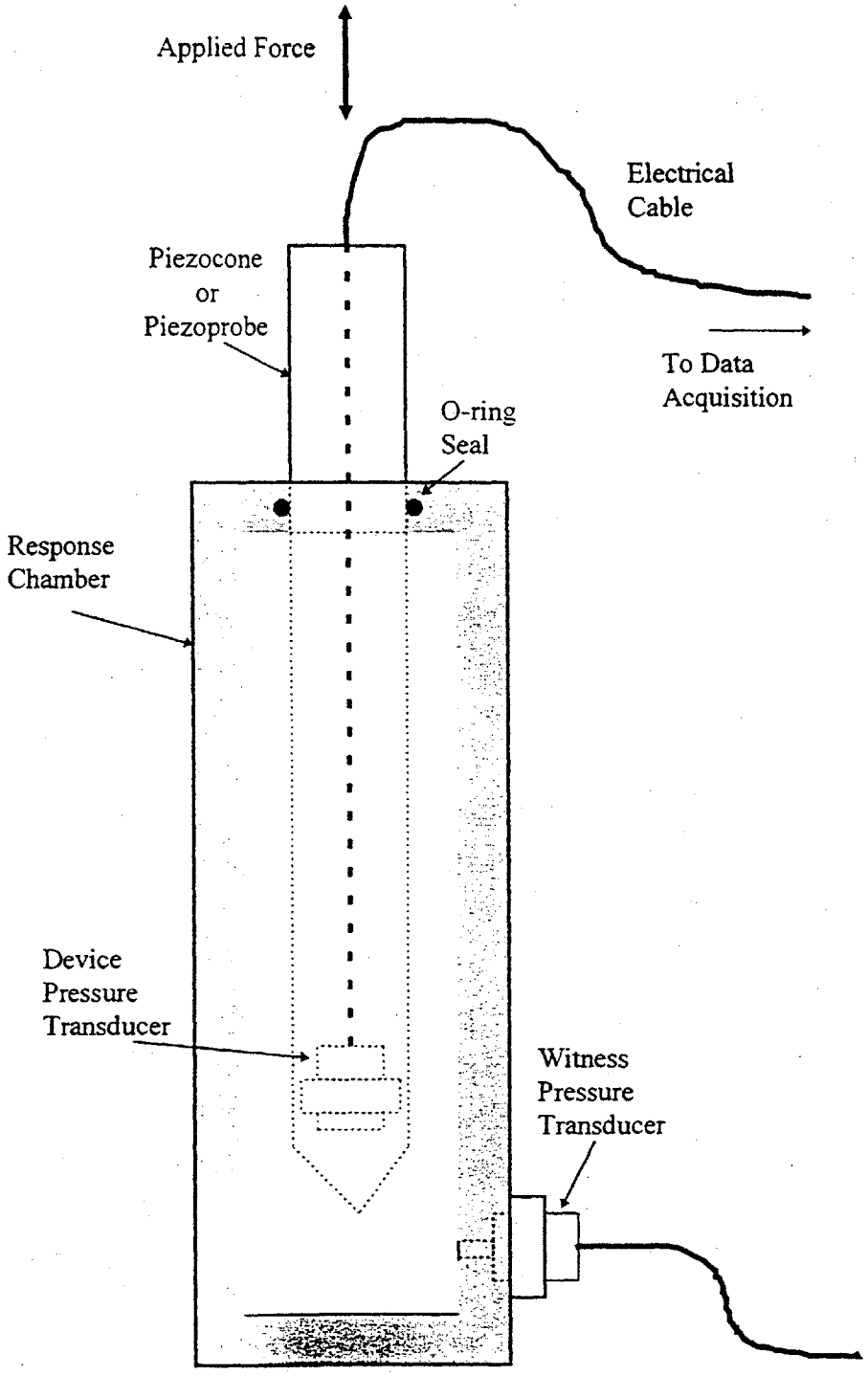

Figure 3.10 Response Chamber (Varney, 1998)

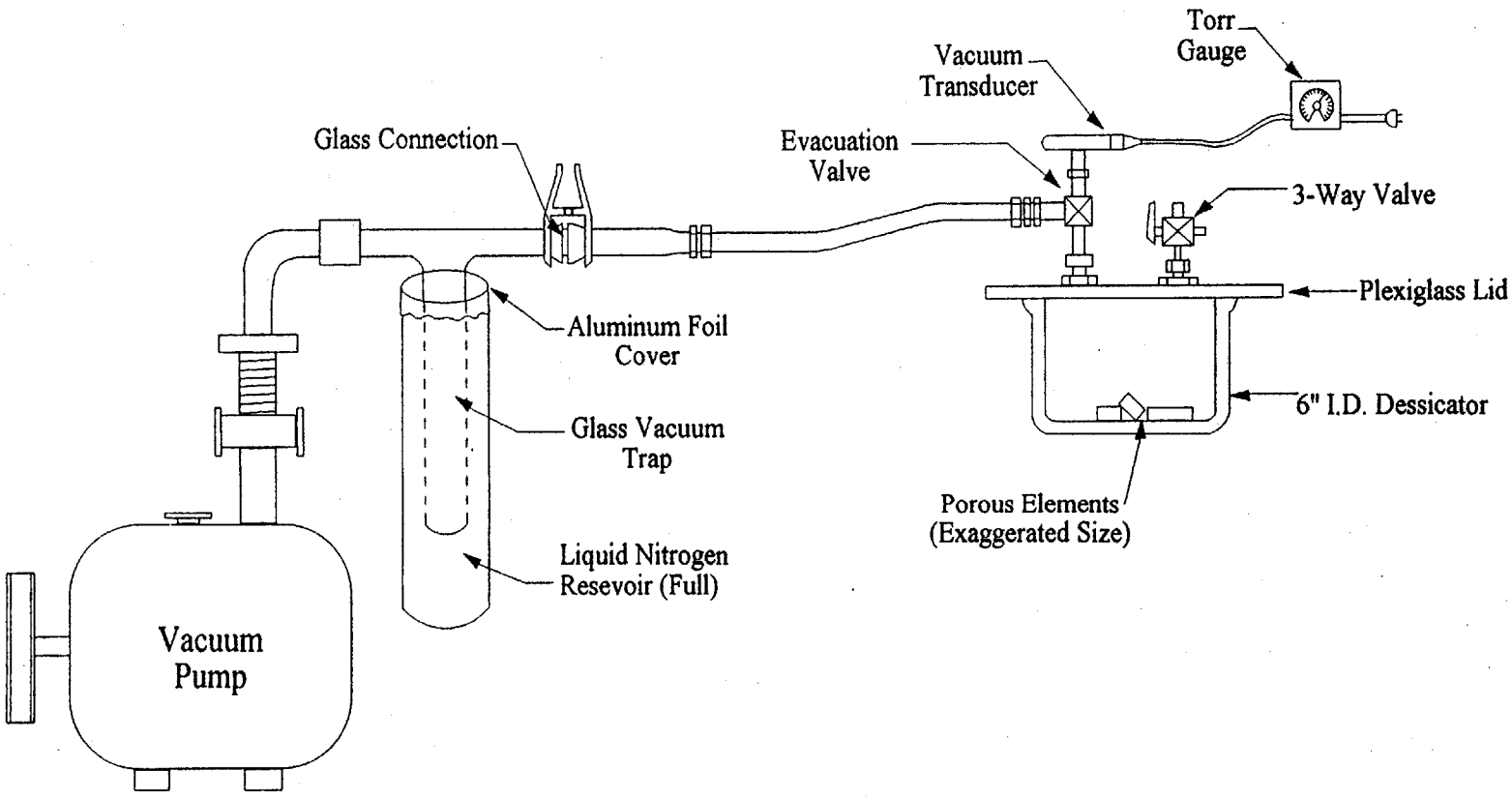

Figure 3.11 Schematic of System used to Evacuate the Chamber in Preparation for Saturation of Filters (Varney, 1998)

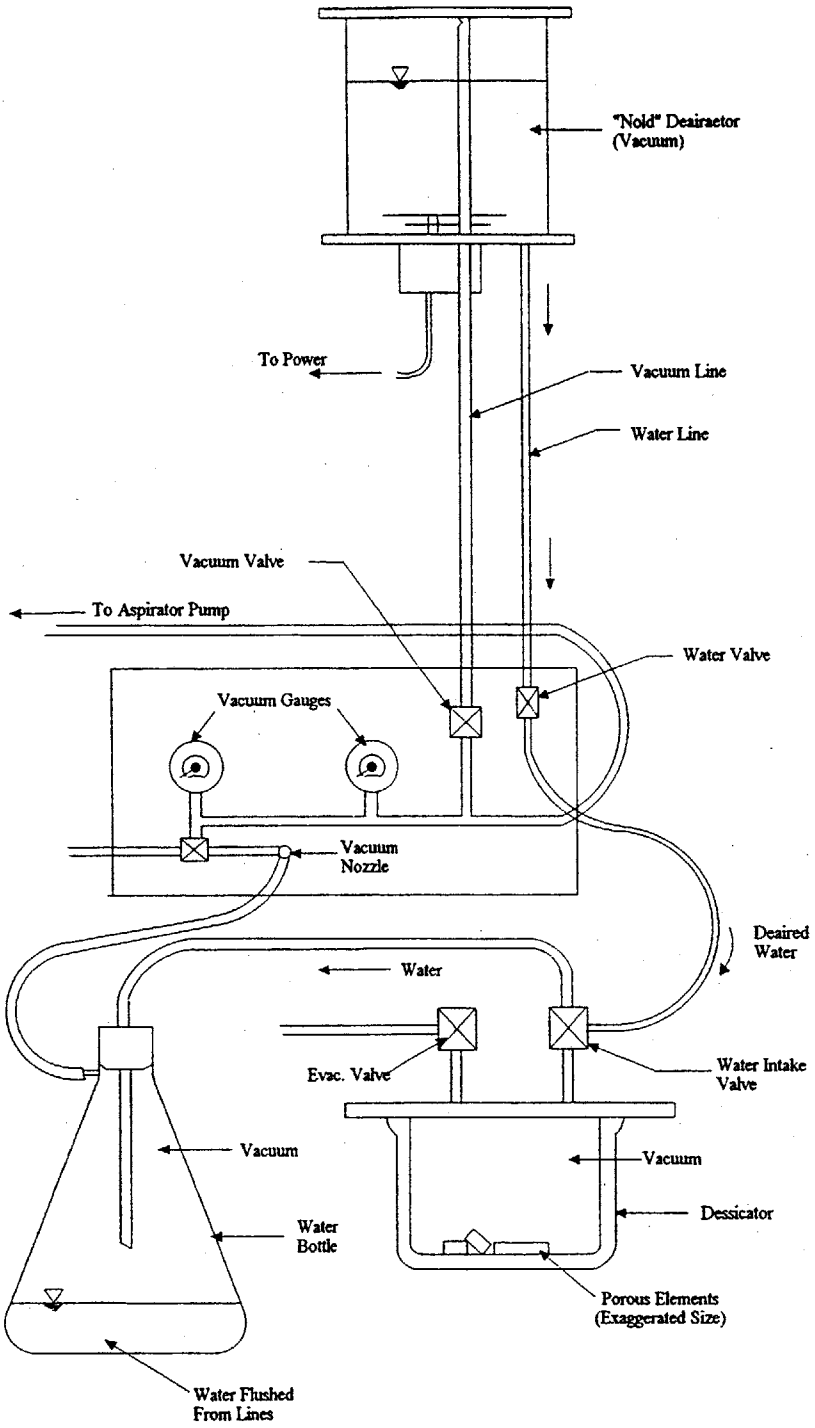

Figure 3.12 Schematic of the Deaired Water System used to Saturate Porous Elements (Varney, 1998)

4 FIELD TEST PROCEDURES

This chapter discusses both the manner in which the field test was conducted and the steps taken to ensure the collection of high-quality data.

4.1 Assembly of T2P

The T2P was assembled at MIT several days before the start of the field test. The first step of assembly was to saturate the tip and shaft filters in the manner described in Section 3.5 of Chapter 3. Four sets of laboratory-saturated filters were available at the start of the field test, for both the tip and shaft pressure pore measurement systems. Once the filters were saturated, the probe tip, needle, and transducer block were placed in a 16 inch-deep, 6 inch-wide, and 32 inch-long Plexiglas container filled with distilled water. These sections were held under water until all conduits were fully saturated, paying careful attention to remove all air bubbles from any threaded sections. The saturated filters were then transferred to the Plexiglas container and the tip, needle, and transducer block were reassembled with the new filters in place. The two pore pressure transducers were held partially underwater and screwed into the submerged transducer block. Rubber gaskets were then placed over both the tip and shaft filters to retard desaturation of the filters. Finally, the remaining components of the probe were reassembled outside of the Plexiglas container.

The T2P, data acquisition system, and support equipment were transported to the field test site in a van on the morning of the first day of the field test. Upon arrival at the site, the electric cable with plastic tubing connected to the T2P was strung through 5-foot lengths of AW drill rod. This was continued until the total length of added drill rod was long enough to allow the probe to reach the deepest penetration depth. The rods containing the electric cable were laid out on the ground during the drilling operation. A set of NX rods was used for the drilling process.

4.2 Borehole Advancement

During the field test, three boreholes (TP1, TP2, and B104A) were advanced using a single drill rig. Boreholes TP1 and TP2 were used to measure penetration,

dissipation and extraction data, and borehole B104A was used to collect soil samples. The locations of these boreholes are shown in Figure 2.2 in Chapter 2. While the boreholes were open, they were kept filled with a mixture of water and cuttings of clay from the drilling process, in order to keep a constant level of stress applied to the base of the hole. For each borehole, a 4-inch diameter casing was driven to a depth of 15 feet, several feet into the clay layer. The casing was then washed to within five feet of the first measurement depth using a tricone rotary bit. Once each borehole was washed to the target depth, the rotary bit was extracted from the hole to allow connection of the T2P or the sampler to the drill rig.

4.3 Penetration, Dissipation, and Extraction Procedures

While the borehole was being advanced with the rotary bit to the desired depth, the initial response of the pore pressure measuring system was evaluated. This was done by inserting the T2P into the water-filled response chamber and sealing it in the manner described in Section 3.4. Pressure measurements from the witness and pore pressure transducers were recorded while one or more pressure pulses were created within the chamber by manually pushing on the back end of the T2P. The resultant pressure pulses ranged from 180 to 830 kPa in magnitude and each lasted approximately one second. The measured responses from the witness and pore pressure transducers were then viewed on the laptop computer screen. If either of the pore pressure transducers did not demonstrate adequate response, the associated filter was replaced and the pressure response was re-evaluated. This was repeated until an acceptable response was achieved (see Section 4.8 for the definition of an adequate response).

Once a satisfactory response was noted for both pore pressure transducers, pore pressure, atmospheric pressure, input voltage, temperature, and depth box measurements were initiated. At this point, the T2P was manually suspended over a 5-gallon bucket of water, with both pore pressure filters beneath the water surface. Initial zero pressure readings were then recorded by hand and with the data acquisition system.

When the target wash depth had been reached and the drill bit extracted from the borehole, the T2P's slotted coupling with AW threads was connected to the drill rods. The slot in this coupling provided a space for the electric cable to exit the interior of the

drill rods. A nylon strap was then used to lift the drill rods against the cross head. Once mechanically attached to the drill string, the tool was lowered to the bottom of the hole. Next, the depth box was affixed to the drill string and the depth box's cord was connected to the casing. At this point, the nylon strap was released so that the cross head could be rapidly removed from the drill rod after penetration. The T2P was then pushed approximately 1.5 meters into the bottom of the borehole at a rate ranging from 1.4 to 3.0 cm/s. The measured penetration rates and distances for each penetration are listed in Table 4.1. 1.5 meters was the largest penetration distance possible, since this is the maximum stroke of the drill rig. During penetration, only pore pressure, temperature, and depth box measurements were recorded.

Once penetration ceased, the cross head was lifted off the rod for all tests except TP1_P6 and TP2_P1. This detachment occurred within 10 to 330 seconds of the end of penetration. For tests TP1_P6 and TP2_P1, the cross head remained in contact with the drill string for at least 10 minutes after the end of penetration.

The T2P then remained at the measurement location while dissipation measurements were recorded for periods ranging from 0.74 to 19.74 hours. Table 4.1 lists the dissipation durations for each test. After approximately 10 minutes of dissipation, input voltage and atmospheric pressure measurements were added to the recorded values.

Once the dissipation period was over, the T2P was extracted from the borehole at rates ranging from 1.3 to 4.0 cm/s. During extraction, only pore pressure, temperature, and depth box measurements were made. Once the probe exited the borehole, atmospheric pressure and input voltage readings were also initiated. After being detached from the drill string, the T2P was cleaned to remove clay from its surface and then once again suspended over a 5-gallon bucket of water, with its pore pressure filters submerged. Final pore pressure zero values were recorded both by hand and with the data acquisition system.

A final evaluation of pore pressure response was then performed using the response chamber in the manner previously described. If the final response was not adequate, the filter associated with the problematic measurement location was changed, requiring a complete disassembly of the tool. The T2P was then reassembled in the

manner described in Section 4.1 and the response was then rechecked until it was judged to be satisfactory.

With the tool and associated drill string removed from the hole, the drill bit and NX rods were able to be re-attached. The borehole was then washed to the new target depth, in preparation for the next penetration.

4.4 Sampling

A standard Shelby sampler was used to collect four samples (NC1, NC2, NC3, and NC4) of the clay deposit from borehole B104A. These samples were collected over depth intervals of 29 to 31 feet (NC1), 32 to 34 feet (NC2), 37 to 39 feet (NC3), and 42 to 44 feet (NC4). As previously mentioned, these samples have not yet been analyzed.

4.5 Data Collection Routines

As mentioned in Section 3.6, seven different channel configurations were used to collect data at various stages of each penetration. These configurations are listed in Table 4.2 and are described below. Each channel configuration file name is composed of the penetration name for which it was used, plus a suffix indicating the type of configuration (e.g., TP1_P1_IR indicates the initial response configuration file for penetration TP1_P1). Table 4.2 includes the respective suffix used for each configuration.

4.5.1 Initial Response Configuration

This configuration was used during the pressure response check performed before each penetration. For these checks, it was vital that the data acquisition system's sampling rate be maximized to capture the brief pressure pulses induced in the chamber. Therefore, only readings from the two pore pressure transducers and the witness pressure transducers were collected in these files. Using an integration time of 0.0125 seconds, these files had a 0.04 second sampling rate.

4.5.2 Prepenetration Configuration

Once a satisfactory initial pressure response was verified, a prepenetration file was activated. These files were used to collect data while the probe was at the surface

and when it was descending into the borehole, prior to penetration. In addition, initial zero pressure values were recorded in these files. A one second sample rate was sufficient for these purposes; therefore, the number of channels recorded did not have to be minimized. Input voltage, temperature, atmospheric pressure, depth, and the tip and shaft pore pressures were recorded with an integration time of 0.1 seconds.

4.5.3 Penetration Configuration

During penetration and the first minutes of dissipation, pore pressure and temperature changes occur quickly. Thus, the maximum scan rate possible was used. The number of recorded channels was reduced to four; namely, temperature, depth, and tip and shaft pore pressures. With an integration time of 0.02 seconds, this configuration had a sample rate of 0.052 seconds. These files were activated shortly before penetration, and terminated approximately 10 minutes after penetration ceased.

4.5.4 Dissipation Configuration

After the first 10 minutes of dissipation, it was no longer necessary to collect data at such a fast sampling rate. Thus, the sampling rate was decreased to one reading every 10 seconds and the integration time was extended to 0.1 seconds. Input voltage, temperature, atmospheric pressure, depth, and the tip and shaft pore pressures were recorded in these files.

4.5.5 Extraction Configuration

Since pressure and temperature change rapidly during extraction of the T2P from the borehole, it was important to collect information at a fast rate during this stage. Hence, only temperature, depth, and the tip and shaft pore pressures were recorded. Using a 0.02 second integration time, a 0.052 scan rate was possible.

4.5.6 After Penetration Configuration

An after penetration file was initiated as soon as the T2P was extracted from the bottom of the borehole. This configuration was used to both collect information as the probe was brought to the surface, and to establish a final zero value. Input voltage,

temperature, atmospheric pressure, and tip and shaft pore pressures were recorded in these files, at the relatively slow rate of 0.5 readings per second, with an integration time of 0.1 seconds.

4.5.7 Final Response Configuration

This configuration was used during the final pressure response check performed after each penetration. As with the initial response checks, it was important that a fast sampling rate be used to capture the brief pressure pulses induced in the chamber. Therefore, only readings from the two pore pressure transducers and the witness pressure transducers were collected in these files. Using an integration time of 0.0125 seconds, these files had a 0.04 second sampling rate.

4.6 Equipment Calibration

Each of the transducers used during the field test (the pore pressure transducers, the witness pressure transducer, the temperature probe, and the atmospheric pressure transducer) were calibrated in the laboratory against physical references. The field data acquisition system and accompanying laptop were used to record data during these calibrations and to evaluate stability, linearity, and hysteresis of the transducers, with the exception of the temperature transducer. All transducers were powered with a constant voltage supply.

The pore pressure transducers and the witness pressure transducer were calibrated against a constant pressure dead weight system for two load/unload cycles. For the original tip pressure transducer, the shaft pressure transducer, and the witness pressure transducer, forty calibrations points were used for each cycle. However, only four calibration points were used to calibrate the tip replacement pressure transducer, because of the limited amount of time available to calibrate this transducer during the field test. The calibration factor for each transducer was then determined using a linear regression line through the resulting data. The linearity of each transducer was evaluated based upon the goodness of fit (R^2 value) of the corresponding linear regression line. Figures 4.1 through 4.4 show the calibration graphs and Table 4.3 provides the calibration factor (slope of the line) and R^2 values for the transducers.

The temperature probe was calibrated in an ice bath with an automatic stirrer. The manufacturer's resistance/temperature curve was used to determine temperature based on the measured resistance of the thermistor. The calibration of the assembled temperature probe was confirmed by placing the probe in an ice bath with an automatic stirrer. Figure 4.5 presents the temperature measurements recorded while the probe was in the ice bath. It is not known whether the temperature fluctuations shown in this figure are indicative of the true temperature changes that occurred within the ice bath, or are due to electrical noise inherent to the temperature measurement system. It should also be noted that the average measured temperature within the ice bath was approximately 31.8°F. It is not clear why the average measured temperature was offset by 0.2°F from the expected ice bath temperature of 32.0°F.

The atmospheric pressure transducer was initially calibrated using the manufacturer's specifications. The calibration and stability of this transducer was then evaluated by comparing the atmospheric pressures measured by the transducer against the corresponding pressure measurements recorded hourly over a 20-hour period by the National Weather Service at Logan Airport in Boston, Massachusetts. The measured data is presented in Figure 4.6. As shown in Figure 4.6, the atmospheric pressure transducer measurements exhibited the same downwards trend as the pressures reported by the national weather service, with some minor fluctuations.

The depth box was calibrated by manually extending the chord in 2-inch intervals to a maximim length of 20 inches, then allowing it to retract, also in 2-inch intervals. The resultant changes in the depth box's output voltage were noted at each interval, during both extension and retraction of the chord. The calibration factor was then determined using a linear regression line through the resulting data. The linearity and hysteresis of the depth box was evaluated based upon the goodness of fit (R^2 value) of the corresponding linear regression line. The calibration data for the depth box are plotted in Figure 4.7.

4.7 Resolution, Noise, and Stability of Transducers

Table 4.4 summarizes the theoretical system resolutions, expected thermal drift, noise as measured in the laboratory and field, and measured mid-term and long-term drift

for the pore pressure transducers, temperature sensor and depth locator box. The theoretical system resolution of each transducer is based upon the range and bit resolution of the data acquisition system, and is the value in engineering units represented by one bit of the analog to digital converter. These numbers are very small and do not have any practical value for interpretation of the field data.

The thermal drift of the transducers, provided by the manufacturer, is the expected measured pressure shift due to a 20°F change in temperature.

The noise of each transducer was evaluated with the field data acquisition system by collecting 50 readings with a measurement duration of 0.02 seconds per reading. This was done both in the field and in the laboratory before the field test. Laboratory and field noise represent the electrical fluctuations, in engineering units, exhibited by each transducer over the 1-second monitoring period. The values of field noise for the shaft and original tip pressure transducers are approximately twice as large as the values measured in the laboratory, while the field noise of the replacement tip transducer is roughly four times greater than the laboratory noise measured by this transducer.

The mid-term drift of each pore pressure transducer used during the field test (the shaft pressure transducer, the original tip pore pressure transducer, and the replacement tip pore pressure transducer) were evaluated in the laboratory by recording pressure measurements for a 14-hour period, with the transducers sitting on a lab bench, exposed to the atmosphere. Changes in atmospheric pressure were taken into account for the absolute pressure transducers. The mid-term drift of the original tip transducer and the shaft transducer were evaluated in the lab before the field test. However, due to time constraints during the field test, the stability of the replacement tip transducer was not assessed until after the field test was over. The data used to calculate the mid-term drift of these transducers is shown in Figures 4.8 through 4.10. As shown in these figures, both the shaft pore pressure transducer and the original tip pore pressure transducer had an average noise band of approximately 1 kPa, while the average noise band for the replacement tip pore pressure transducer was 4 kPa. The shaft pore pressure transducer exhibited no drift in its pressure fluctuations. The original tip pore pressure transducer exhibited a 1.6 kPa drop in pressure during the first 30 minutes of the measurement

exhibited a 1.6 kPa drop in pressure during the first 30 minutes of the measurement period, then a rise to its approximate original pressure over the next 14 hours. In contrast, the measured pressures from the replacement tip transducer drifted consistently downwards by 18 kPa over the period. Given these results, it is apparent that the noise and stability of the replacement tip transducer, as measured in the lab, was significantly worse than either of the other two pore pressure transducers. The level of noise exhibited by the replacement tip transducer, relative to the other pore pressure transducers, is consistent with the increased capacity of this transducer; however, the drift is not. The drift of the witness pressure transducer was not evaluated, since this transducer was only used to measure rapid pressure pulses over a short period of time.

The long-term drift of each pore pressure transducer is defined as the largest shift in initial zero pressure values measured by that transducer over the course of the field test.

The practical accuracy of the pore pressure measurement system during the field test is controlled by the long-term stability of the pore pressure transducers, as measured in the field. Field stability can be affected by either factors inherent to the pore pressure measurement system, or external sources. Ideally, the stability of the pressure measurements should be identical in both the lab and field; however, the harsh environment encountered in the field will typically have some effect on the system. During the field test, the initial zero value recorded before each penetration was selected as the voltage value corresponding to zero pressure for that penetration. This value was then used in all subsequent voltage/pressure calculations for that penetration. Thus, eight different initial zero pressure values were used for the eight penetrations performed over the course of the field program. The long-term drift of the pore pressure measurement system was evaluated by examining fluctuations in the initial zero pressure values that were recorded during the field test. The drift of initial zero pressure values are plotted versus time for both the shaft and replacement tip pore pressure transducers in Figure 4.11. The initial zero value for the original tip pore pressure transducer was not included in this figure, since it was only used for the first penetration.

It can be seen from Figure 4.11 that the initial zero pressures measured at the tip exhibit a general downward trend over the 28-hour period that this transducer was in use

the previous section, the tip pore pressure transducer exhibited an 18 kPa pressure drop over a 14-hour laboratory stability test. Therefore, it is likely that the drop in initial zero values measured by this transducer is related to the stability of the transducer, and not to external sources.

The shaft pore pressure transducer proved to be more stable. As indicated in Figure 4.11, the initial zero pressure values from this transducer had a maximum drift of 6.44 kPa over a 24-hour period, and do not exhibit a trend with time. The shaft pore pressure transducer is an absolute transducer; hence, shaft pore pressure measurements can be affected by changes in atmospheric pressure. Figure 4.11 also provides a comparison between the fluctuations in initial zero pressures measured at the shaft and the fluctuations in atmospheric pressure measured by the atmospheric pressure transducer and the National Weather Service. From this figure, it is apparent that the fluctuations in initial zero pressure values measured at the shaft were unrelated to changes in atmospheric pressure over the course of the field test.

Table 4.5 lists the pressure difference between each penetration's initial and final zero pressure values, for both the tip and shaft pressure transducers. Figure 4.12 plots the drift in initial and final zero pressure values measured at the tip and Figure 4.13 shows the fluctuations in initial and final zero pressure values measured at the shaft.

For each transducer, the magnitude and trend of the drift in final zero pressure values are consistent with the drift of initial zero pressure values. Therefore, the pressure difference between each penetration's initial and final zero pressure values was likely caused by electrical drift of the transducers over the dissipation period.

4.8 Pressure Response Evaluation

As discussed in the previous section, the pore pressure response of both the tip and shaft pressure measurement systems was measured before and after each penetration. This was done to confirm that the tip and shaft filters remained fully saturated, and to verify that both pore pressure transducers were operational. The witness pressure transducer, being in direct contact with the water within the response chamber, provided an independent measurement of pressure.

A satisfactory pressure response by the T2P's two pore pressure transducers was defined as one in which the measured pressures from all three transducers closely matched, with no time lag in pressure measurements. This was a purely visual assessment made in the field. Table 4.1 lists the results for the final response evaluation for each penetration and Figures 4.14 through 4.21 show the initial and final responses for the eight penetration and dissipation tests. Zero pressure was considered to be the initial pressure in the response chamber before the pressure pulse was applied. No attempt was made to control the starting or ending pressures; therefore, the final pressure did not return to zero. As shown in Table 4.1, all final responses from the shaft pore pressure transducer were adequate. However, Figures 4.14, 4.17, and 4.19 indicate that there were poor final responses at the tip for TP_P1, TP_P4, and TP1_P6. A poor response is very obvious, since there is virtually no change in measured pressure during the 5-second data collection period. For several response checks, the witness transducer did not record the maximum applied pressure, as shown in the final response for TP1_P3 in Figure 4.16. It is believed that this occurred when the maximum allowable pressure was exceeded for the witness transducer.

The extraction process causes negative pore pressures to develop around the probe; these negative pressures are a function of a number of variables, including probe geometry, soil strength, extraction rate, and soil permeability. The negative pore pressures that occur during extraction can cause cavitation and the loss of pressure response. It is likely that the relatively small surface area of the tip filter caused it to become de-saturated more rapidly than the larger shaft filter. For all penetrations, replacement of the de-saturated tip filters resulted in adequate pressure responses. Of course, this required complete re-saturation of the tool from scratch, using the method described in Section 4.1.

4.9 Equipment Problems During the Field Test

Several equipment problems were encountered during the field test. When the T2P was brought to the surface after the first penetration (TP1_P1) on the second day of the field test, it was discovered that the thin shaft at the tip of the probe (the needle) was bent

by approximately ½ the diameter of the shaft (i.e., it was bent by 3mm). This apparently occurred during penetration of the T2P into the BBC.

A much more serious problem occurred after the TP1_P1 extraction. The extraction took place on a very cold morning and it was discovered that pore water within the conduit linked to the tip transducer flash froze upon exposure to the atmosphere after TP1_P1, within several minutes of extracting the probe from the borehole. The expansion of the water in this conduit caused the original tip transducer diaphragm to burst. No replacement pore pressure transducer was available in the field at that time.

When attempting to disassemble the probe in order to exchange the transducer and the bent needle, the spin collar linking the coupling with the drive shaft seized. Thus, the probe could not be disassembled and was returned to the MIT machine shop for repairs. In hindsight, it appears that stainless-on-stainless galling had occurred between the spin collar and the AW coupling. At the machine shop, the clearance between the collar and the coupling was increased, allowing the T2P to be easily disassembled. The tip pore pressure transducer was replaced with a transducer from the MIT lab and the bent needle was straightened, thus allowing the field program to continue.

Before the second penetration (TP1_P2), the T2P needle was not sufficiently tightened to the transducer block before penetration. This oversight allowed a hydraulic connection to form between the tip and shaft pore pressure transducers. Thus, the resulting pore pressure measurements from the tip and shaft transducers are identical for this penetration.

In addition to the equipment problems discussed above, the thermistor wires were damaged during re-assembly of the probe after the first penetration, causing the temperature sensor became inoperable. Therefore, only temperature data for the first penetration of the field test is included in this thesis.

Penetration Date	Penetration	Wash Depth (m)	Penetration Length (m)	Nominal Tip Depth (m)	Nominal Tip Elevation (m)	Average Penetration Speed (cm/s)	Dissipation Period (hours)	Tip Final Response	Shaft Final Response
12/14/05	TP1_P1	4.64	1.46	6.10	-1.10	2.8*	17.79	NG	OK
12/16/05	TP1_P2	5.70	1.31	7.01	-2.01	1.9	0.74	OK	OK
12/16/05	TP1_P3	7.06	1.32	8.38	-3.38	2.2	1.36	OK	OK
12/16/05	TP1_P4	8.67	1.29	9.96	-4.96	1.5	1.38	NG	OK
12/16/05	TP1_P5	10.03	1.40	11.43	-6.43	1.7	16.41	OK	OK
12/17/05	TP1_P6	11.47	1.33	12.80	-7.80	3.0	1.28	NG	OK
12/17/05	TP2_P1	6.99	1.39	8.38	-3.38	2.0	1.25	OK	OK
12/17/05	TP2_P2	8.53	1.38	9.91	-4.91	1.4	19.74	OK	OK

*Penetration rate for TP1_P1 fluctuated significantly. Listed rate is for the last segment of penetration.

Table 4.1 Summary of Installation Details

Configuration Type	Configuration Name	Number of Recorded Channels	Integration Time (seconds)	Sample Rate (seconds)
Initial Response	penetration name + _IR	3	0.0125	0.04
Prepenetration	penetration name + _PP	6	0.1	1
Penetration	penetration name + _P	4	0.02	0.052
Dissipation	penetration name + D	6	0.1	10
Extraction	penetration name + _EXT	4	0.02	0.052
After Penetration	penetration name + _AP	5	0.1	0.5
Final Response	penetration name + _FR	3	0.0125	0.04

Table 4.2 Field Test Channel Configurations

Measurement	Transducer	R^2	Calibration Factor
Tip Pore Pressure	Original, Kulite absolute	0.99998	-224480.37 kPa/V/V
Tip Pore Pressure	Replacement, Kulite gauge	0.9999997	-454855.45 kPa/V/V
Shaft Pore Pressure	Kulite absolute	0.999998	-225793.88 kPa/V/V
Depth	Depth Locator Box	0.9998	67.0812 in/V/V
Temperature	General Electric Thermistor	NA	NA

Table 4.3 Calibration Factors and Goodness of Fit (R^2)

Measurement	Transducer	System Resolution	Thermal Drift	Laboratory		Field	
				Noise	Mid-term Drift	Noise	Long-term Drift
Tip Pore Pressure	Original, Kulite absolute	$5.6x10^{-4}$ kPa	6.90 kPa	$4.4x10^{-2}$ kPa	1.6 kPa	$2.1x10^{-1}$ kPa	NA
Tip Pore Pressure	Replacement, Kulite gauge	$1.1x10^{-3}$ kPa	13.79 kPa	$1.1x10^{-1}$ kPa	18 kPa	$4.8x10^{-1}$ kPa	28
Shaft Pore Pressure	Kulite absolute	$5.6x10^{-4}$ kPa	6.90 kPa	$4.4x10^{-2}$ kPa	0	$2.0x10^{-1}$ kPa	6 kPa
Depth	Depth Locator Box	$3.2x10^{-5}$ inches	NA	Not Measured	Not Measured	$5.2x10^{-3}$ inches	NA
Temperature	General Electric Thermistor	9.3x10-5 °F	NA	$1.8x10^{-2}$ °F	Not Measured	$2.5x10^{-2}$ °F	NA

Note: Thermal drift is based on a 20°F temperature change.

Table 4.4 Resolution, Noise, and Drift of Transducers

Penetration	Tip Pressure Change (Kpa)	Shaft Pressure Change (Kpa)
TP1_P1*	No Final Response	-0.16
TP1_P2	-11.00	2.37
TP1_P3	-9.48	-1.61
TP1_P4	No Final Response	-2.19
TP1_P5*	-31.78	-12.92
TP1_P6	No Final Response	0.56
TP2_P1	1.93	-0.91
TP2_P2*	36.12	8.49

* Indicates an overnight test.

Table 4.5 Pressure Change Between Initial and Final Zero Pressure Values

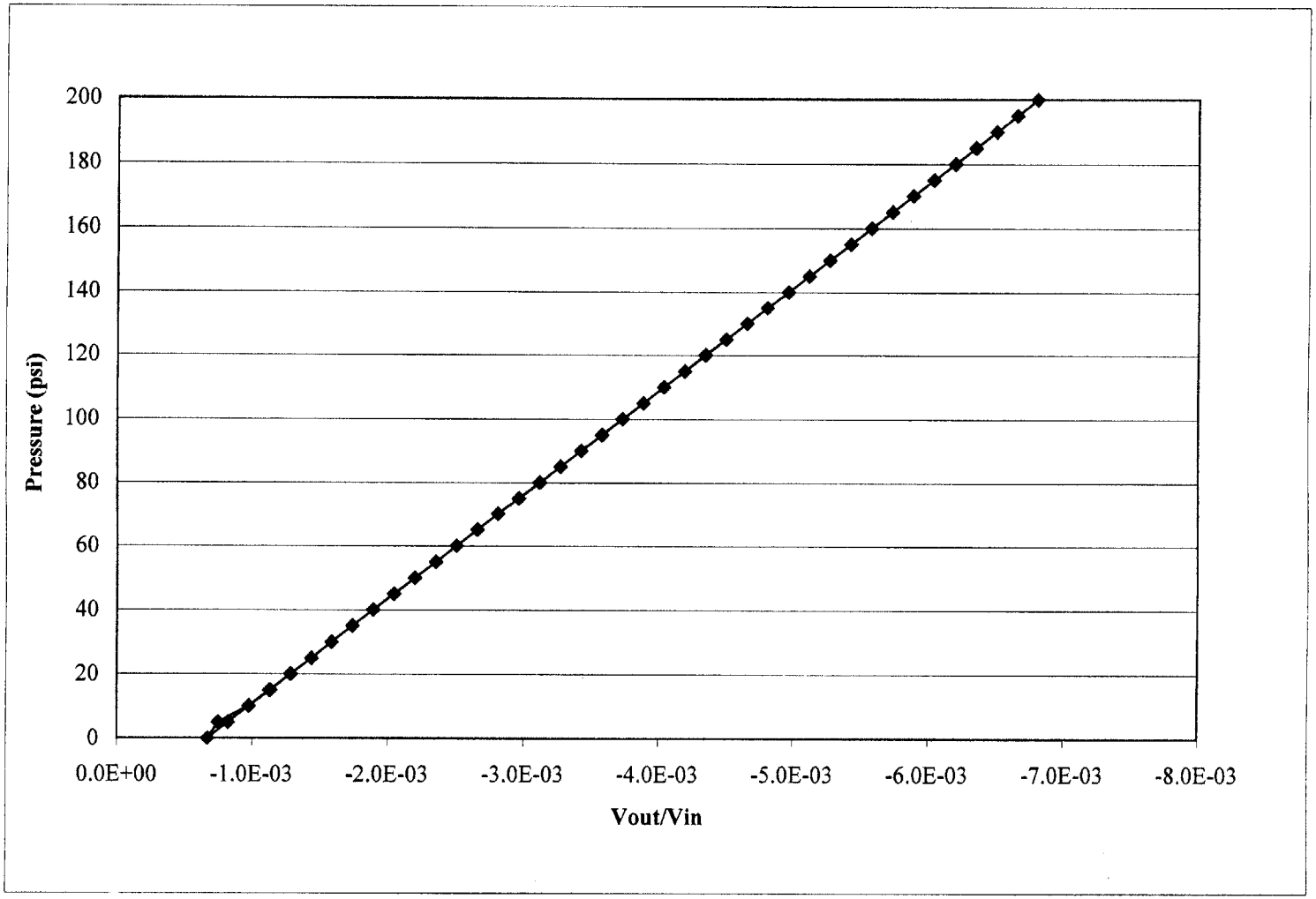

Figure 4.1 Calibration of Original Tip Pore Pressure Transducer

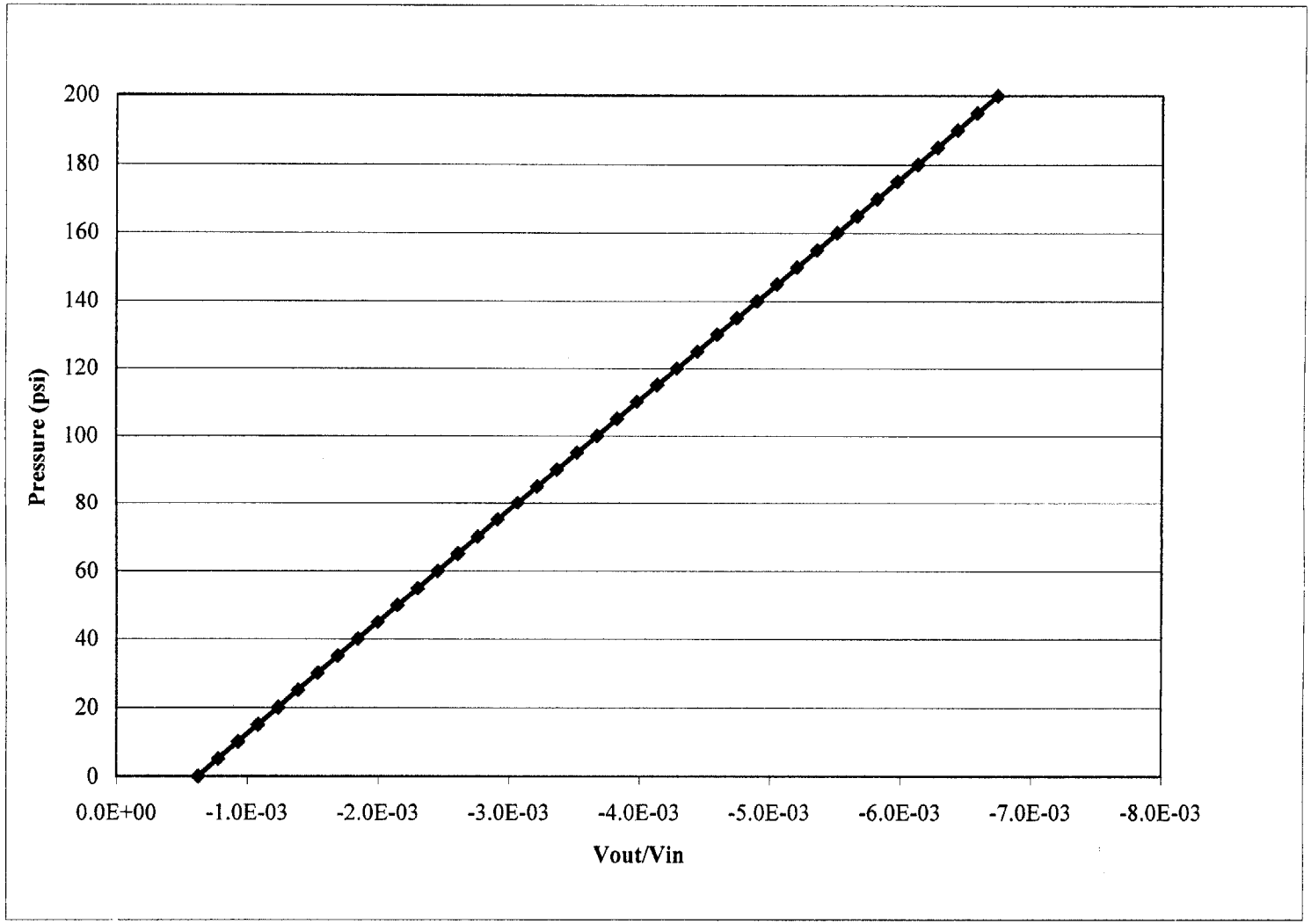

Figure 4.2 Calibration of Shaft Pore Pressure Transducer

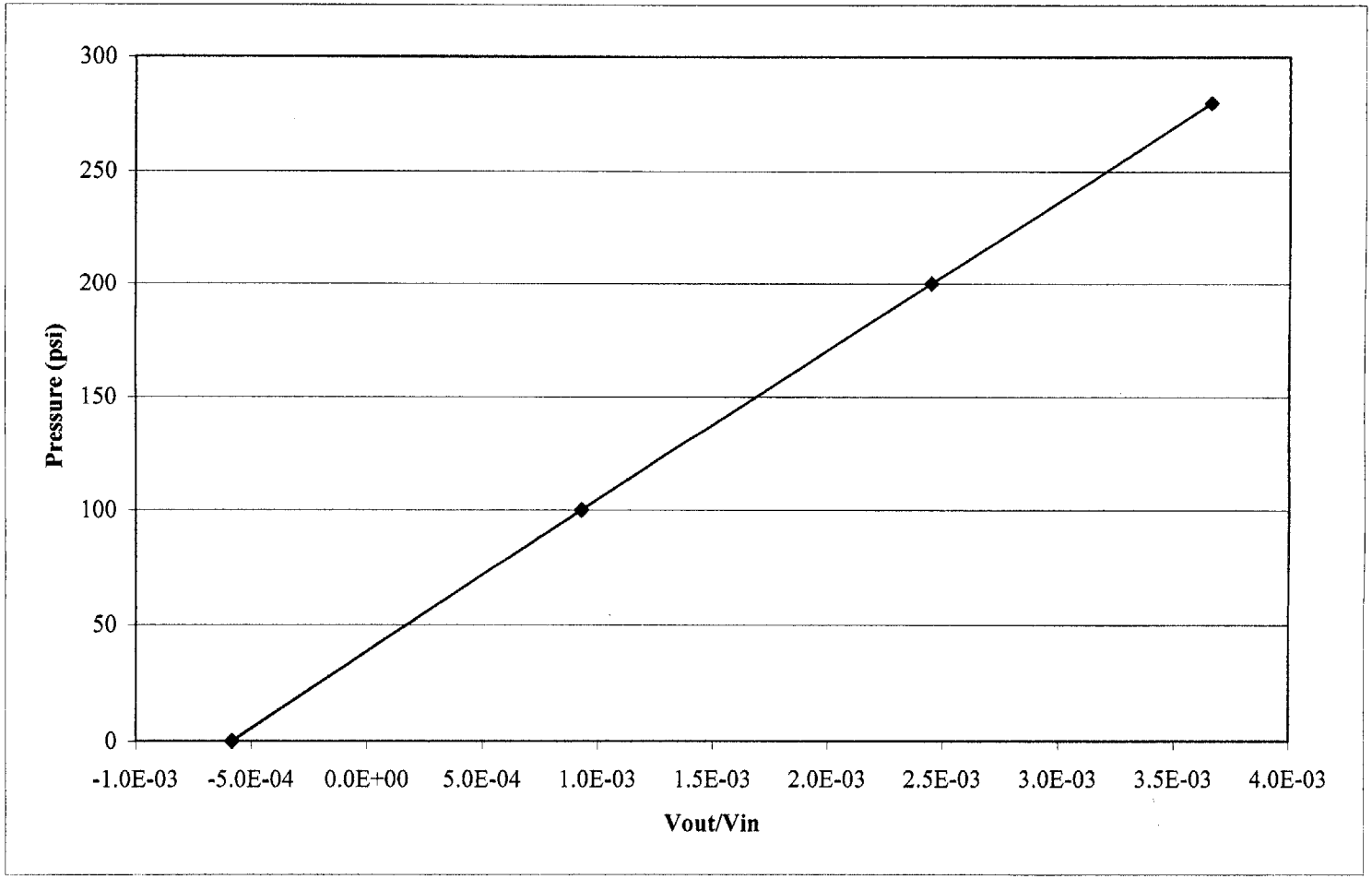

Figure 4.3 Calibration of Replacement Tip Pore Pressure Transducer

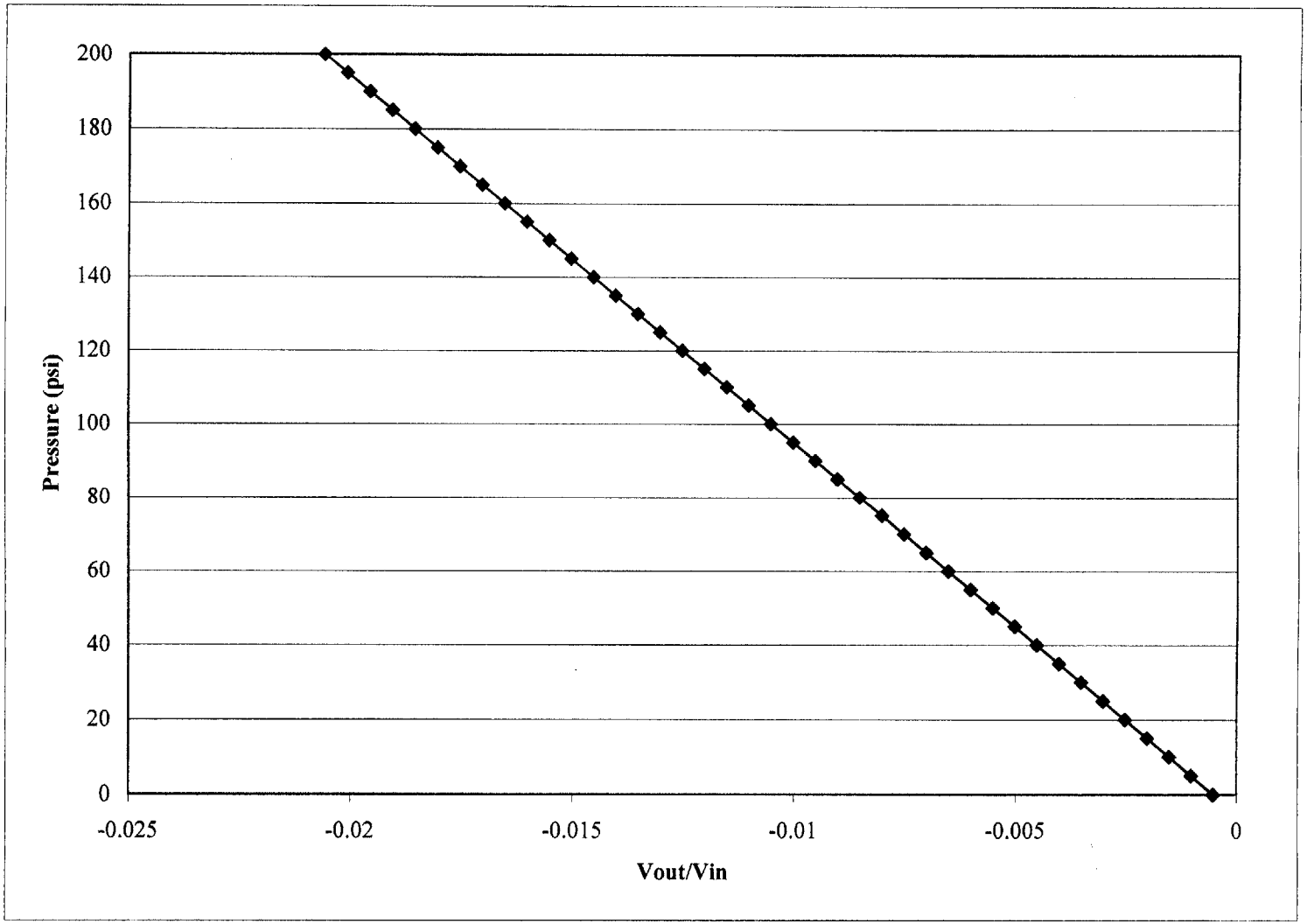

Figure 4.4 Calibration of Witness Pressure Transducer

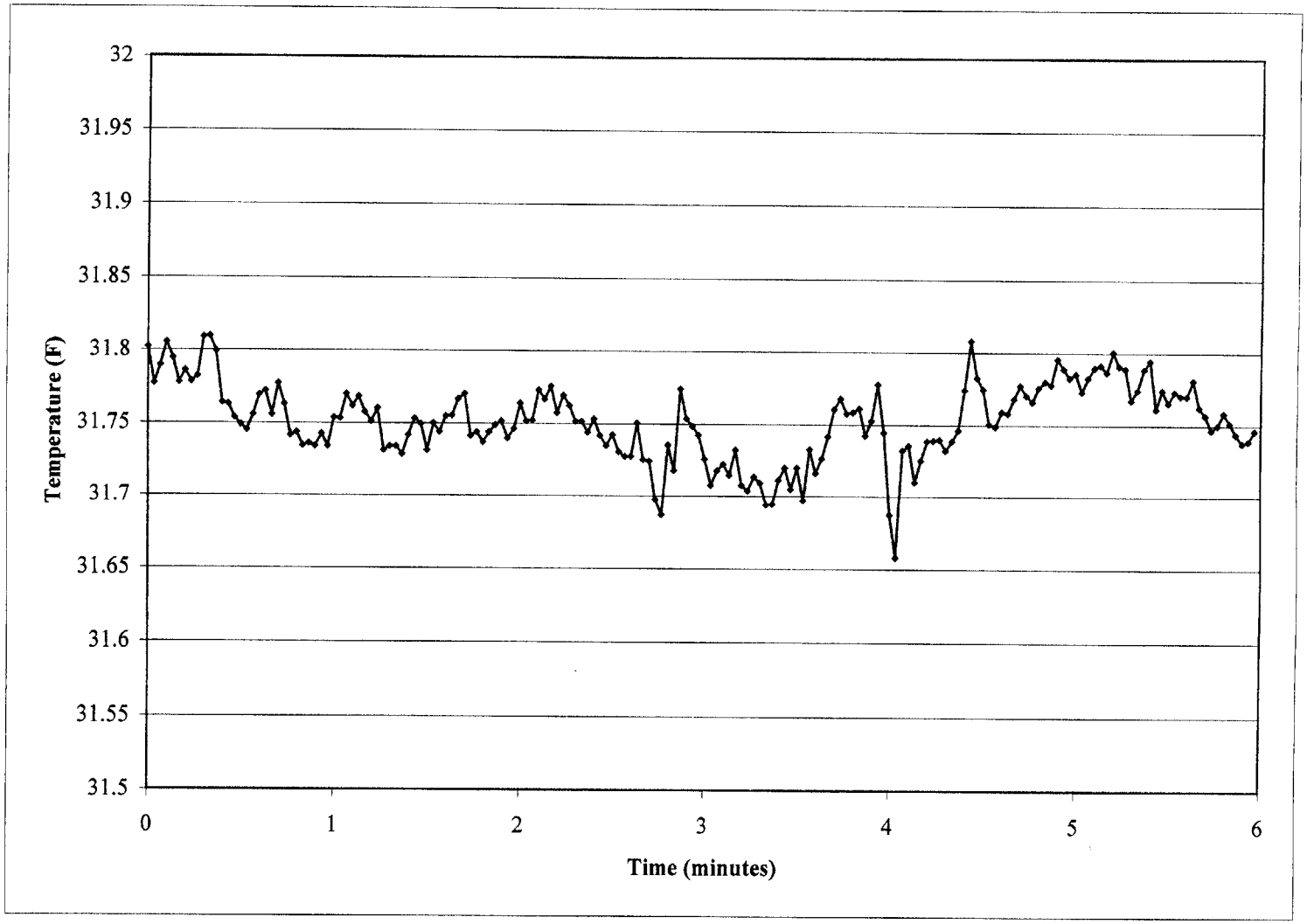

Figure 4.5 Calibration of Temperature Probe in Ice Bath

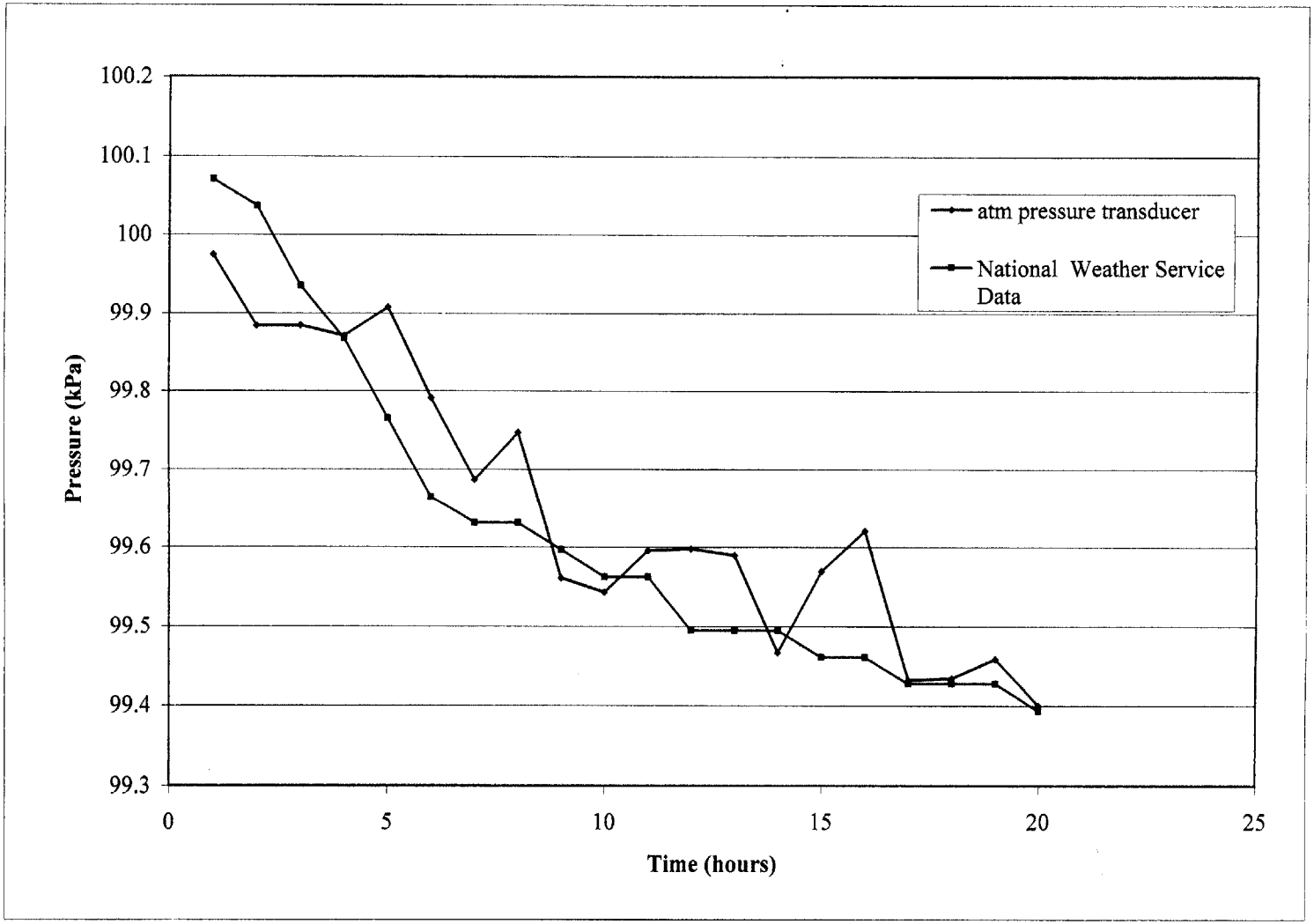

Figure 4.6 Laboratory Stability Test of Atmospheric Pressure transducer

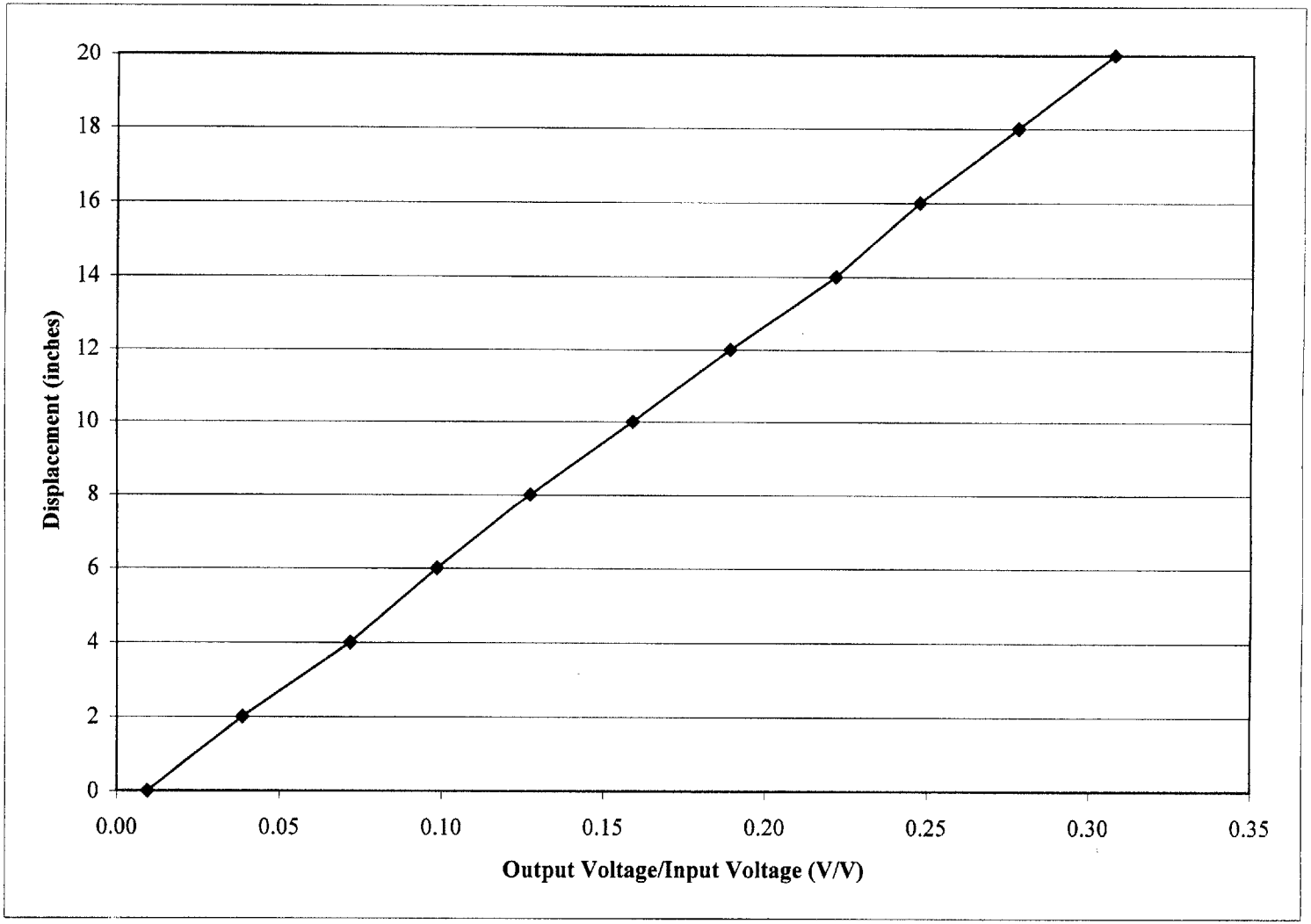

Figure 4.7 Calibration of Depth Box

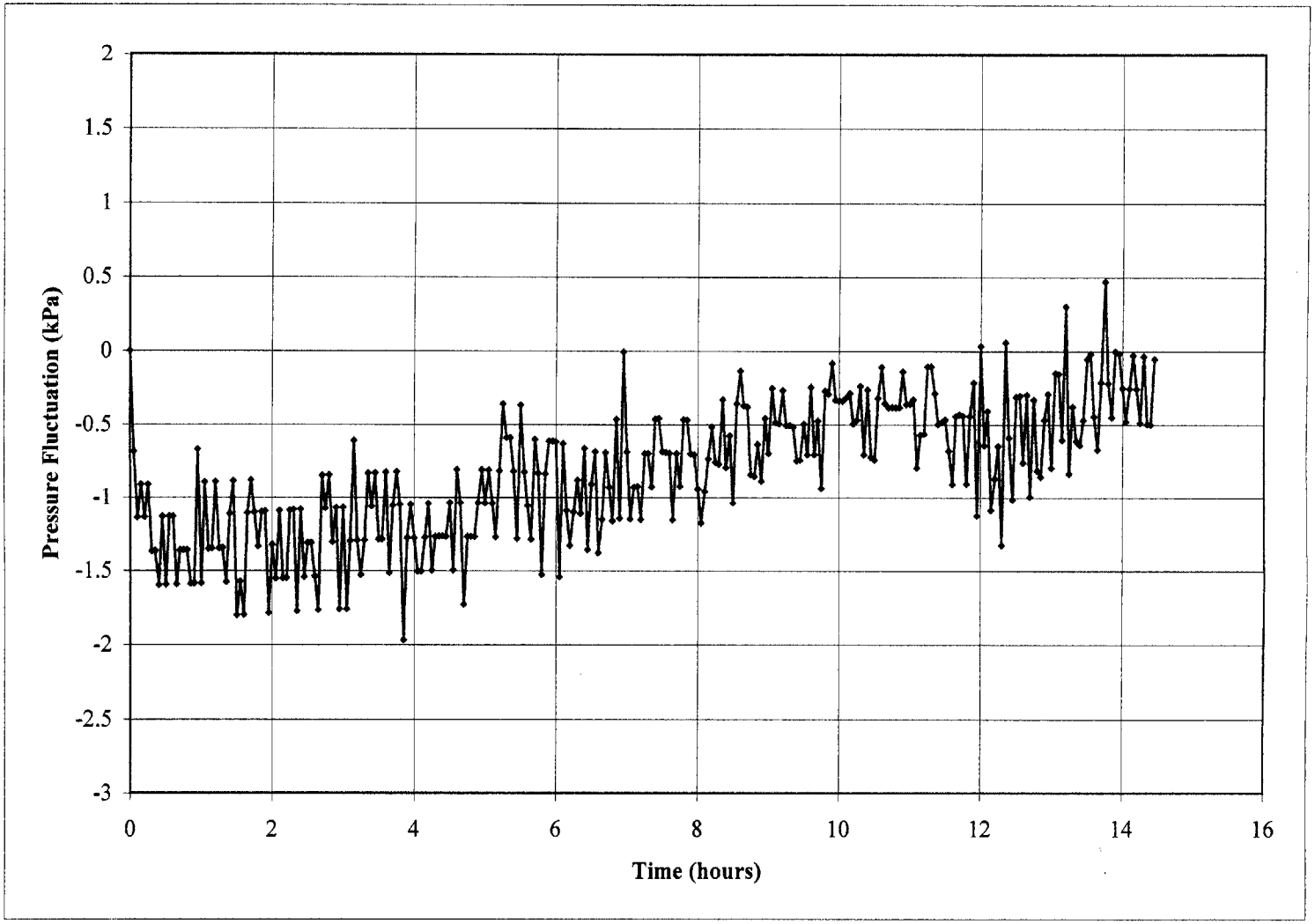

Figure 4.8 Laboratory Stability Test of Original Tip Pore Pressure Transducer

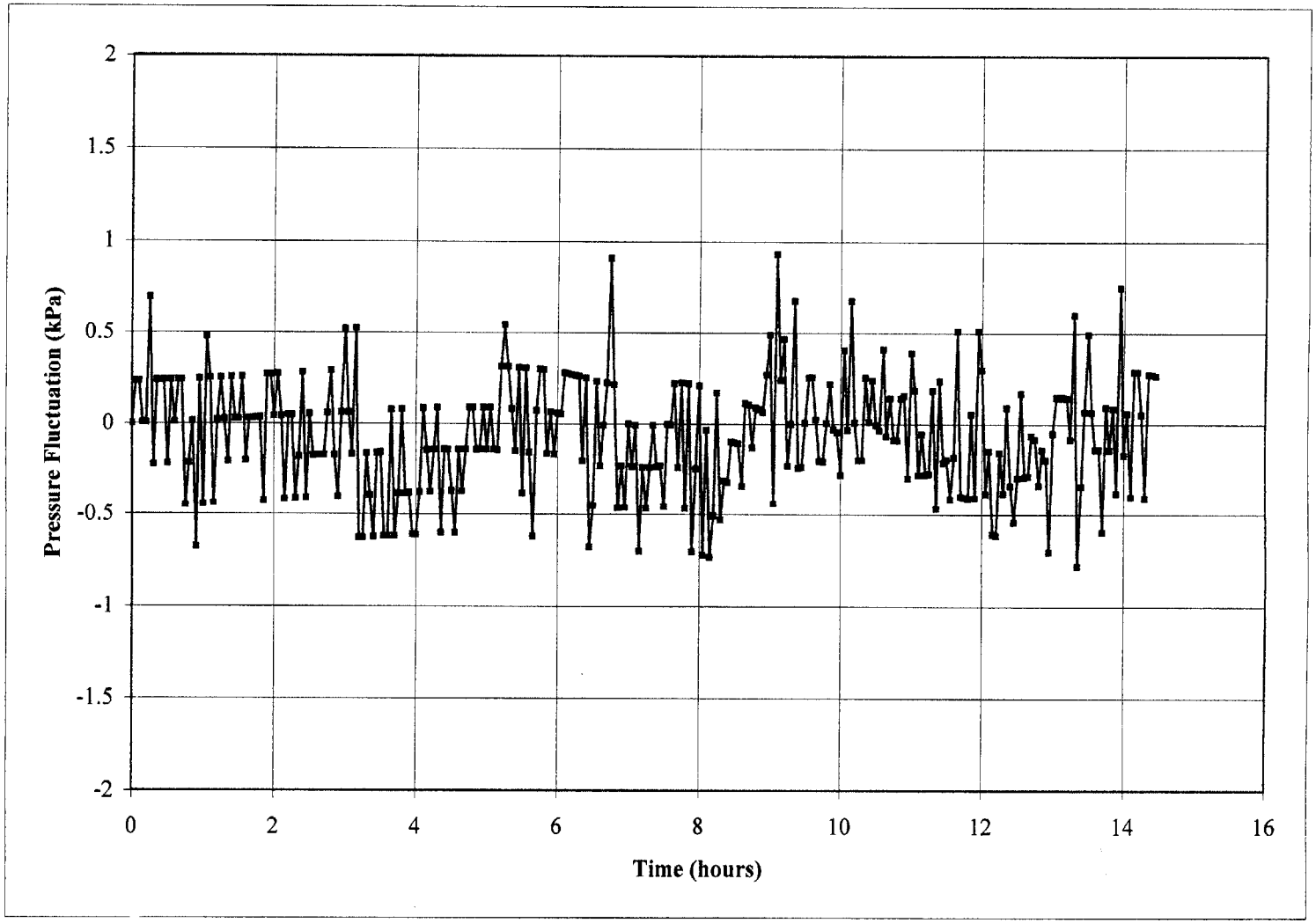

Figure 4.9 Laboratory Stability Test of Shaft Pore Pressure Transducer

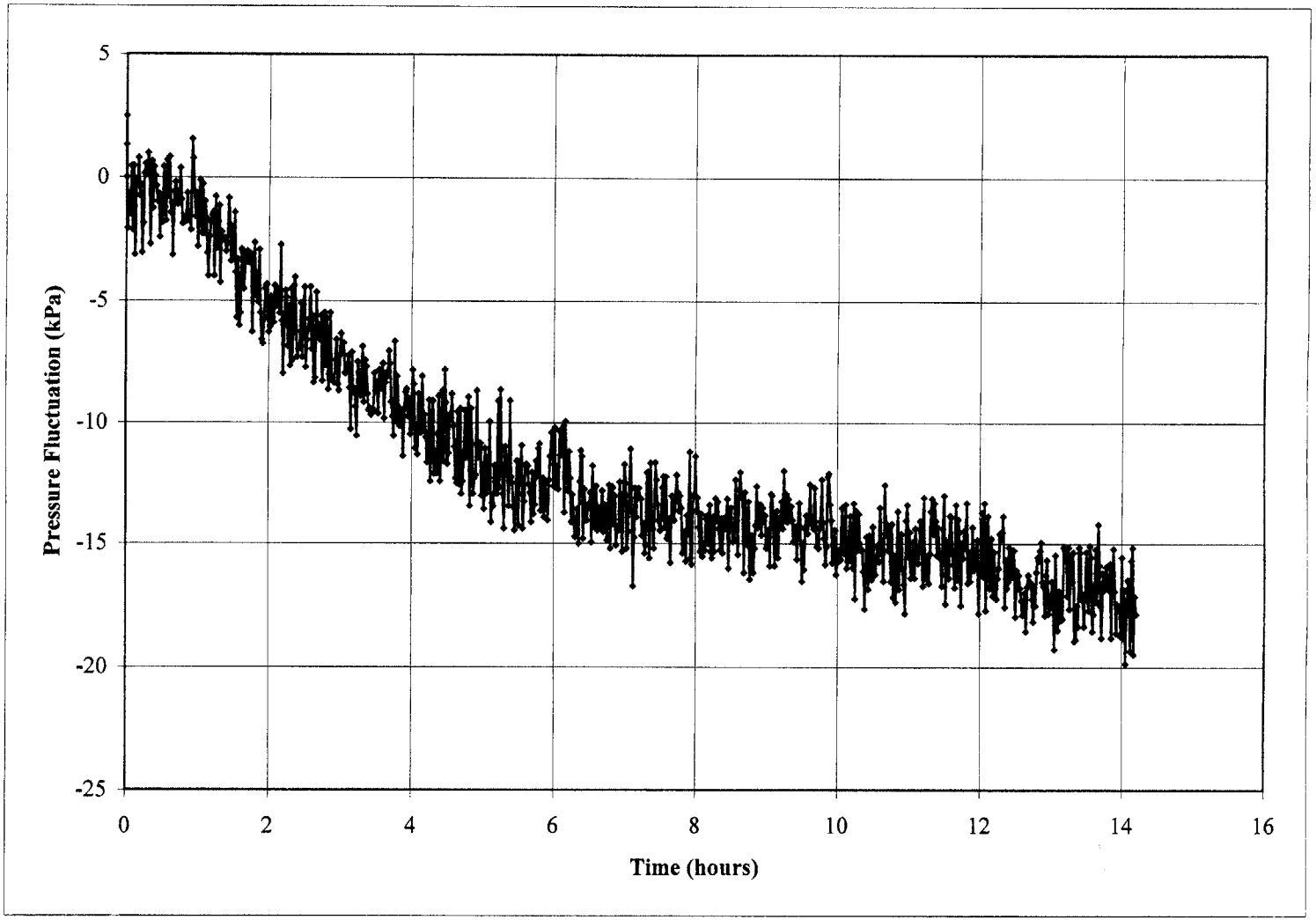

Figure 4.10 Laboratory Stability Test of Replacement Tip Pore Pressure Transducer

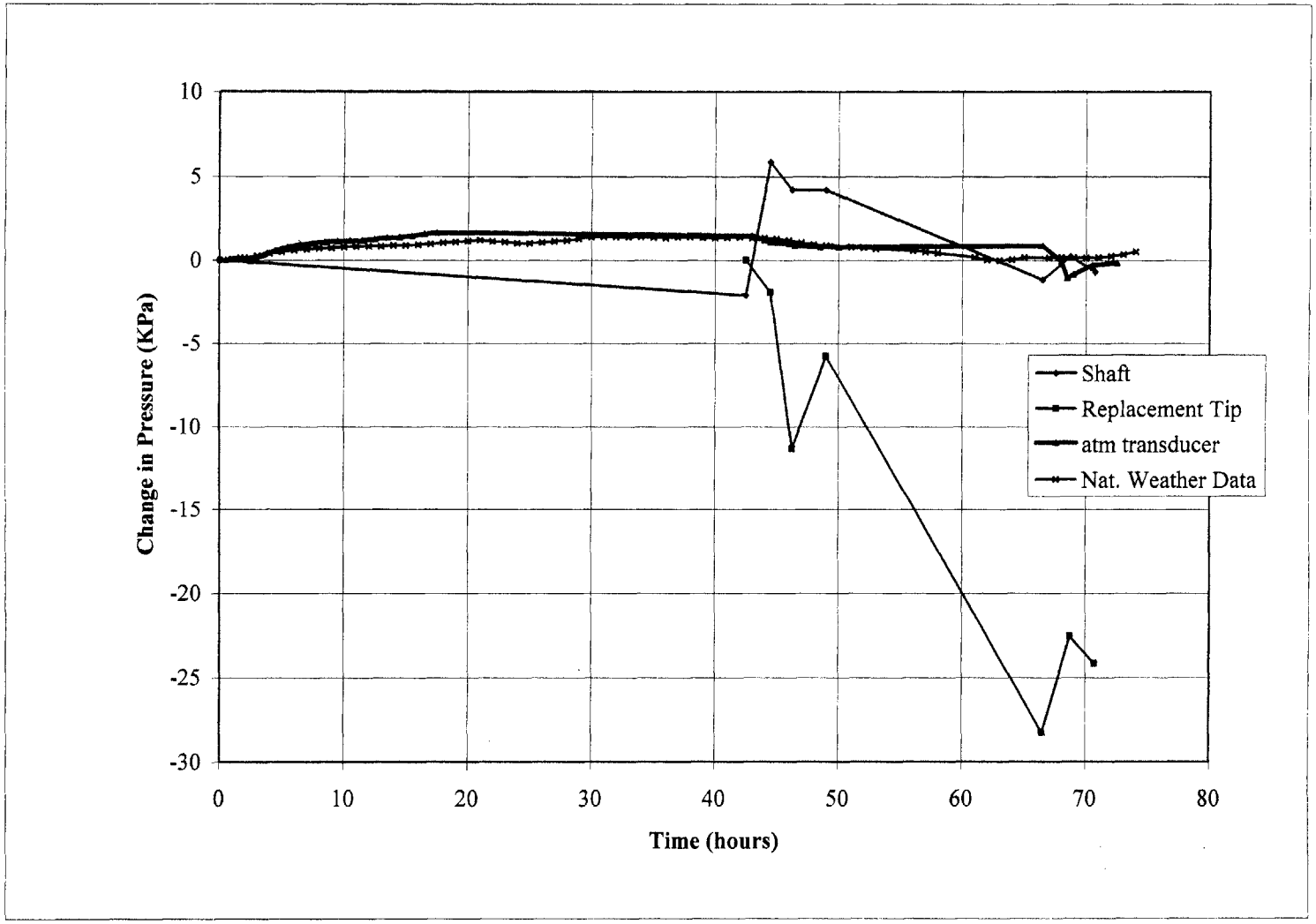

Figure 4.11 Change in Initial Zero Pressure Values for the Pore Pressure Transducers

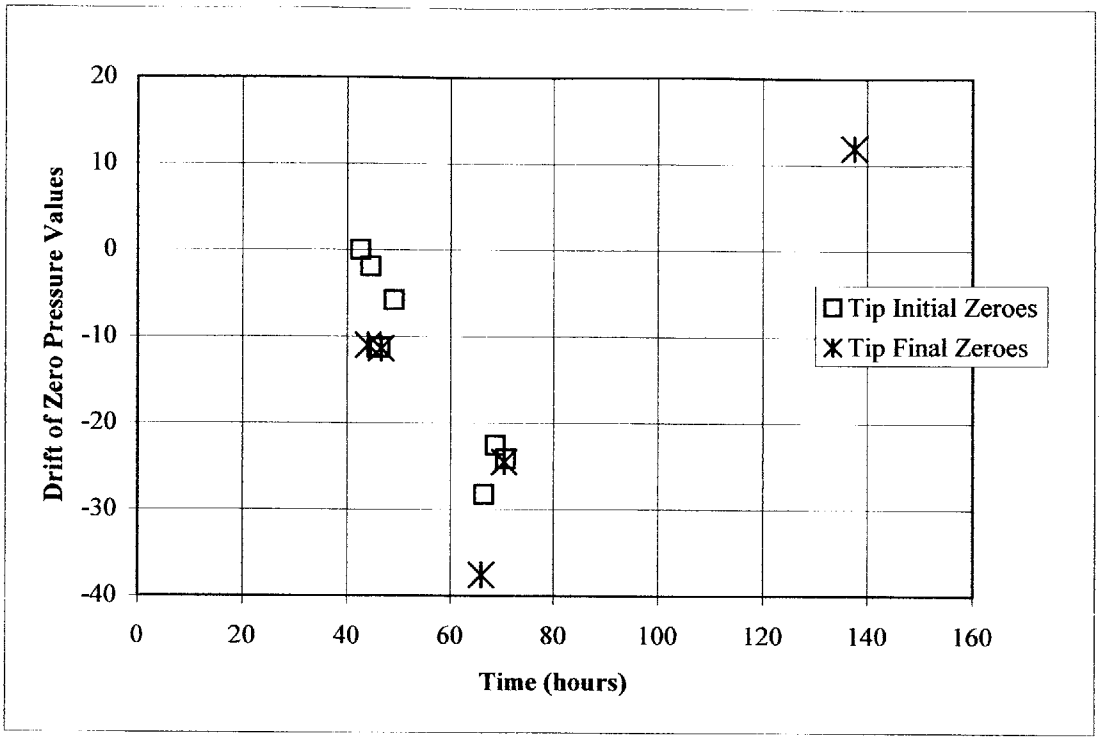

Figure 4.12 Drift of Initial and Final Zero Pressure Values Measured at the Tip

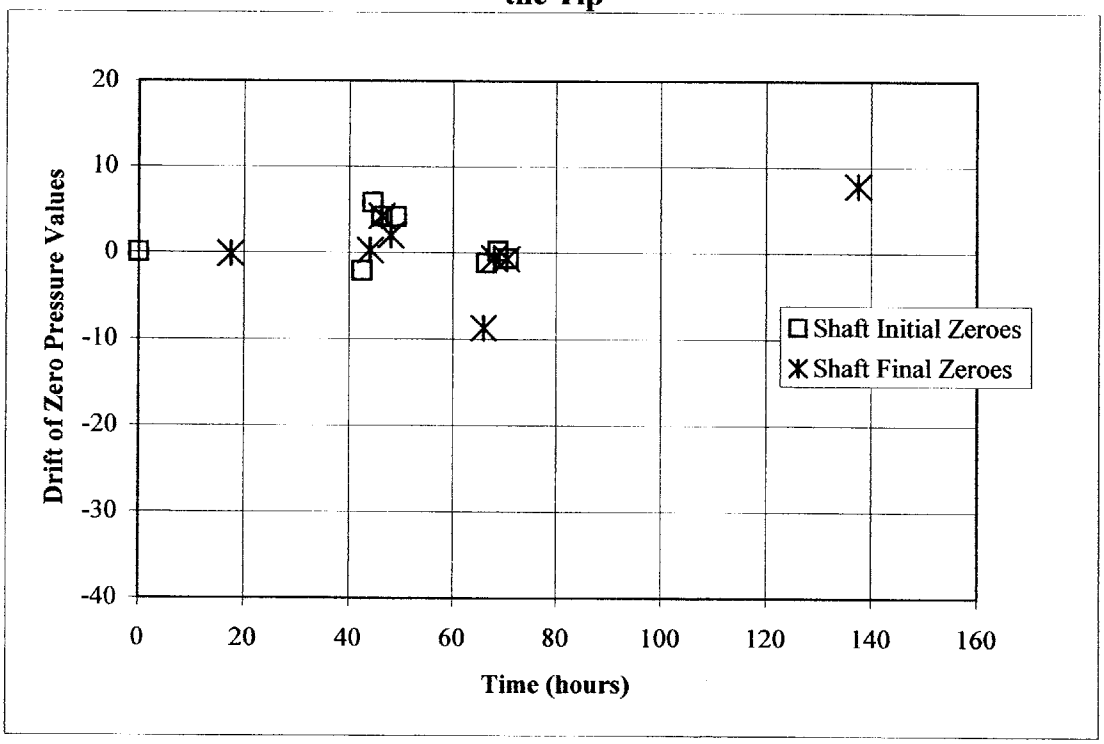

Figure 4.13 Drift of Initial and Final Zero Pressure Values Measured at the Shaft

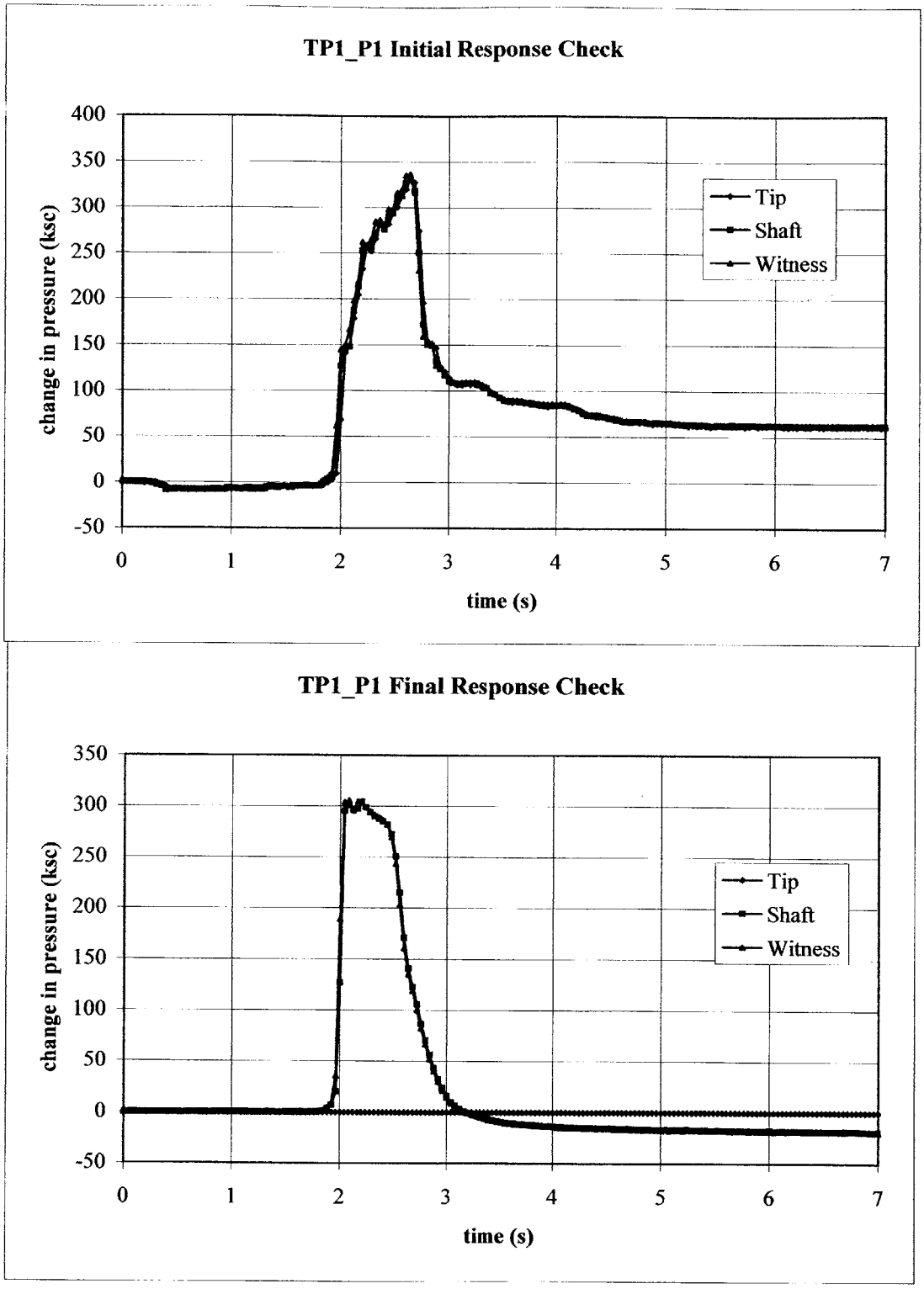

Figure 4.14 - Initial and Final Response Checks for TP1_P1

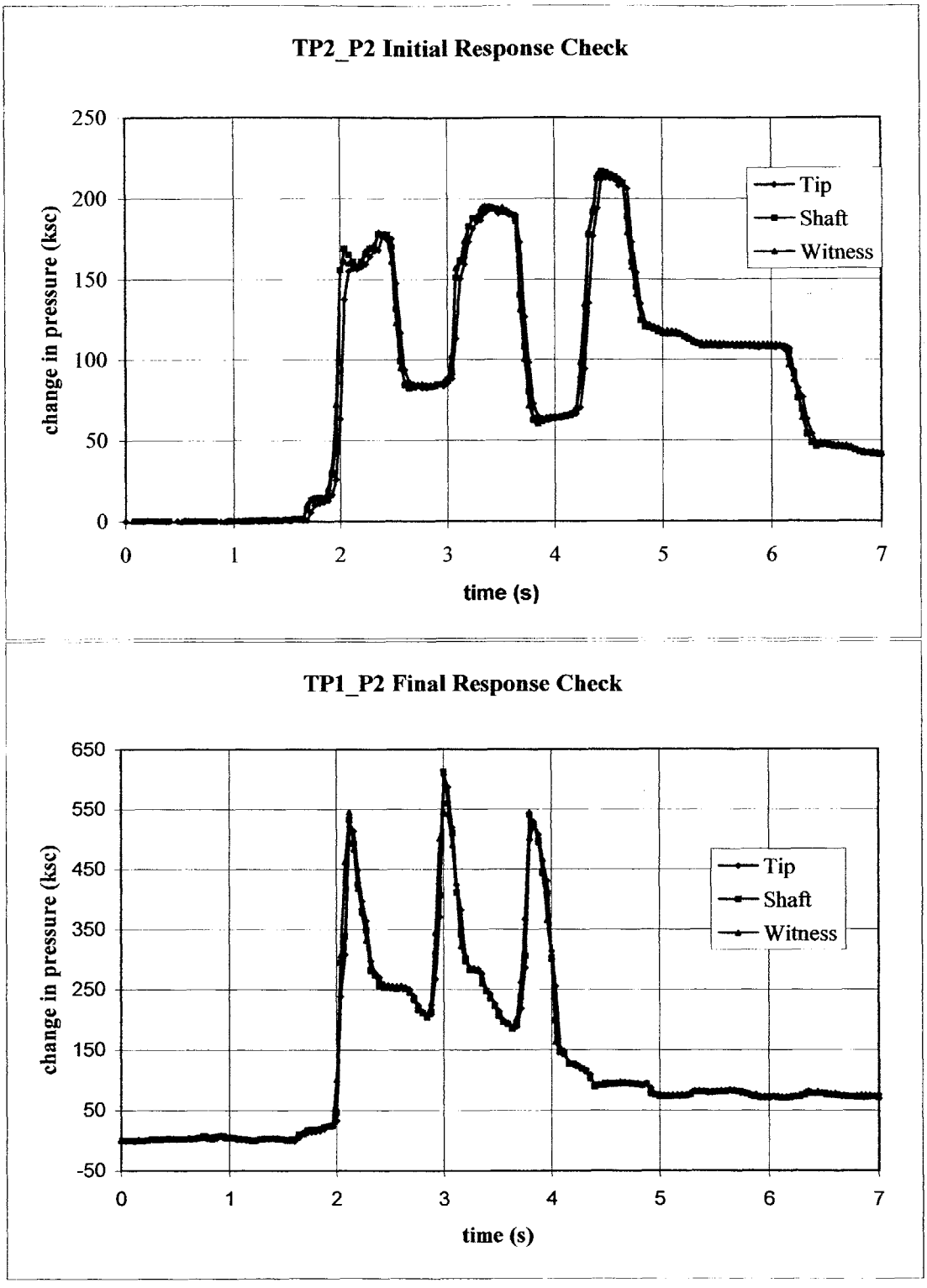

Figure 4.15 - Initial and Final Response Checks for TP1_P2

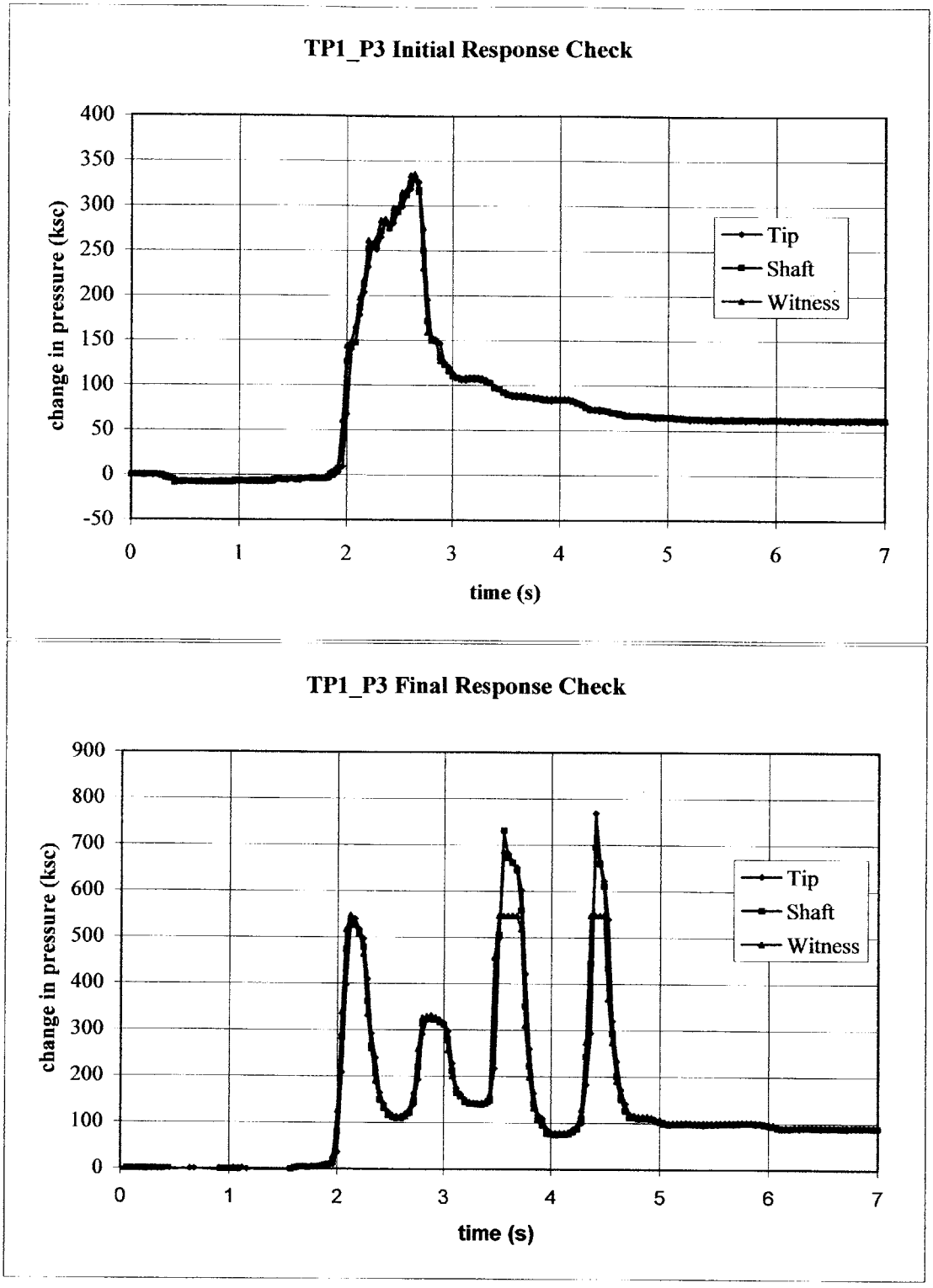

Figure 4.16 - Initial and Final Response Checks for TP1_P3

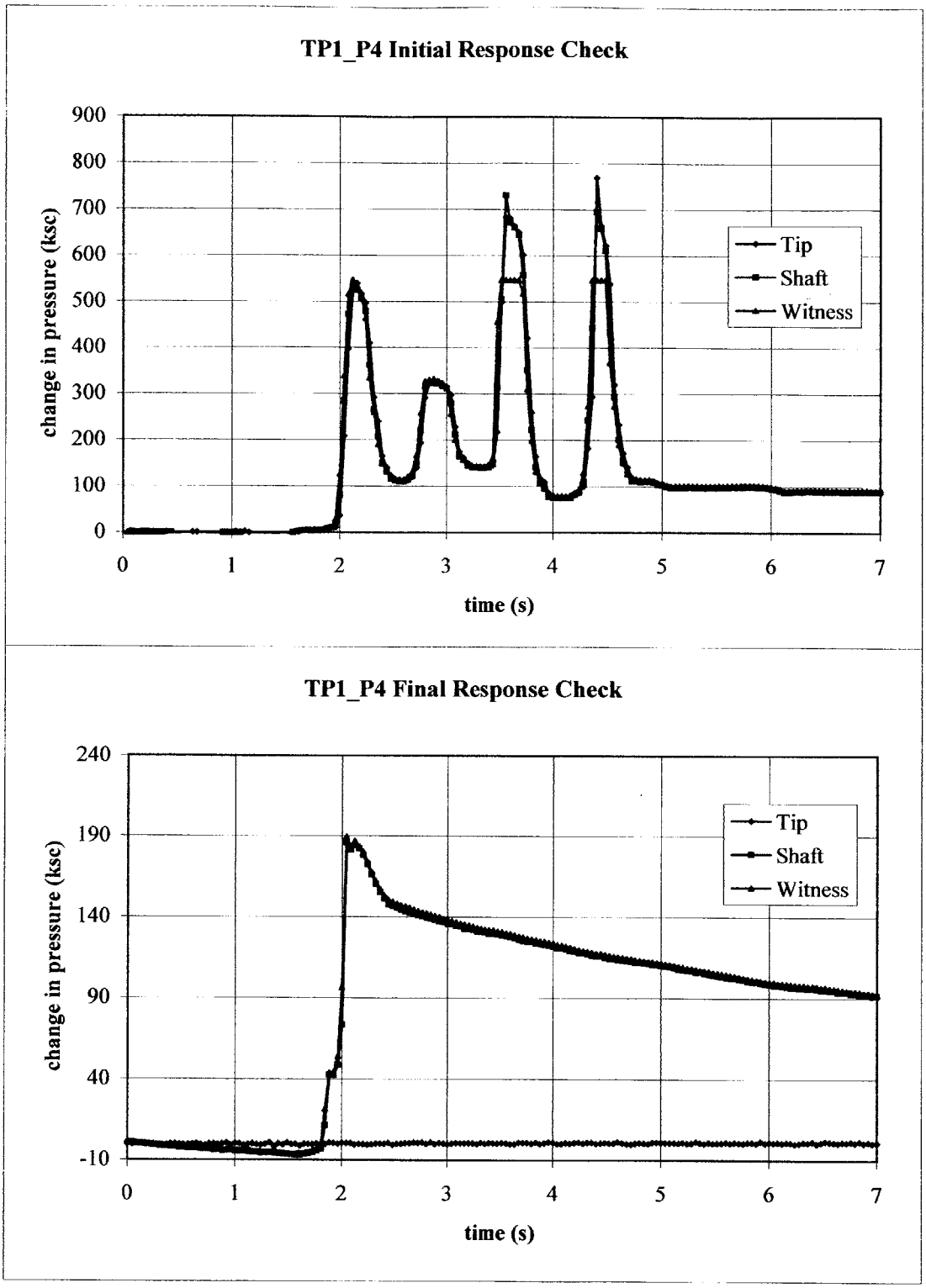

Figure 4.17 - Initial and Final Response Checks for TP1_P4

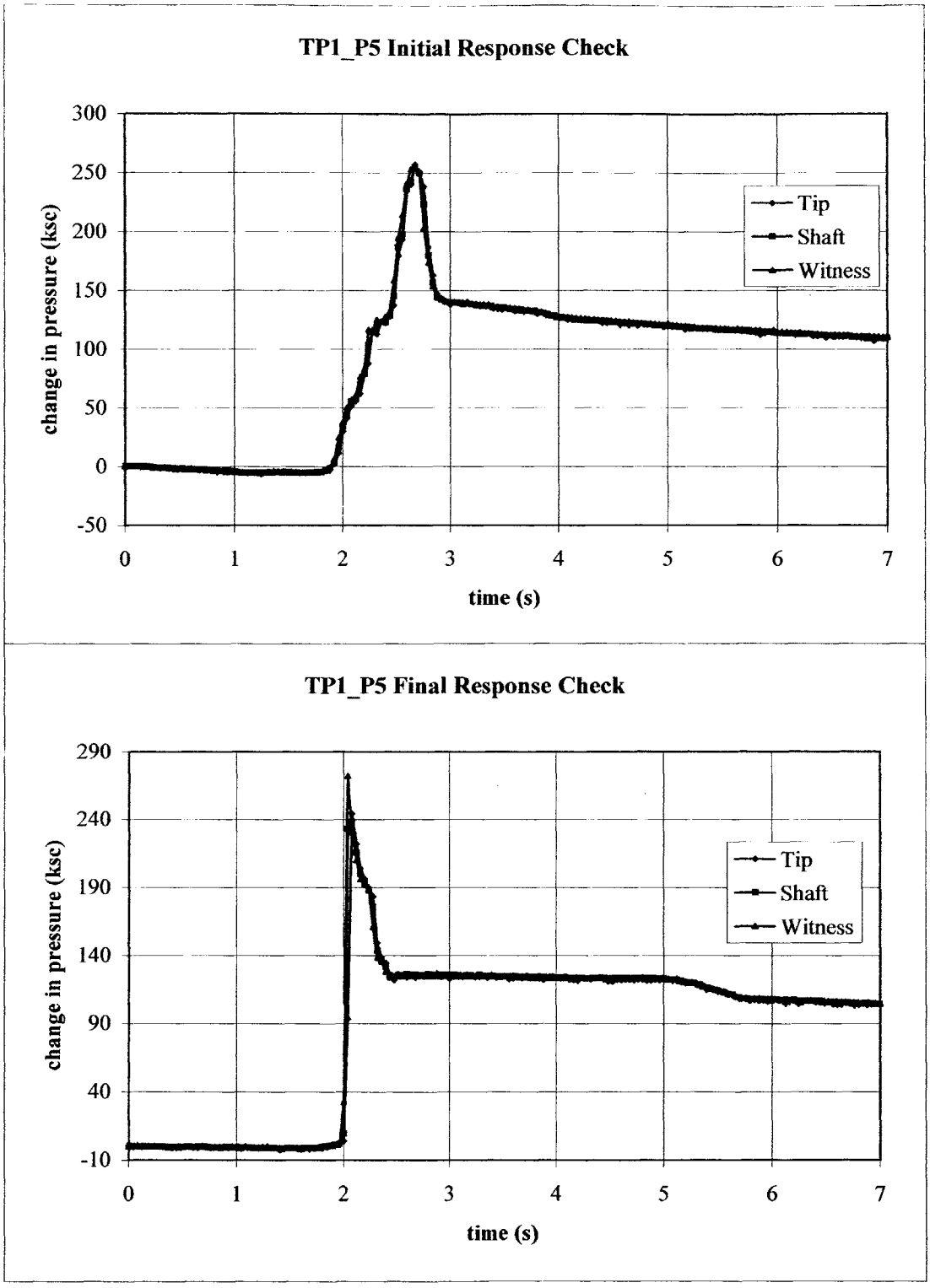

Figure 4.18 - Initial and Final Response Checks for TP1_P5

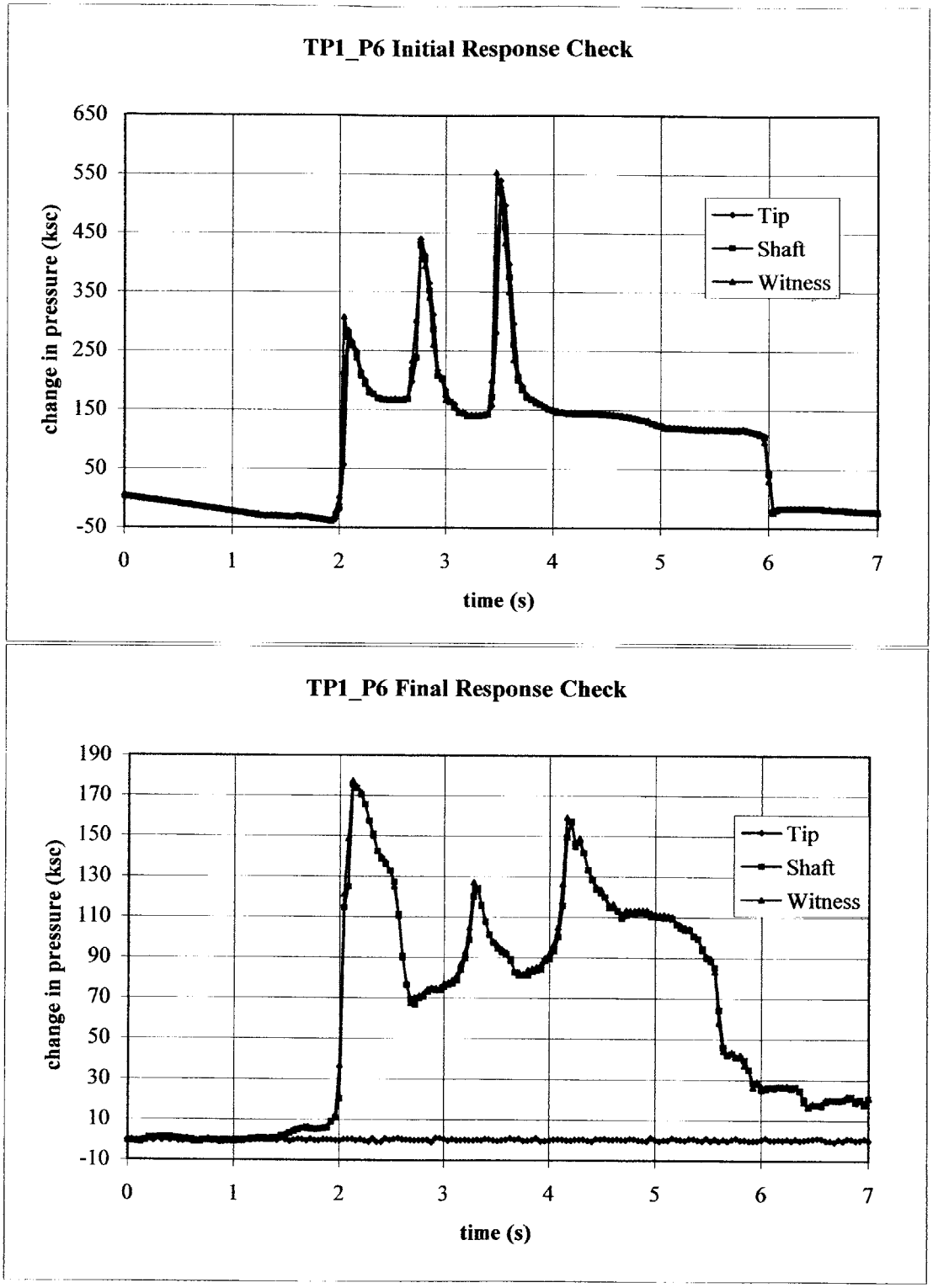

Figure 4.19 - Initial and Final Response Checks for TP1_P6

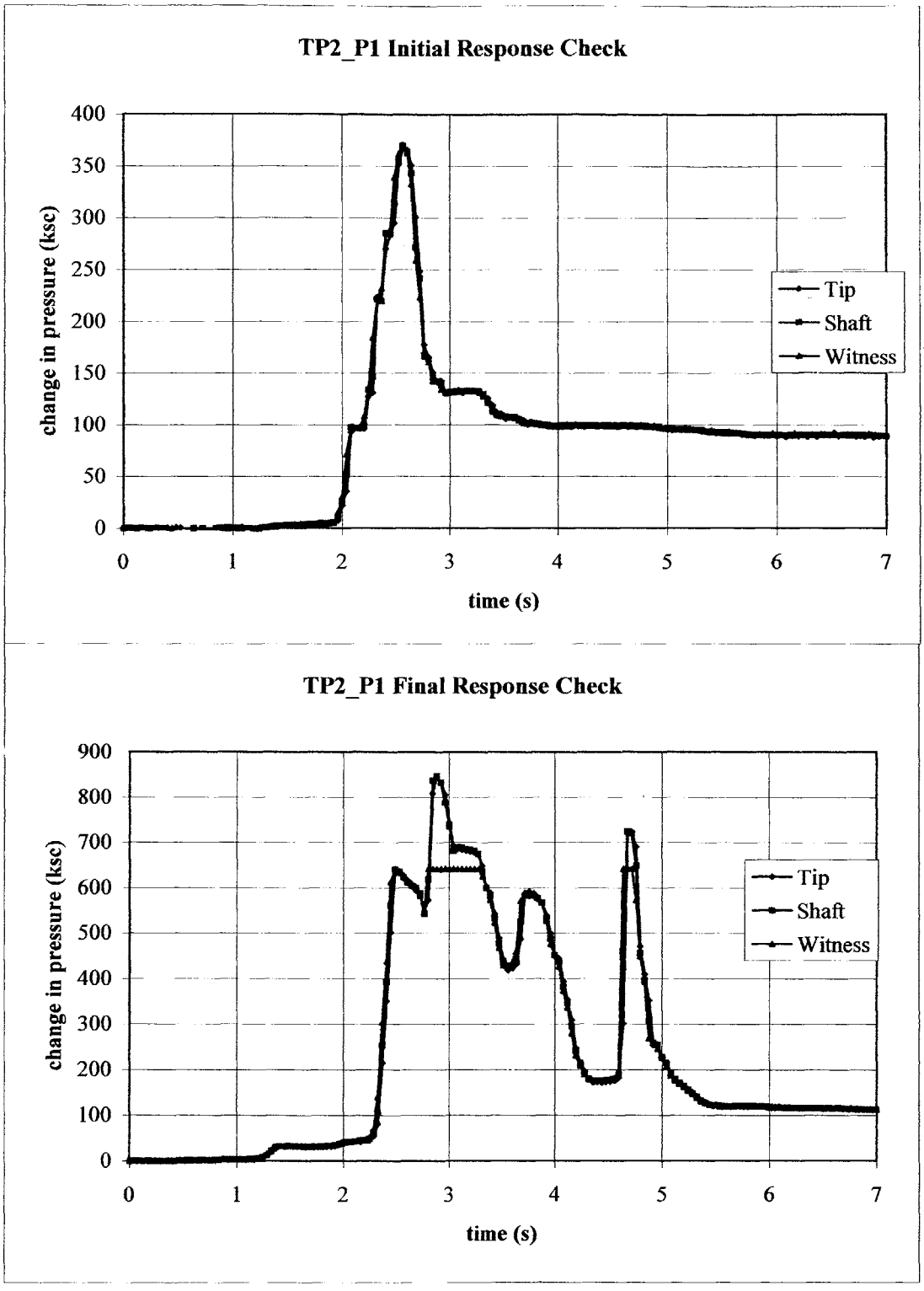

Figure 4.20 - Initial and Final Response Checks for TP2_P1

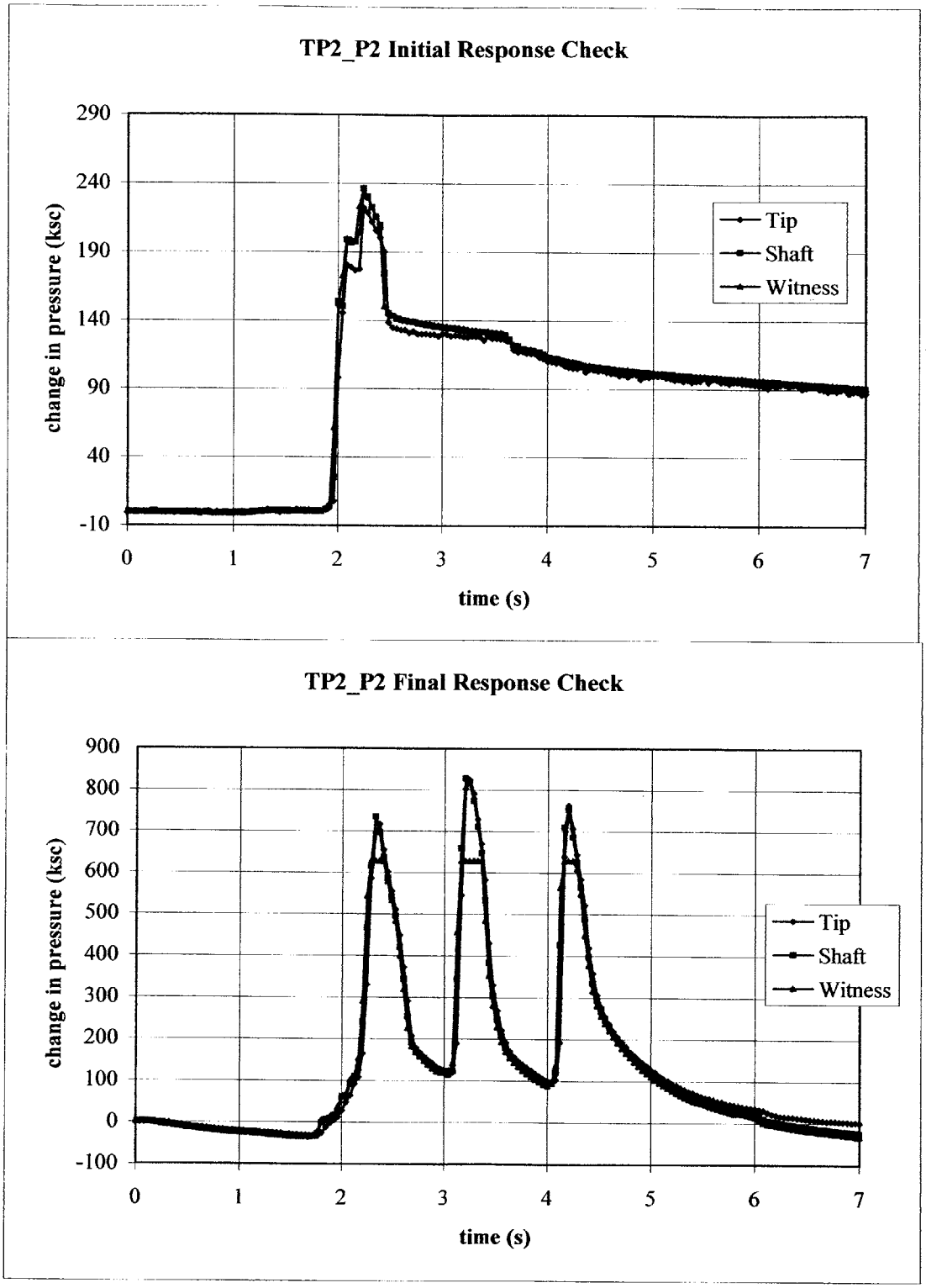

Figure 4.21 - Initial and Final Response Checks for TP2_P2

5 FIELD DATA

In this chapter, the pore pressure and temperature measurements collected during the field test are presented in three sections: 1) penetration records; 2) dissipation records; and 3) extraction records.

5.1 Penetration Records

Eight penetrations took place during the 4-day field test. These penetrations are labeled TP1_P1, TP1_P2, TP1_P3, TP1_P4, TP1_P5, TP1_P6, TP2_P1, and TP2_P2. For each penetration, the letters and number preceding the underscore refer to the borehole in which the penetration took place. The number following the underscore indicates the order in which the penetration took place in the corresponding borehole. Thus, TP1_P1 refers to the first penetration in borehole TP1, TP1_P2 refers to the second penetration in borehole TP1, etc.

As mentioned in Chapter 3, two different tip geometries were used during the field test. The original probe geometry, with the lower filter located just above the probe tip, was used for all penetrations except TP2_P1. The altered probe geometry, with the lower filter located 5.6 cm above the tip, was used for penetration TP2_P1.

5.1.1 Penetration Rate

The changes in penetration depth with time for all eight penetrations are plotted in Figures 5.1 through 5.8. Although the operator of the drill rig attempted to keep the penetration rates for all penetrations consistent, the penetration rates varied between 1.4 and 3.0 cm/sec (refer to Table 4.1 for a summary of the penetration rates).

Out of the eight penetrations, only TP1_P1 experienced significant penetration rate fluctuations during penetration, as shown in Figure 5.1. From 12.5 to 15 seconds after the start of penetration TP1_P1, the tool penetrated a very soft zone, causing the tool to rapidly descend and the drill string to lose contact with the crosshead over this period. From 15 to 26 seconds into penetration, the tool remained motionless, while the crosshead regained contact with the drill rods. From approximately 26 to 44 seconds after the start of penetration, the penetration rate stabilized. However, from 44 to 62

seconds into penetration, an additional drill rod had to be added to the drill string before penetration could continue. At approximately 62 seconds after the start of penetration, steady penetration resumed.

For TP1_P5, the tool descended rapidly during the last few seconds of penetration. It is not known why this occurred.

5.1.2 Temperature Measurements

As mentioned in Chapter 4, pore pressure and temperature measurements were recorded during T2P installation at each depth. Unfortunately, the temperature sensor within the T2P was functional only during the first penetration of the field test (TP1_P1). Temperature data from all subsequent penetrations could not be collected because of equipment problems and will not be presented. Temperature data from penetration TP1_P1 is shown in Figure 5.9. Figure 5.9a shows the change in temperature during penetration versus time, Figure 5.9b plots the penetration depth with time, and Figure 5.9c illustrates how the temperature changed with penetration depth.

During penetration, temperature remained relatively constant as the T2P descended between 4.64 and 5.34 meters below ground surface (bgs). It is believed that the T2P's tip had not yet penetrated the bottom of the borehole at these depths. Instead, it is likely that the tip was actually still in driller's mud until depth 5.48 meters bgs. This was due to a miscommunication between the drillers concerning the true depth of the borehole at the time of penetration. The relatively constant temperature measurements recorded above 5.34 meters bgs support this conclusion.

Once the probe tip descended beyond 5.48 meters bgs, the measured temperature rose rapidly from 53.4°F to approximately 54.8°F, most likely due to heat caused by friction between the tip and the soil. Measured temperatures then dropped to 53.8°F in a fairly linear fashion over the remainder of the penetration distance, with the exception of two rapid temperature decreases. From Figure 5.9, it is apparent that the two rapid drops in temperature that occurred at 5.5 meters bgs and 5.89 meters bgs were the result of the 10 to 15 second halts in movement that occurred at these depths during penetration. As discussed in Chapter 4, the probe tip bent during TP1_P1 and may have been in contact

with a rock or other obstacle during this penetration. This may have affected the temperature data.

5.1.3 Pore Pressure Measurements

As discussed in Section 4.6, the initial zero value recorded before each penetration was selected as the voltage value corresponding to zero pressure for that penetration. This value was then used in all subsequent voltage/pressure calculations for the data collected during the penetration. Thus, eight different initial zero pressure values were used for the eight penetrations performed over the course of the field program. Each initial zero pressure reading was recorded by the data acquisition system and visually confirmed on the computer screen. The initial zero pressure values used for the eight penetrations, dissipations, and extractions are listed in Table 5.1.

For each penetration, the accuracy of the voltage/pressure calculations was verified by confirming that the tip, shaft, and witness pressure transducers all recorded equal pressures during the application of the pressure pulse for that penetration's initial response test, as was shown in Figures 4.2 through 4.9. The original dissipation data has undergone a minor amount of filtering to eliminate fluctuations that were obviously caused by electrical noise.

5.1.3.1 Individual Penetrations

Figures 5.10 through 5.17 present the penetration pressure data. These figures show the change in penetration depth with time (plot a), the measured pore pressures versus time (plot b), and pore pressure versus the change in penetration depth (plot c). These figures indicate that shaft pore pressures are consistently larger than those measured at the tip. To quantify this effect, the ratios of tip pore pressures to shaft pore pressures versus penetration depth are plotted in Figures 5.18 through 5.23. Penetration data recorded when the shaft filter had obviously not yet entered undisturbed soil are not included in Figures 5.18 through 5.23. These ratios generally range from 0.7 to 0.8 for TP1_P4, TP1_P5, TP1_P6, and TP2_P2, with an average of approximately 0.75. However, the ratios for TP1_P3 and TP1_P2 were significantly lower and both had an

average of roughly 0.55. It is interesting to note that penetrations TP1_P3 and TP2_P1 occurred at the same depth. The altered probe geometry used in TP2_P1 may have caused this ratio to have a wider range and a lower average magnitude than those from the other penetrations. It is not known why this ratio also differed significantly during TP1_P3, since the original probe geometry was used for this penetration and the penetrated soil was normally consolidated, as it was for the other penetrations. The ratios for TP1_P1 and TP1_P2 are not shown, since the probe tip bent during penetration TP1_P1 and the needle shaft was not sufficiently tightened to the transducer block before penetration TP1_P2, creating a hydraulic connection between the two pore pressure transducers.

After penetrations TP1_P1, TP1_P2, TP1_P3, and TP1_P4, the drillers did not add additional driller's mud to the borehole during extraction of the drill string used to bore the hole. The resulting drop in mud level caused a bearing capacity failure at the base of the borehole after each of these penetrations. As the borehole base collapsed, a shear zone was created and the horizontal effective stress increased relative to the vertical effective stress at the bottom of the hole. The effect of this shear zone can be seen in the penetration records for TP1_P3, TP1_P4, and TP1_P5, by noting the initial slow increase in measured pore pressures that occurred as the probe penetrated this disturbed zone. As measured at the shaft, the depths of the shear zones below the bases of the boreholes ranged from approximately 45 cm (4.4 times greater than the diameter of the hole) for TP1_P5 to roughly 70 cm (6.9 times larger than the borehole hole diameter) for TP1_P4. There does not appear to be a relationship between the vertical extent of the shear zone and penetration depth. After penetration TP1_P5, the drillers maintained the mud level in the borehole during all extractions; thus, shear zone effects are less prominent for the subsequent penetrations. However, even with a constant stress level maintained on the base of the borehole, the penetration records for TP2_P1 and TP2_P2 indicate that the tool must penetrate a minimum of roughly 20 cm (2.0 times greater than the borehole diameter) before steady-state penetration pressures are reached.

The variations in pore pressure with depth measured by both the tip and shaft transducers indicate the presence of thin seams of silt or sand. Generally, these layers

range from 1 to 10 centimeters in thickness. Pore pressure measurements made at the tip appear more sensitive to the presence of layering within the deposit. It is likely that soil disturbance caused by shaft penetration is considerably greater than disturbance from penetration by the relatively thin tip. Consequently, a larger shear zone exists around the shaft. Thus, pore pressure measurements made at the shaft do not reflect the small-scale variations with the deposit as well as those recorded at the tip.

The altered probe geometry was used for penetration TP2_P1. By comparing the penetration data from TP2_P1 with the other penetration records, it is apparent than changing the lower filter location decreased the sensitivity of the resulting pore pressure measurements to layering effects. In fact, with this geometry, shaft pore pressure measurements more accurately reflect soil layering than those made at the tip.

5.1.3.2 Piecewise Penetration

Figure 5.24 presents the combined pore pressure measurements versus depth for penetrations TP1_P3, TP1_P4, TP1_P5, TP1_P6, and TP2_P2. The initial portions of the penetration records, collected when the either tip or shaft filter was descending through the mud column or disturbed soil, are not included in these figures. Hydrostatic pressures were calculated by assuming the water table depth is 2.1 m and vertical effective stresses were determined using the relationship between vertical effective stress and depth shown in Figure 2.5, with the weight of the Route 1 bridge taken into account. To evaluate the T2P piecewise penetration pressures, the data measured at the shaft are compared with the continuous piezocone profiles performed at the Newbury site by Jakubowski (2004), presented in Figure 2.8, and the T2P tip measurements are compared with the piezoprobe piecewise penetration data collected at the Saugus site by Varney (1998) and shown in Figure 2.10.

The piezocone used by Jakubowski had a constant outer diameter of approximately 3.6 cm, with a tip angle of 60°. A pore pressure filter was located on the shaft of the piezocone, just above the tip (u_2 position). At corresponding depths, all T2P shaft pore pressures are larger than those measured by the piezocone. This effect is most significant for penetrations above 10 meters bgs.

Normalized excess pore pressure is defined as the pressure difference between the penetration pore pressure and hydrostatic pore pressure, divided by the vertical effective stress ($(u_{pen}- u_o)/\sigma_v'$). From 8 to 12 meters bgs, in the normally consolidated clay, the average normalized excess pore pressure measured at the T2P shaft is approximately 3.7. Over the same depth interval, the average normalized excess pore pressure from Jakubowski's piezocone data equals approximately 3.1. In comparison, the piezocone profile performed by Varney (1998) in normally consolidated BBC at the Saugus site produced an average value of 3.5 for $(u_{pen}- u_o)/\sigma_v'$, which is similar to the the T2P shaft value.

The average normalized value of excess pore pressure from T2P tip measurements between 8 to 12 meters bgs is 2.7. This is similar to the average value of 2.5 from piezoprobe penetration measurements in normally consolidated BBC at the Saugus site.

The T2P pore pressure measurements exhibit little, if any, trend with depth. The short depth interval over which T2P penetrations were performed (5.5 meters) may have prevented this expected trend from being apparent in the penetration data.

5.2 Dissipation Records

Because of the previously mentioned problems encountered during TP1_P1 (bent tip) and TP1_P2 (hydraulic connection between the two transducers), the pore pressure data from these dissipations is not reliable and will not be used for interpretation. The dissipation records for TP1_P1 and TP1_P2 are included in Appendix A.

The pore pressure dissipation records for remaining penetrations are presented in Figures 5.25 through 5.30. The top plot (a) in each figure depicts pore pressure versus time on a logarithmic scale for each dissipation record. The bottom plot (b) presents data from the same dissipation record in terms of normalized pore pressure versus time on a logarithmic scale. Varney (1998) defined normalized pore pressure as the increment of pore pressure above hydrostatic pressure, divided by the difference between the installation pressure and hydrostatic pressure (i.e. $(u-u_o)/(u_i-u_o)$). Zero time is selected as the moment continuous penetration ceased, as calculated from depth box measurements.

The installation pore pressure (u_i) is chosen as the magnitude of pressure measured at the end of continuous penetration, also determined by depth box measurements. The elevation of the water table was not measured during the T2P field test. Hydrostatic pressure (u_o) is calculated by assuming that the water table is located 2.1 meters bgs, as measured at the site by Paikowsky and Hart (1998). As was shown in Figure 2.4, water table elevation measurements collected at the Newbury test site over a six-month period generally ranged from 1.75 and 2.5 bgs; thus a water table depth of 2.1 meters bgs represents an average value and appears to be a reasonable assumption.

Figures 5.31 through 5.36 show the changes in depth and pore pressure that occurred during the last 5 seconds of penetration and the first 10 seconds of dissipation. These figures illustrate that relatively minor fluctuations of tool position at the end of penetration can have a significant impact on pore pressures around a penetrometer. TP1_P3, TP1_P6, and TP2_P1 had consistent penetration rates during the last few seconds of penetration, with sharp transitions from penetration to dissipation and no fluctuations in tool position, as shown in Figures 5.31, 5.34, and 5.35. However, for TP1_P4, TP1_P5, and TP2_P2, sudden changes in tool position occurred during the last few seconds of penetration, leading to abrupt drops in pore pressure around the probe, as indicated in Figures 5.32, 5.33, and 5.36. For all three of these penetrations, the tool moved slightly upwards just before penetration ceased, with rises of roughly 0.5 cm for TP1_P4, 0.4 cm for TP1_P5, and 0.8 cm for TP2_P2. These small changes in probe position were enough to cause sudden and significant reductions in pore pressure at both the tip and shaft pressure measurement locations. The corresponding pressure drops ranged from approximately 100 kPa at the shaft filter for TP1_P5, to 180 kPa at the tip for TP2_P2. These pressure drops may reflect broad changes in the stress field around the tool that are not accounted for in the theoretical model. This discrepancy between the theoretical model and the stress distribution in the field may lead to problems in the interpretation of the dissipation data.

The upward shift in tool position seen in these penetrations may have been caused by a rebound of the AW coupling as it was pushed into the sediment; however, the reason for this behavior is not certain at this time.

5.2.1 Influence of Electrical Noise on Dissipation Data

Figure 5.27 shows that measurements of dissipated pressure made at the tip during TP1_P5 exhibit significant fluctuations from 1 second to 400 seconds into dissipation. It is likely that these fluctuations were due to problems with the tip pore pressure transducer's electrical connections, since pressure measurements made at the upper filter did not display these fluctuations.

Normalized pore pressures from TP1_P5 become significantly negative approximately 100,000 seconds into dissipation, which is physically unrealistic since dissipated pore pressures would not be expected to drop below hydrostatic values. The most negative normalized pore pressure value of –0.21 measured at the tip corresponds to a pore pressure approximately 33.1 KPa below hydrostatic. As was shown in Table 4.4, the final zero pressure value measured at the tip was 31.78 KPa lower than the initial tip zero pressure value. Thus, the negative normalized pore pressures recorded during this dissipation were probably caused by electrical drift of the tip transducer. Additionally, the electrical fluctuations exhibited by the tip pressure transducer earlier in the dissipation record for TP1_P5 also support the likelihood of transducer problems during this penetration.

During dissipation of TP1_P6, the pore pressures measured at both the tip and shaft undergo a gradual increase from roughly 1,800 to 3,200 seconds into dissipation, and then drop sharply. In addition, the pressures measured by the atmospheric pressure transducer also gradually rose and then suddenly decreased over this period. Since all the pressure transducers behaved this way concurrently, it is likely that these pressure variations were related to a problem with the data acquisition system.

The dissipation record from TP2_P2 also displays some irregularities. Figure 5.30 shows that a significant jump in dissipated pore pressures measured at the tip occurred from approximately 7,100 to 17,900 seconds into dissipation. A smaller, but significant rise in pore pressures measured at the upper filter and in atmospheric pressures measured by the atmospheric pressure transducer also occurred during this time interval. Therefore, it is likely that these pressure jumps are linked to a problem that occurred with the data acquisition system, and not an individual transducer.

As in the case of TP1_P5, tip normalized pore pressures from TP2_P2 become significantly negative approximately 23,000 seconds into dissipation, which cannot be indicative of true dissipation behavior. This discrepancy was clearly caused by electrical drift of the tip transducer.

5.2.2 Detachment Effects on Dissipation

As mentioned in Chapter 4, the drill rods linking the T2P to the drill rig were detached from the crosshead within 10 to 330 seconds of the start of dissipation during all penetrations except TP1_P6 and TP2_P1, effectively causing a slight change in applied load to occur. The time periods between the start of dissipation and the detachment of the drill rods from the cross head for each penetration are listed in Table 5.2. By comparing the times listed in this table with the respective dissipation records for each penetration, it is apparent that this detachment had little effect on the measured dissipated pore pressures.

5.3 Extraction Records

Figures 5.37 through 5.42 present the extraction data from TP1_P3, TP1_P4, TP1_P5, TP1_P6, TP2_P1, and TP2_P2. The top plot in each figure (a) depicts the change in depth versus time during extraction. The bottom plot (b) shows the pressures measured by the tip and shaft pressure transducers versus time during extraction. The third plot in each figure (c) presents the change in pressure versus extraction depth. Depth box measurements were not recorded during the TP1_P4 extraction; therefore, only changes in pore pressure with time are shown for this extraction.

The figures indicate that, with the exception of TP2_P1, tip pressures drop dramatically upon the start of extraction and typically rapidly become negative. These sudden reductions in tip pressures range from approximately 70 kPa for TP1_P6 to approximately 165 kPa for TP1_P5, and most likely reflect a combination of suction between the probe and the soil and the unloading effects of extraction. Subsequent reductions in pressure around the tip may be caused by shear-induced dilation of the clay around the tip, as the surrounding soil becomes overconsolidated during extraction.

Shaft pressures generally drop more gradually during extraction than tip pressures. This is not surprising, since unloading effects should have less influence on pore pressures around the shaft than on those near the tip. Therefore, after a small, initial pressure drop around the shaft due to soil suction, the subsequent, generally gradual reductions in shaft pressures are likely due to shear-induced dilation of the now-overconsolidated clay.

The pressures measured at the tip filter in the extraction record from TP2_P1 reflect the altered probe geometry utilized during this penetration. These pressures rise by approximately 100 kPa during the initial stages of extraction, and then drop rapidly to negative values as extraction continues. The altered location of the lower filter (now 6.7 cm above the tip) should reduce the influence of unloading effects; therefore, it is not surprising that a significant initial drop in pressure was not measured. However, it is not known why the pressures measured at this location actually increase significantly before eventually becoming negative.

For TP1_P5 and TP2_P2, the T2P remained in the borehole over night. It should be noted that pressures measured at the shaft during these extractions became significantly more negative than those measured at the shaft during the other extractions. Hence, there appears to be a correlation between shaft extraction pressures and the length of time the T2P remains embedded in the clay.

With the exception of TP1_P6, once the probe was removed from the boreholes and the filters were wiped clean of clay, pressures measured at both the tip and shaft returned to positive values. For TP1_P4 and TP1_P6, as previously mentioned, there was no final response measured at the tip; thus, the tip filter had to be replaced after these extractions.

Penetration	Date and Time of Reading	Input Voltage (V)	Tip Initial Zero Pressure Voltage (V)	Shaft Initial Zero Pressure Voltage (V)
TP1_P1	12/14 1:35pm	12.889	-4.889E-03	-5.444E-03
TP1_P2	12/16 7:56am	13.070	6.700E-03	-5.400E-03
TP1_P3	12/16 9:53am	12.941	6.688E-03	-5.802E-03
TP1_P4	12/16 11:45am	12.790	6.874E-03	-5.640E-03
TP1_P5	12/16 2:34pm	12.756	6.701E-03	-5.624E-03
TP1_P6	12/17 7:59am	12.302	7.072E-03	-5.133E-03
TP2_P1	12/17 10:23am	12.331	6.933E-03	-5.220E-03
TP2_P2	12/17 12:28pm	12.330	6.976E-03	-5.172E-03

Table 5.1 Initial Zero Pressure Voltages

Penetration Name	Detachment Time from Start of Dissipation
TP1_P1	330.1 seconds
TP1_P2	20.6 seconds
TP1_P3	16.0 seconds
TP1_P4	40.4 seconds
TP1_P5	10.0 seconds
TP1_P6	> 10 minutes*
TP2_P1	> 10 minutes*
TP2_P2	28.9 seconds

*The exact detachment times from the beginning of dissipation for TP1_P6 and TP2_P1 were not recorded.

Table 5.2 Time from the Beginning of Dissipation to the Moment the Cross Head Was Removed from the Drill String

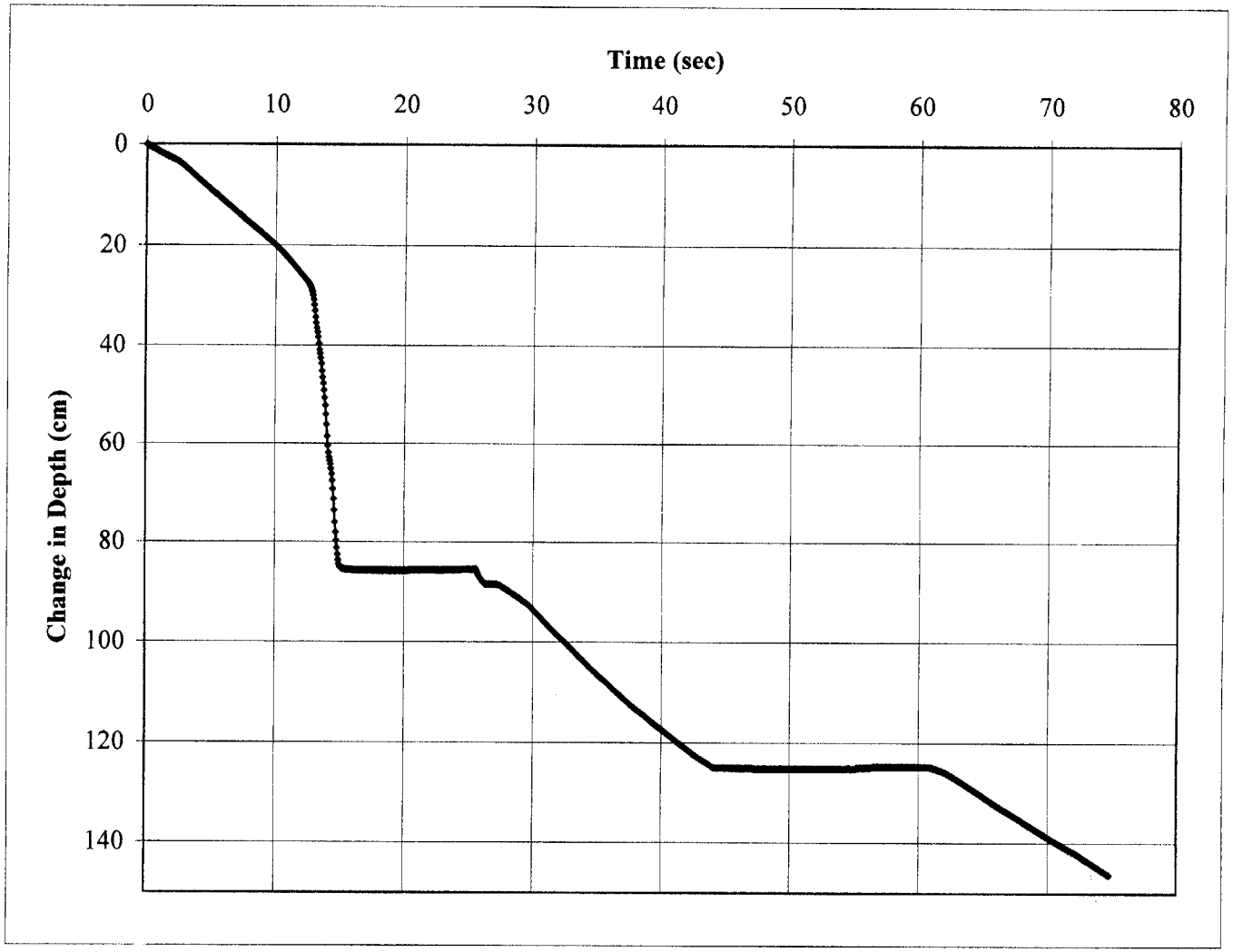

Figure 5.1 TP1_P1 Change in Depth vs. Time During Penetration

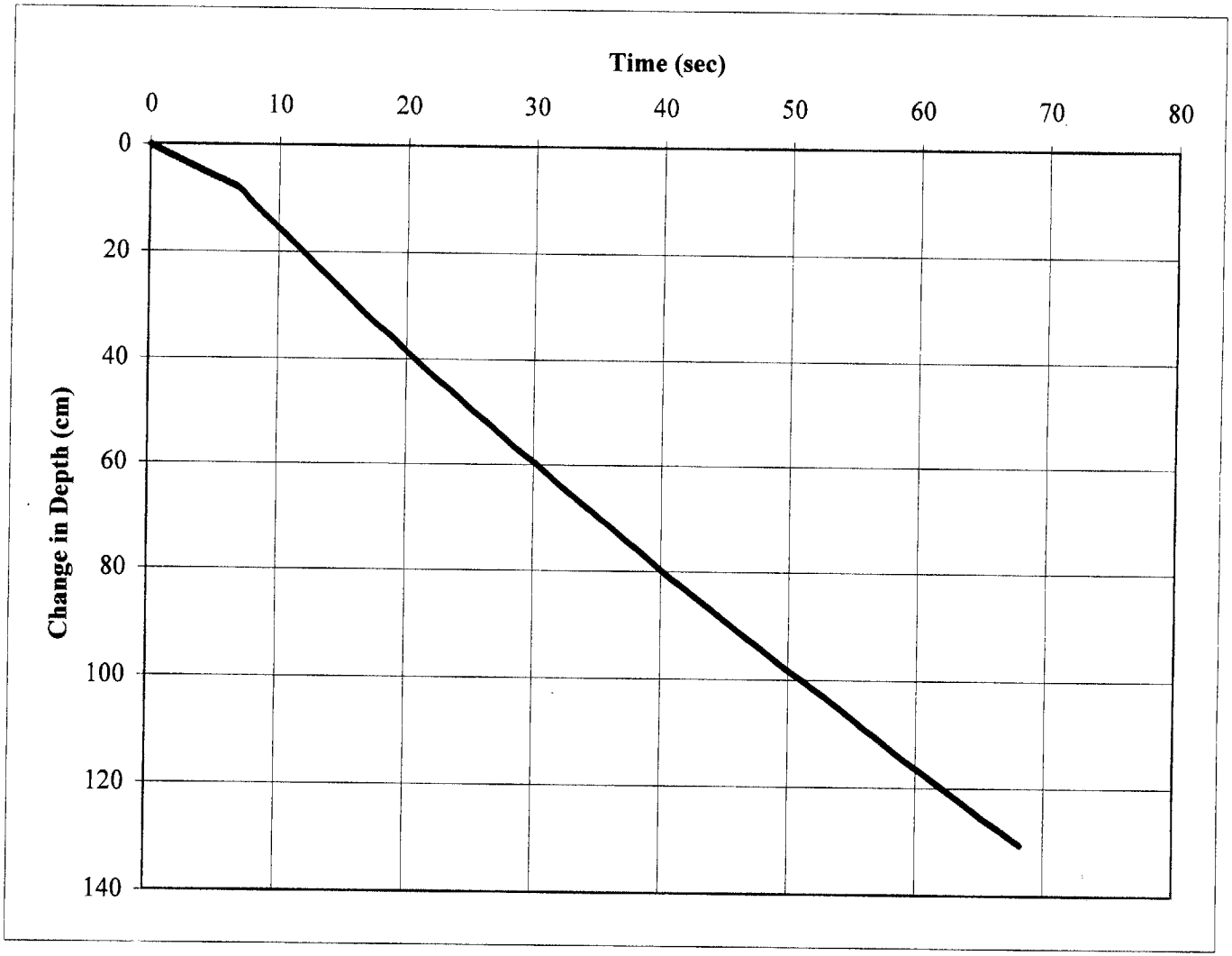

Figure 5.2 TP1_P2 Change in Depth vs. Time During Penetration

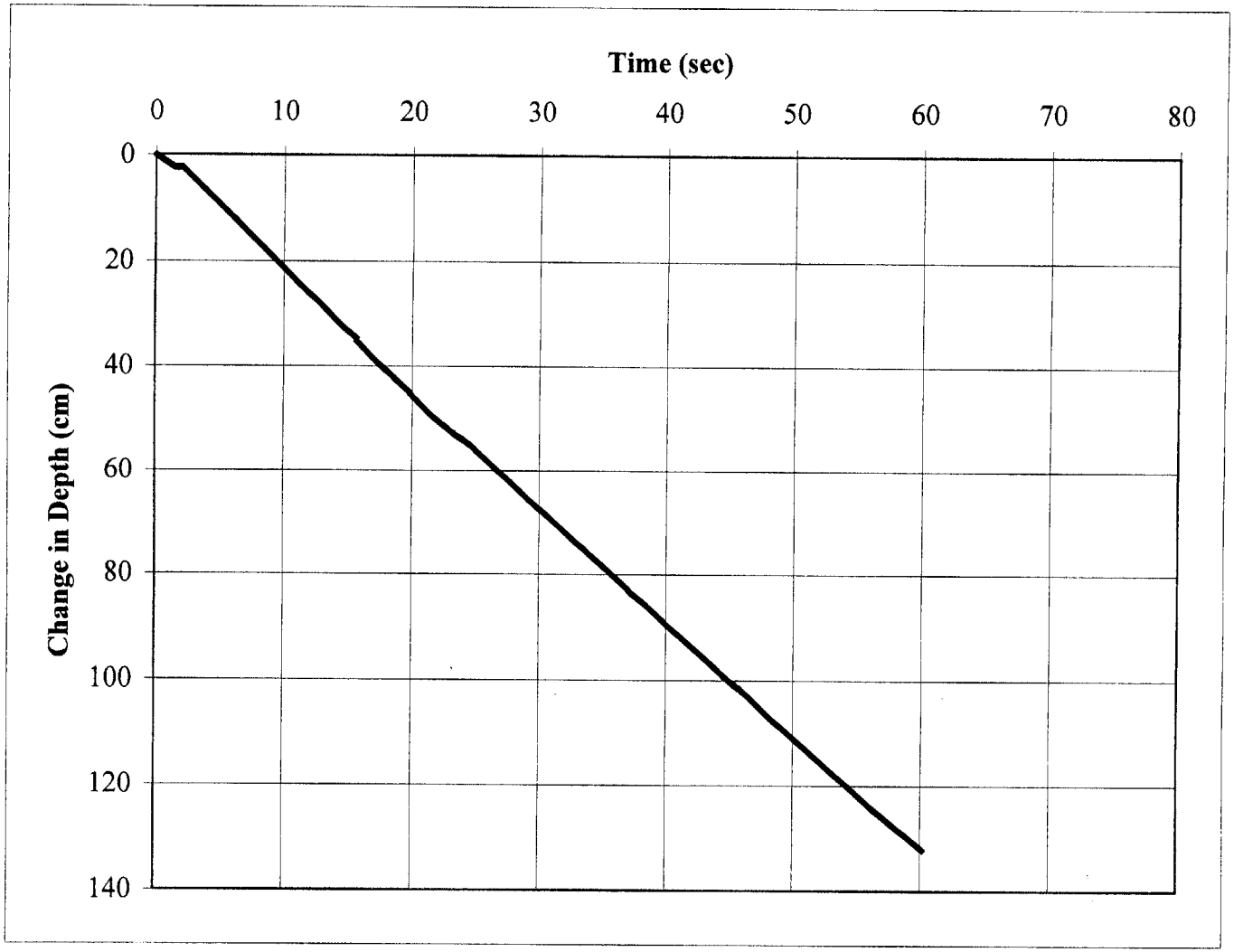

Figure 5.3 TP1_P3 Change in Depth vs. Time During Penetration

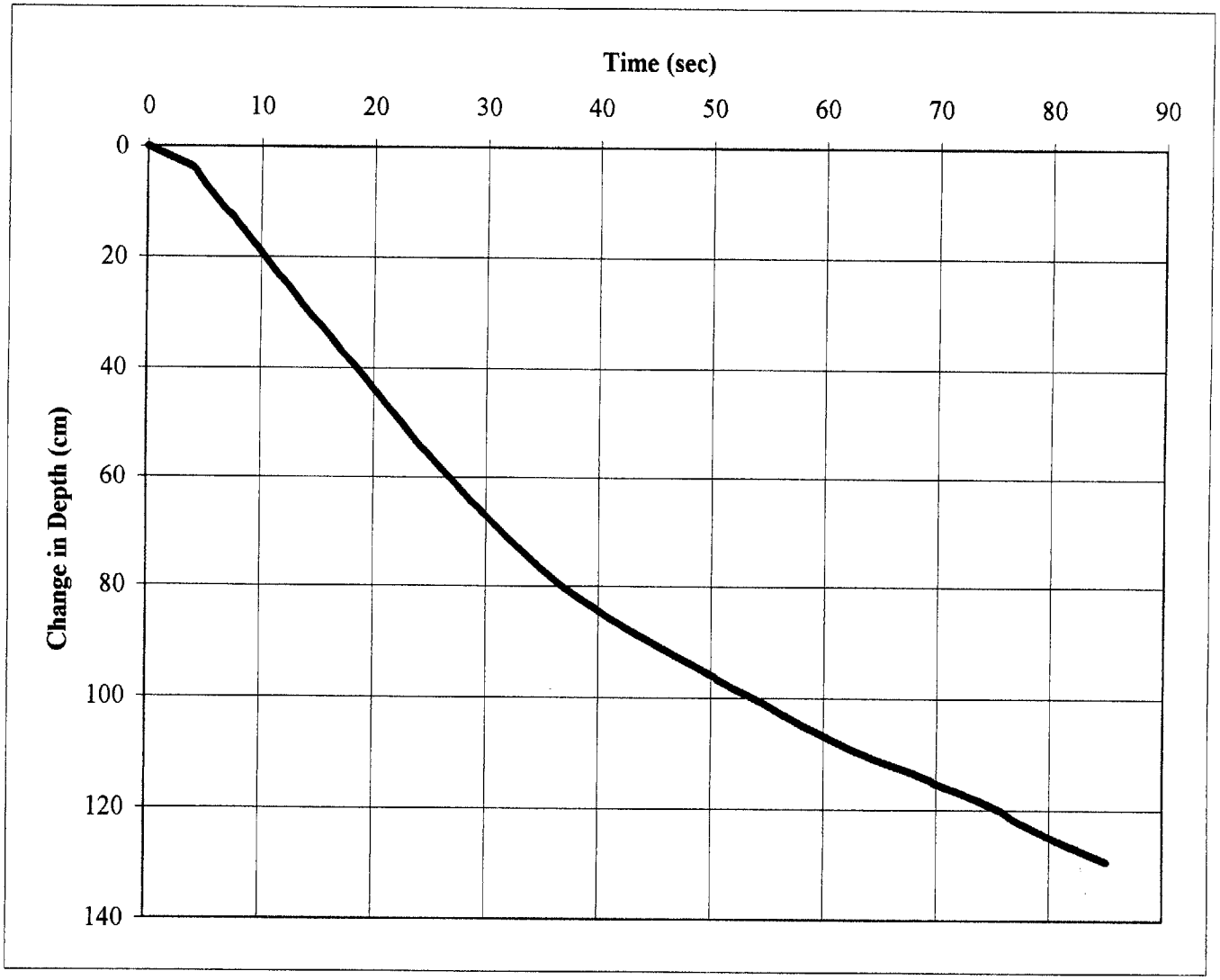

Figure 5.4 TP1_P4 Change in Depth vs. Time During Penetration

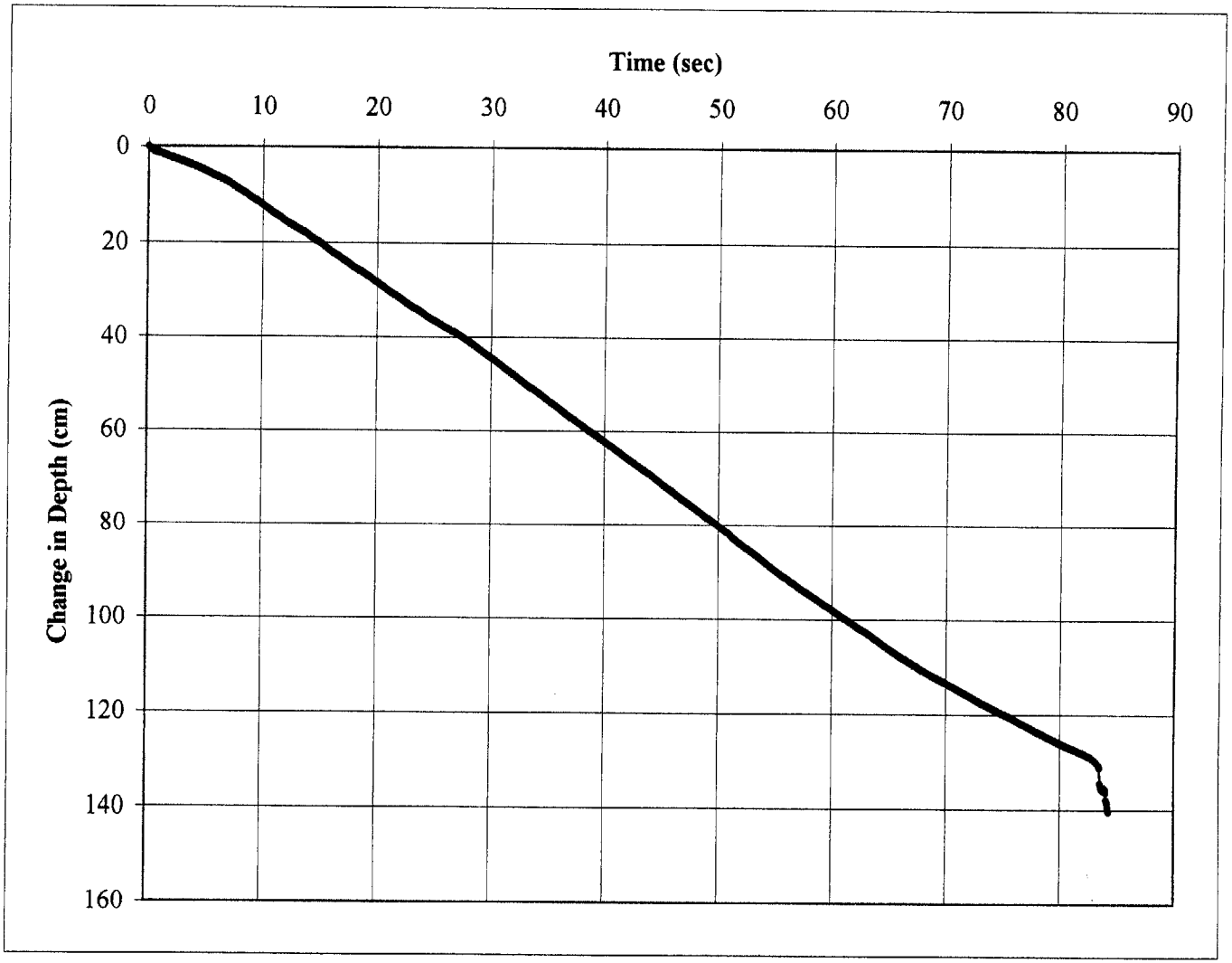

Figure 5.5 TP1_P5 Change in Depth vs. Time During Penetration

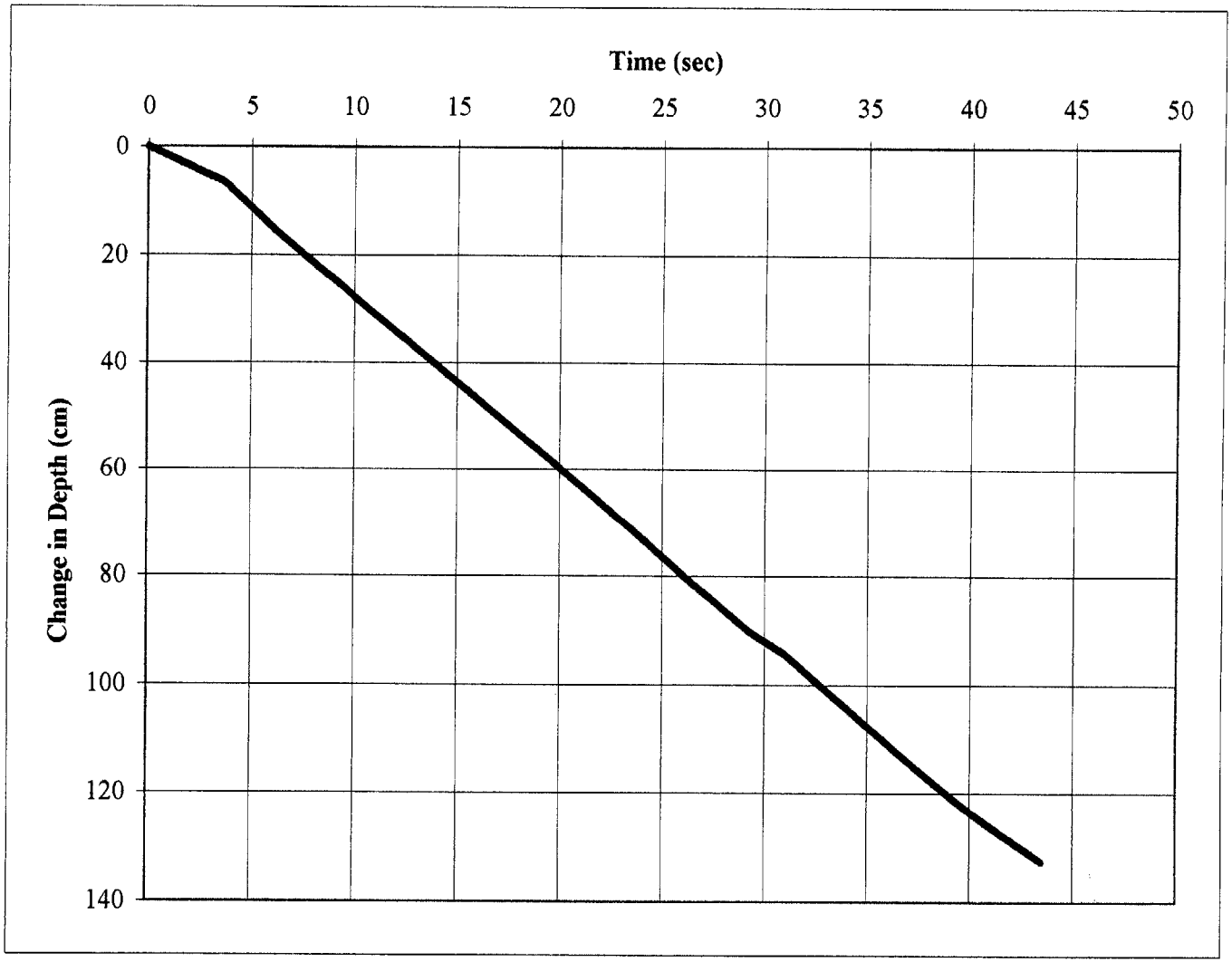

Figure 5.6 TP1_P6 Change in Depth vs. Time During Penetration

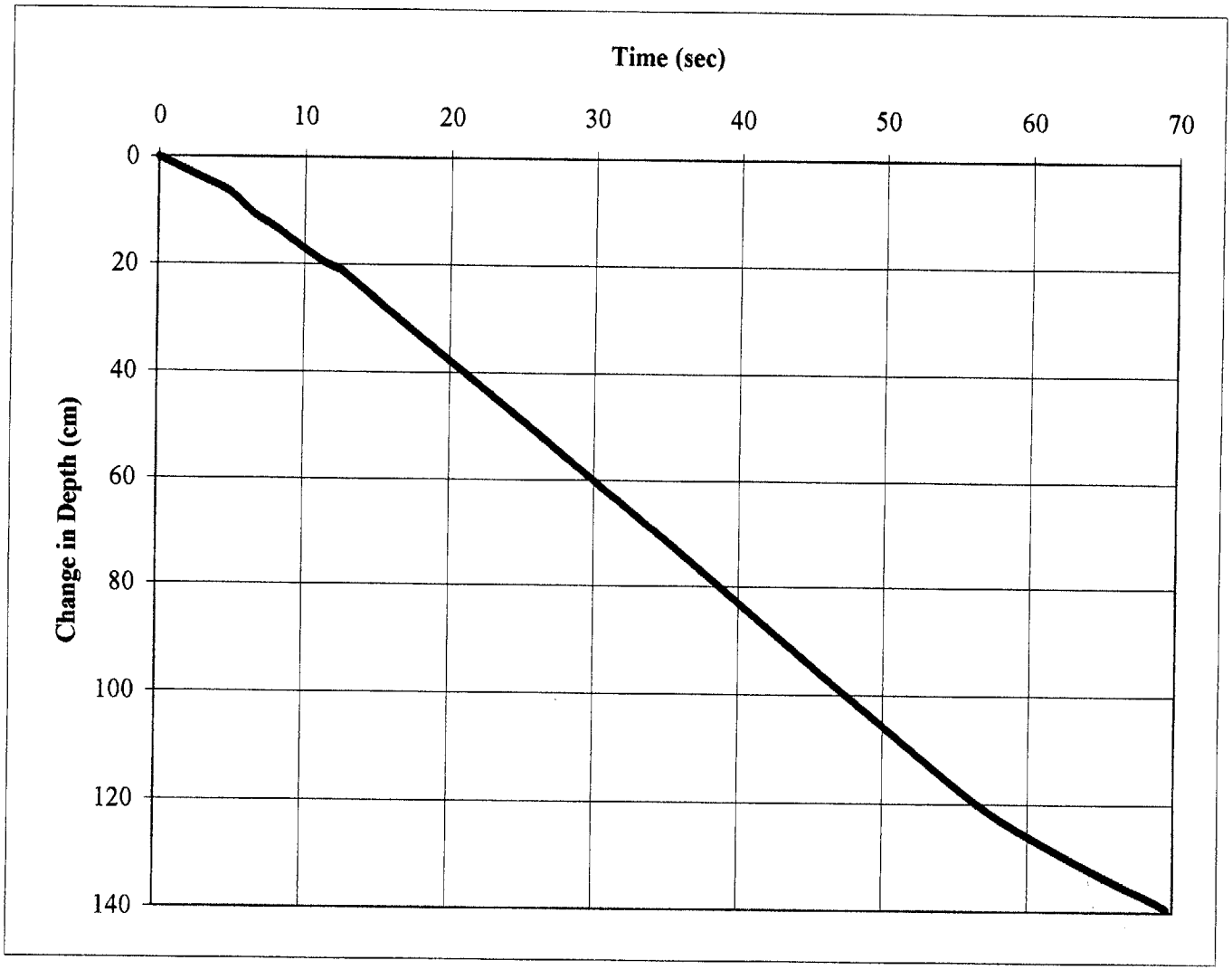

Figure 5.7 **TP2_P1 Change in Depth vs. Time During Penetration**

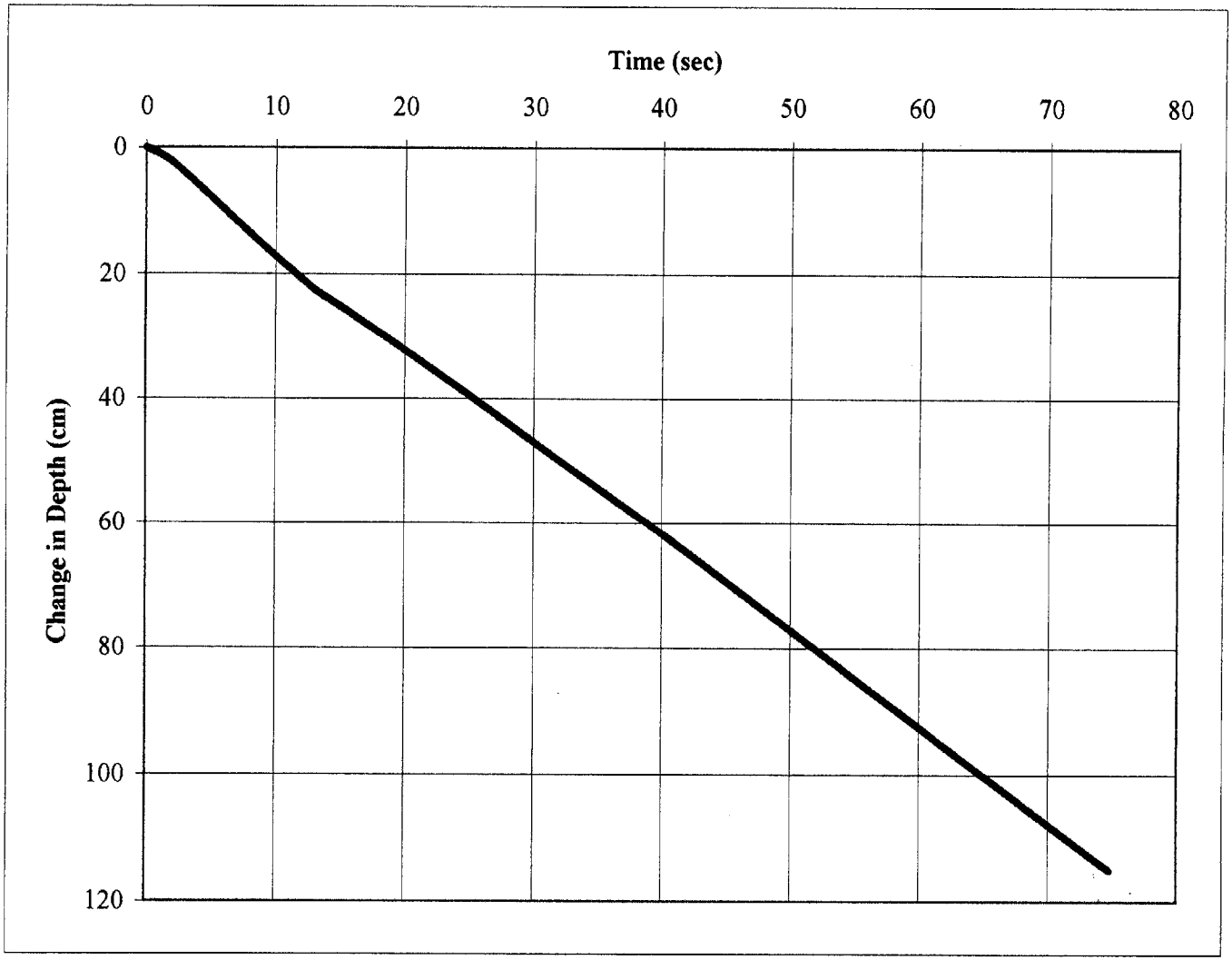

Figure 5.8 TP2_P2 Change in Depth vs. Time During Penetration

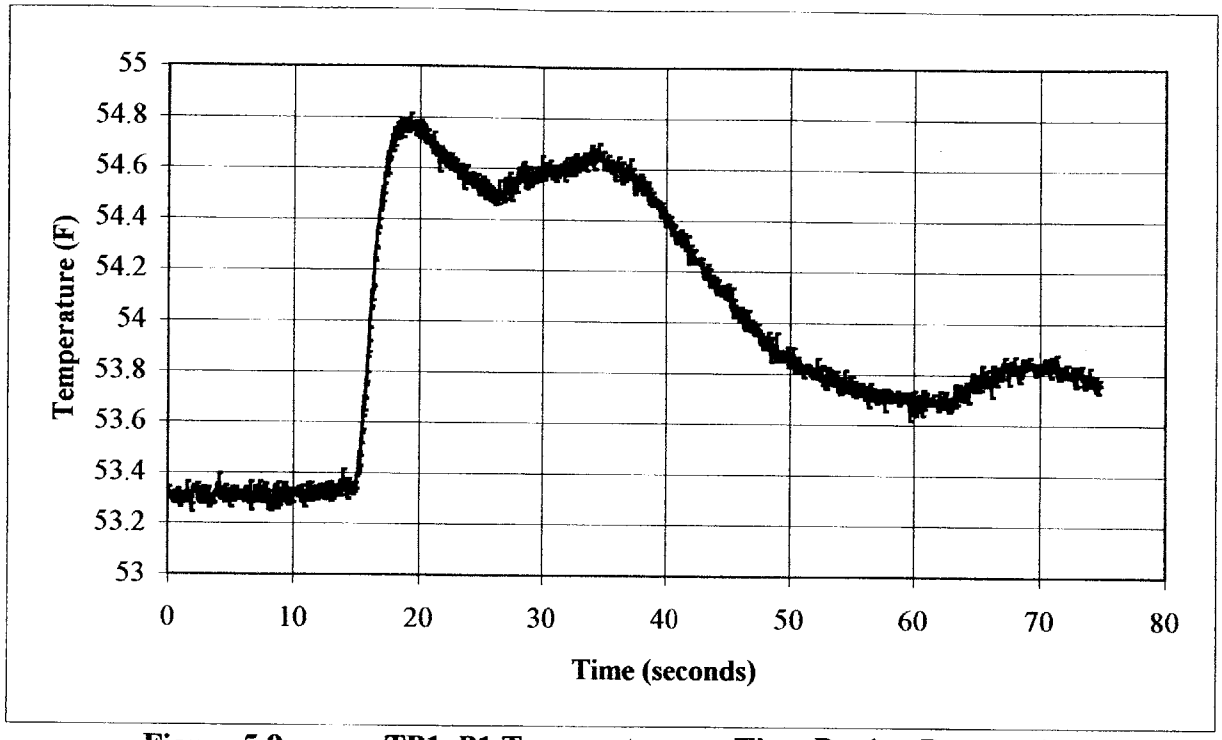

Figure 5.9a TP1_P1 Temperature vs. Time During Penetration

b) Depth vs. Time During Penetration

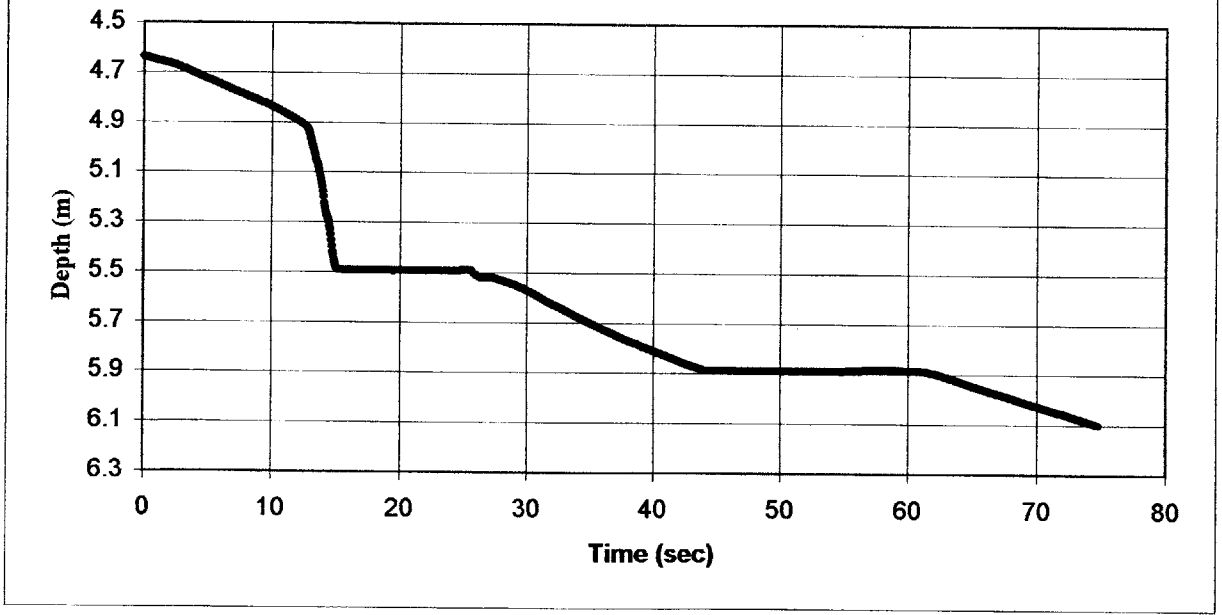

Figure 5.9b TP1_P1 Depth vs. Time During Penetration

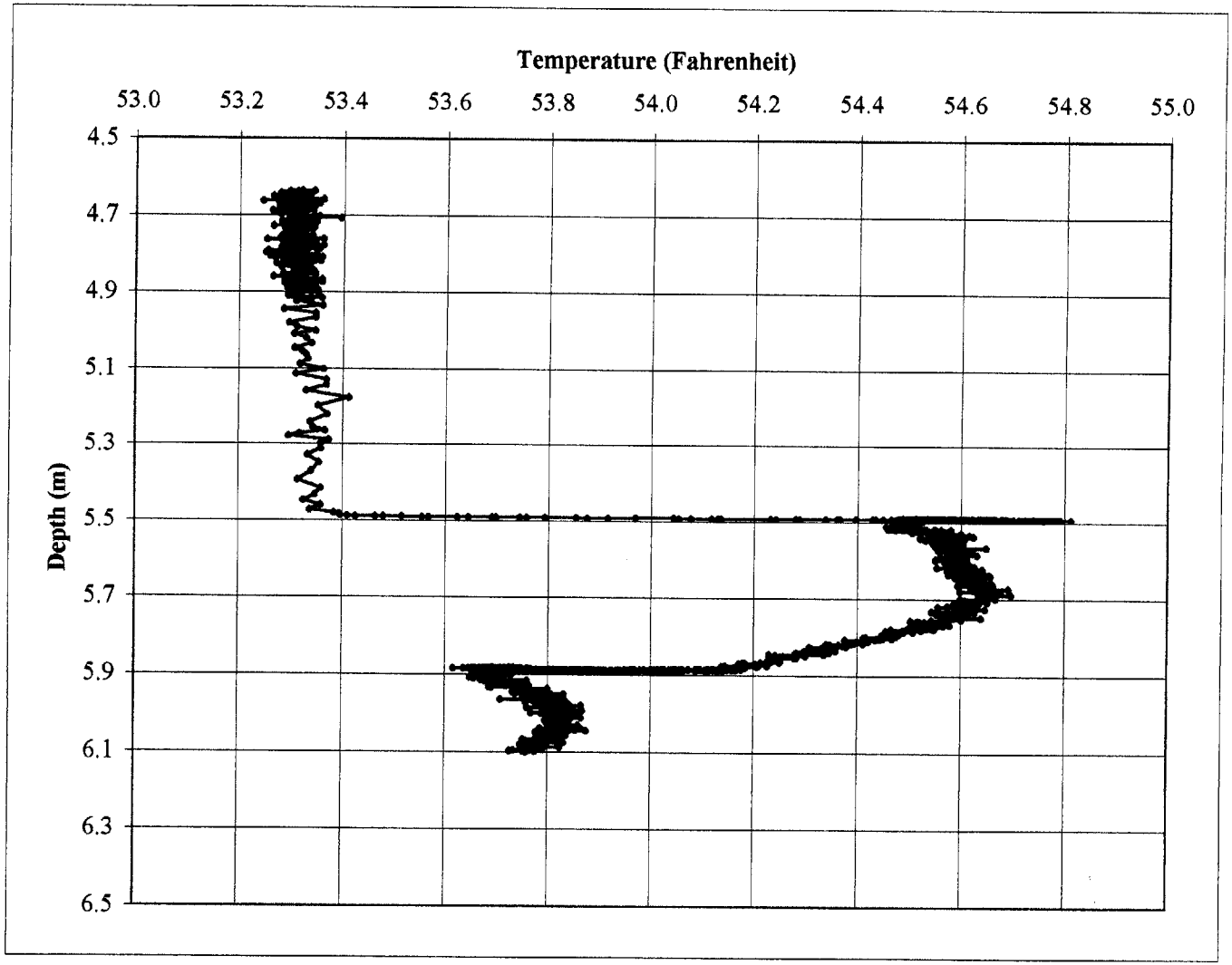

Figure 5.9c TP1_P1 Temperature vs. Depth During Penetration

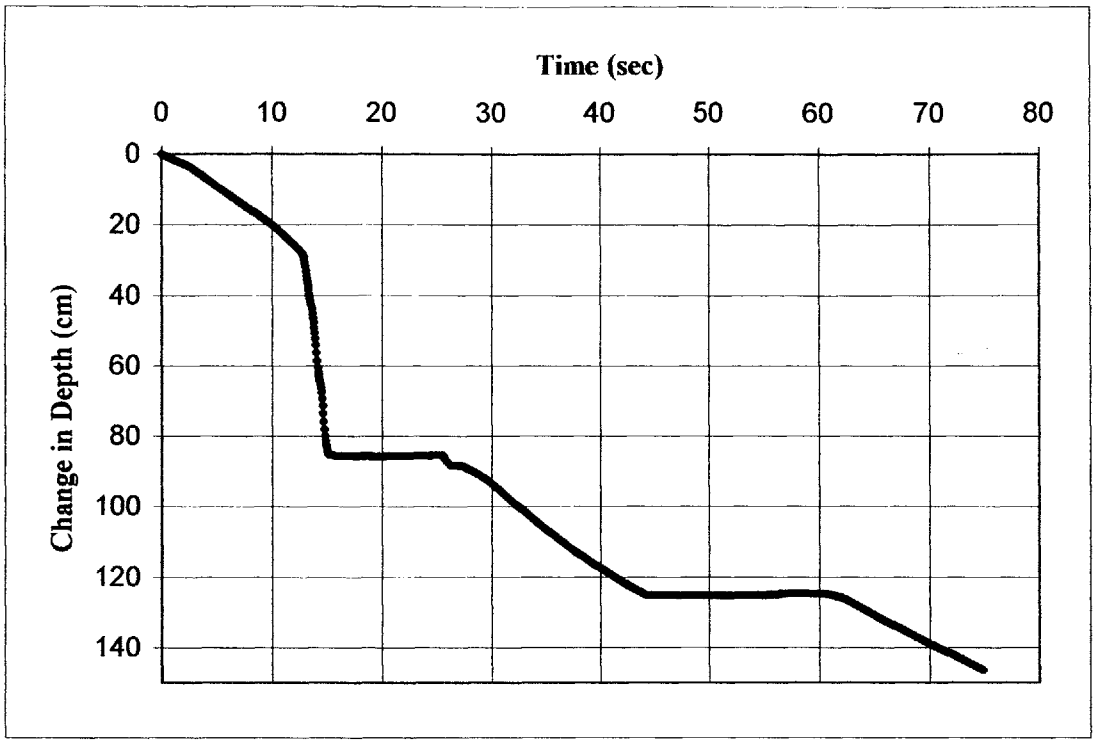

Figure 5.10a TP1_P1 Change in Depth vs. Time During Penetration

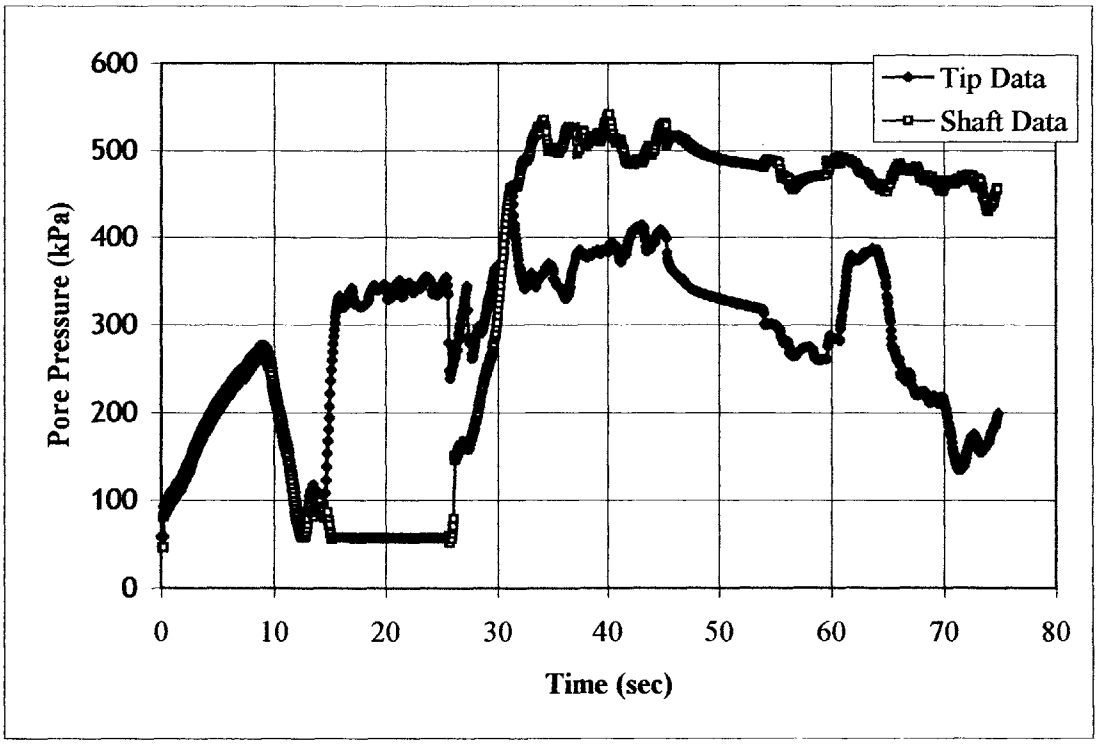

Figure 5.10b TP1_P1 Penetration Pore Pressure vs. Time

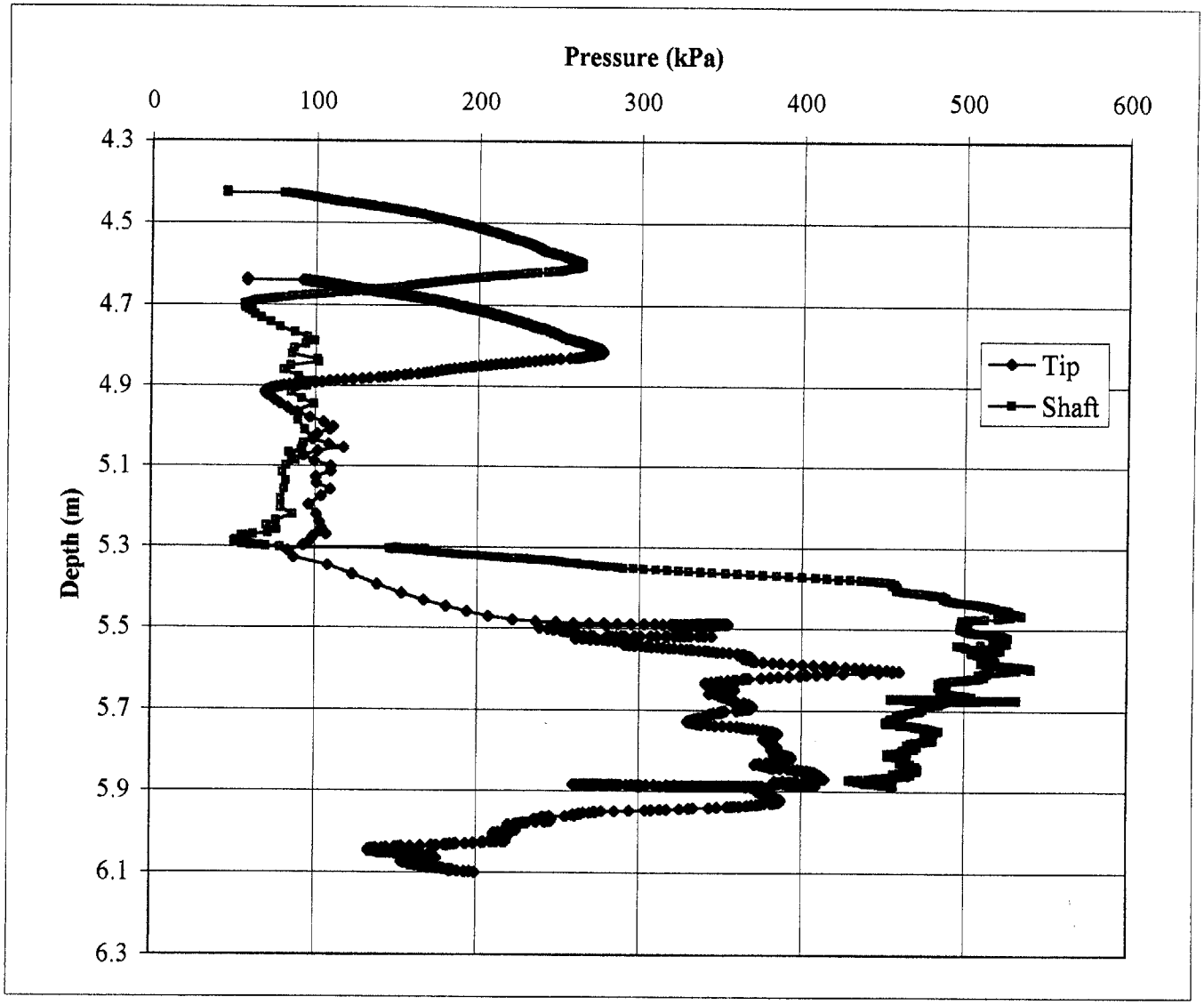

Figure 5.10c TP1_P1 Pressure vs. Depth During Penetration

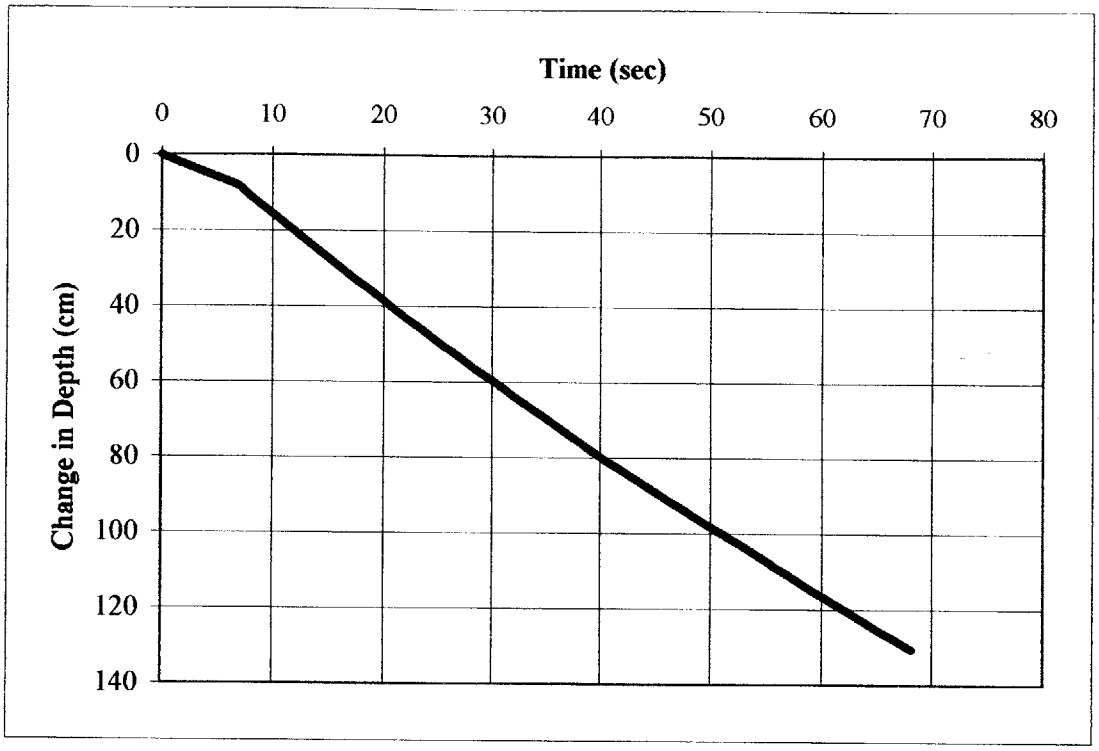

Figure 5.11a TP1_P2 Change in Depth vs. Time During Penetration

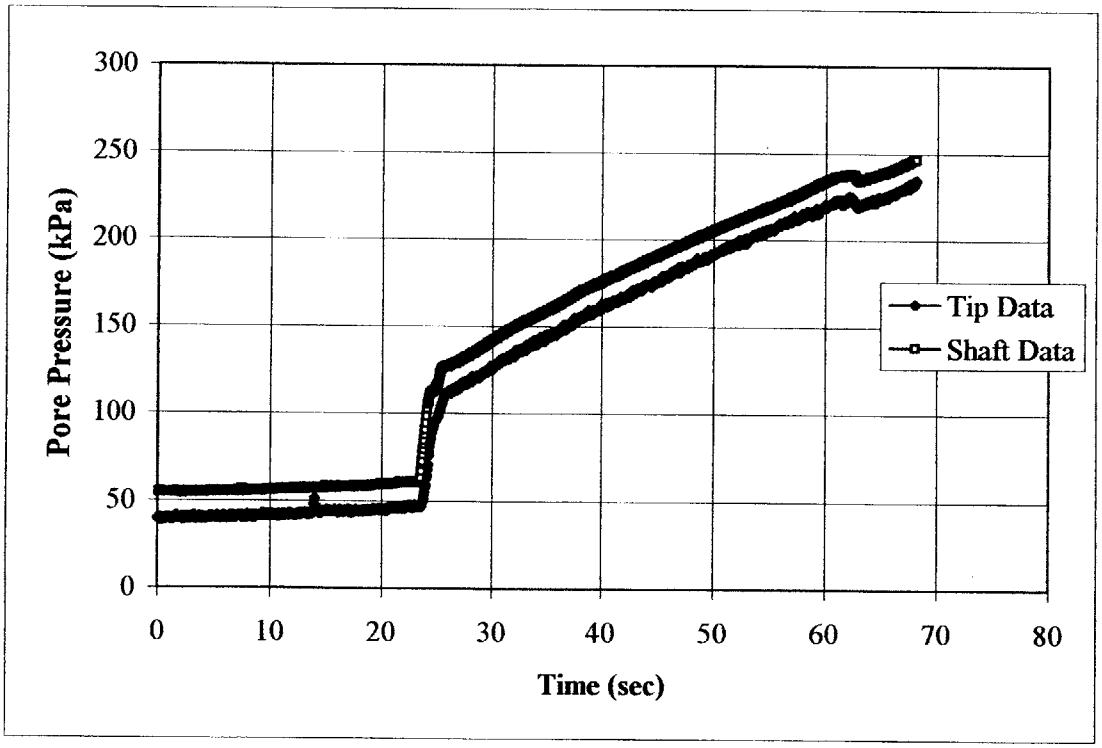

Figure 5.11b TP1_P2 Penetration Pore Pressure vs. Time

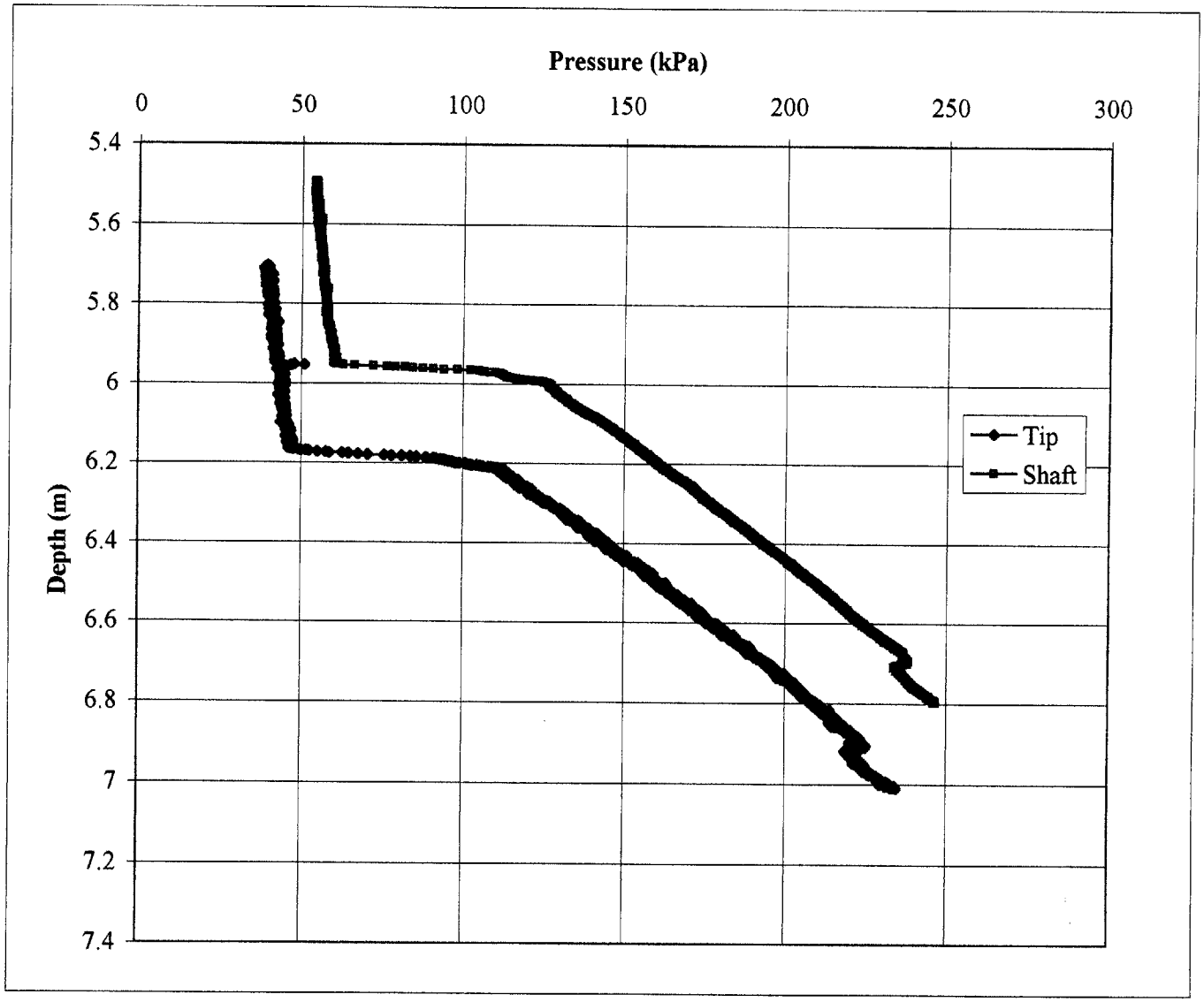

Figure 5.11c TP1_P2 Pressure vs. Depth During Penetration

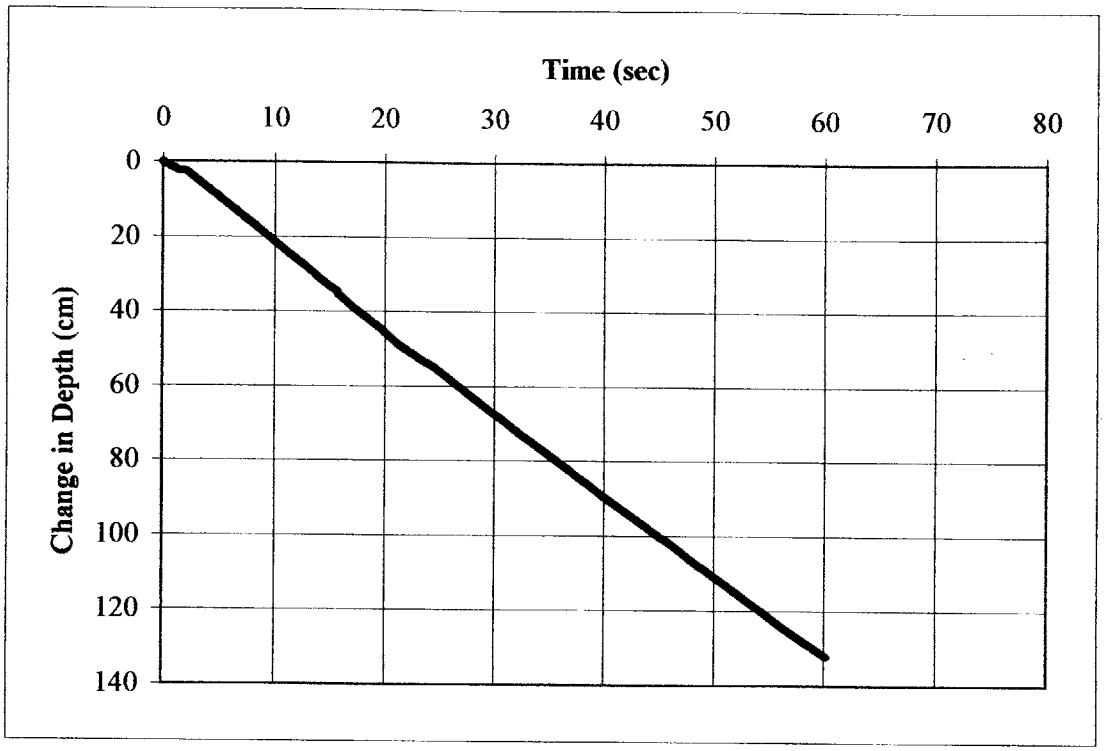

Figure 5.12a **TP1_P3 Change in Depth vs. Time During Penetration**

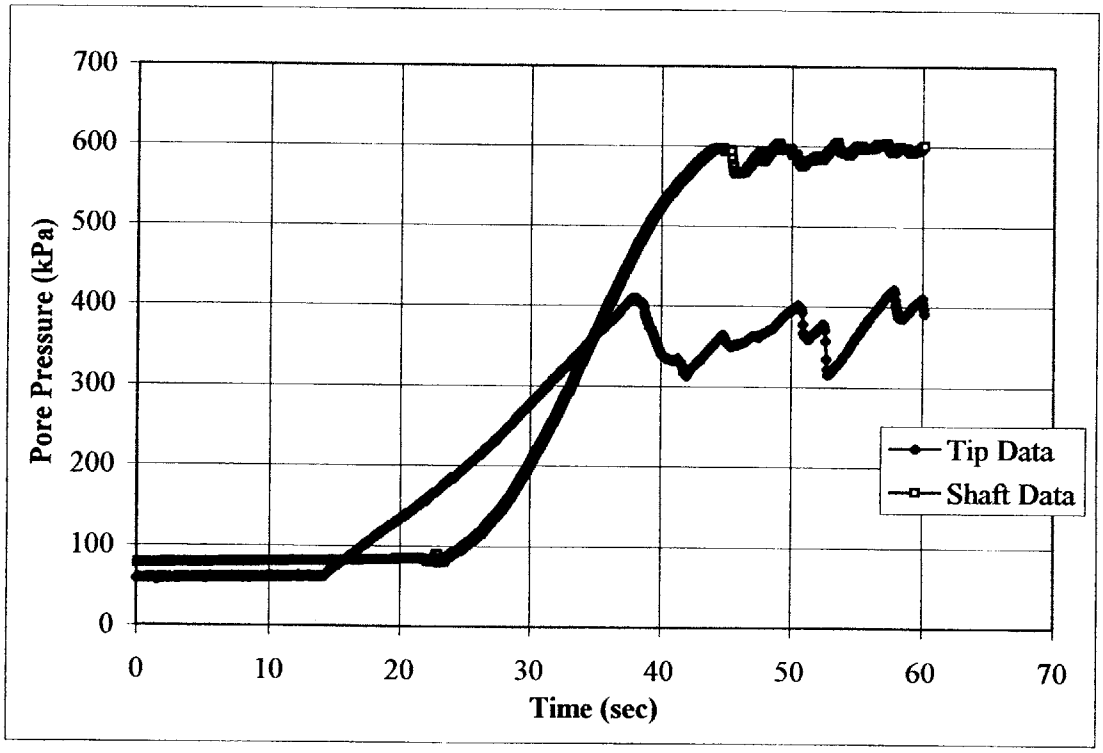

Figure 5.12b **TP1_P3 Penetration Pore Pressure vs. Time**

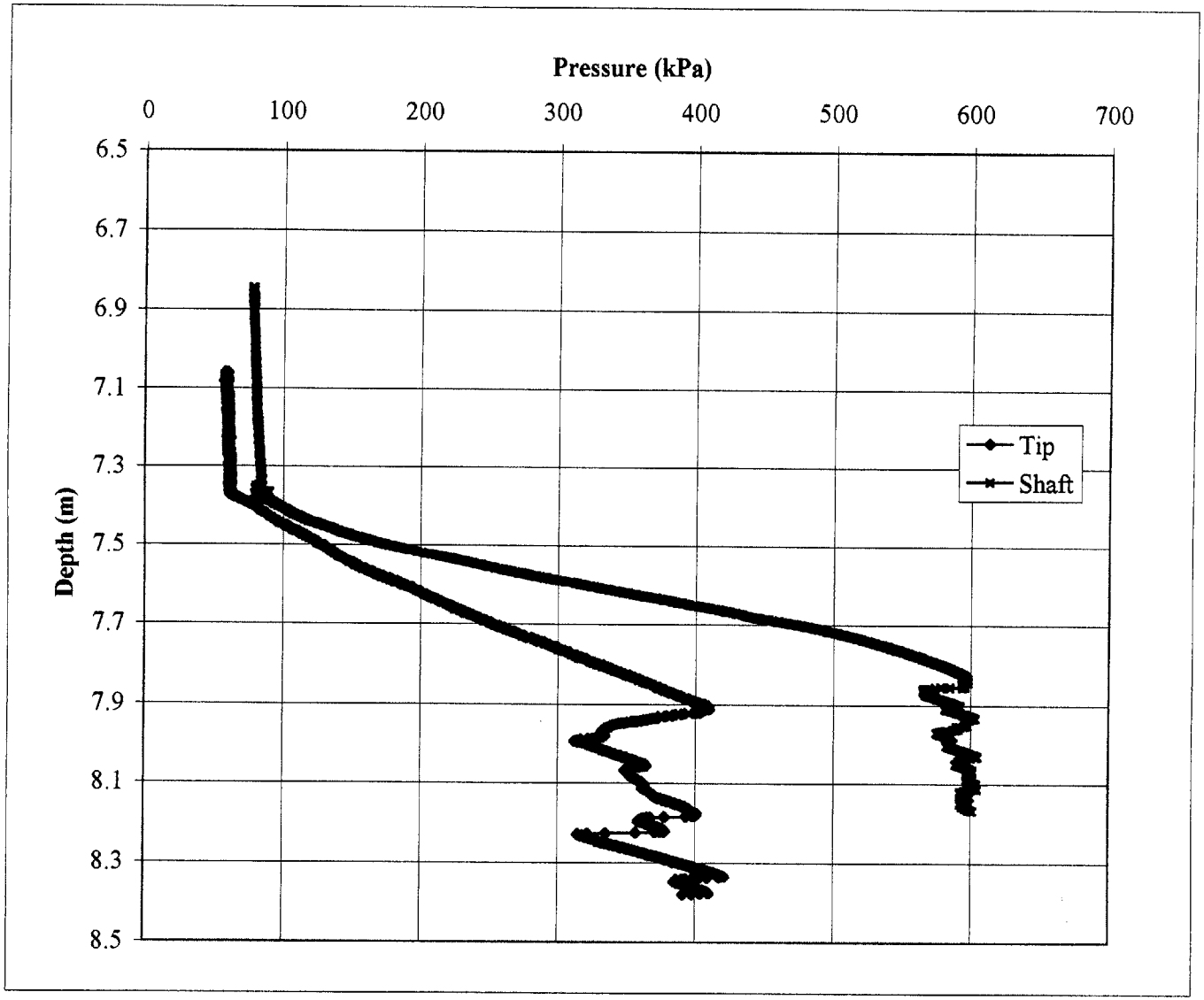

Figure 5.12c TP1_P3 Pressure vs. Depth During Penetration

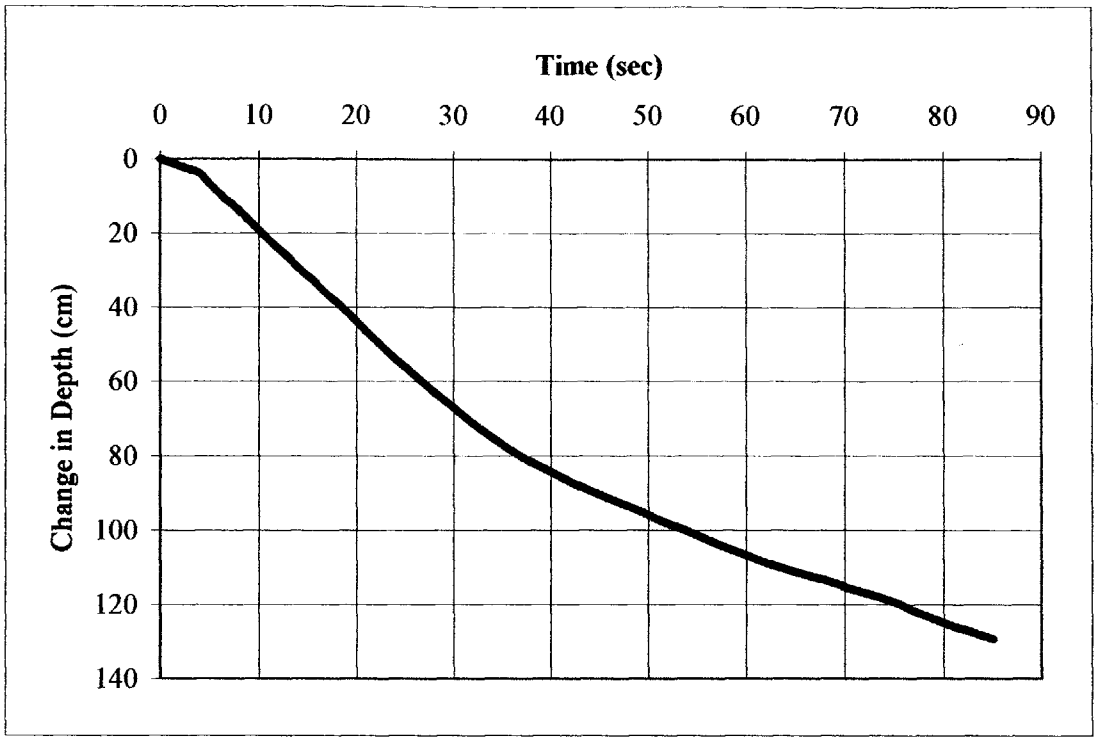

Figure 5.13a TP1_P4 Change in Depth vs. Time During Penetration

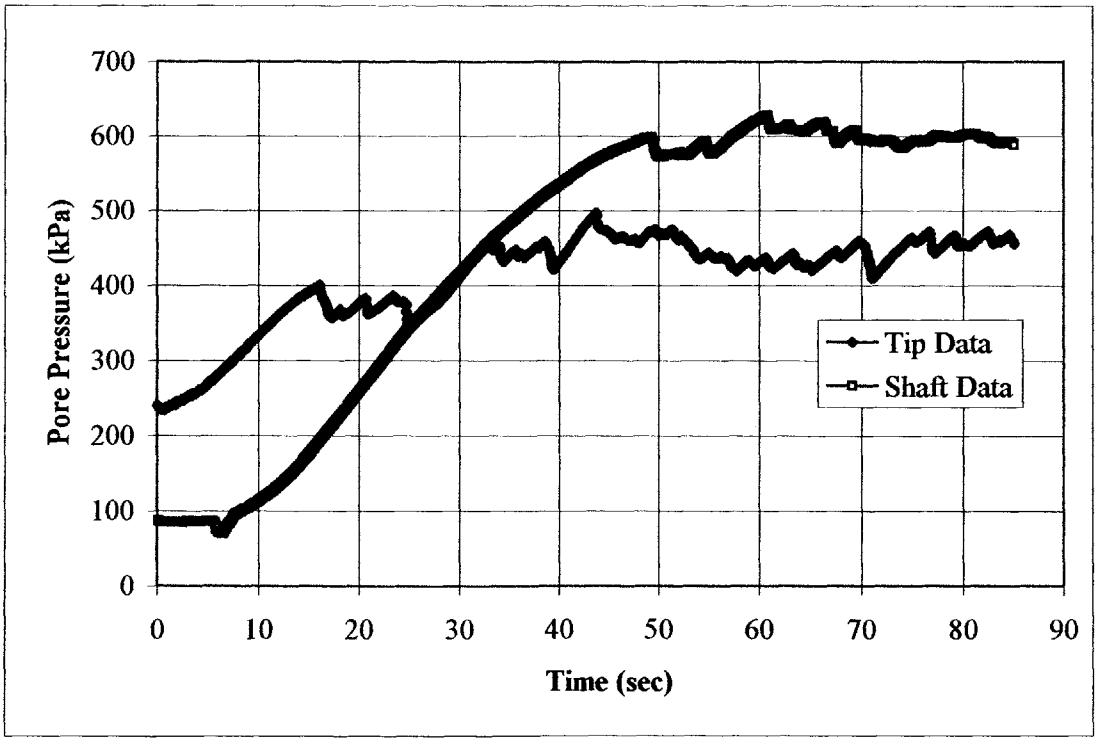

Figure 5.13b TP1_P4 Penetration Pore Pressure vs. Time

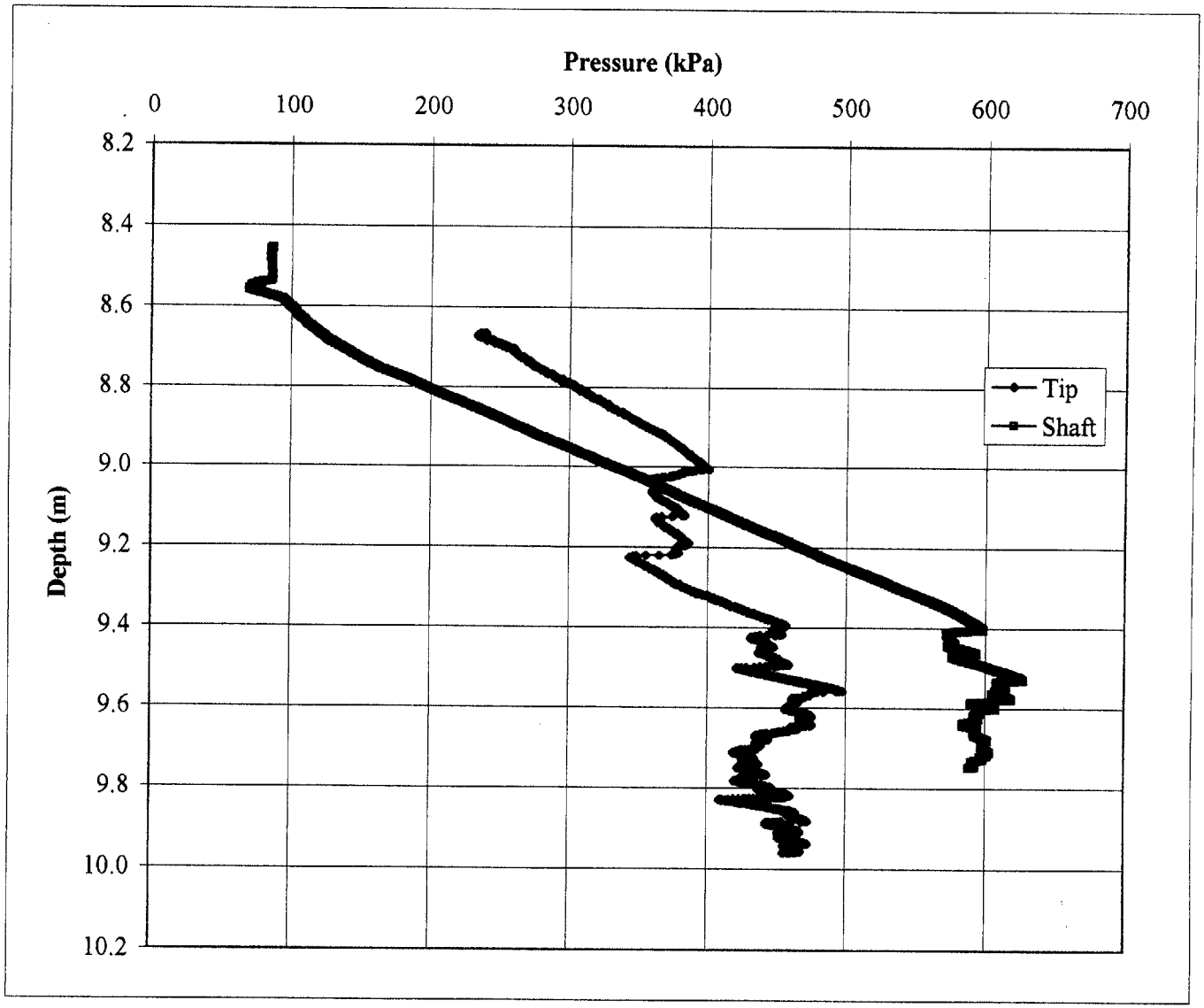

Figure 5.13c TP1_P4 Pressure vs. Depth During Penetration

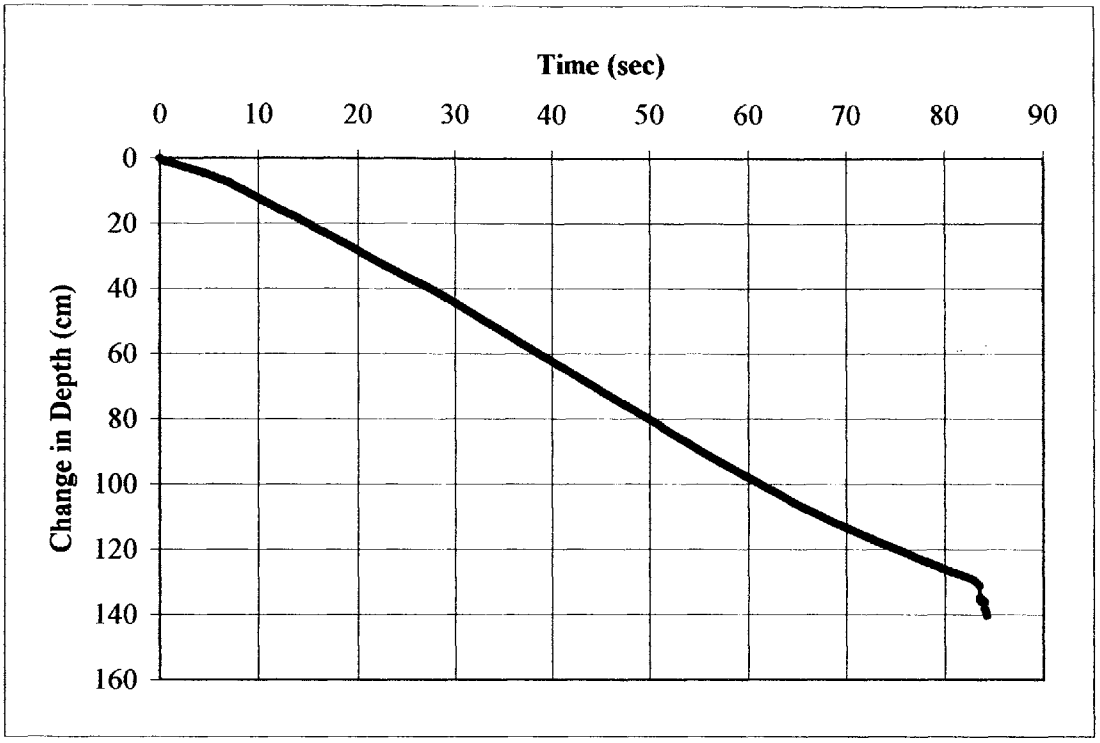

Figure 5.14a TP1_P5 Change in Depth vs. Time During Penetration

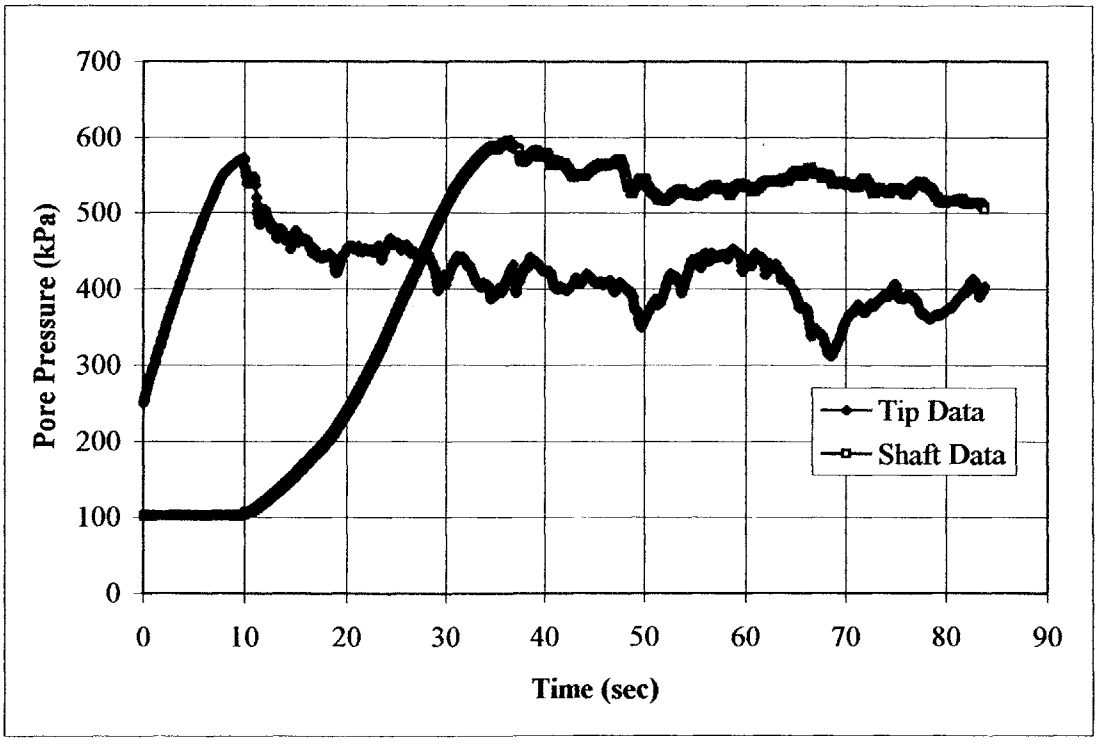

Figure 5.14b TP1_P5 Penetration Pore Pressure vs. Time

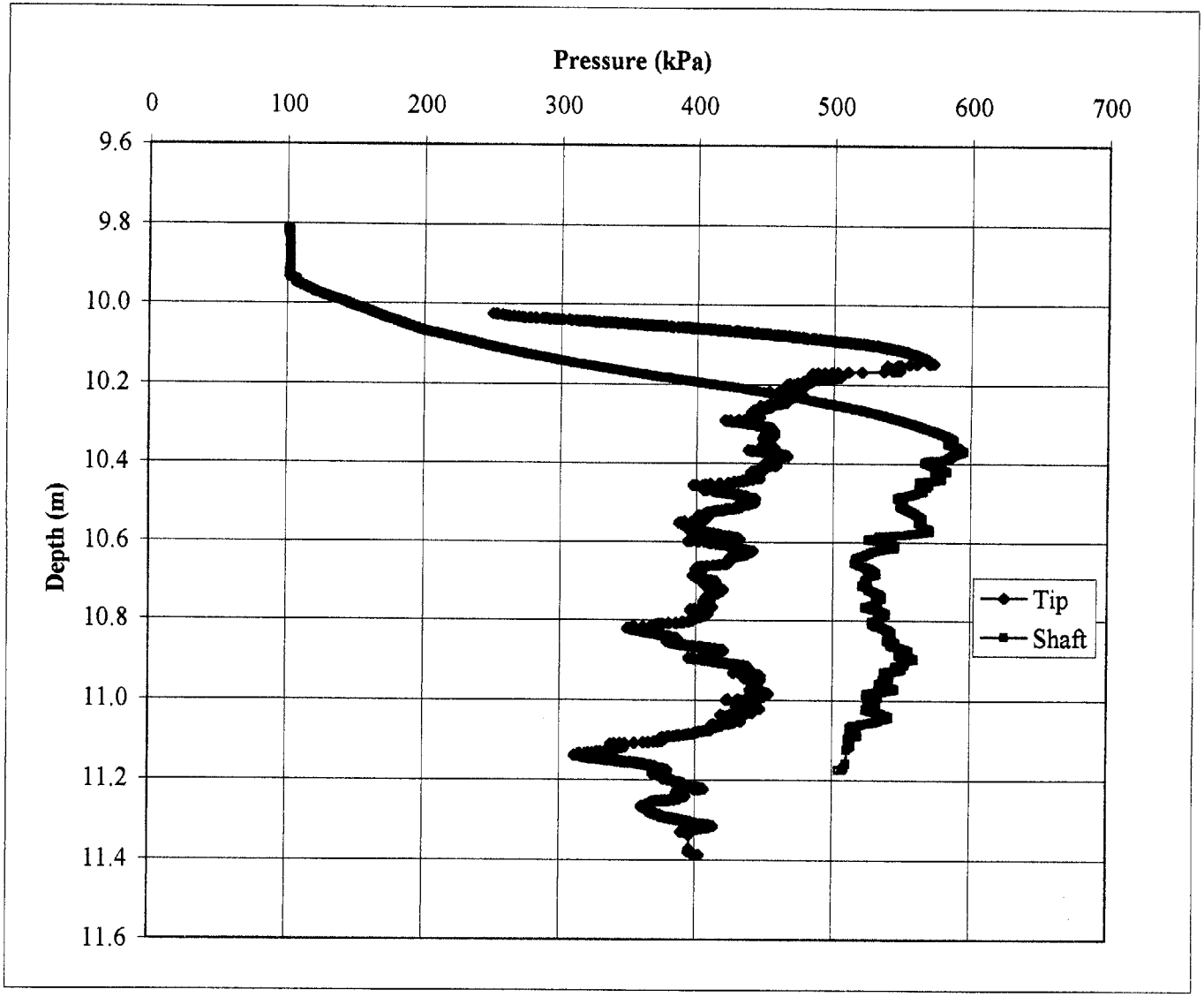

Figure 5.14c TP1_P5 Pressure vs. Depth During Penetration

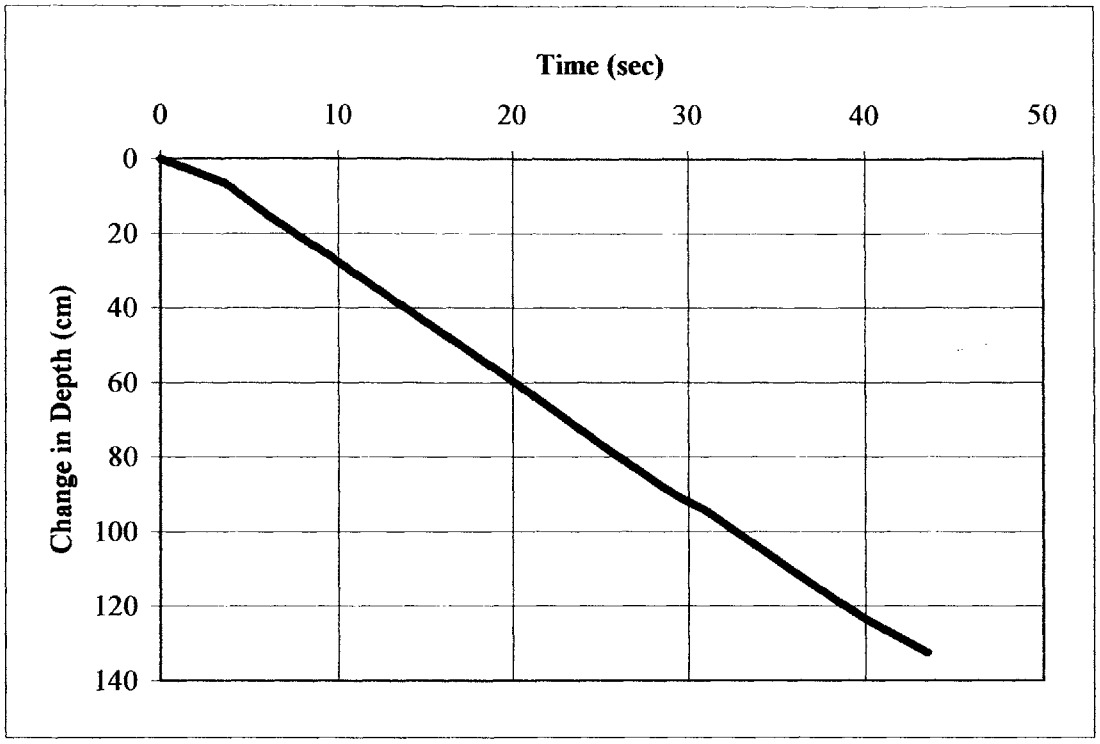

Figure 5.15a TP1_P6 Change in Depth vs. Time During Penetration

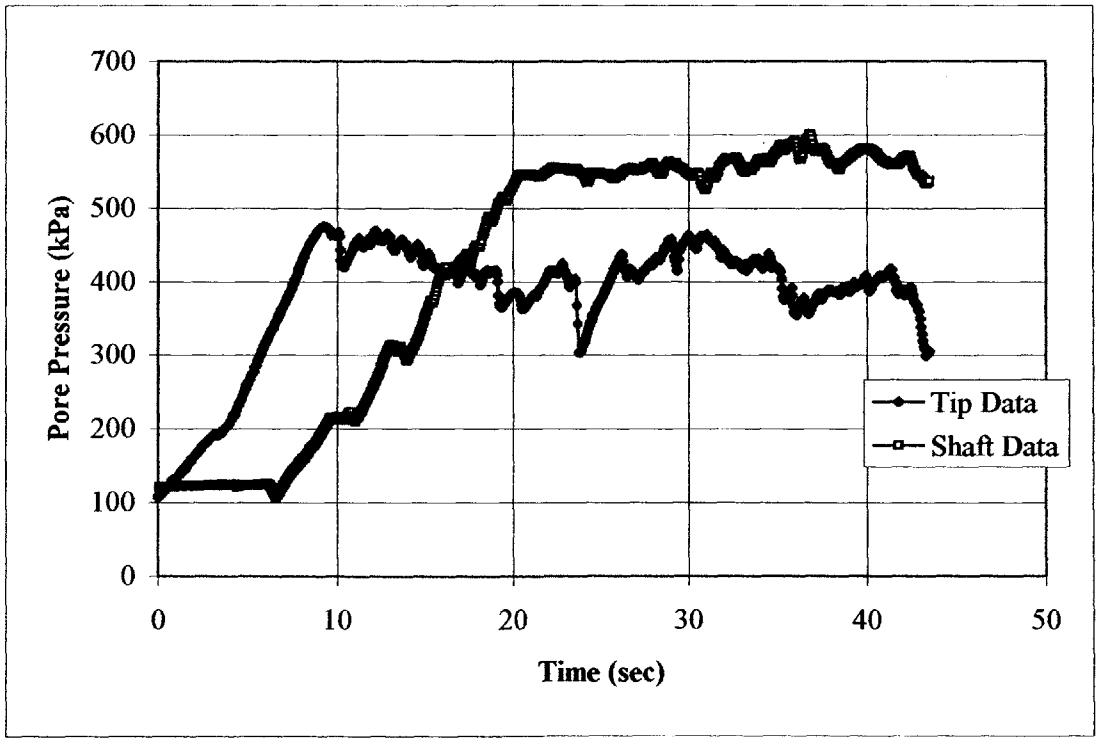

Figure 5.15b TP1_P6 Penetration Pore Pressure vs. Time

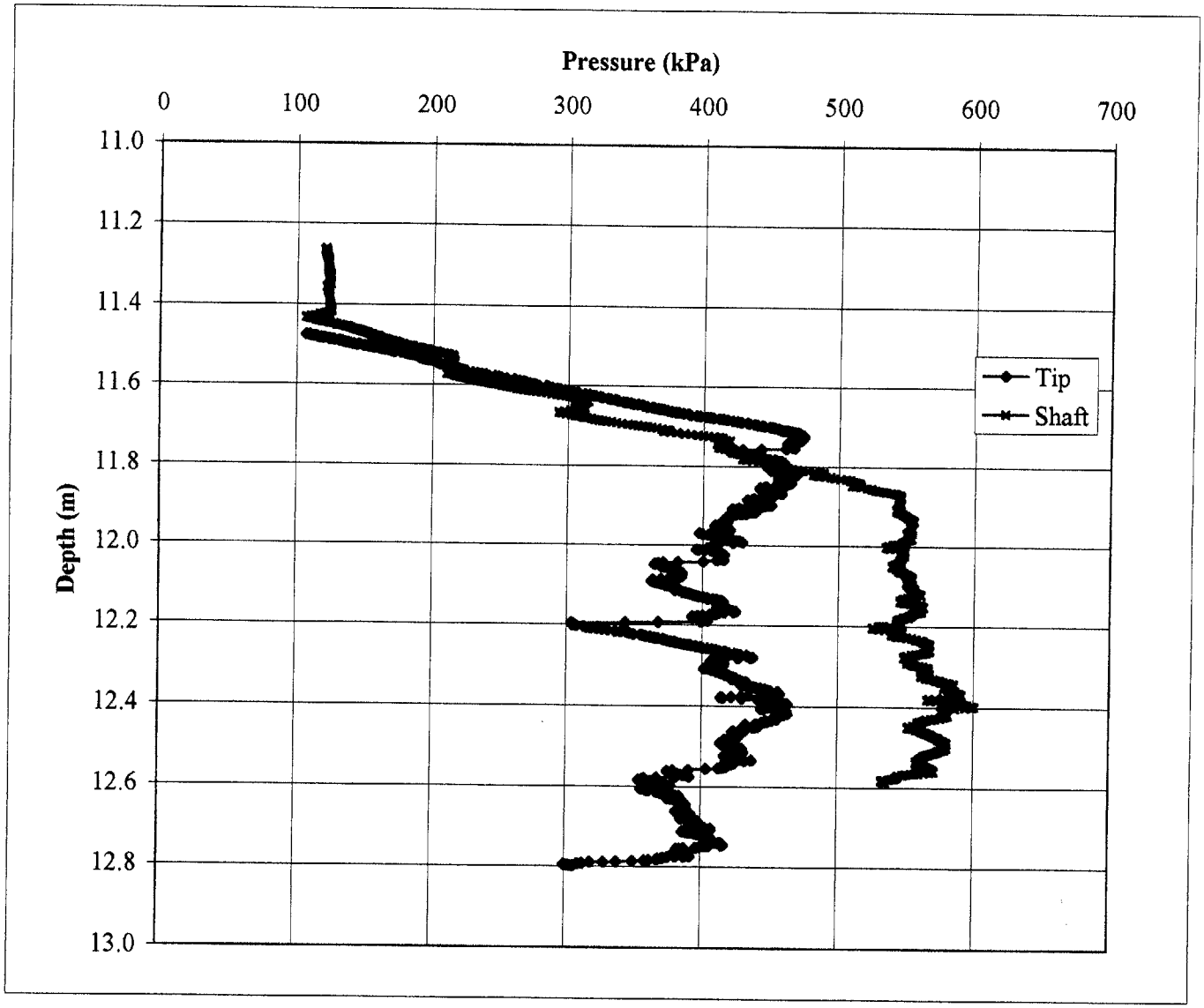

Figure 5.15c TP1_P6 Pressure vs. Depth During Penetration

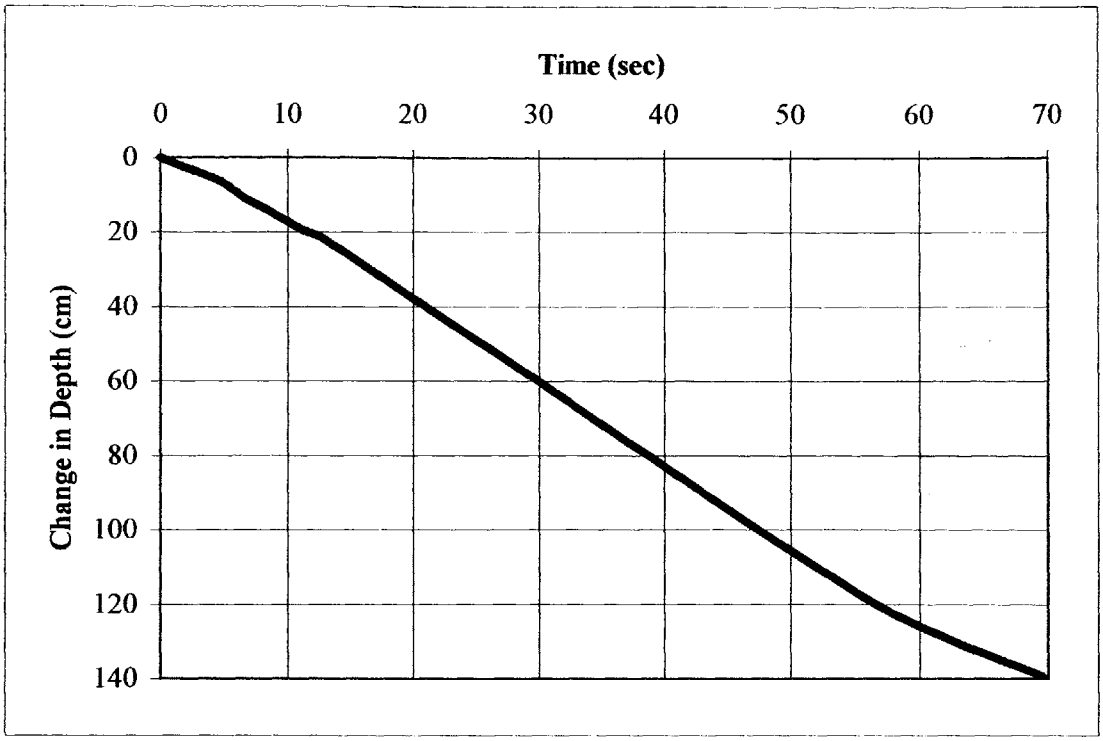

Figure 5.16a TP2_P1 Change in Depth vs. Time During Penetration

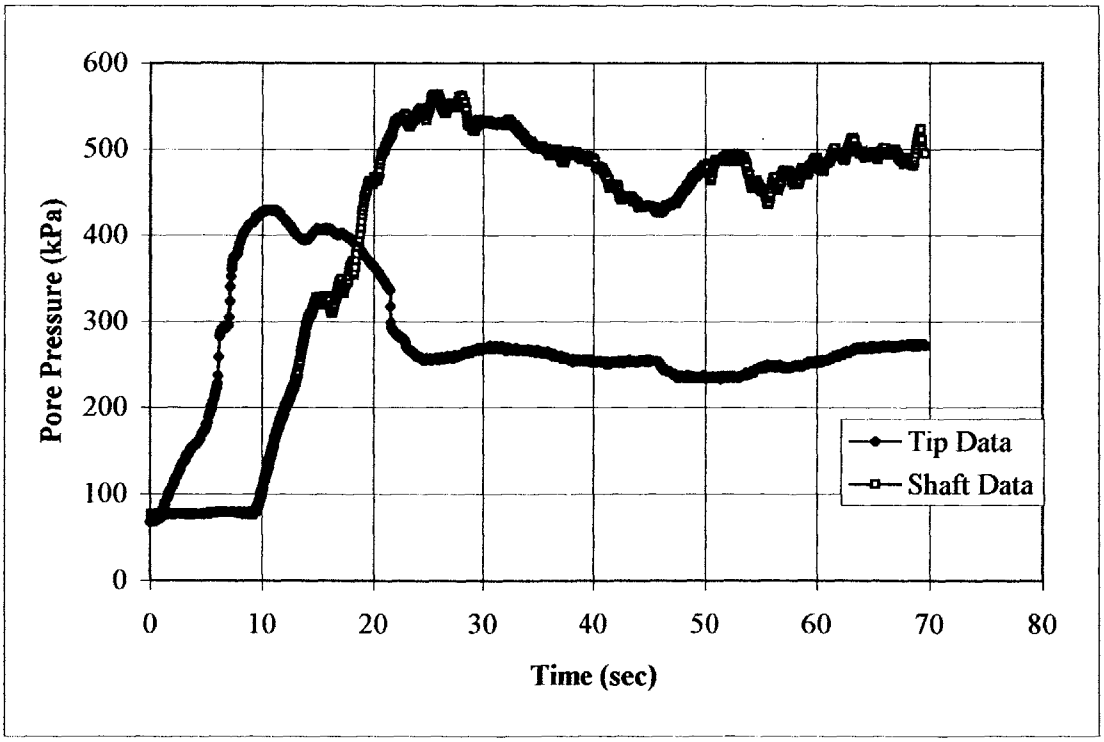

Figure 5.16b TP2_P1 Penetration Pore Pressure vs. Time

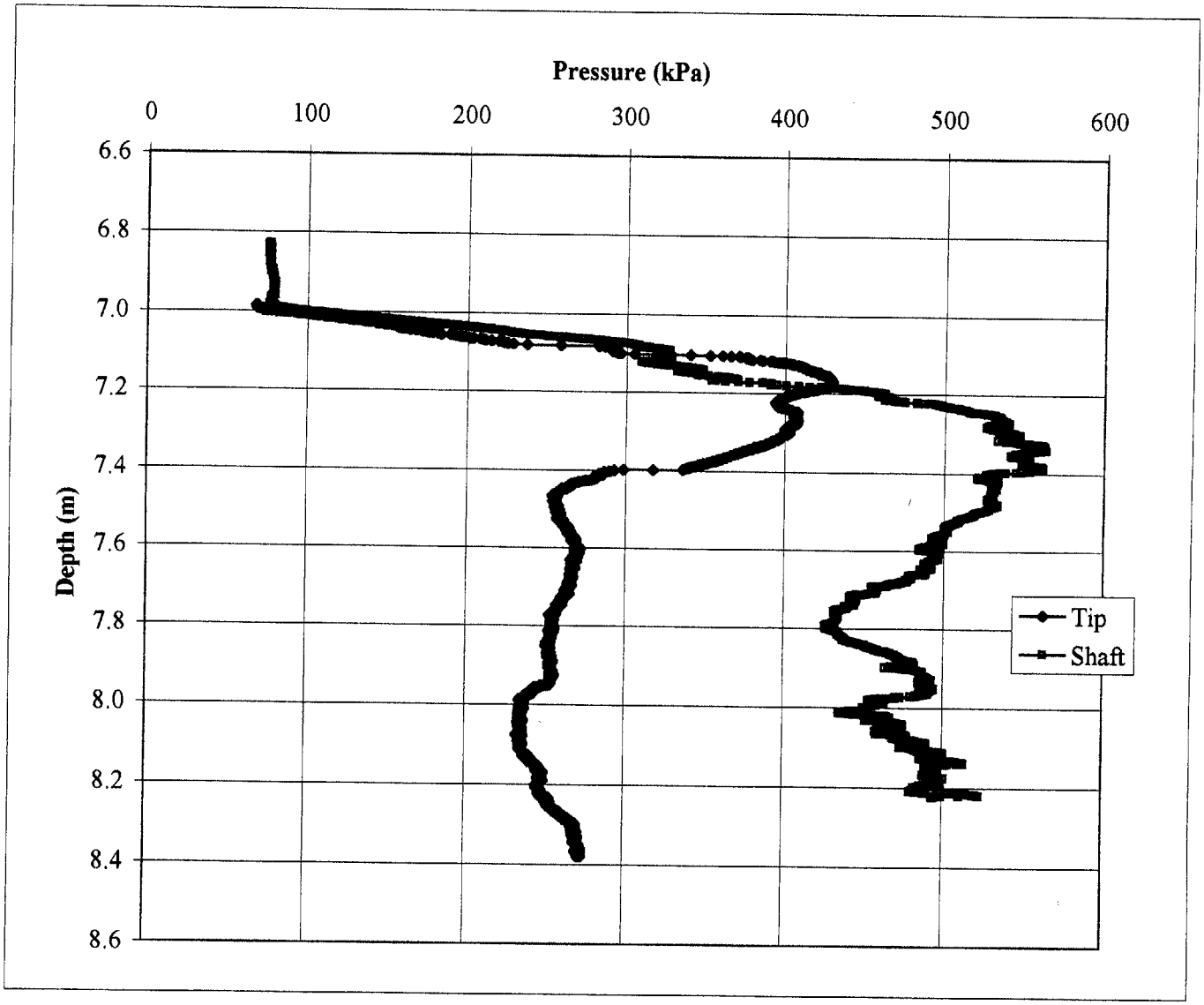

Figure 5.16c TP2_P1 Pressure vs. Depth During Penetration

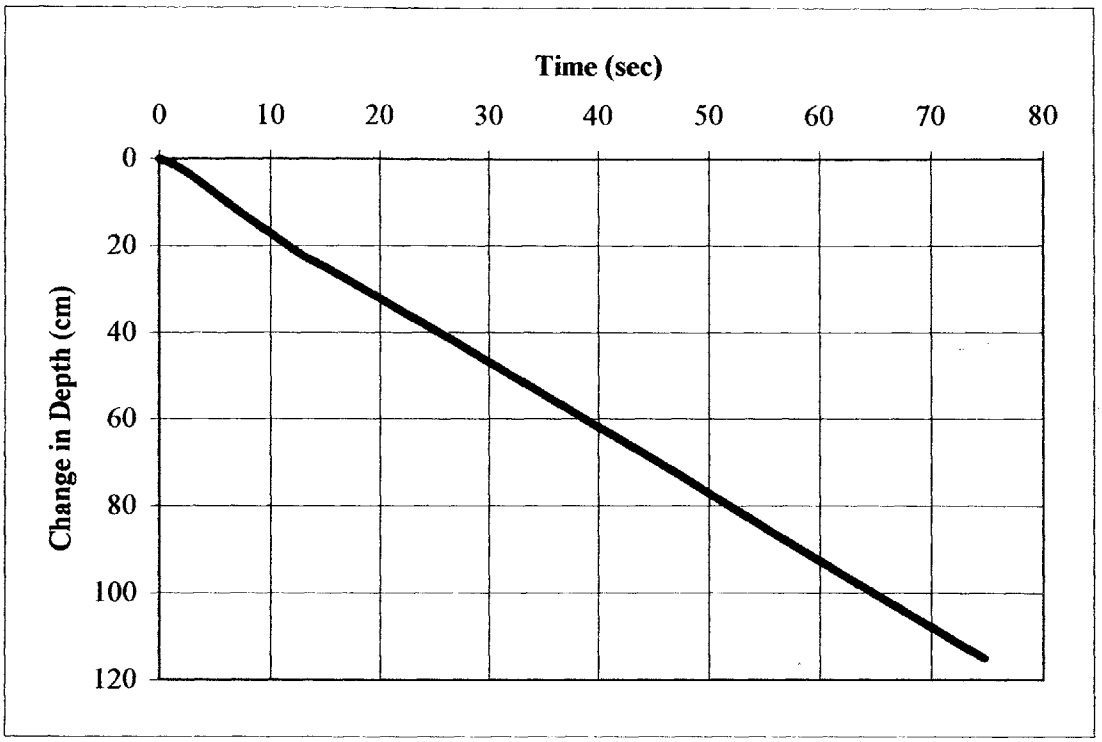

Figure 5.17a TP2_P2 Change in Depth vs. Time During Penetration

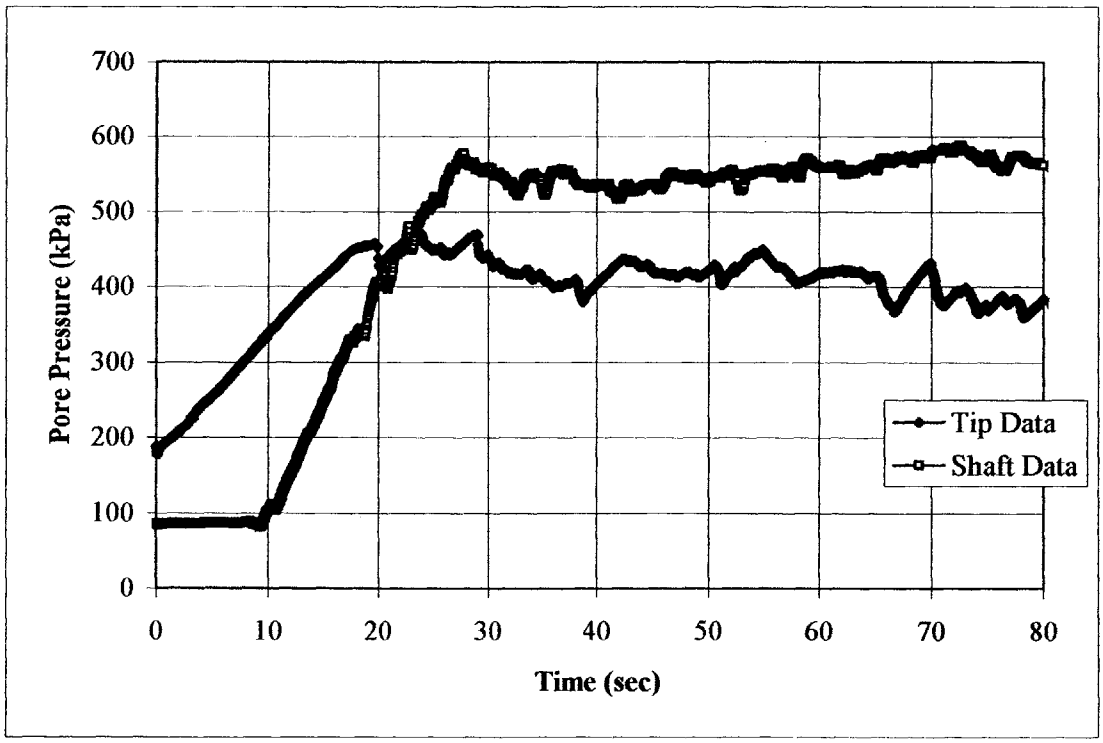

Figure 5.17b TP2_P2 Penetration Pore Pressure vs. Time

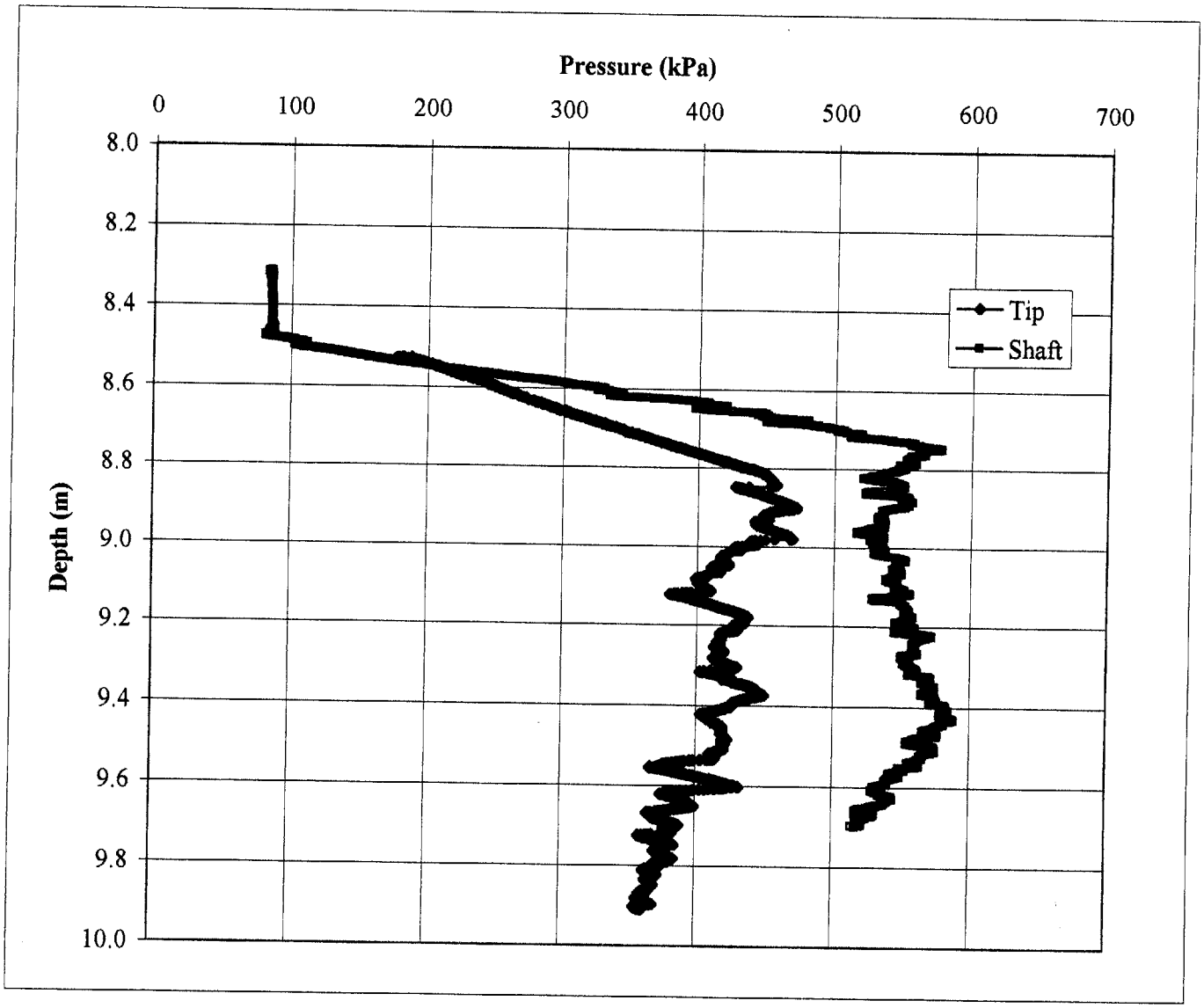

Figure 5.17c TP2_P2 Pressure vs. Depth During Penetration

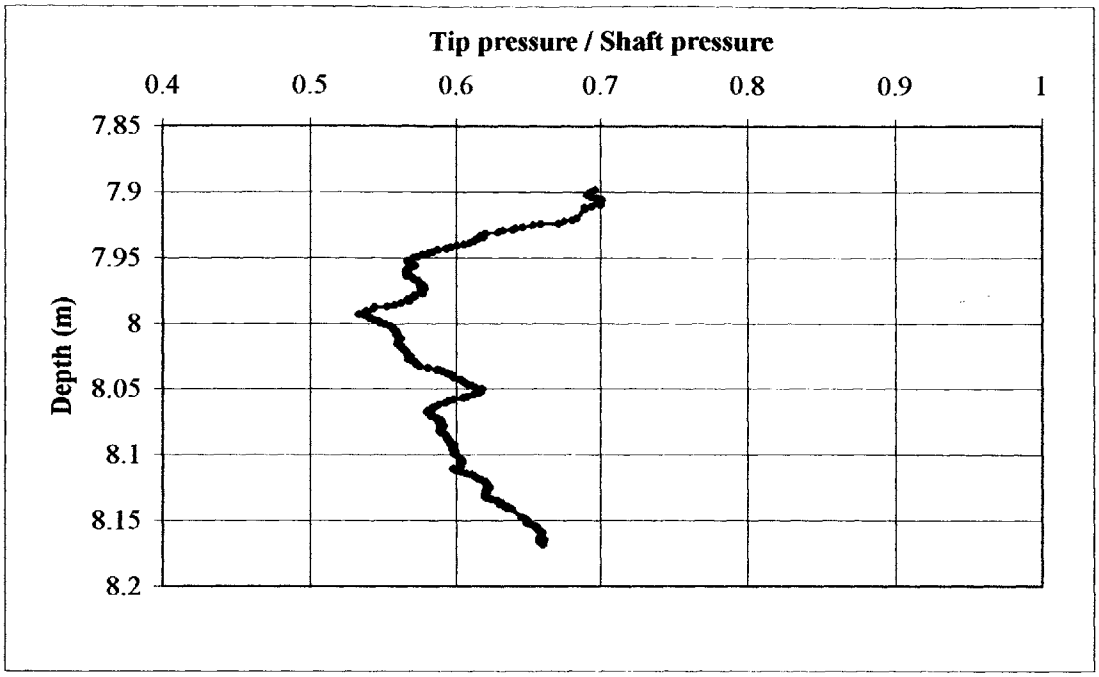

Figure 5.18 Ratio of Tip Pore Pressure Over Shaft Pore Pressure versus Depth During Penetration TP1_P3

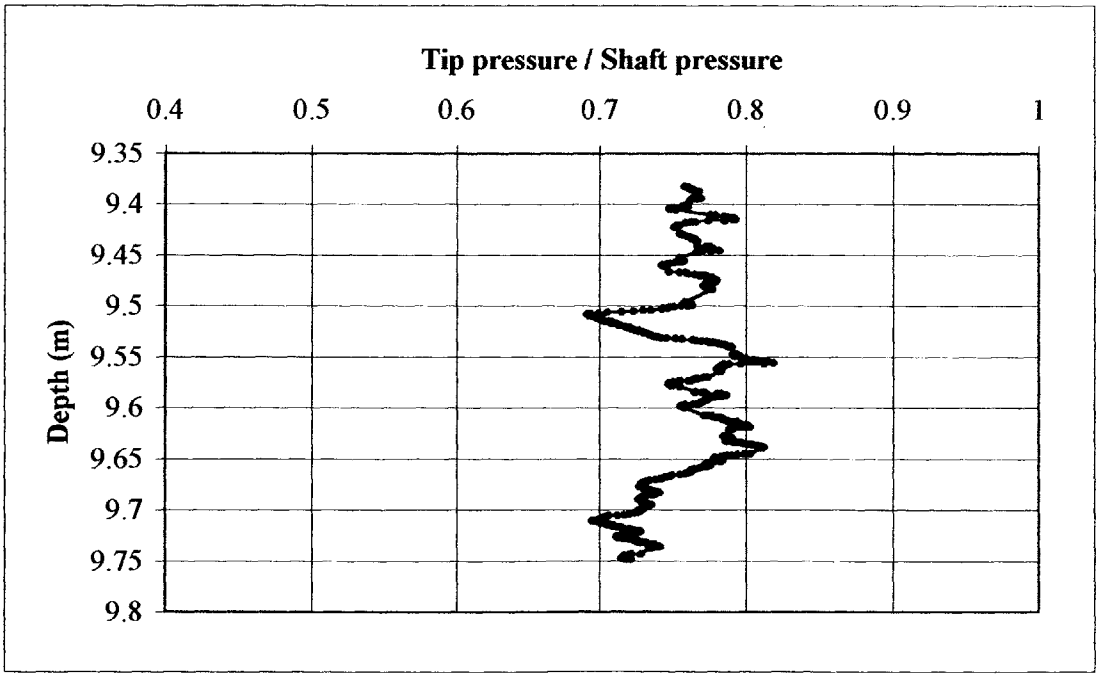

Figure 5.19 Ratio of Tip Pore Pressure Over Shaft Pore Pressure versus Depth During Penetration TP1_P4

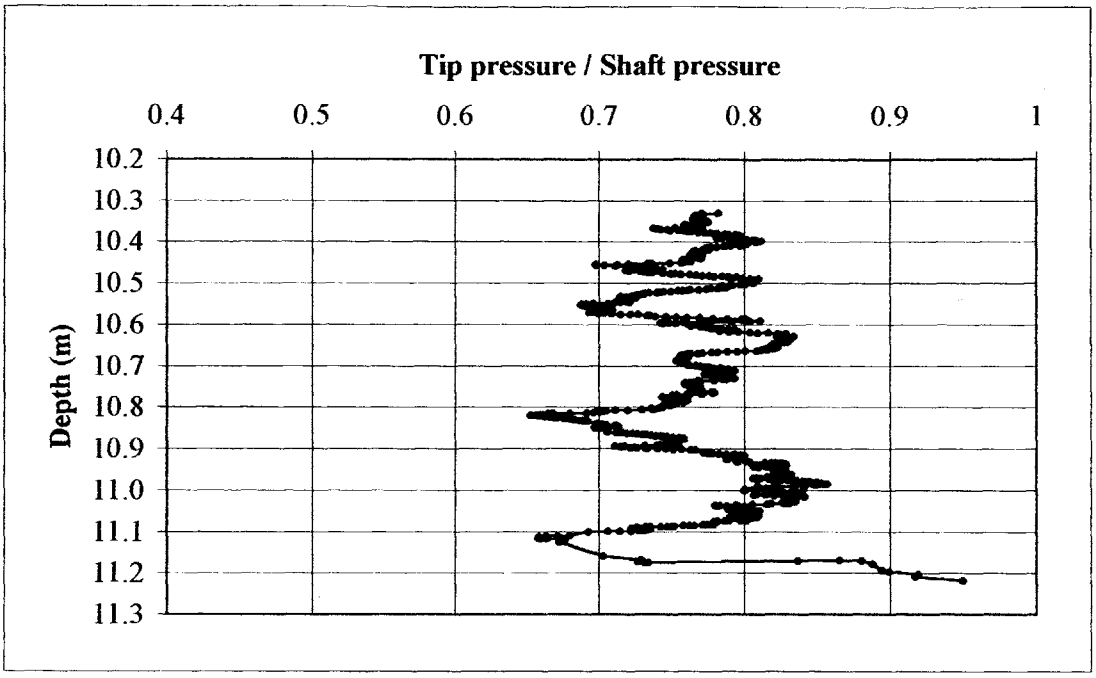

Figure 5.20 Ratio of Tip Pore Pressure Over Shaft Pore Pressure versus Depth During Penetration TP1_P5

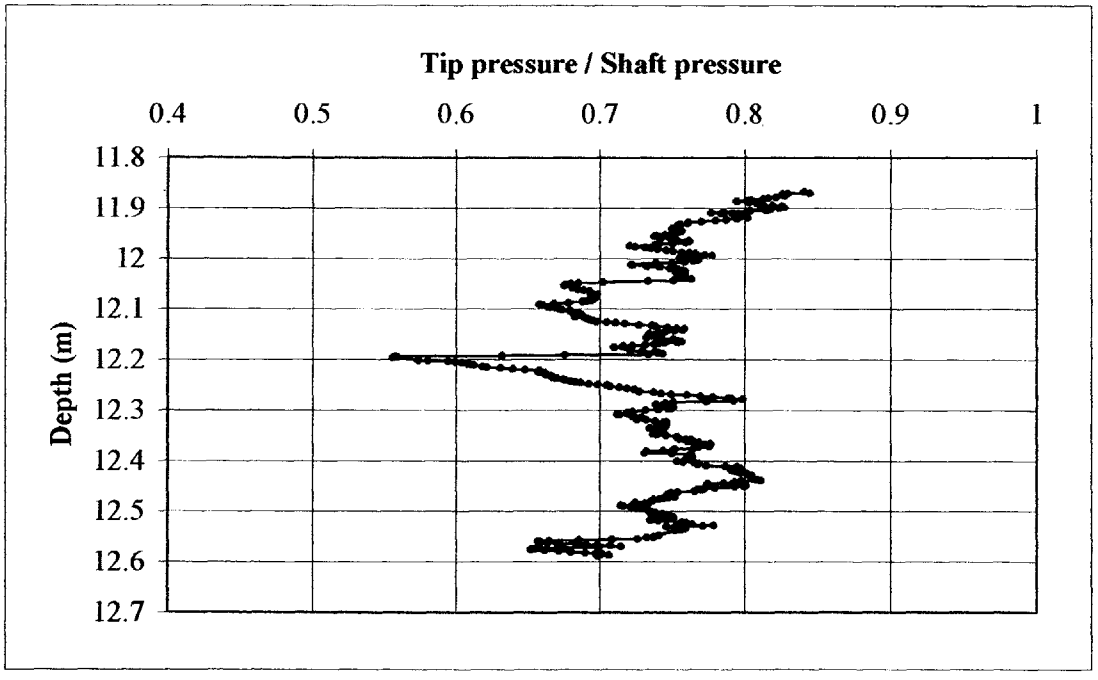

Figure 5.21 Ratio of Tip Pore Pressure Over Shaft Pore Pressure versus Depth During Penetration TP1_P6

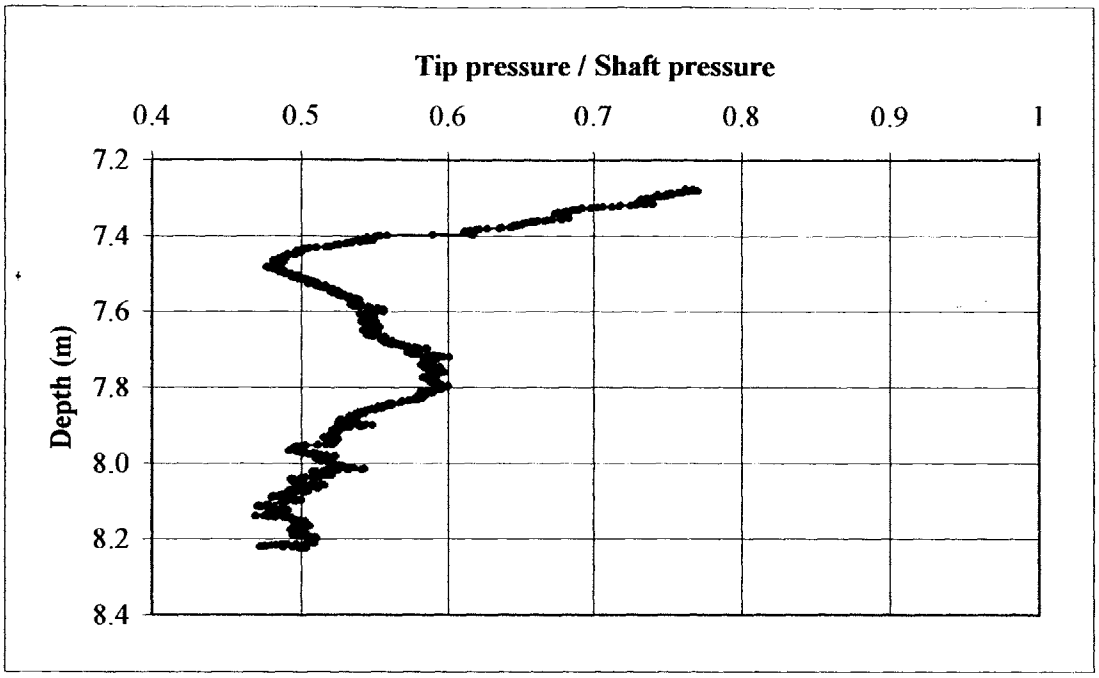

Figure 5.22 Ratio of Tip Pore Pressure Over Shaft Pore Pressure versus Depth During Penetration TP2_P1

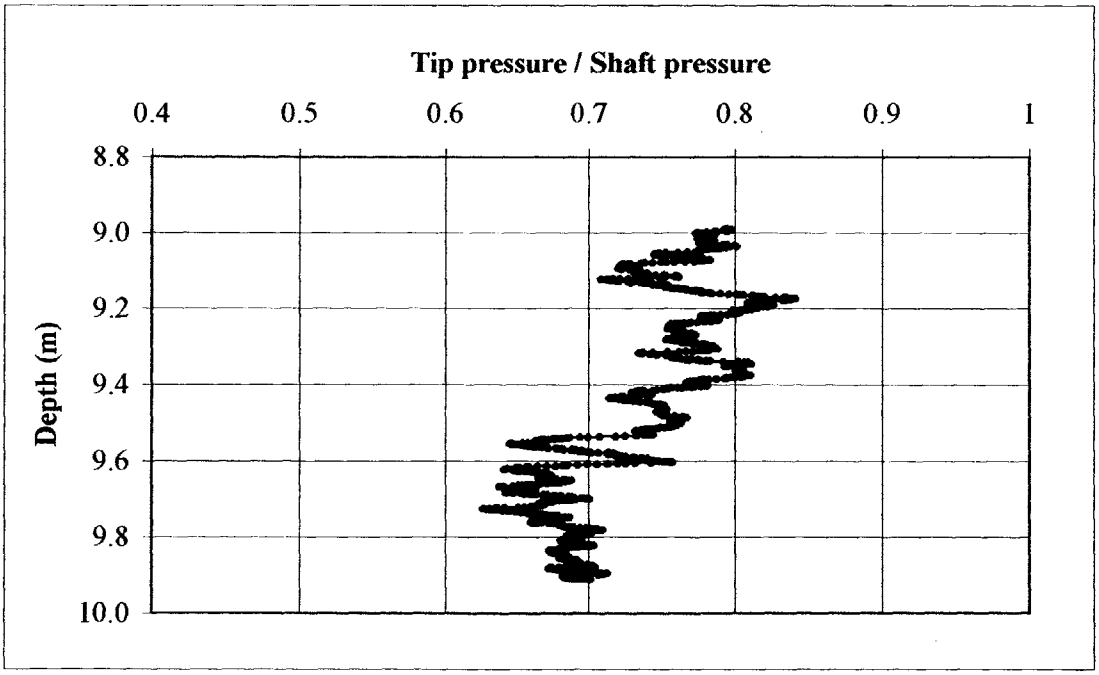

Figure 5.23 Ratio of Tip Pore Pressure Over Shaft Pore Pressure versus Depth During Penetration TP2_P2

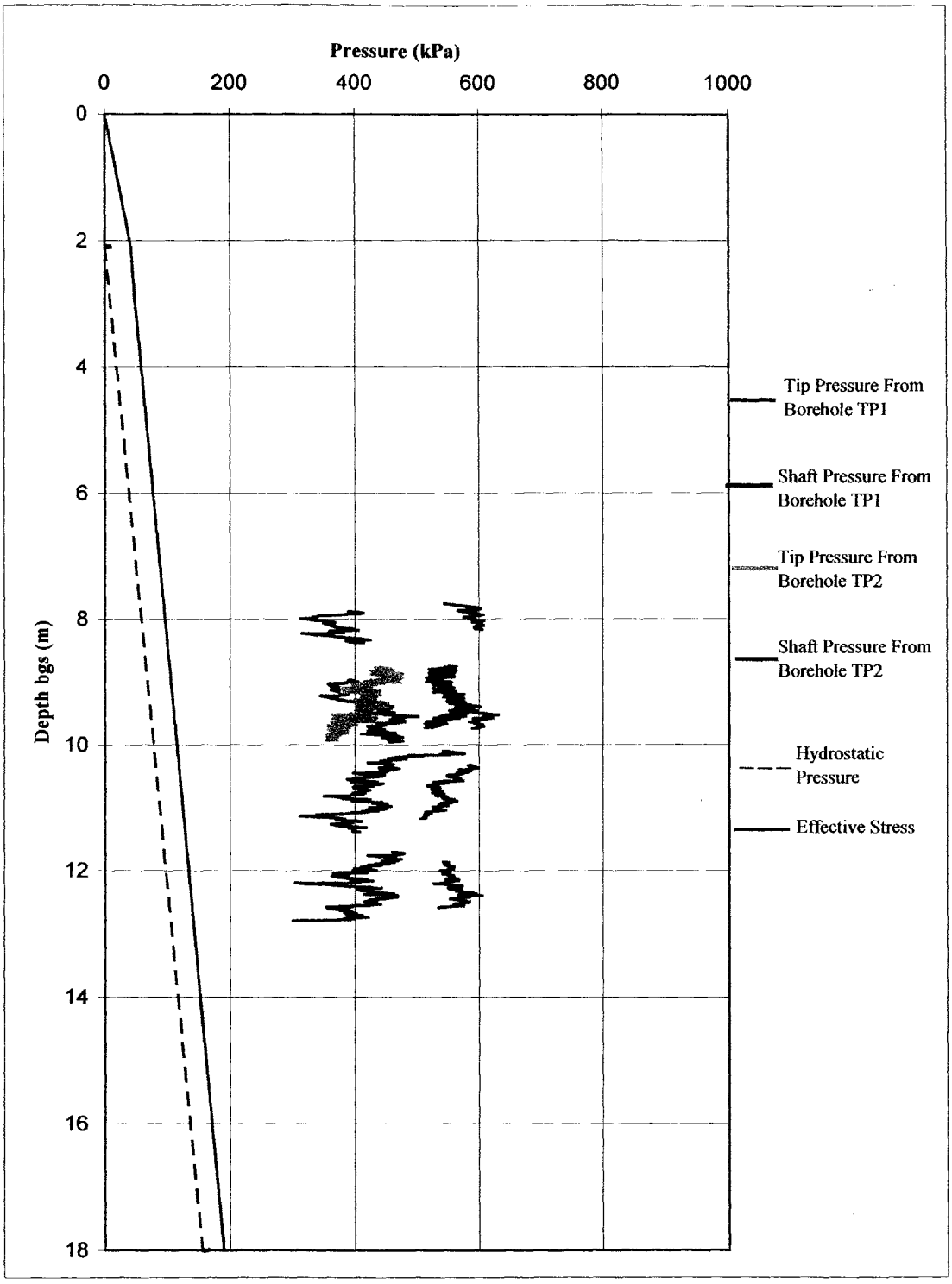

Figure 5.24 Combined Penetration Plots from TP1_P3, TP1_P4, TP1_P5, TP1_P6, and TP2_P2

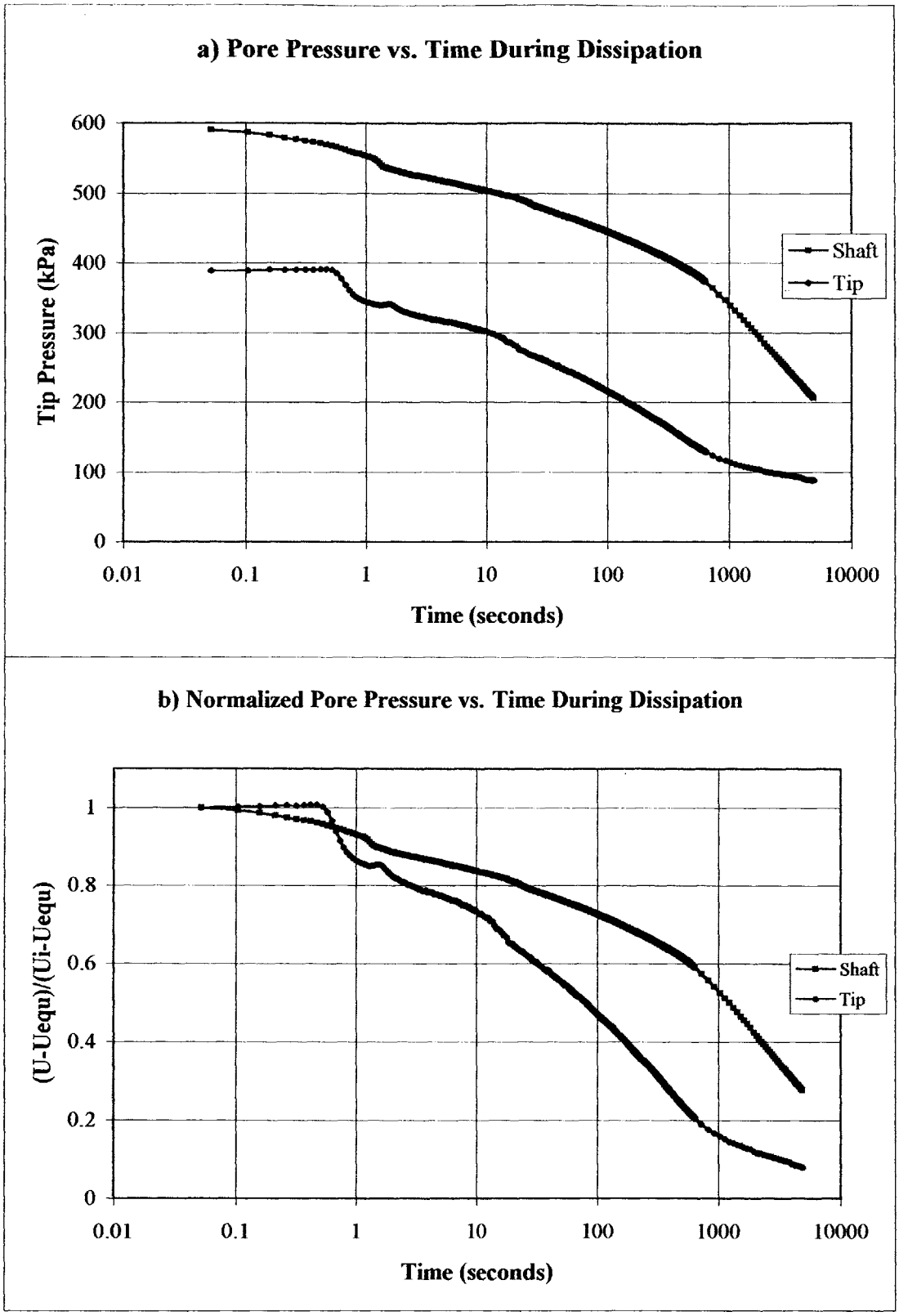

Figure 5.25 - TP1_P3 Dissipation Data

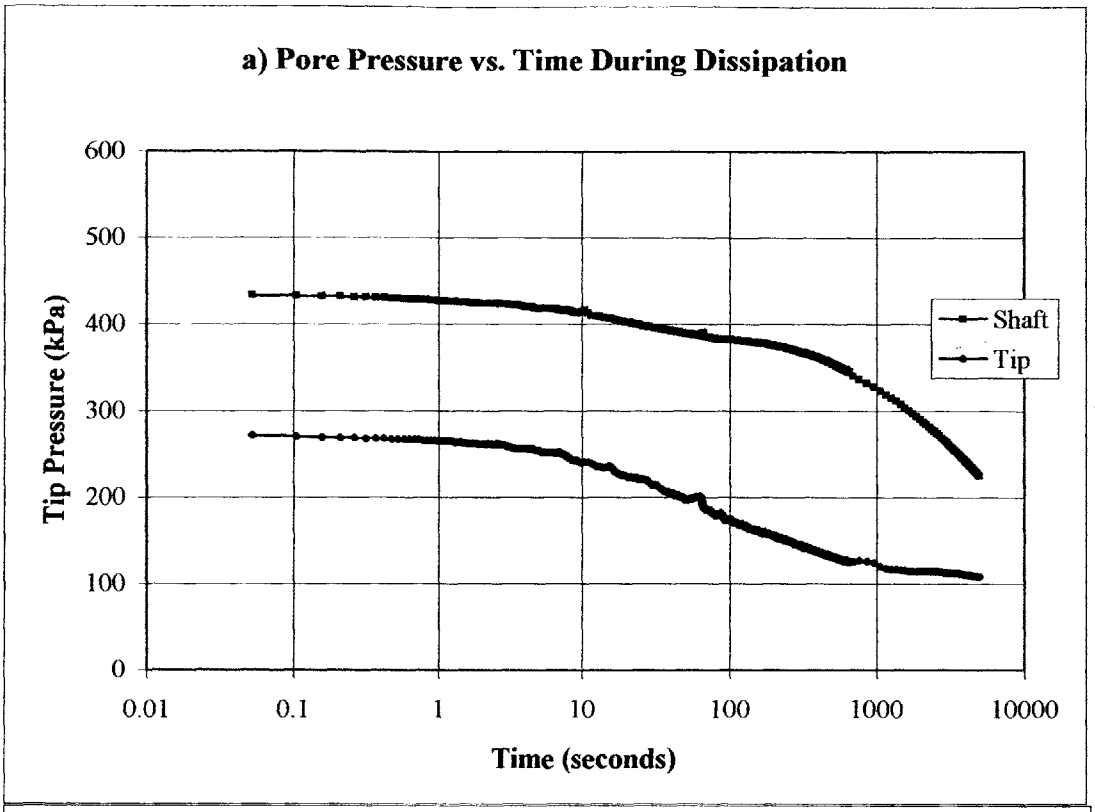

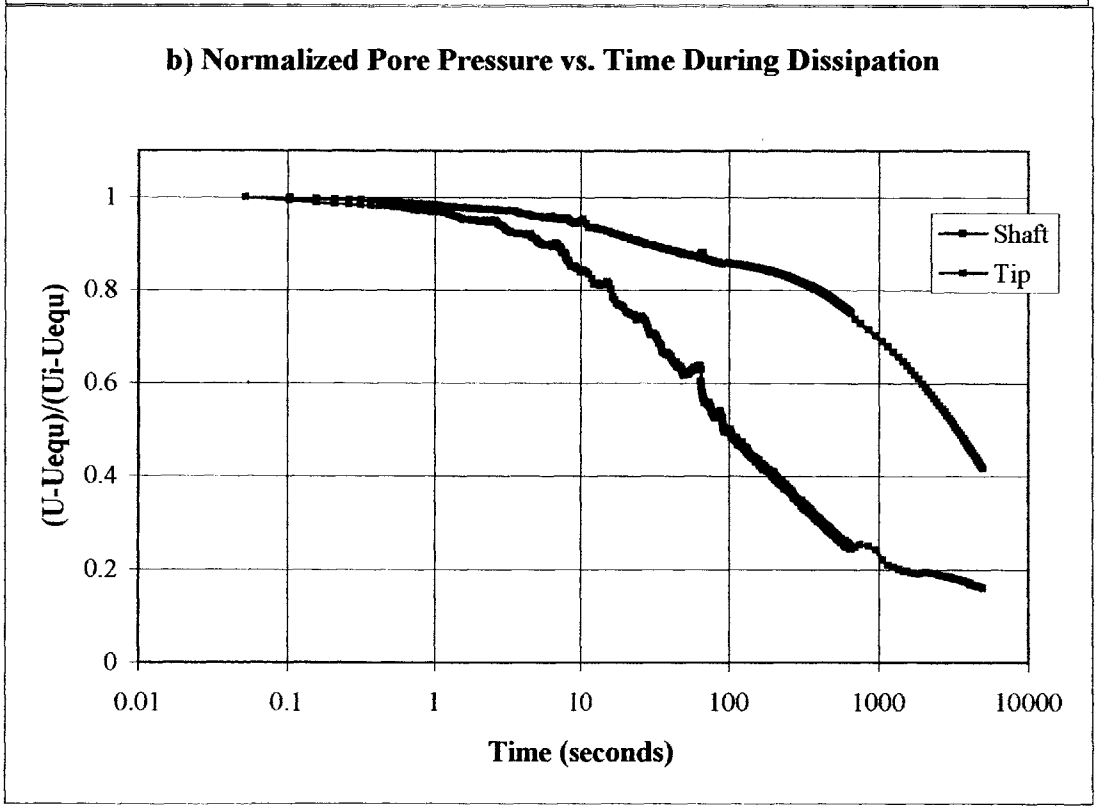

Figure 5.26 - TP1_P4 Dissipation Data

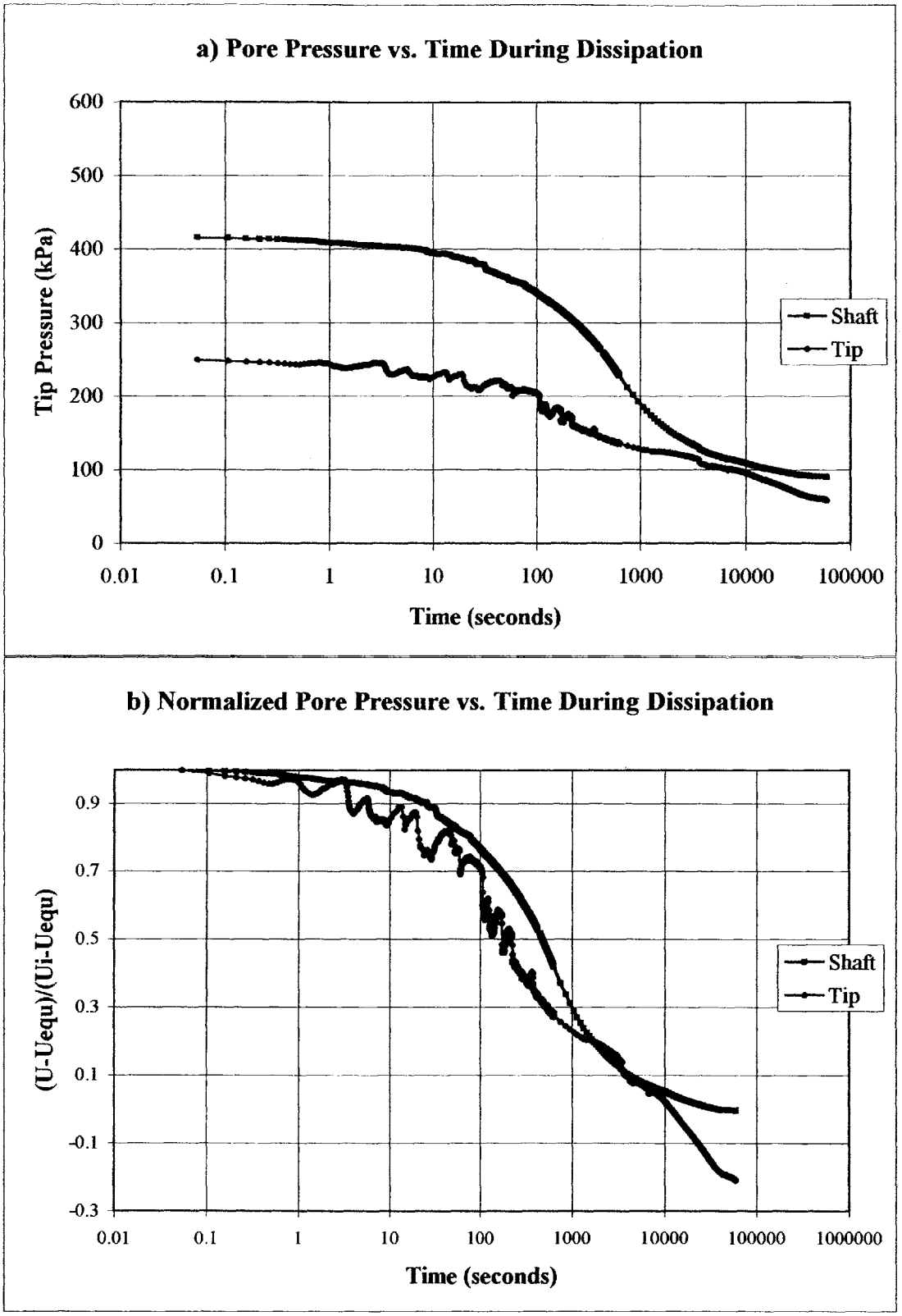

Figure 5.27 - TP1_P5 Dissipation Data

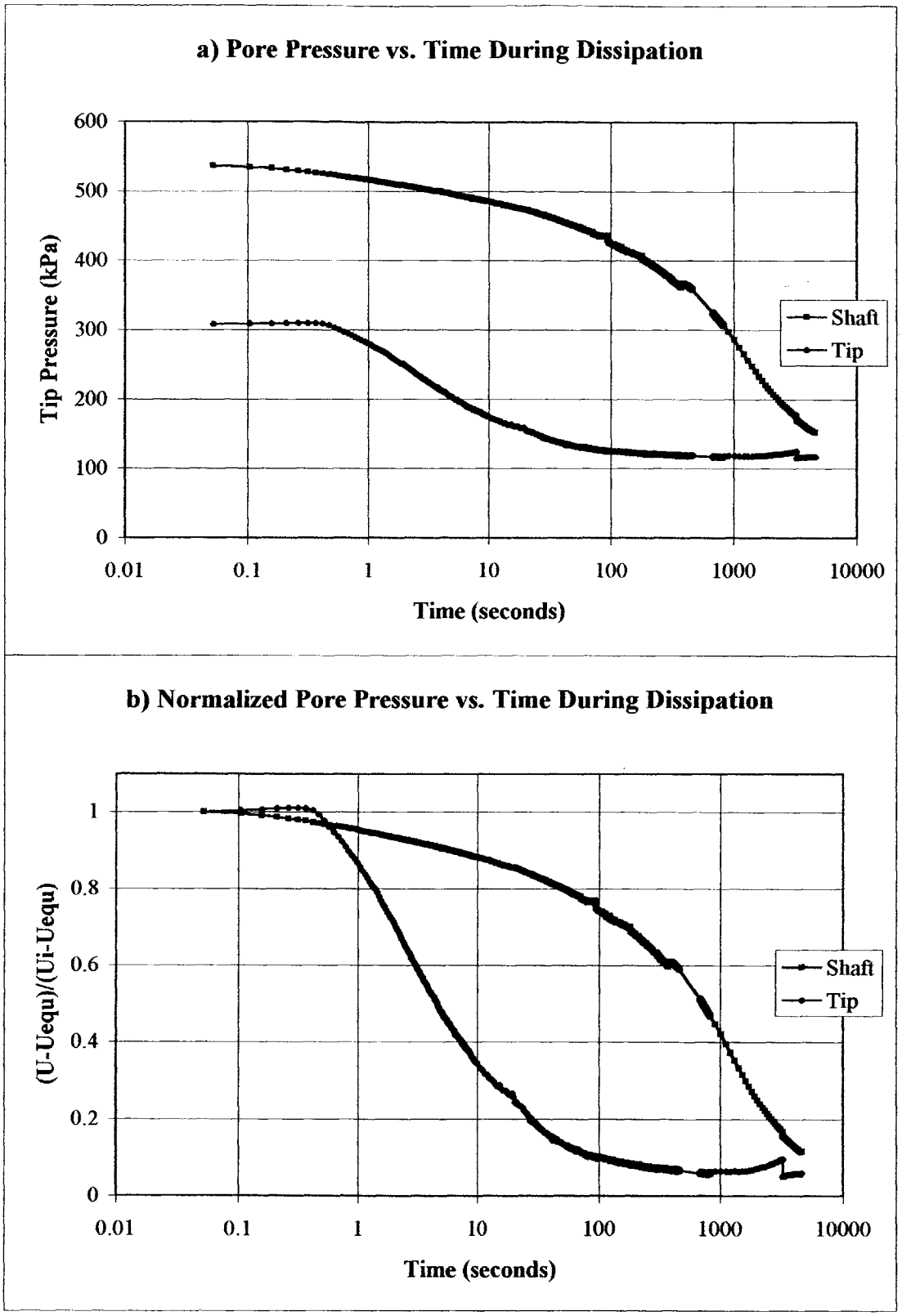

Figure 5.28 - TP1_P6 Dissipation Data

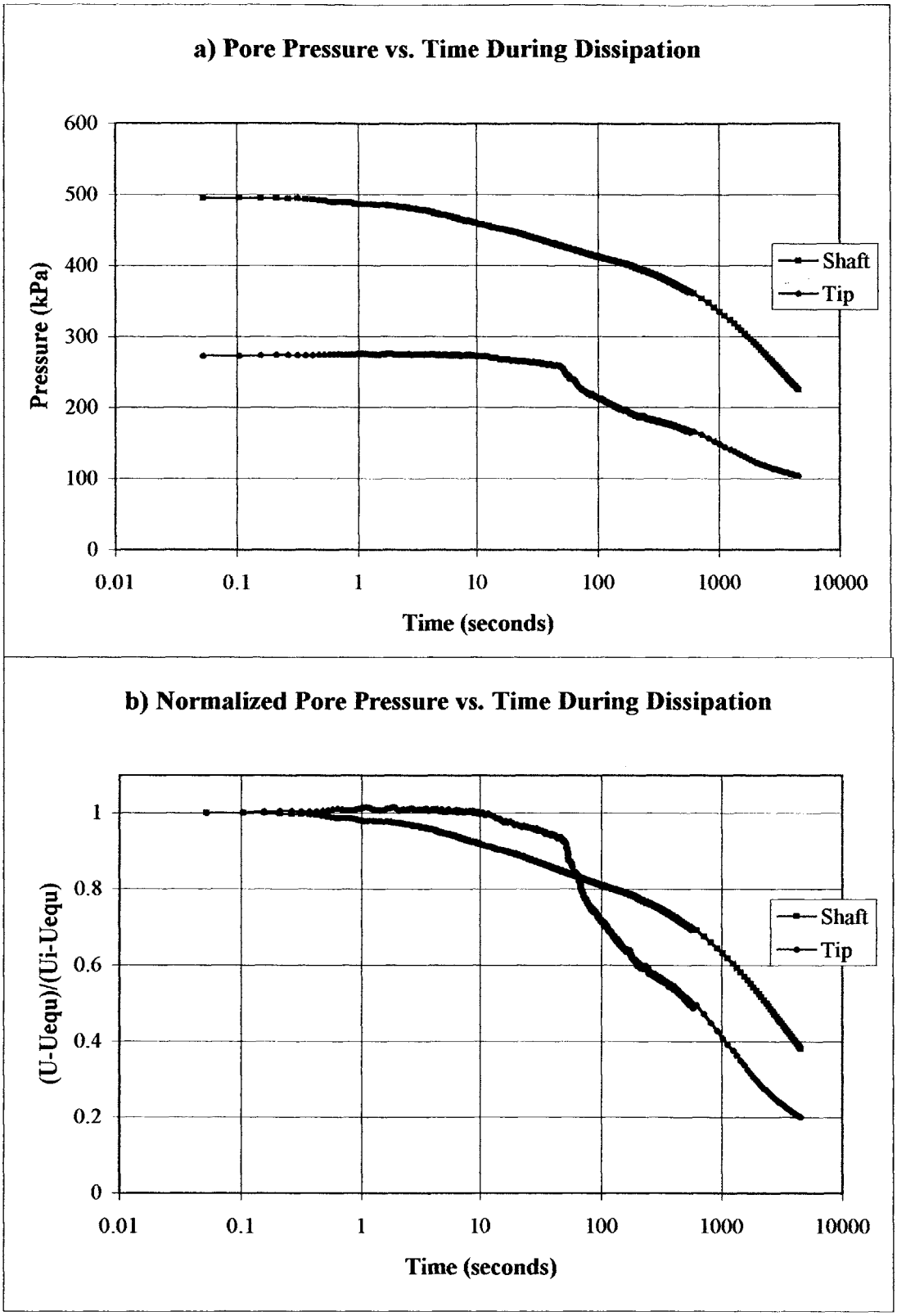

Figure 5.29 - TP2_P1 Dissipation Data

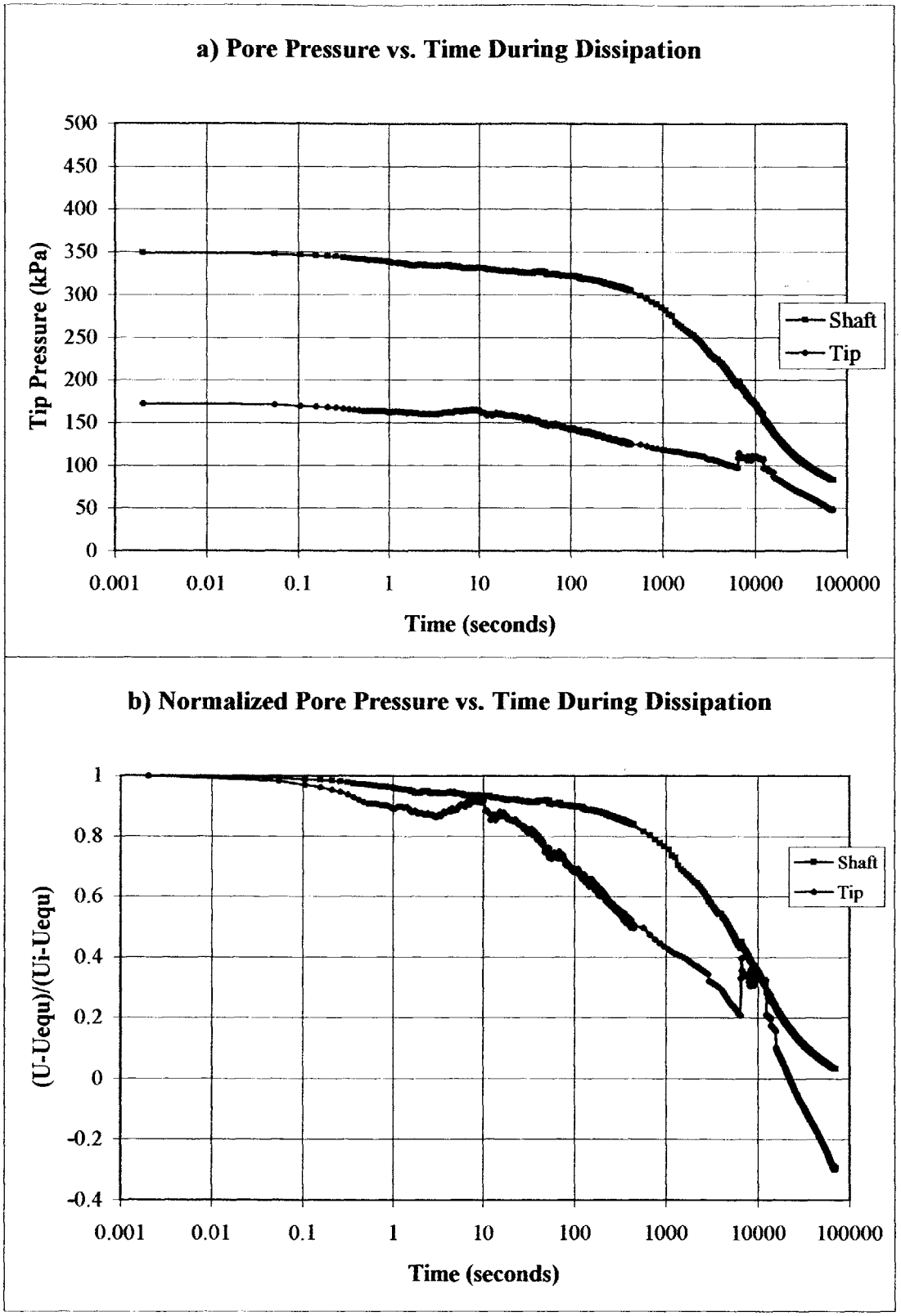

Figure 5.30 - TP2_P2 Dissipation Data

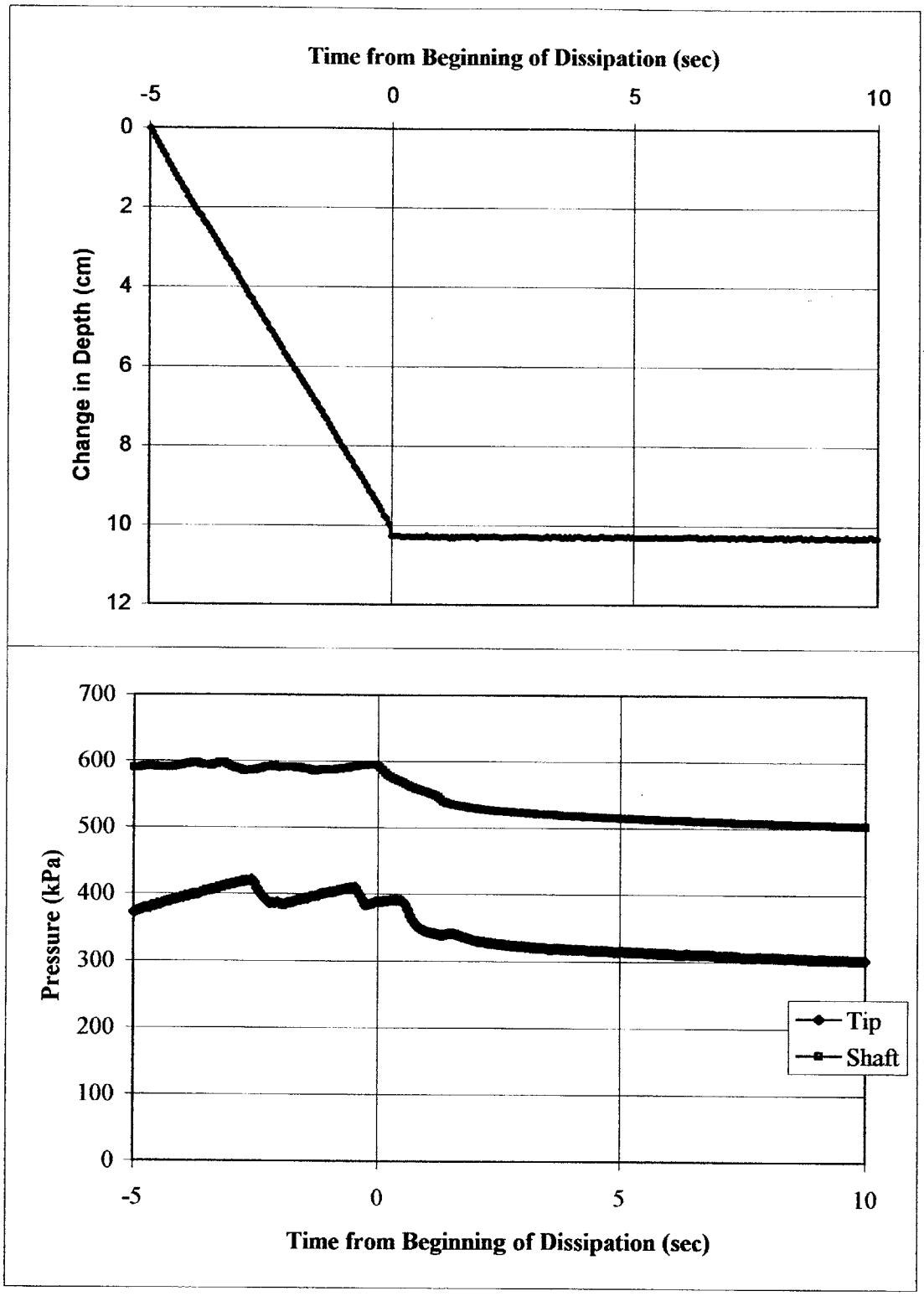

Figure 5.31 TP1_P3 Installation Effects on Pore Pressure Record

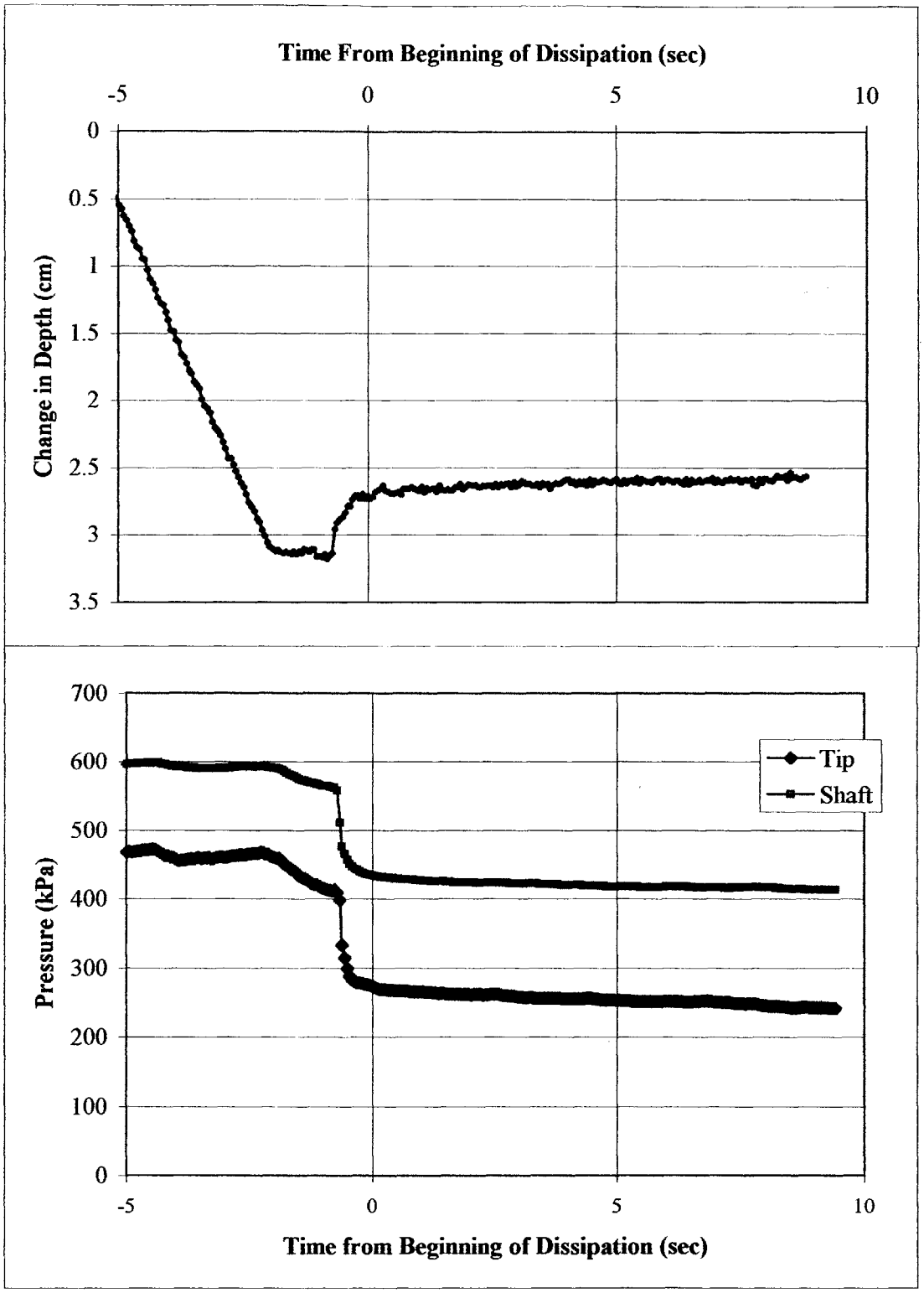

Figure 5.32 TP1_P4 Installation Effects on Pore Pressure Record

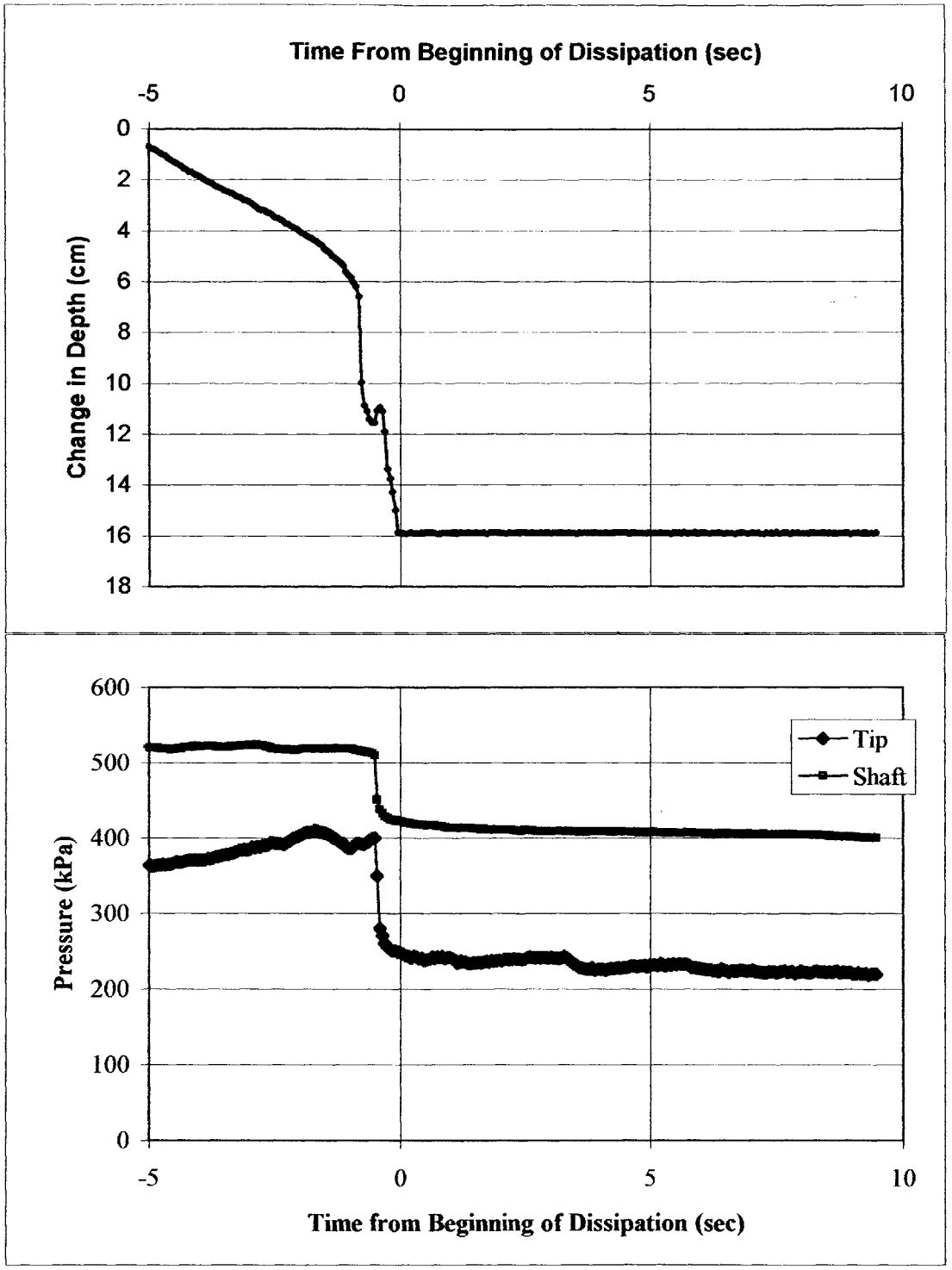

Figure 5.33 TP1_P5 Installation Effects on Pore Pressure Record

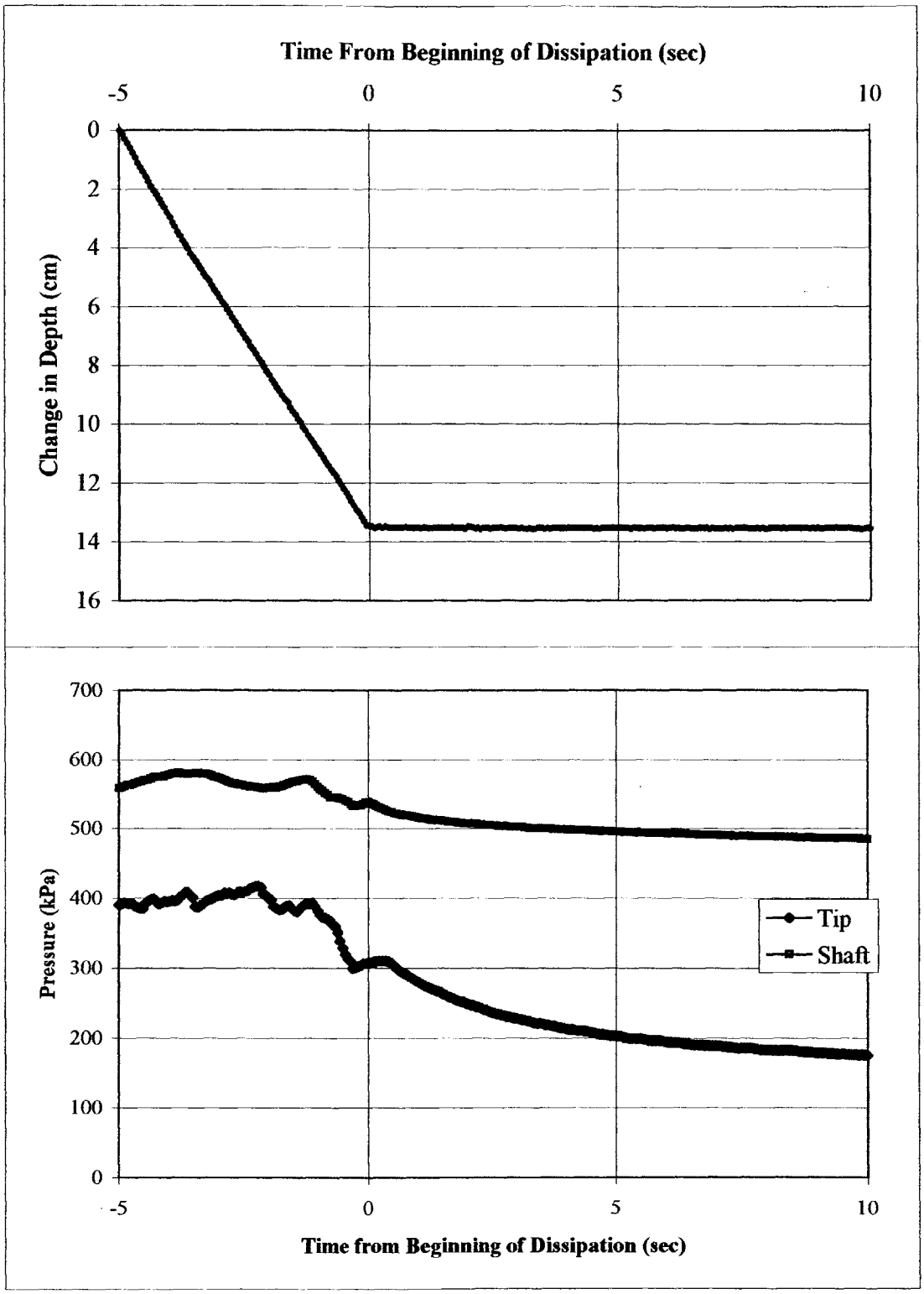

Figure 5.34 TP1_P6 Installation Effects on Pore Pressure Record

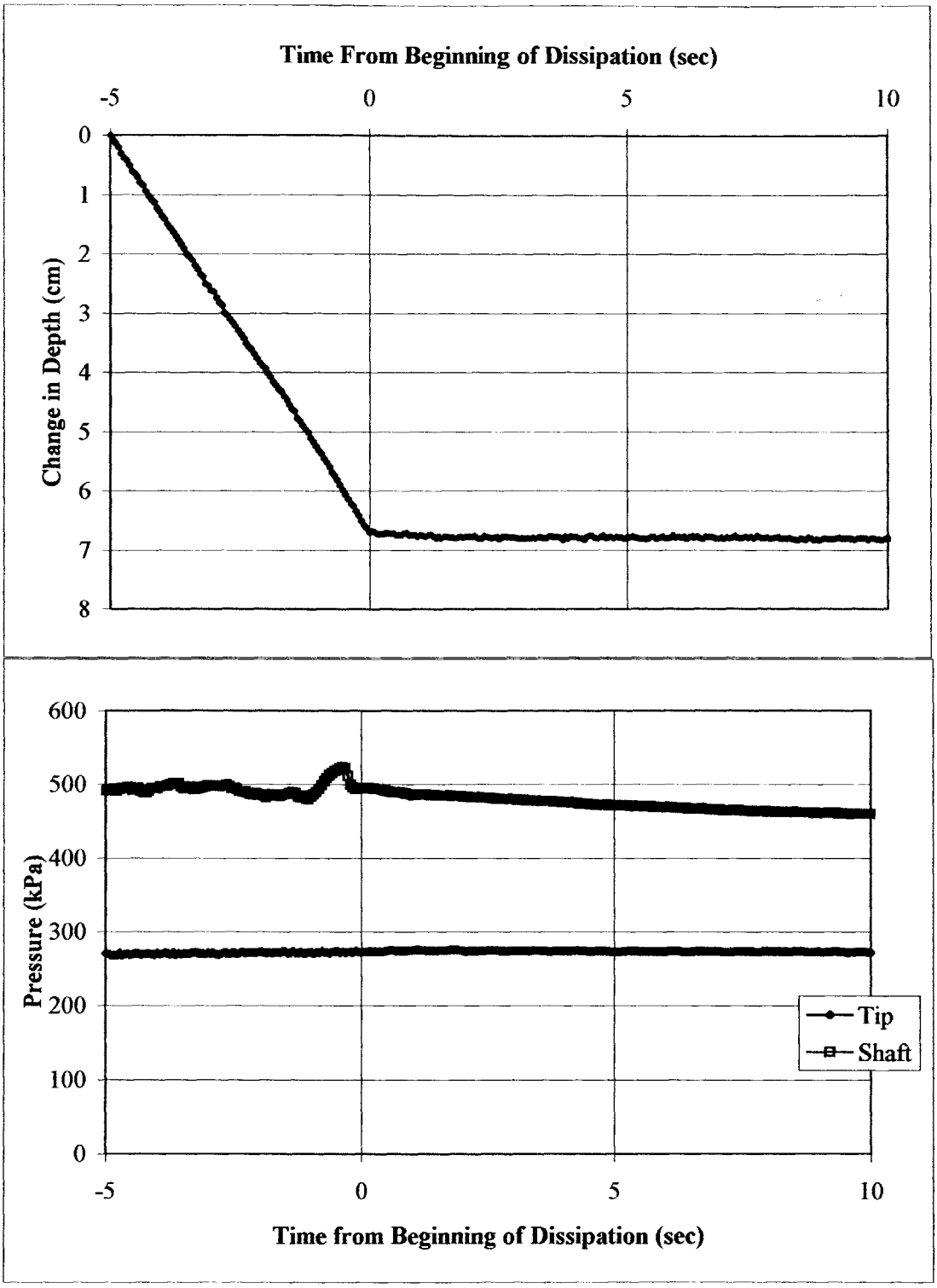

Figure 5.35 TP2_P1 Installation Effects on Pore Pressure Record

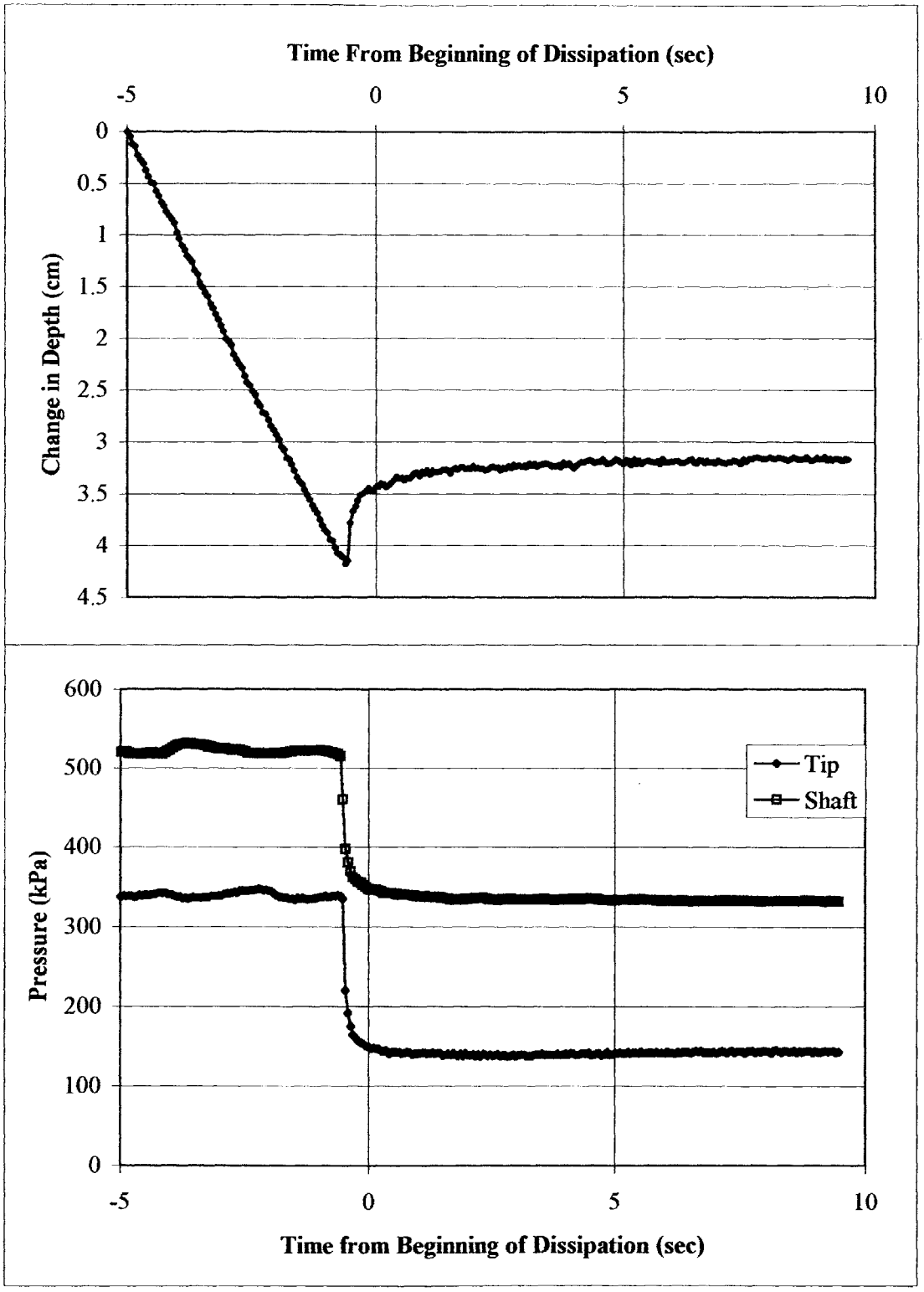

Figure 5.36 TP2_P2 Installation Effects on Pore Pressure Record

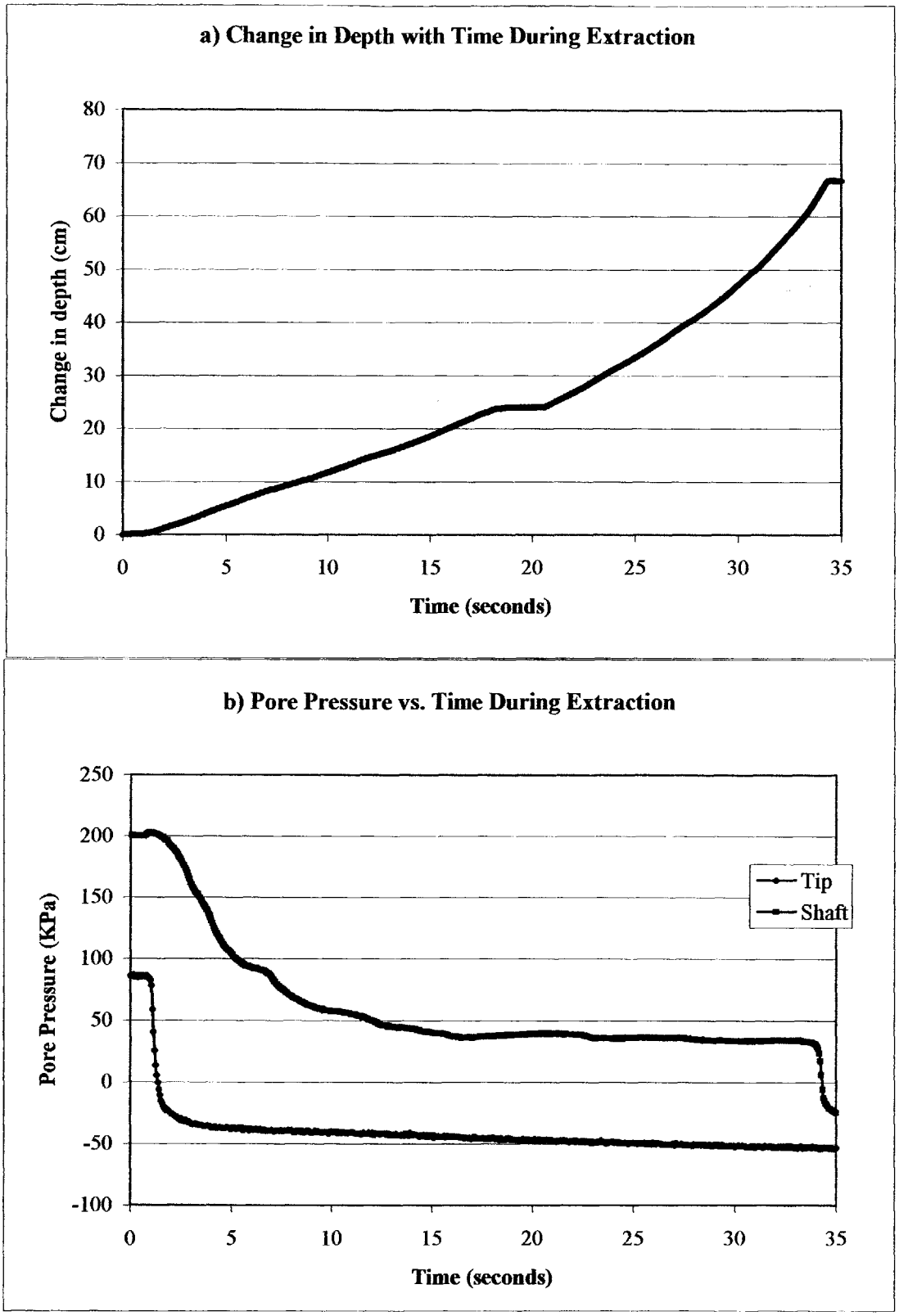

Figure 5.37 TP1_P3 Extraction Data

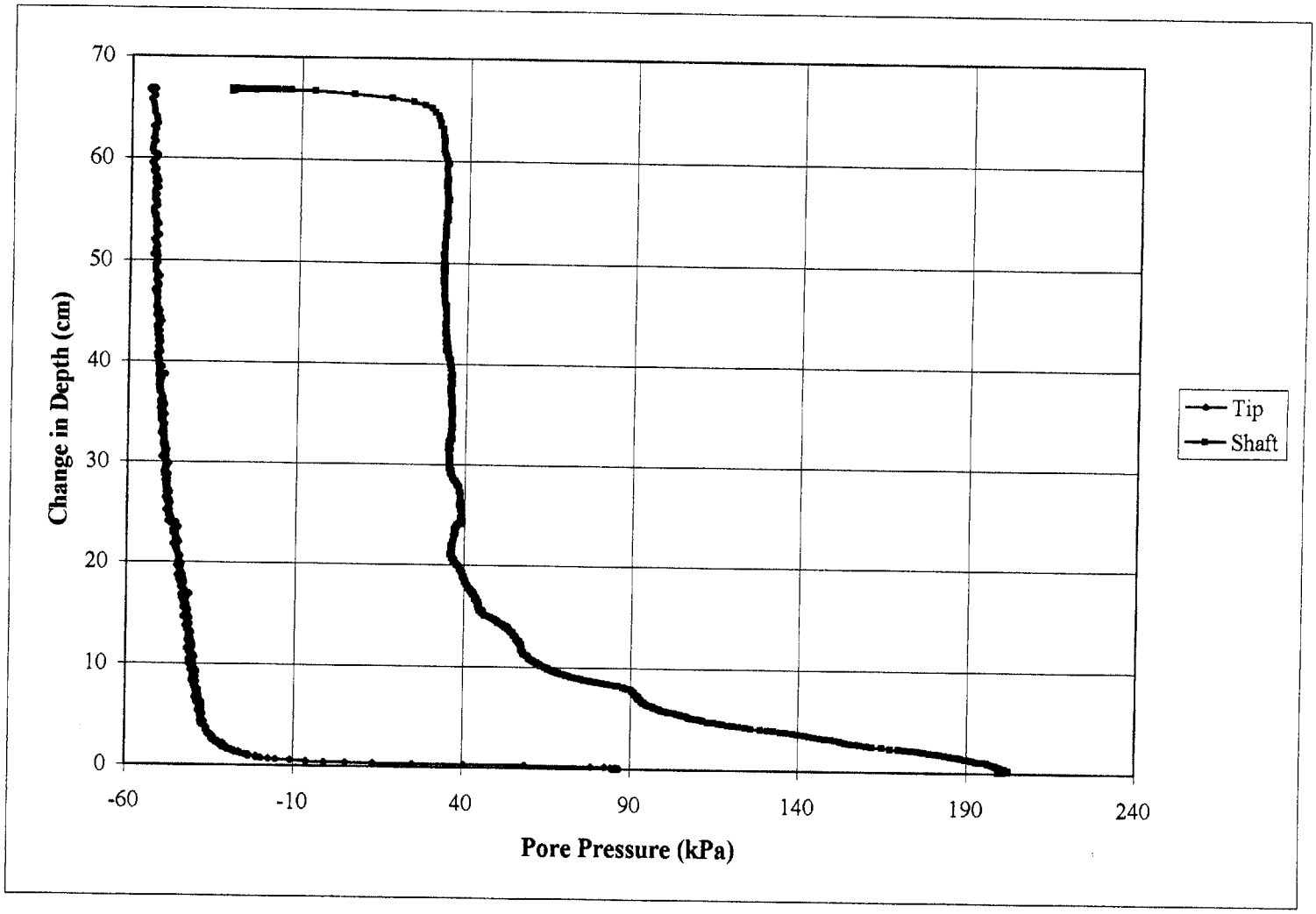

Figure 5.37c TP1_P3 Extraction Data - Pressure vs. Depth

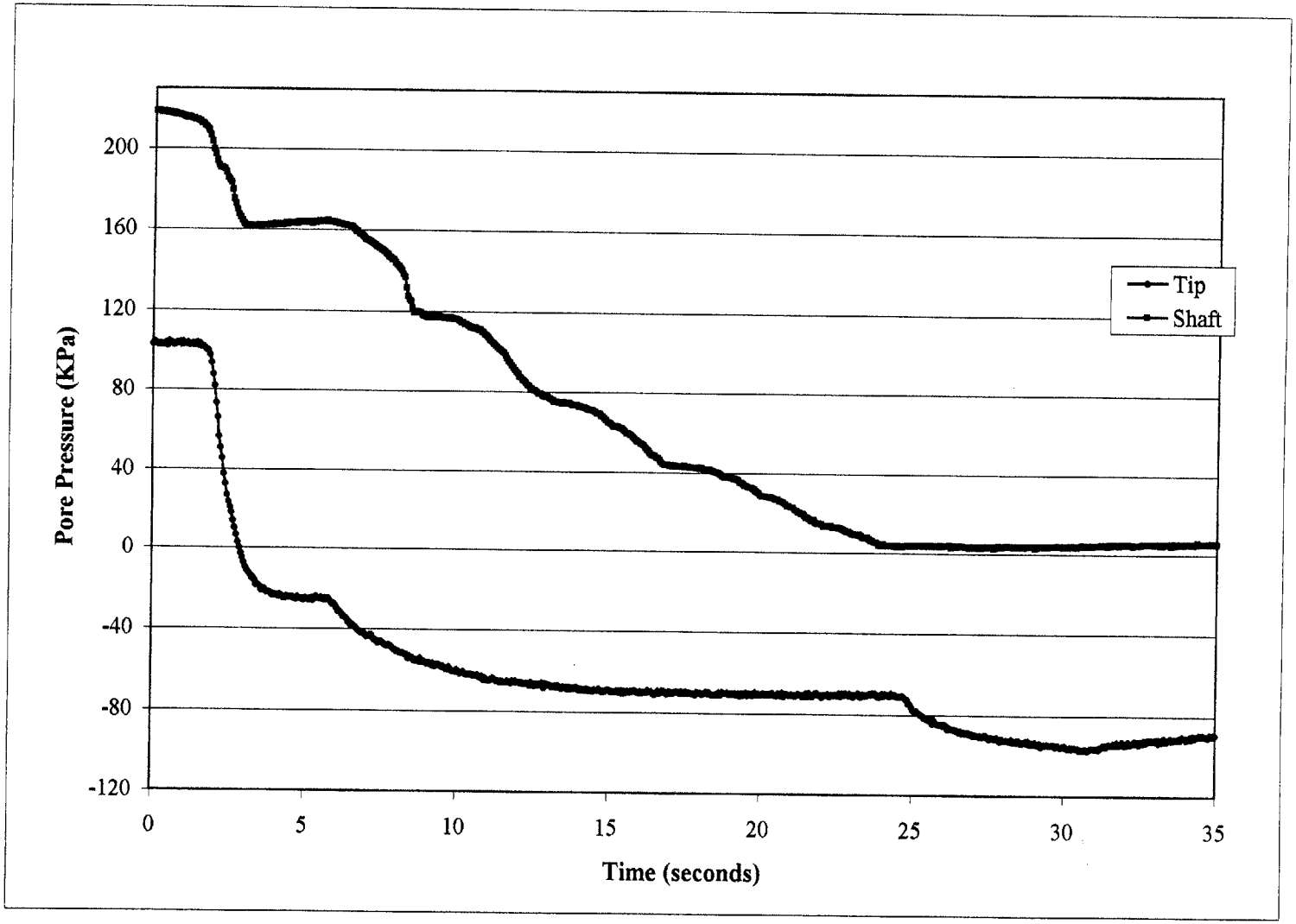

Figure 5.38 **TP1_P4 Extraction Data - Pressure vs. Time During Extraction**

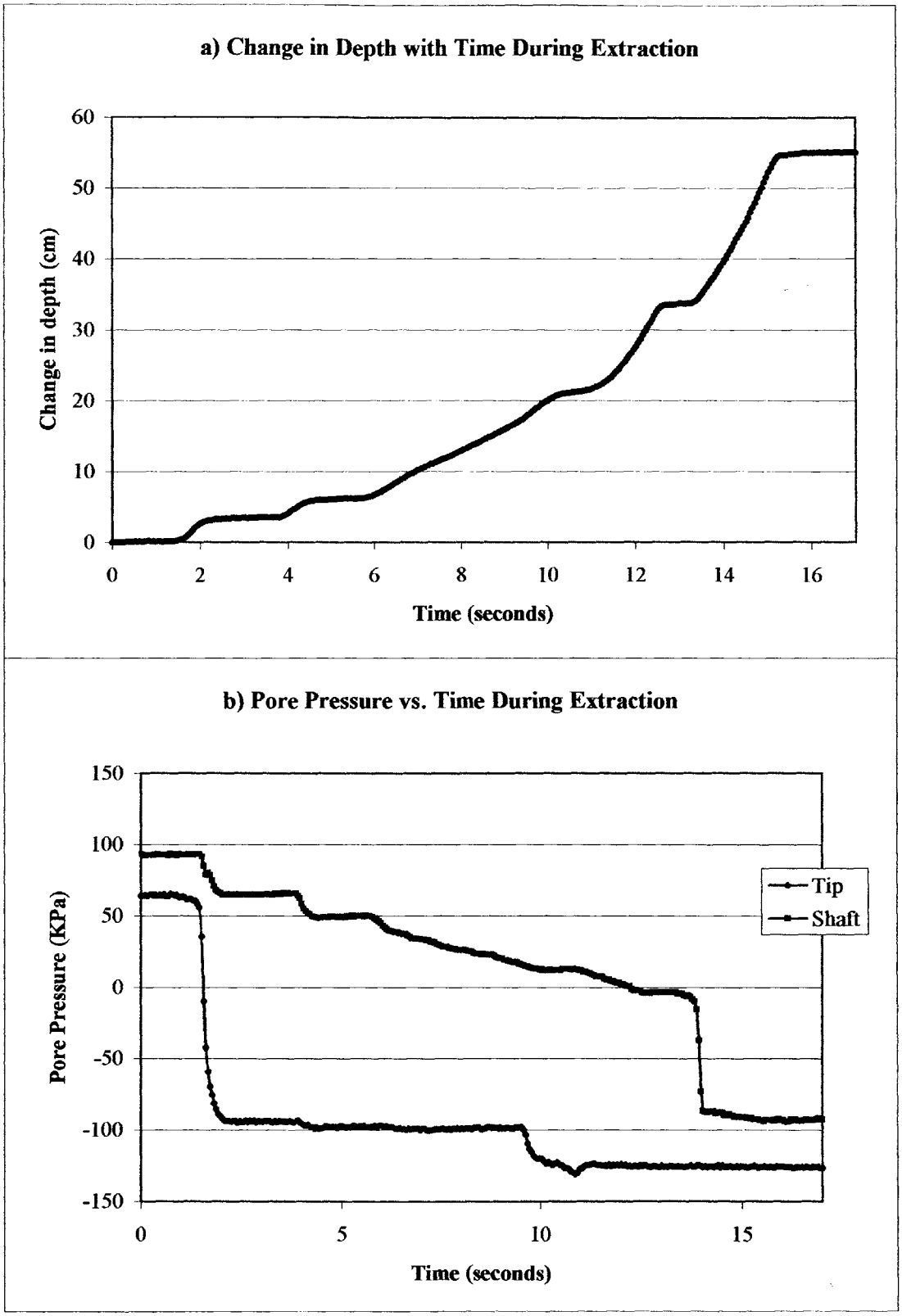

Figure 5.39 TP1_P5 Extraction Data

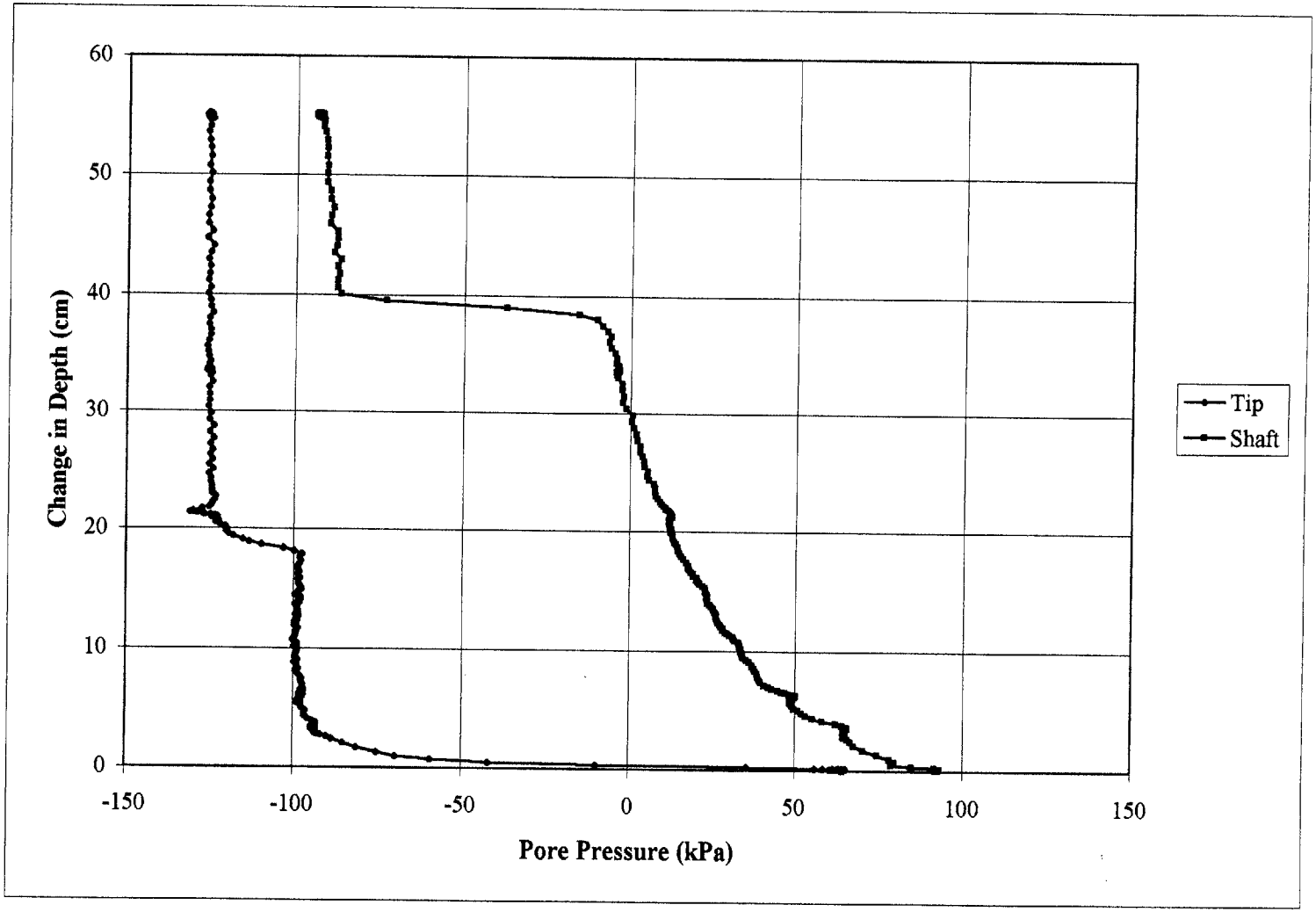

Figure 5.39c TP1_P5 Extraction Data - Pressure vs. Depth

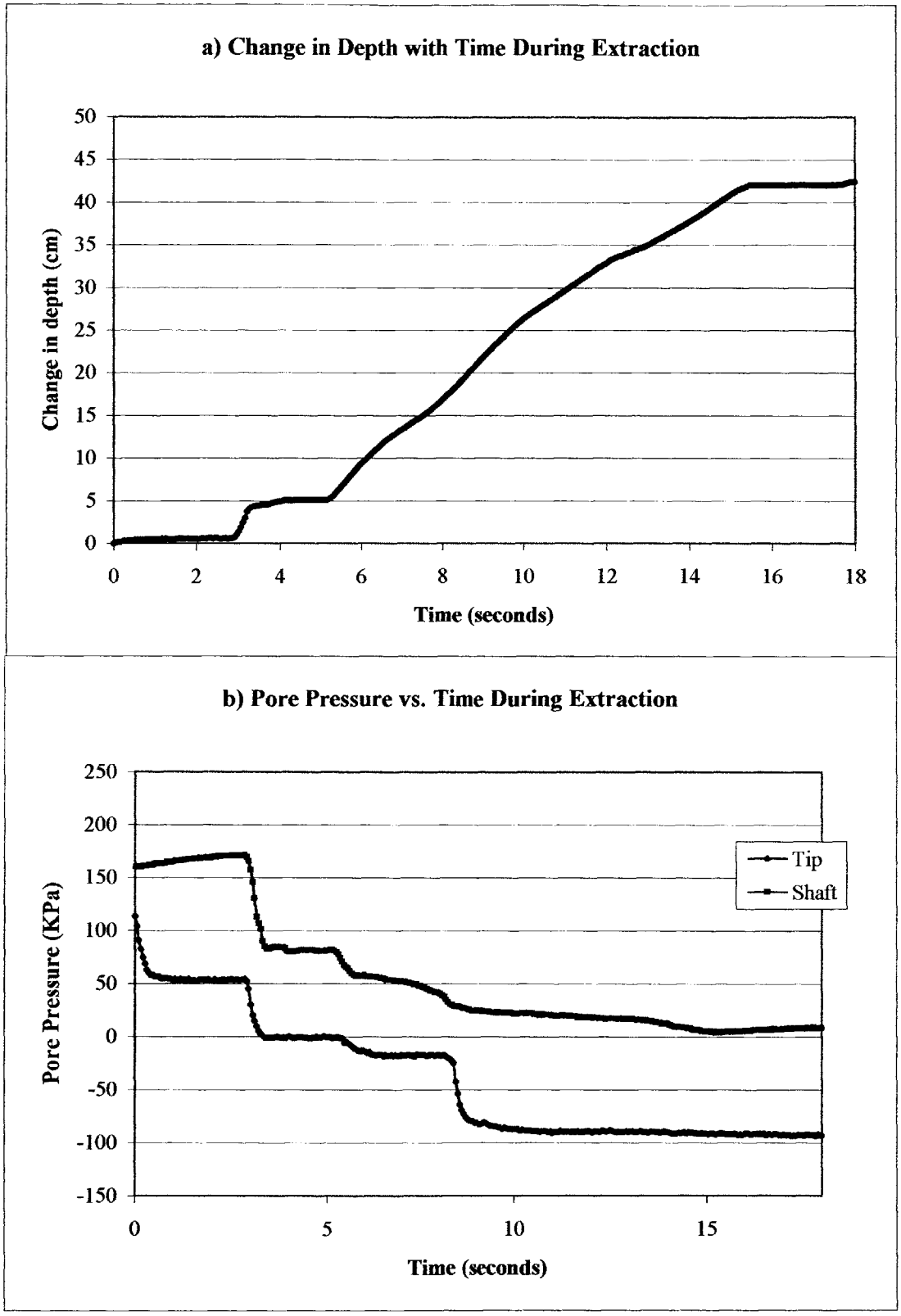

Figure 5.40 TP1_P6 Extraction Data

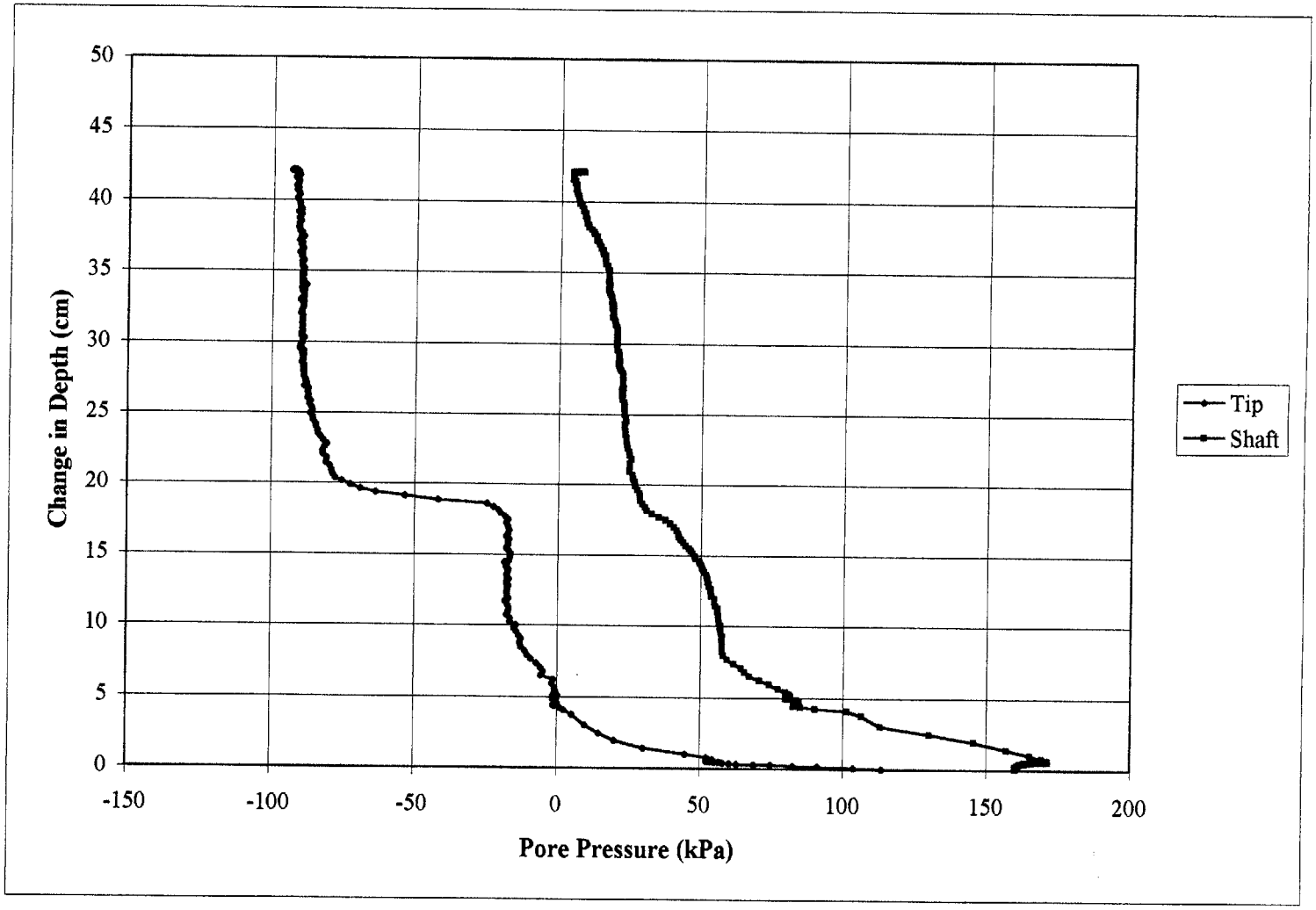

Figure 5.40c TP1_P5 Extraction Data - Pressure vs. Depth

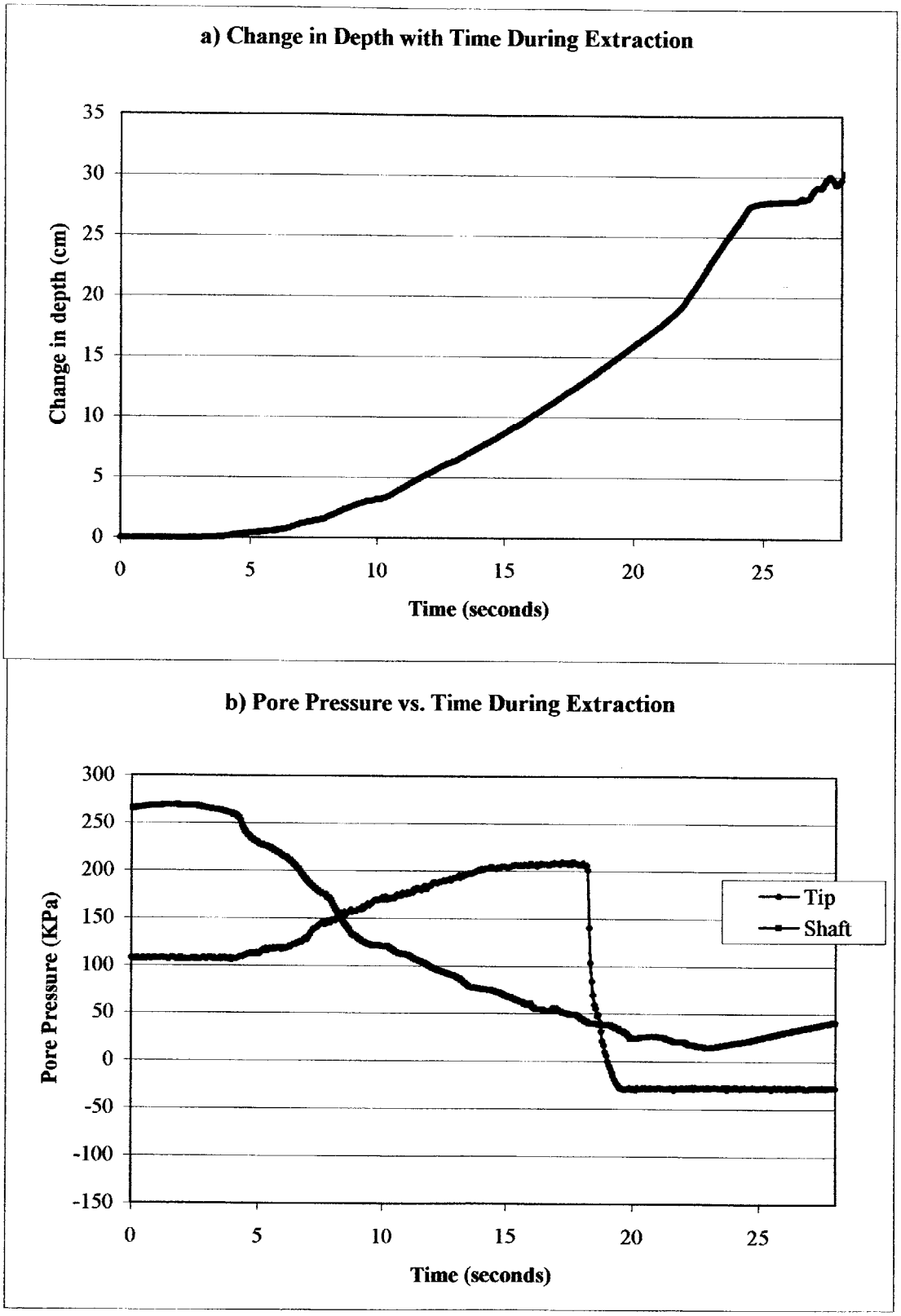

Figure 5.41 TP2_P1 Extraction Data

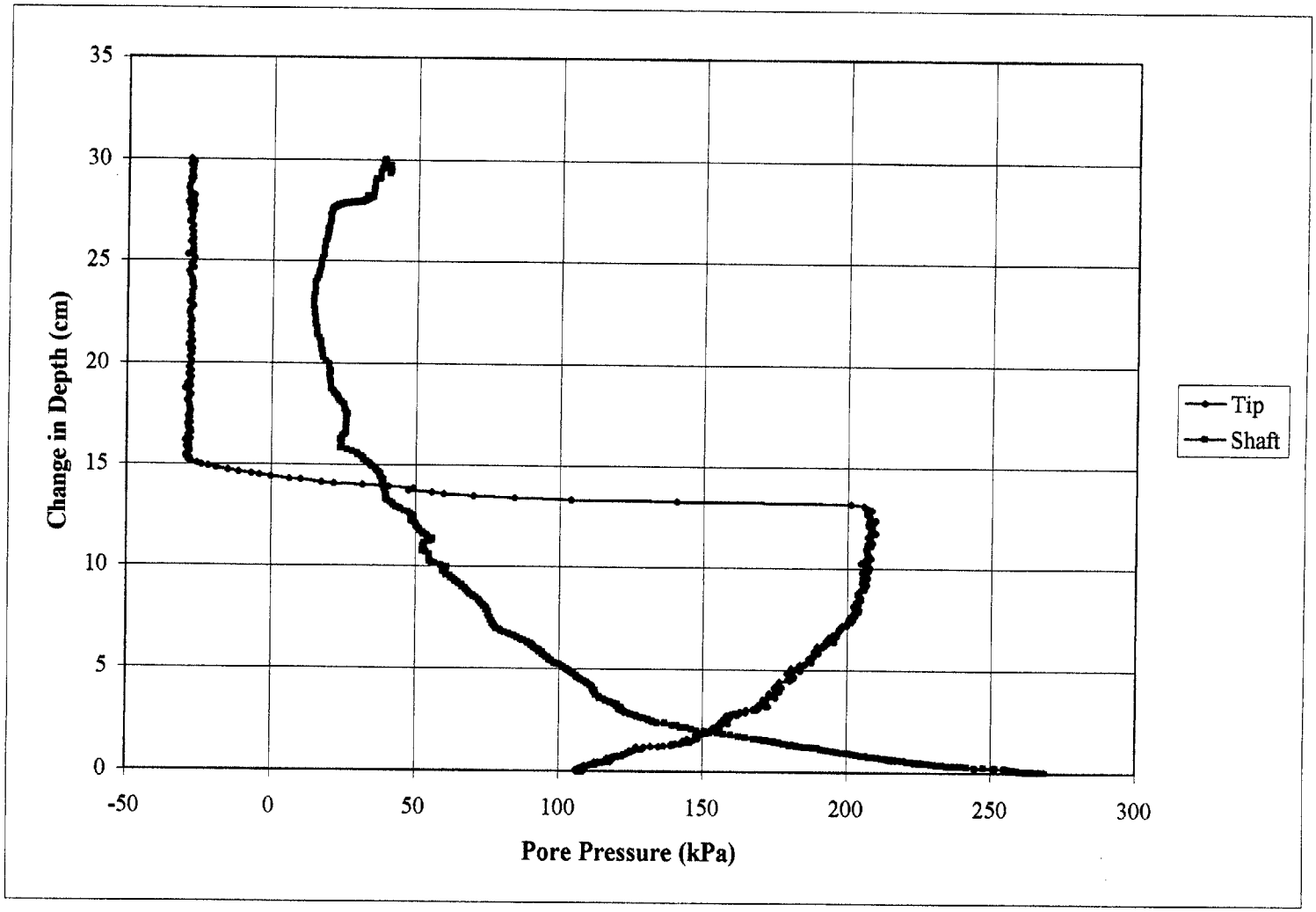

Figure 5.41c TP2_P1 Extraction Data - Pressure vs. Depth

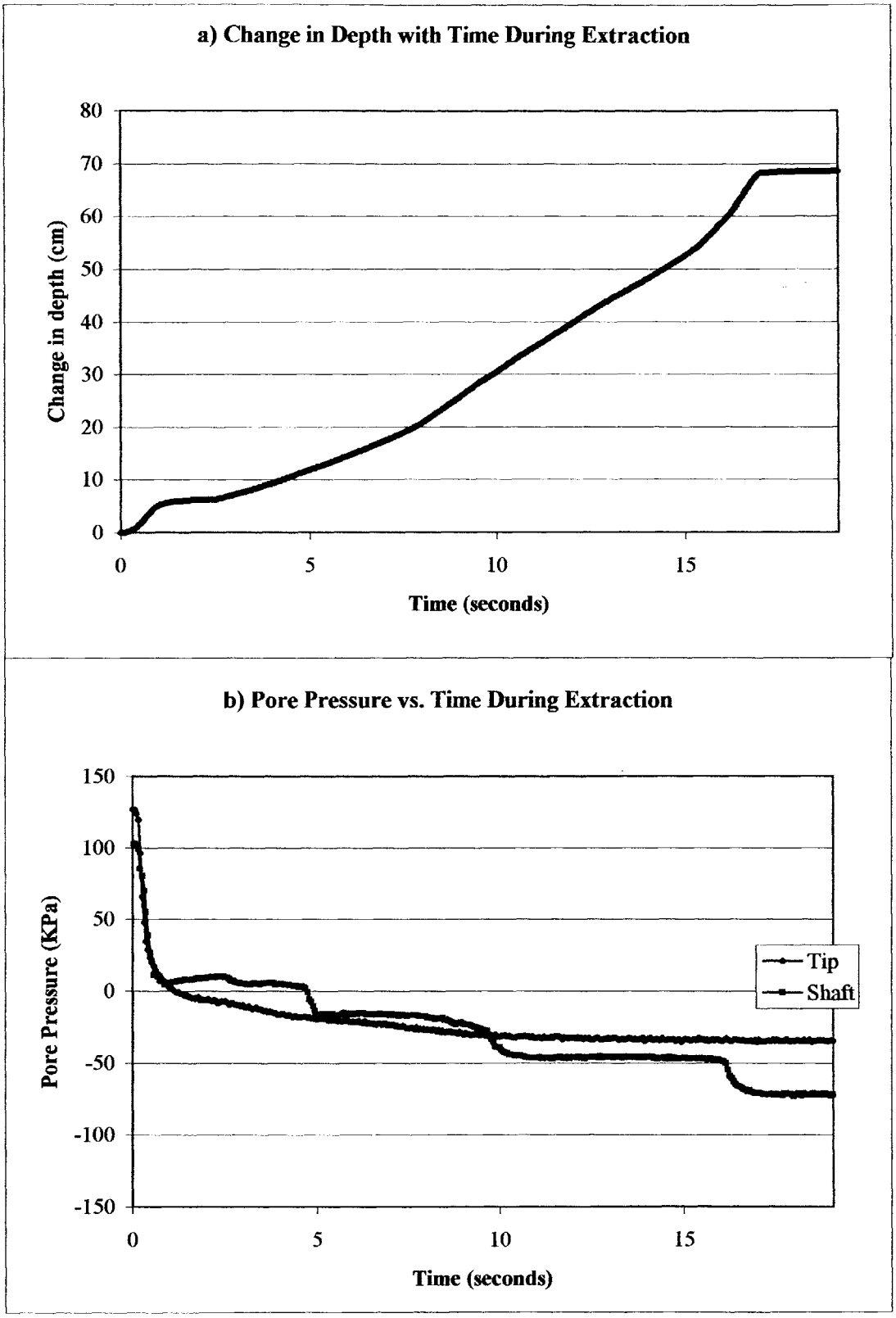

Figure 5.42 TP2_P2 Extraction Data

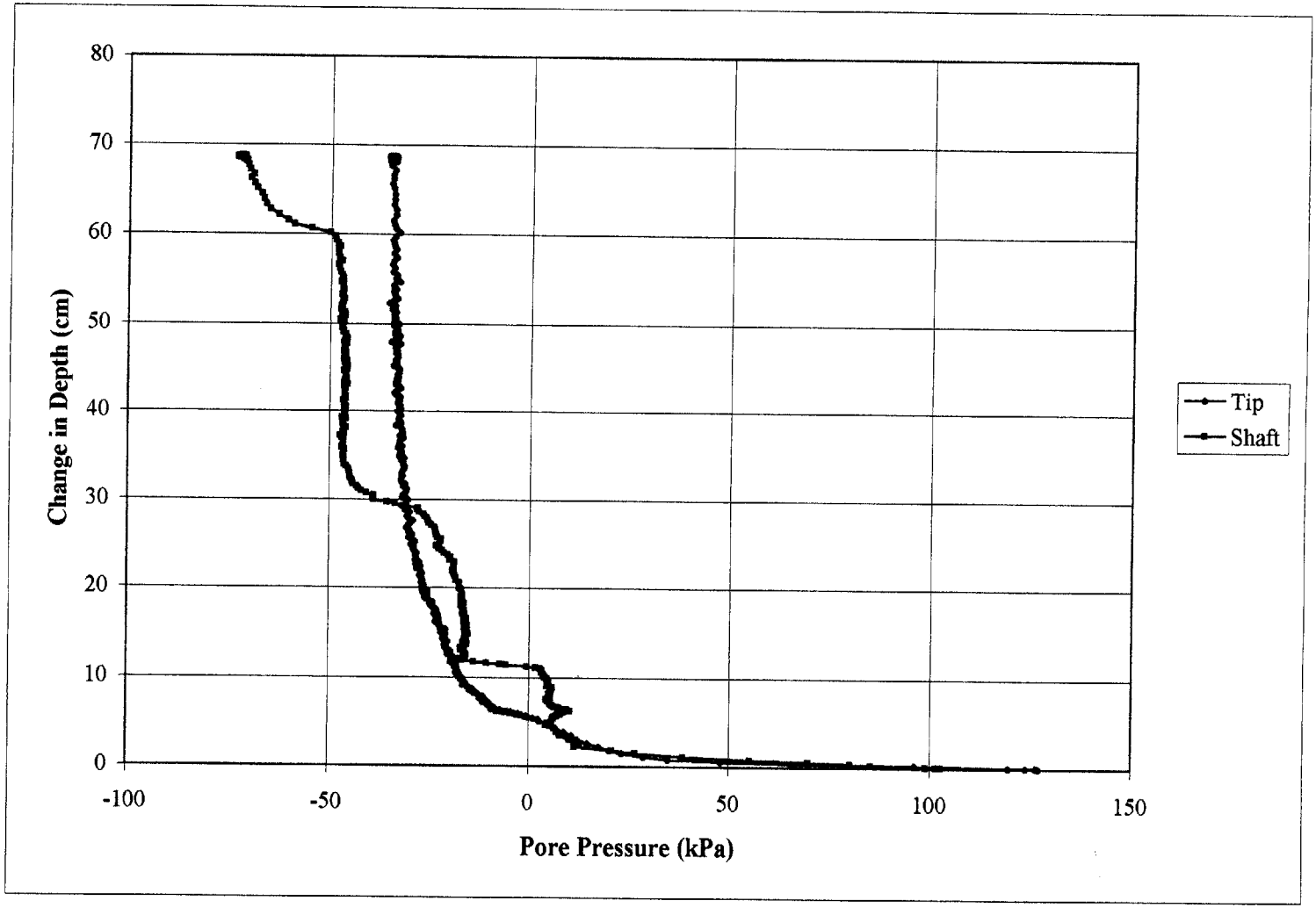

Figure 5.42c TP2_P2 Extraction Data - Pressure vs. Depth

6 INTERPRETATION OF FIELD DATA

In this chapter, the dissipation data is further evaluated and a number of methods are used to extrapolate in-situ pore pressure (u_o) and soil hydraulic conductivity (k) from the T2P field data. Section 6.1 examines differences between the T2P dissipation curves, Section 6.2 compares the time required for fifty percent dissipation (t_{50}) of excess pore pressures for the T2P with values of t_{50} from Varney's piezoprobe and piezocone data, Section 6.3 discusses the "brake points" exhibited in the T2P dissipation records, Section 6.4 examines the effectiveness of several methods for calculating u_o from dissipation records, and Section 6.5 evaluates a technique for determining k from pore pressure measurements.

6.1 Comparison of Dissipation Data

To compare the dissipation rates from each penetration, the normalized dissipated pore pressures measured at the tip and shaft filter locations are plotted versus time on a logarithmic scale in Figures 6.1 and 6.2, respectively, for penetrations TP1_P3, TP1_P4, TP1_P5, TP1_P6, and TP2_P2. The dissipation data from TP2_P1 was not included, since a different probe geometry was used for this penetration. It is apparent from Figures 6.1 that there are significant differences in the dissipation rates from the five penetrations, as measured at the tip filter location. The normalized pore pressures measured at the tip from TP1_P3 and TP1_P6 show a slight initial rise before the onset of dissipation; in contrast, the normalized pore pressures from the other penetrations continuously dissipate from the end of penetration. By examining the plot of pore pressure versus penetration depth for TP1_P6 in Figure 5.15c, it can be seen that this penetration ceased when the tip filter was located in a layer with relatively low generated excess pore pressure, causing the ratio of tip to shaft pressures to drop significantly below the average value for this penetration. Therefore, the tip value of installation pore pressure (u_i) used to calculate the resultant normalized pore pressures for this dissipation does not appear representative of the general soil behavior of the deposit. In addition, the ratio of tip to shaft pore pressures during penetration TP1_P3 was considerably lower than for other penetrations, as was mentioned in Section 5.1.3.1. Hence, the initial rises

in tip normalized pore pressure that occurred after penetrations TP1_P3 and TP1_P6 may have been caused by the influence of the relatively large pressure pulse from the shaft initially affecting pressure measurements made at the tip. However, it is not clear why the tip normalized pore pressures from TP1_P6 then drop off so quickly after the initial rise, relative to the other dissipation records.

As shown in Figure 6.2, the dissipation curves measured at the shaft are more uniform than those recorded at the tip and none of the shaft data exhibit the initial pressure increases seen in the TP1_P3 and TP1_P6 tip dissipation records. However, dissipations at the shaft for TP1_P3, TP1_P5, and TP1_P6 proceed more rapidly than for TP1_P4 and TP2_P2. These variations in the dissipation rates may be due to differences in the hydraulic conductivity of the layers in which dissipation at the shaft occurred for the five dissipations shown in this figure.

6.2 Time for 50% Dissipation (t_{50})

The time for 50% dissipation (t_{50}) is defined as the amount of time required for dissipation of 50% of the pressure difference between the installation pore pressure and the hydrostatic pore pressure. The values of t_{50} for each T2P penetration, calculated separately for tip and shaft pore pressure measurements, are listed in Table 6.1 and plotted versus depth in Figures 6.3. The t_{50} values from TP2_P1 are not included in these figures because of the altered probe geometry used for this penetration.

The t_{50} values measured at the tip vary from 4.6 seconds for TP1_P6 to 431 seconds for TP2_P2, with an average of 157 seconds and a standard deviation of 164 seconds. The relatively rapid drop in excess pore pressure measured at the tip during the initial stages of TP1_P6 dissipation caused the TP1_P6 value of t_{50} to be far smaller than the tip values of t_{50} from the remaining dissipations.

The shaft t_{50} values range from 479 seconds for TP1_P5 to 4925 seconds for TP2_P2, with an average of 2164 seconds and a standard deviation of 1944 seconds.

Varney (1998) measured t_{50} values from dissipation data collected during penetrations of FMMG piezoprobes and standard piezocones in normally consolidated BBC at the Saugus site. The resulting t_{50} values are shown in Table 6.2. The t_{50} values measured with the piezoprobes ranged from 27 to 114 seconds, with an average of 80

seconds and a standard deviation of 25 seconds. The piezocone t_{50} values varied from 1261 to 1822 seconds, with an average of 1541 seconds and a standard deviation of 175 seconds. By comparing the t_{50} values measured at the T2P tip with those measured with the FMMG piezoprobes, it can be seen that the time for 50% dissipation as measured at the T2P tip is generally longer than that measured with the piezoprobes. In addition, there is more scatter in the T2P tip data, suggesting more significant layering within the Newbury clay deposit than at the Saugus site.

The average t_{50} value measured at the T2P shaft is also larger than the average piezocone value. The standard deviation of the T2P shaft values is greater than that of the piezocone values, also supporting the hypothesis of more severe variability within the Newbury deposit.

6.3 Brake Points

From the plots of normalized pore pressures versus time on a logarithmic scale, it is apparent that normalized pressures measured at the tip of the T2P dissipate differently than those measured at the shaft. As described by Varney (1998) and mentioned in Chapter 2, normalized pore pressures measured at the tip typically decrease more rapidly than those measured at the shaft, and generally exhibit an inflection point or "brake point" at which the rate of change of normalized pore pressures significantly decreases. It is believed that this brake point occurs as the pressure pulse generated by the penetration of the larger diameter cone begins to affect pressure measurements made at the tip. Tip normalized pore pressure measurements from penetrations TP1_P3, TP1_P4, and TP1_P6 all display brake points. These points occur at dissipated pore pressure ratios ranging from 18 to 25% and occur from 31 to 828 seconds into dissipation. As mentioned in Chapter 2, Varney (1998) found that FMMG piezoprobe dissipation records from the Saugus site produced brake points at dissipated pore pressure ratios ranging from 10 to 20%.

6.4 Determination of In-situ Pore Pressure (u_o)

A variety of methods have been used to determine values of in-situ pore pressure from full or partial dissipation records. These methods include the evaluation of

complete dissipation records, the Inverse Time (1/t) Extrapolation method, and the Two Point Intersection Method (Sutabutr, 1998 and Whittle et al., 1997). These three methods will be used to evaluate u_o from the T2P field data, presented in Chapter 5.

6.4.1 Full Dissipation

Excess pore pressures generated from the penetration of a clay deposit by the T2P dissipate over time. Once full dissipation is complete, pore pressures measured at both the tip and shaft should equal in-situ pore pressures. Varney (1998) found that full dissipation of excess pore pressures due to the penetration of both piezoprobes and piezocones in BBC at the Saugus site took anywhere from 28 to 83 hours. Therefore, only overnight dissipation records from the T2P field test will be evaluated for the determination of in-situ pore pressures.

Of the eight penetrations performed during the field test, only TP1_P1, TP1_P5, and TP2_P2 involved overnight dissipations; for the remaining penetrations, the tool was removed from the borehole within 0.74 to 1.38 hours of the start of dissipation. Table 6.3 lists the measurement durations for the eight T2P penetrations.

Figures 6.4 through 6.6 show the TP1_P1, TP1_P5, and TP2_P2 dissipation records for tip and shaft pore pressure measurements. In each figure, the top plot (a) presents the dissipation record from pressure measurements made at the tip, and the bottom plot (b) depicts the pressure measurements made at the shaft. The final pore pressure values recorded at the end of each dissipation time interval (u_{diss}) are included in the figures, along with the respective calculated value of u_o. In order to account for electrical drift of the transducers over the monitoring periods, each figure also provides the final measured pore pressure value calculated using the final zero pressure value recorded at the end of each dissipation. Table 6.4 lists the ratio for each penetration of the final recorded tip and shaft pressure values to the corresponding hydrostatic pressures (u_{diss}/u_o). In this table, u_{diss} was calculated using both the initial zero pressure value and the final zero pressure value recorded for each dissipation.

The duration of the TP1_P1 dissipation record was 17.8 hours. For TP1_P1, the final pore pressures measured at the tip or shaft are significantly larger than the assumed

in-situ values. Full dissipation at either the tip or shaft most likely had not taken place by the time the final pressure measurements were made.

TP1_P5 dissipation was monitored for 16.4 hours. The value of u_{diss} measured at the shaft (90.17 KPa) is close to the assumed shaft in-situ pore pressure (89.32 KPa). However, u_{diss} measured at the tip (58.43 KPa) is considerably less than u_o at the tip (91.53 KPa), which is not realistic. As was shown in Table 4.5, the changes between initial and final zero pressure values measured at the tip and shaft for TP1_P5 were -31.78 and -12.92 KPa, respectively. Therefore, electrical drift of the two pore pressure transducers may have significantly affected the final measurements of pore pressure. If the tip and shaft values for u_{diss} are adjusted to account for the corresponding zero pressure changes, u_{diss} for the tip equals 90.21 KPa and u_{diss} for the shaft becomes 103.09 KPa. If these adjusted values represent the true dissipated pore pressures, dissipation around the tip may have been complete at the end of the measurement period.

Dissipation data for TP2_P2 was recorded for 19.7 hours. At the end of the monitoring period, u_{diss} at the shaft (83.52 KPa) approached the shaft in-situ value (74.41 KPa), while u_{diss} at the tip (48.81 KPa) dropped significantly below the tip u_o (76.76 KPa). However, unlike TP1_P5, the change from initial to final zero pressure values cannot explain the unrealistically low value of u_o measured at the tip for TP2_P2, since the final zero pressure reading was recorded several days after the monitoring period ended; therefore, this final zero pressure value cannot be used to evaluate u_{diss} for TP2_P2.

It appears likely that the TP1_P5 and TP2_P2 final shaft pore pressure measurements approached the hydrostatic values. The data also suggest that the dissipation monitoring periods were of insufficient duration to achieve hydrostatic conditions at the tip; thus, dissipation records recorded at the tip must be longer than 20 hours in order to reach the in-situ pore pressure, which is consistent with Varney's data from the Saugus site. However, there clearly was a significant problem with electrical drift of the tip transducer, adding to the difficulty in drawing conclusions from the data.

6.4.2 Inverse Time (1/t) Extrapolation

As mentioned in Chapter 1, the inverse time (1/t) extrapolation method is a technique used to estimate in-situ pore pressures from incomplete dissipation records.

For this method, dissipated pore pressure measurements are plotted against the inverse of time on a natural scale, with zero time selected as the moment penetration ceased. A tangent line is then extended from the final portion of the dissipation data, and the in-situ pore pressure ($u_{1/t}$) is chosen as the intersection pore pressure at $1/t = 0$. As the dissipation measurement duration increases, the accuracy of this technique in estimating u_o improves.

This method was used to evaluate $u_{1/t}$ from dissipation records TP1_P3, TP1_P4, TP1_P5, TP1_P6 and TP2_P2 at 100, 166.7, 250, 500, and 1000 seconds after the start of dissipation. The TP2_P1 dissipation record was not included in this analysis due to the altered tip geometry used for this dissipation. Figures 6.7 through 6.11 illustrate how this technique was used to calculate $u_{1/t}$ from TP2_P2 tip and shaft dissipation records. From these figures, it is apparent that dissipated pore pressures, when plotted as a function of inverse time, become non-linear at large inverse time scales. Hence, the 1/t extrapolation method overestimates u_o when large inverse time ranges are used (Varney, 1998).

For this technique, the error is defined as the difference between the calculated value of $u_{1/t}$ and the assumed value of the in-situ pore pressure (u_o), normalized by the pressure increment from u_o to the installation pore pressure value (u_i), i.e. $(u_{1/t}- u_o)/(u_i- u_o)$. As previously suggested, electrical drift of the transducers and the relatively short timeframe of the T2P dissipations may have prevented the final measured pore pressures during dissipation (u_{diss}) from equaling the respective in-situ values, particularly for the tip data. Therefore, in order to eliminate the influence of electrical drift of the transducers during dissipation and the uncertainty if dissipated pressures reached equilibrium values, the error in $u_{1/t}$ is evaluated relative to u_o instead of u_{diss} for the T2P data. In addition, it is unlikely that electrical drift of the transducers had a significant impact on the first 1000 seconds of the dissipation records; thus, using a range of t from 100 to 1000 seconds should prevent electrical drift from influencing the results of the inverse time extrapolation method.

Tables 6.5 and 6.6 list the calculated values of $u_{1/t}$ determined at selected points on the dissipation curves, and the corresponding errors for each value. Figures 6.12 and 6.13 plot the error values as a function of elapsed dissipation time (t), normalized by the

time for 50% dissipation for each penetration (i.e., as a function of t/t_{50}). Figure 6.12 presents the values as a function of t/t_{50} using a natural scale and Figure 6.13 plots the values against the logarithm of t/t_{50}. The top plots (a) in these figures indicate that the TP1_P6 tip data has a much greater range of t/t_{50} values than does the tip data from the other T2P dissipations. This is due to the fact that the value of t_{50} from TP1_P6 (4.6 sec) is far smaller than any other value of t_{50} from the remaining dissipations, as is shown in Tables 6.1 and 6.5.

Figures 6.14 and 6.15 present results from 1/t extrapolation performed on complete dissipation records from piezoprobe and piezocone penetrations performed in BBC at the Saugus site by Varney (1998). Also included in these figures are data from model predictions for both the piezoprobe and piezocone. The 1/t extrapolation was performed on the Saugus data at time intervals after the start of dissipation of 100, 166.7, 250, 500, 1,000, 10,000, 16,667, and 25,000 seconds. Because of similarities in geometry, the T2P tip data will be compared with Varney's piezoprobe results and the T2P shaft data will be contrasted with the piezocone results. To evaluate the accuracy of the inverse time extrapolation method with the piezoprobe and piezocone data, Varney (1998) compared each calculated value of $u_{1/t}$ to the corresponding final measured dissipated pore pressure (u_{diss}), rather than the assumed in-situ pore pressure value (u_o). The piezoprobe and piezocone dissipation records were of sufficient length for full dissipation to occur and u_{diss} can be assumed to equal the equilibrium pore pressure. However, the T2P records were generally too short to allow for full dissipation; thus, this method of error evaluation could not be performed with the T2P data.

For the T2P tip data, the error drops below 10% at a normalized time of approximately 6, corresponding to an average monitoring time of 942 seconds. In contrast, the error from the measured piezoprobe data becomes less than 10% at a normalized time of roughly 3, which corresponds to a monitoring period of 240 seconds.

For the T2P shaft data, the error becomes less than 10% at a normalized time of approximately 2, corresponding to an average time of 4328 seconds. The error from the piezocone data drops below 10% at a normalized time of 3.5, corresponding to an average measurement period of 5,871 seconds.

From these results, it seems likely that inverse time extrapolation will predict in-situ pore pressures within 10% accuracy from either T2P tip or piezoprobe dissipation records in reasonable periods of time for routine use in sub-seafloor explorations. However, the average length of the monitoring periods required for estimation of in-situ pressures from dissipation records measured either with a piezocone or at the T2P shaft appears to be too long to use routinely for marine investigations.

6.4.3 Two-Point Intersection Method

The two-point intersection method, described in Chapters 1 and 2, was used to estimate in-situ pore pressures from the TP1_P3, TP1_P4, and TP1_P6 dissipation records. Intersection points did not occur for the TP1_P5, TP2_P1, or TP2_P2 dissipation data. It is not surprising that the TP2_P1 record does not exhibit an intersection point, since an altered tip geometry was used for this dissipation. However, the reasons for the lack of intersection points in the TP1_P5 and TP2_P2 data are not as obvious. As discussed in Chapter 5, sudden changes in tool position occurred during the last few seconds of these penetrations, leading to abrupt drops in pore pressure around the probe. These pressure drops had the effect of reducing the values of installation pore pressure (u_i) used in all subsequent calculations of dissipated excess pore pressures (u_i-u) and excess pore pressure ratios ($(u-u_o)/(u_i-u_o)$), possibly preventing the intersection point from being apparent in the TP1_P5 and TP2_P2 data.

The top plots (a) in Figures 6.16 through 6.18 present dissipated excess pore pressures versus time on a logarithmic scale for the three T2P dissipations that had intersection points. The bottom plots (b) in these figures show the corresponding normalized pore pressure data. Table 6.7 lists the relevant data for these dissipations, including the calculated values of u_{2pt}. As discussed in Chapter 2, the theoretical results predict that the intersection point will occur at 92% dissipation of excess pore pressure at the T2P tip. Thus, by measuring u_i and the tip pore pressure at the time of intersection (u), the in-situ pressure is calculated by setting $(u-u_{2pt})/(u_i-u_{2pt}) = 0.088$, where u_{2pt} is the in-situ pore pressure calculated using the two-point intersection method.

In order to evaluate the accuracy of the method among dissipations, u_{2pt} was compared with the assumed hydrostatic in-situ pore pressure (u_o), and then normalized by

the interval from the installation pore pressure to the hydrostatic pore pressure (i.e, $(u_{2pt}-u_o)/(u_i-u_o)$). As shown in Table 6.7, values of this ratio, calculated using the two-point intersection method on T2P dissipation data, range from –0.03 for TP1_P6 to 0.11 for TP1_P4, with an average ratio of 0.04 and a standard deviation of 0.07. The time from the start of each dissipation to the intersection point (t_p) ranged from 525 to 2769 seconds, with an average value of 1641 seconds and a standard deviation of 1122 seconds.

In comparison, Varney (1998) used the two-point matching method to calculate in-situ pore pressures from piezoprobe and piezocone dissipation records measured in BBC at the Saugus site. A tapered probe capable of making simultaneous pressure measurements at two locations along its surface was not available at the time. Instead, piezoprobe and piezocone dissipation records, measured at identical depths within boreholes in close proximity, were combined to determine the intersection point that would have occurred if a dual pressure probe had been used. Using this approach, the time required to reach the intersection point from the beginning of dissipation ranged from 517 to 7225 seconds, with an average of 3543 seconds and a standard deviation of 2102 seconds. Hence, the time required to reach the intersection condition appears to be significantly shorter for the T2P than for the other devices.

As in the case of the inverse time extrapolation method, Varney (1998) used the values of dissipated pore pressure (u_{diss}) to evaluate the accuracy of the two-point intersection method with the piezoprobe and piezocone data, rather than the assumed in-situ pore pressure value (u_o). Once again, the use of u_{diss} for purposes of comparison was acceptable for the Saugus data, since the piezoprobe and piezocone dissipation records were of sufficient length for full dissipation to occur and u_{diss} can be assumed to equal the equilibrium pore pressure. The values of the resulting ratio (i.e., $(u_{2pt}-u_{diss})/(u_i-u_{diss})$) from the piezoprobe and piezocone data ranged from –0.05 to 0.11, with an average of –0.01 and a standard deviation of 0.04.

There are several possible reasons why the average accuracy of the two-point intersection method was greater when applied to the combined piezoprobe and piezocone data from Saugus than when used on the T2P dissipations recorded at the Newbury site. First, significantly fewer dissipations were conducted for the T2P field test than were

performed using the piezoprobes and piezocones at Saugus; hence, the limited T2P data set may not accurately represent the true capabilities of the tool. As previously mentioned, transducer drift and pressure fluctuations due to faulty electrical connections significantly affected much of the T2P tip dissipation data. In addition, the changes in the stress field that probably occurred when the position of the tool shifted at the end of penetration TP1_P4 are not accounted for in the theoretical model. Hence, this discrepancy between the theoretical model and the stress distribution in the field may have caused problems when applying the two point intersection method to the TP1_P4 dissipation data. As previously mentioned, the same site was not used for all devices; consequently, the influence of variability within and among the soil deposits cannot be discounted in these results. Model predictions of the normalized pore pressure at the intersection point (U_p) assume a homogeneous soil deposit. As suggested in Chapter 5, the T2P tip penetration data indicated significant layering within the Newbury site clay layer; therefore, the accuracy of the predicted value of U_p may have been reduced by this stratigraphy. Additionally, the fact that the T2P values of u_{2pt} were compared to an assumed value of u_o, instead of a measured value of u_{diss}, may also have affected the results.

6.4.4 Comparison of Methods for Estimating In-Situ Pore Pressure

Since Varney (1998) found that it took a minimum of 28 hours to reach full dissipation of penetration-induced pore pressures, and the longest T2P monitoring period was 19.7 hours, it is uncertain whether full dissipation occurred for any of the overnight T2P dissipations. A subsequent T2P field test involving longer dissipation periods is necessary to evaluate the accuracy of T2P long-term dissipation measurements.

To compare the effectiveness of the inverse time extrapolation method with the two-point intersection method, predictions of $u_{1/t}$ were made for TP1_P3, TP1_P4, and TP1_P6 at similar dissipation times as was required for the corresponding intersection points to occur. The resulting ratios of $(u_{1/t}-u_o)/(u_i-u_o)$ can then be compared to the respective ratios of $(u_{2pt}-u_o)/(u_i-u_o)$ calculated at the same dissipation times. Table 6.8 tabulates these ratios.

From this table, it can be seen that the two-point intersection method consistently produces more accurate measurements of in-situ pore pressure that the inverse time extrapolation method does at similar dissipation times.

6.5 Determination of Hydraulic Conductivity (k)

The T50 matching method, described in Chapter 1, was used to estimate the hydraulic conductivity of the BBC deposit from tip and shaft pore pressure measurements made during dissipations TP1_P3, TP1_P4, TP1_P5, TP1_P6, and TP2_P2. This method was not used on the TP2_P2 dissipation record because model predictions were not available for the altered probe geometry used during this penetration. K_o was assumed to equal 0.5 and vertical effective stresses were determined from the effective stress profile shown in Figure 2.5. The resulting values of hydraulic conductivity calculated from tip and shaft dissipation measurements are listed in Tables 6.9 and 6.10, respectively, and are plotted versus depth in Figure 6.19.

The values of hydraulic conductivity calculated from the tip pressure measurements range from 1.8×10^{-8} to 1.4×10^{-6} cm/s, with an average value of 3.3×10^{-7} cm/sec and a standard deviation of 6.1×10^{-7} cm/s. The values of k from the shaft dissipation records range from 2.6×10^{-8} to 2.4×10^{-7} cm/s, with an average of 1.1×10^{-7} cm/sec and a standard deviation of 8.7×10^{-8} cm/s. As shown in Figure 6.19, hydraulic conductivity generally increases with depth, as calculated from the tip and shaft data. For TP1_P3, TP1_P4, and TP2_P2, the values of k determined from tip measurements are relatively consistent with those calculated from shaft data. However, the hydraulic conductivity values from the tip differ significantly from those at the shaft for dissipations TP1_P5 and TP1_P6. It is possible that the tip and shaft were located in layers with considerably different hydraulic conductivities while these dissipations were occurring.

As was shown in Figure 2.13, Varney (1998) found that laboratory measurements of the hydraulic conductivity of the normally consolidated portion of the Saugus BBC deposit ranged from approximately 2.5×10^{-8} to 1.5×10^{-7} cm/sec. With the exception of the value of k calculated from TP1_P6 tip data (1.4×10^{-6} cm/sec), Varney's findings are consistent with the values of k from the T50 matching method applied to the T2P

dissipation data. These results support the validity of this method when used on partial T2P dissipation records.

Penetration Number	Tip Depth (m)	Tip t_{50} (sec)	Shaft Depth (m)	Shaft t_{50} (sec)
TP1_P3	8.38	80.2	8.17	1228.2
TP1_P4	9.96	97.8	9.75	3469.3
TP1_P5	11.43	172.0	11.22	478.8
TP1_P6	12.80	4.6	12.59	720.8
TP2_P1	8.38	531.1	8.17	2357.5
TP2_P2	9.91	431.2	9.70	4924.5

Table 6.1 Time to 50% Dissipation (t_{50}) for T2P

Piezoprobe Depth (m)	Piezoprobe t_{50} (sec)	Piezocone Depth (m)	Piezocone t_{50} (sec)
25.94	114	25.81	1530
25.97	84	26.02	1822
28.98	27	28.86	1513
29.02	94	29.07	1606
32.03	80	31.91	1701
32.07	71	32.12	1377
35.08	76	34.96	1261
35.11	94	35.17	1521

Table 6.2 Piezoprobe and Piezocone t_{50} values from the Saugus Site (Varney, 1998)

Penetration	Dissipation Time (hrs)	Dissipation Time (sec)
TP1_P1	17.79	64049
TP1_P2	0.74	2660
TP1_P3	1.36	4883
TP1_P4	1.38	4964
TP1_P5	16.41	59091
TP1_P6	1.28	4607
TP2_P1	1.25	4517
TP2_P2	19.74	71061

Table 6.3 Dissipation Measurement Durations

	u_{diss} from initial zero values		u_{diss} from final zero values	
Penetration	Tip (u_{diss}/u_o)	Shaft (u_{diss}/u_o)	Tip (u_{diss}/u_o)	Shaft (u_{diss}/u_o)
TP1_P1	1.44	1.28	*	1.28
TP1_P5	0.64	1.01	0.99	1.15
TP2_P2	0.64	1.12	**	**

* There was no final response from the tip transducer for TP1_P1; thus, no final zero value was recorded.

** The final zero value for TP2_P2 was not recorded until several days after the last pore pressure measurement. Therefore, it was not included in the analysis.

Table 6.4 Ratio of Final Measured Pore Pressure (u_{diss}) to Assumed In-Situ Value (u_o), Using Both Initial and Final Zero Pressure Values

Penetration	Depth bgs (m)	t_{50} (sec)	u_i (kPa)	u_o (kPa)	t (sec)	$u_{1/t}$ (kPa)	t/t50	$(u_{1/t} - u_o)/(u_i - u_o)$
TP1_P3	8.38	80.2	388.56	61.61	100	173.78	1.2	0.34
					166.7	142.69	2.1	0.25
					250	123.52	3.1	0.19
					500	91.8	6.2	0.09
					1000	87.69	12.5	0.08
TP1_P4	9.96	97.8	271.36	77.11	100	129.93	1.0	0.27
					166.7	127.34	1.7	0.26
					250	108.12	2.6	0.16
					500	108.11	5.1	0.16
					1000	95.2	10.2	0.09
TP1_P5	11.43	172.0	249.29	91.53	100	285.01	0.6	1.23
					166.7	160.35	1.0	0.44
					250	118.95	1.5	0.17
					500	116.37	2.9	0.16
					1000	113.56	5.8	0.14
TP1_P6	12.80	4.6	307.94	104.97	100	116.76	21.7	0.06
					166.7	116.76	36.2	0.06
					250	116.76	54.3	0.06
					500	116.76	108.7	0.06
					1000	116.76	217.4	0.06
TP2_P2	9.91	431.2	172.79	76.62	100	136.88	0.2	0.63
					166.7	122.23	0.4	0.47
					250	120.65	0.6	0.46
					500	113.05	1.2	0.38
					1000	106.46	2.3	0.31

Table 6.5 Inverse Time Extrapolation Method for Determination of u_o – Tip Data

Penetration	Depth bgs (m)	t_{50} (sec)	u_i (kPa)	u_o (kPa)	t (sec)	$u_{1/t}$ (KPa)	t/t50	$(u_{1/t} - u_o)/(u_i-u_o)$
TP1_P3	8.16	1228.2	590.33	59.40	100	413.46	0.1	0.67
					166.7	391.45	0.1	0.63
					250	372.59	0.2	0.59
					500	330.86	0.4	0.51
					1000	261.1	0.8	0.38
TP1_P4	9.74	3469.3	433.42	74.90	100	368.58	0.0	0.82
					166.7	360.04	0.0	0.80
					250	345.60	0.1	0.76
					500	314.49	0.1	0.67
					1000	286.68	0.3	0.59
TP1_P5	11.22	478.8	415.68	89.32	100	285.01	0.2	0.60
					166.7	266.58	0.3	0.54
					250	227.36	0.5	0.42
					500	158.22	1.0	0.21
					1000	112.81	2.1	0.07
TP1_P6	12.58	720.8	536.74	102.76	100	381.38	0.1	0.64
					166.7	357.55	0.2	0.59
					250	322.53	0.3	0.51
					500	264.20	0.7	0.37
					1000	165.12	1.4	0.14
TP2_P2	9.7	4924.5	349.43	74.41	100	313.6	0.0	0.87
					166.7	306.09	0.0	0.84
					250	298.9	0.1	0.82
					500	274.82	0.1	0.73
					1000	243.78	0.2	0.62

Table 6.6 Inverse Time Extrapolation Method for Determination of u_o – Shaft Data

Penetration	Depth (m)	U_p	u_i at tip (kPa)	(u_i-u) at tip (kPa)	dissipation time (sec)	u_o at tip (kPa)	u_{2pt} (kPa)	$(u_{2pt}-u_o)/(u_i-u_o)$
TP1_P3	8.38	0.088	388.6	284.3	1628.2	61.6	76.94	0.047
TP1_P4	9.96	0.088	271.4	158.3	2769.3	77.1	97.83	0.107
TP1_P6	12.8	0.088	307.9	189.8	525.0	105.0	99.71	-0.026

Table 6.7 T2P Two-Point Matching Data

Penetration	dissipation time (sec)	u_{2pt} (kPa)	Tip $u_{1/t}$ (kPa)	Shaft $u_{1/t}$ (kPa)	Tip $(u_{1/t}-u_o)/(u_i-u_o)$	Shaft $(u_{1/t}-u_o)/(u_i-u_o)$	$(u_{2pt}-u_o)/(u_i-u_o)$
TP1_P3	1628.2	76.9	87.7	216.8	0.080	0.296	0.047
TP1_P4	2769.3	97.8	104.5	173.2	0.141	0.274	0.107
TP1_P6	525.0	99.7	116.8	264.2	0.058	0.372	-0.025

Table 6.8 Comparison Between Inverse Time Extrapolation and Two-Point Matching Methods for T2P Data

Penetration	σ_v' (kg/cm^2)	σ' (kg/cm^2)	t_{50} (sec)	Depth (m)	k (cm/sec)
TP1_P3	0.93	0.31	80.2	8.38	1.1E-07
TP1_P4	1.05	0.35	97.8	9.96	8.1E-08
TP1_P5	1.16	0.39	172	11.43	4.1E-08
TP1_P6	1.27	0.42	4.6	12.8	1.4E-06
TP2_P2	1.05	0.35	431.2	9.91	1.8E-08
				Average =	3.3E-07
				Std. Dev.=	6.1E-07

Figure 6.9 Values of Hydraulic Conductivity (k) from the T_{50} Matching Method – T2P Tip Data

Penetration	σ_v' (kg/cm^2)	σ' (kg/cm^2)	t_{50} (sec)	Depth (m)	k (cm/sec)
TP1_P3	0.91	0.30	1228.2	8.17	1.2E-07
TP1_P4	1.03	0.34	3469.3	9.75	3.7E-08
TP1_P5	1.14	0.38	478.8	11.22	2.4E-07
TP1_P6	1.25	0.42	720.8	12.59	1.5E-07
TP2_P2	1.03	0.34	4924.5	9.70	2.6E-08
				Average =	1.1E-07
				Std. Dev. =	8.7E-08

Figure 6.10 Values of Hydraulic Conductivity (k) from the T_{50} Matching Method – T2P Shaft Data

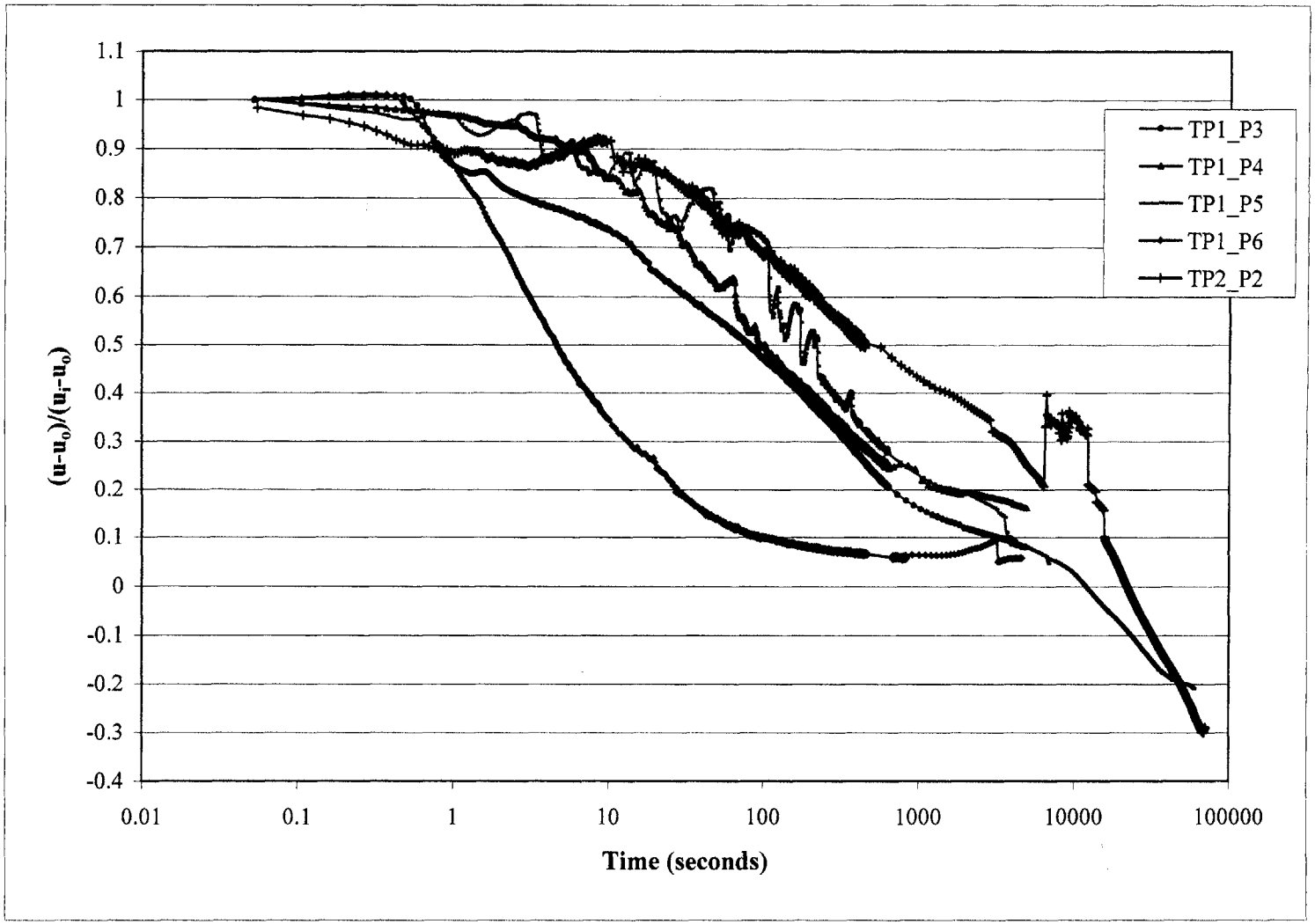

Figure 6.1 Combined Normalized Dissipated Pore Pressure Records from Tip Measurements

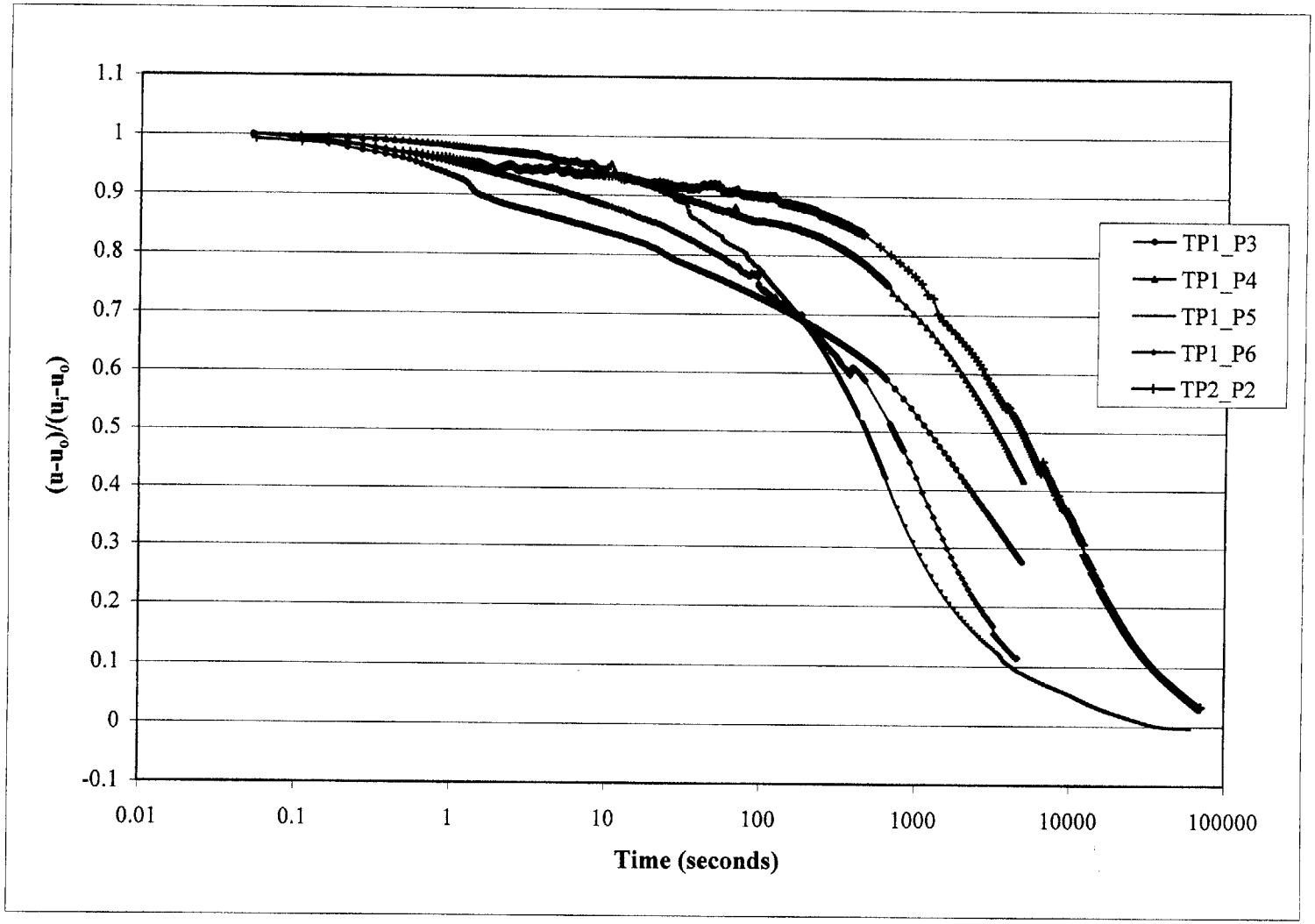

Figure 6.2 **Combined Normalized Dissipated Pore Pressure Records from Shaft Measurements**

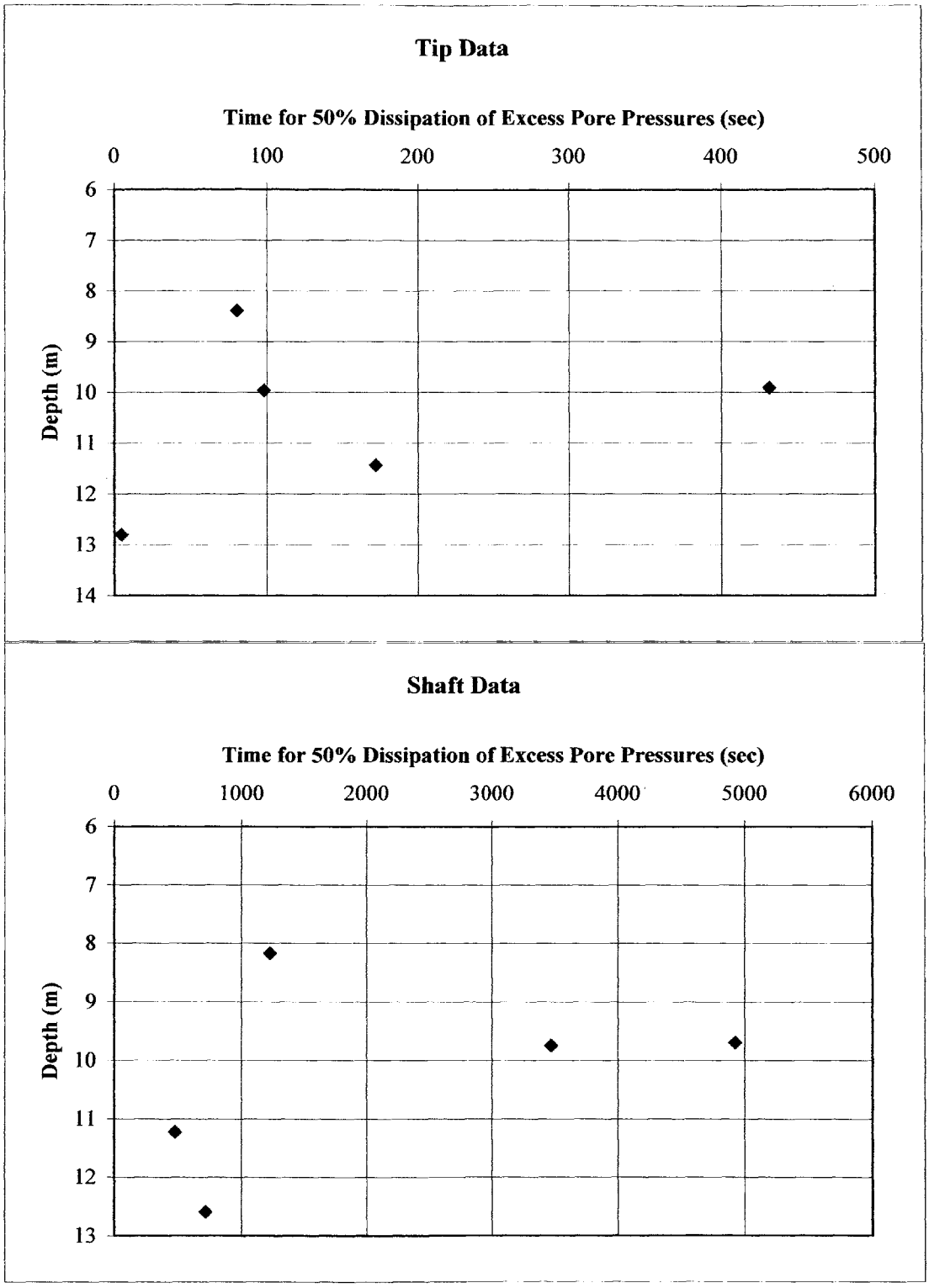

Figure 6.3 Values of t_{50} from T2P Dissipation Data

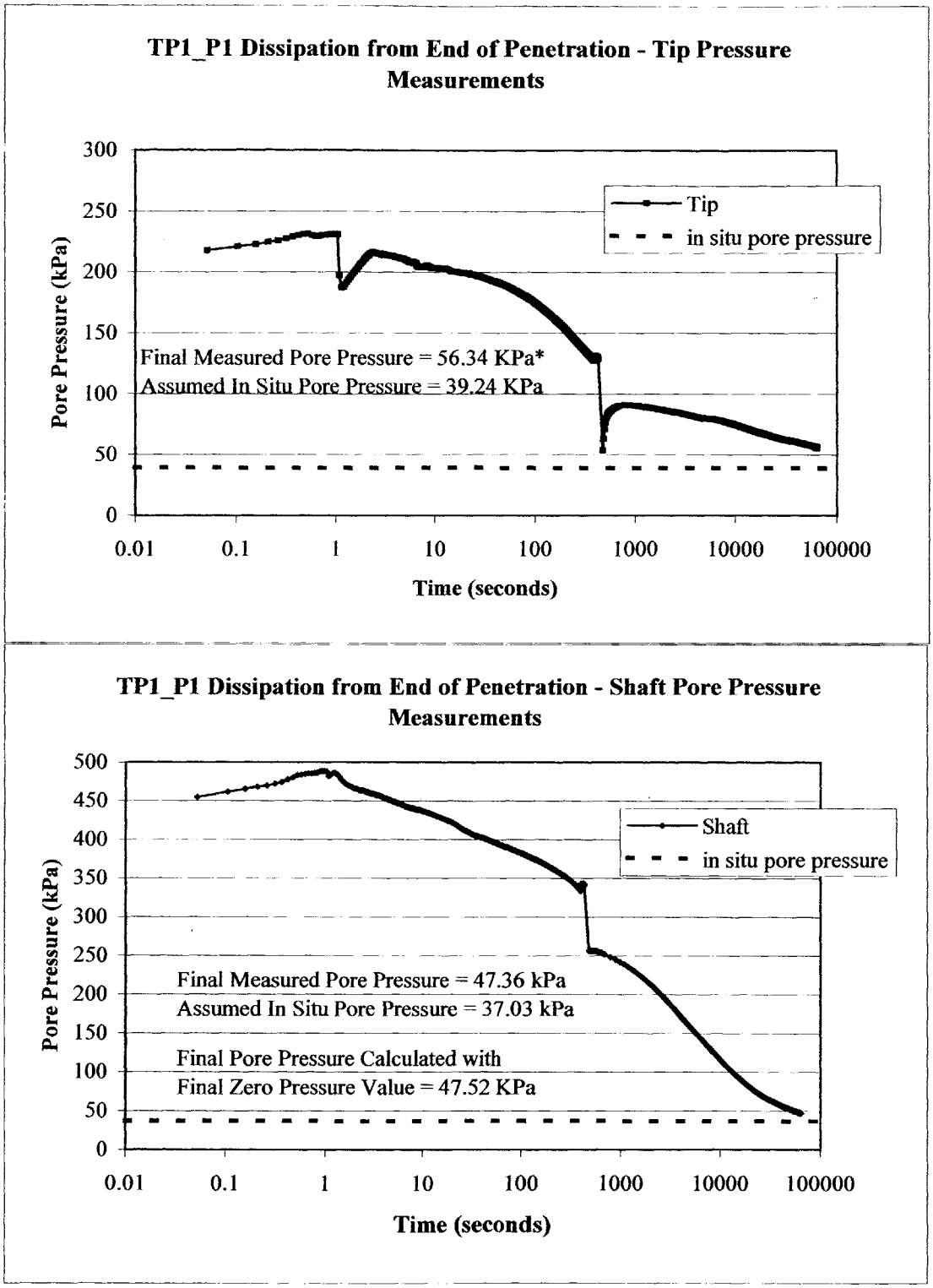

* There was no final response from the tip transducer, thus no final zero value was recorded

Figure 6.4 Tip and Shaft Dissipation Records for TP1_P1

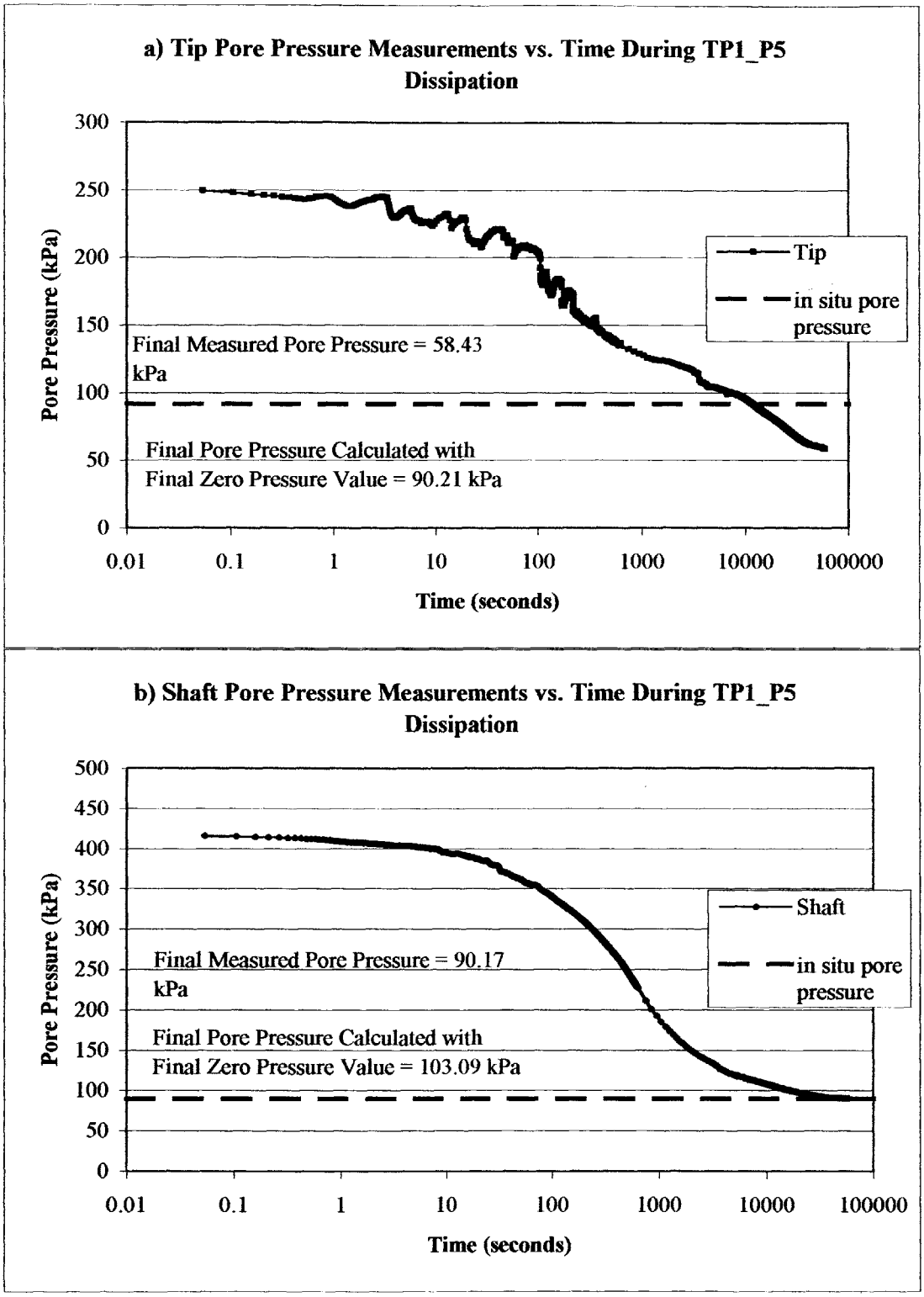

Figure 6.5 Tip and Shaft Dissipation Records for TP1_P5

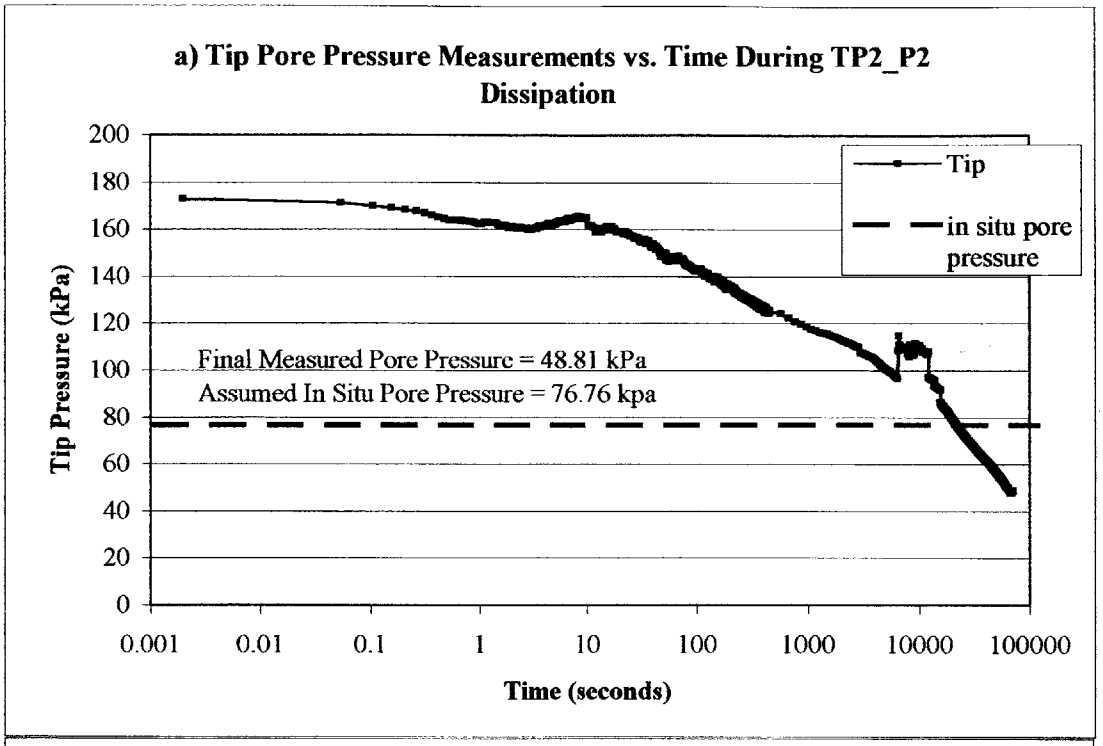

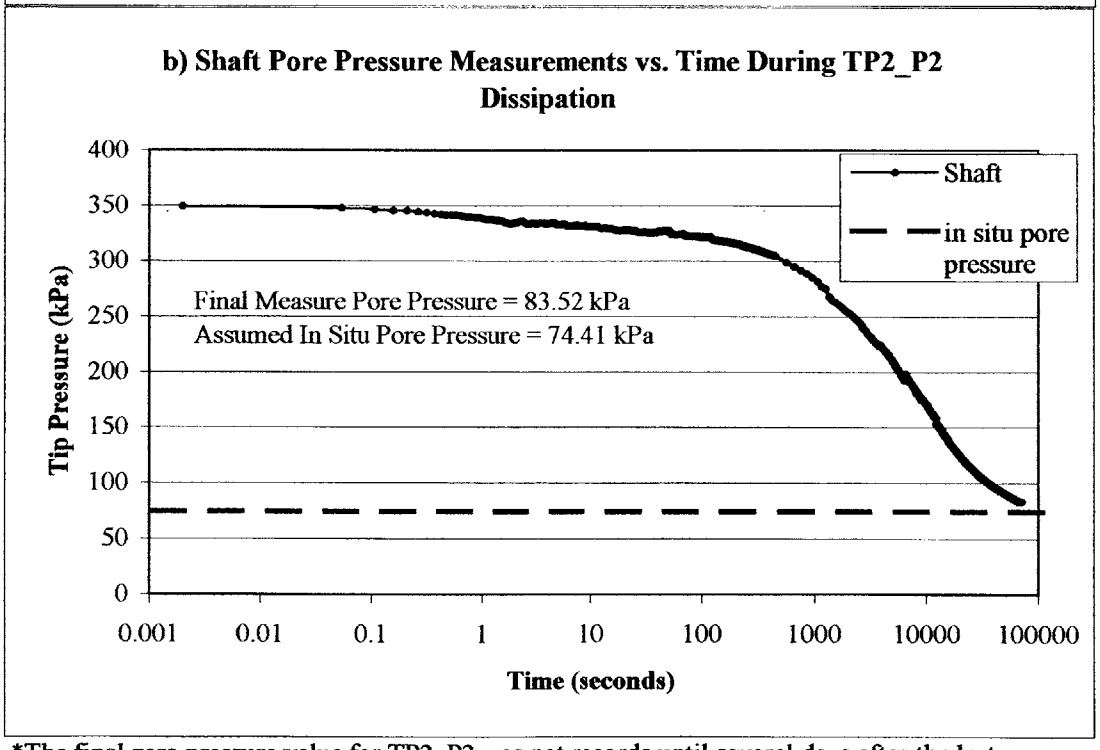

*The final zero pressure value for TP2_P2 was not records until several days after the last pore pressure measurement. Therefore, it is not included in the analysis.

Figure 6.6 Tip and Shaft Dissipation Records for TP2_P2

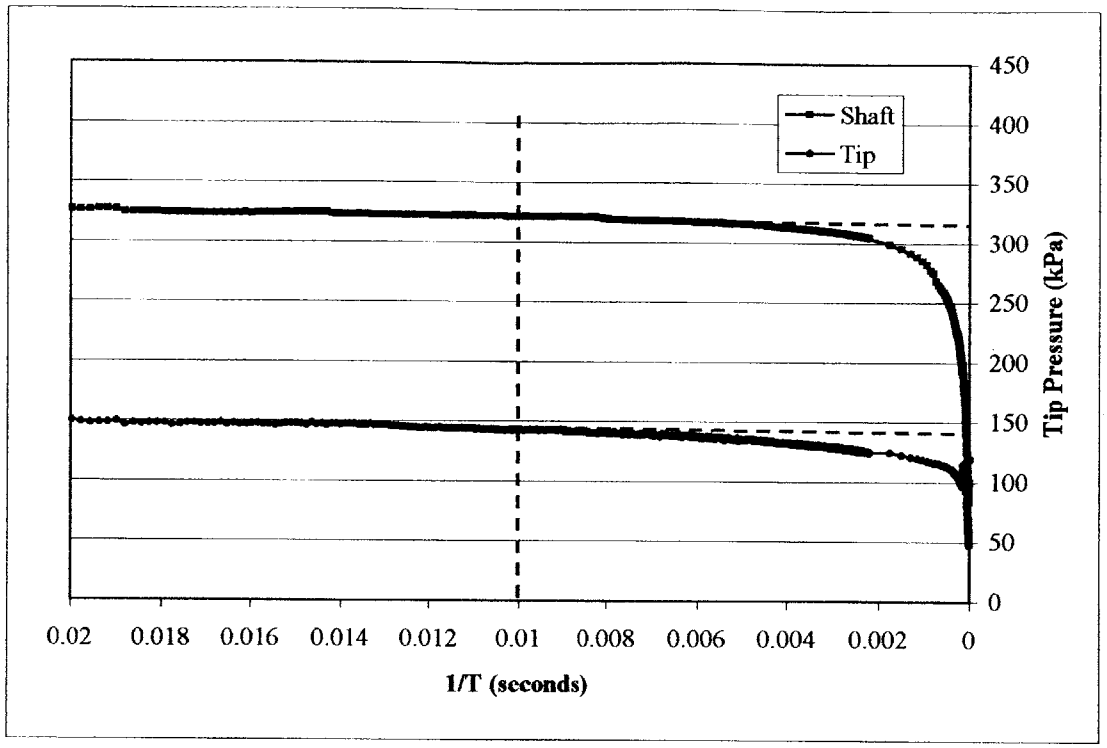

Figure 6.7 1/t Method on TP2_P2 Dissipation Record with t = 100 sec

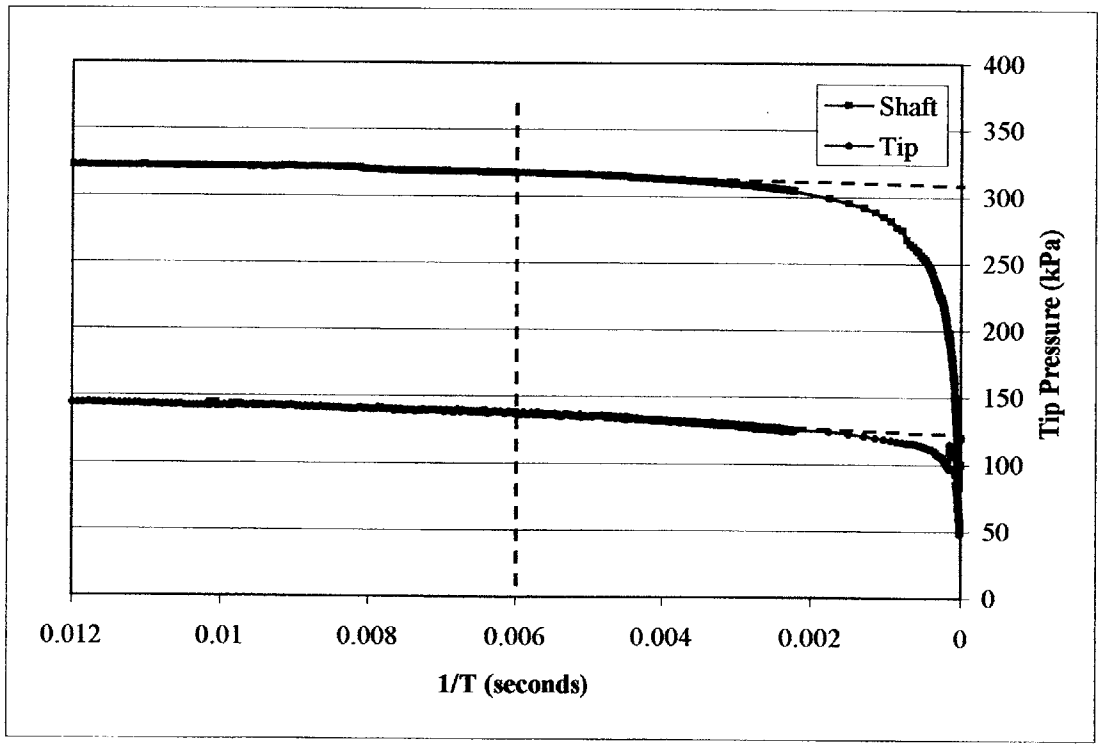

Figure 6.8 1/t Method on TP2_P2 Dissipation Record with t = 166.7 sec

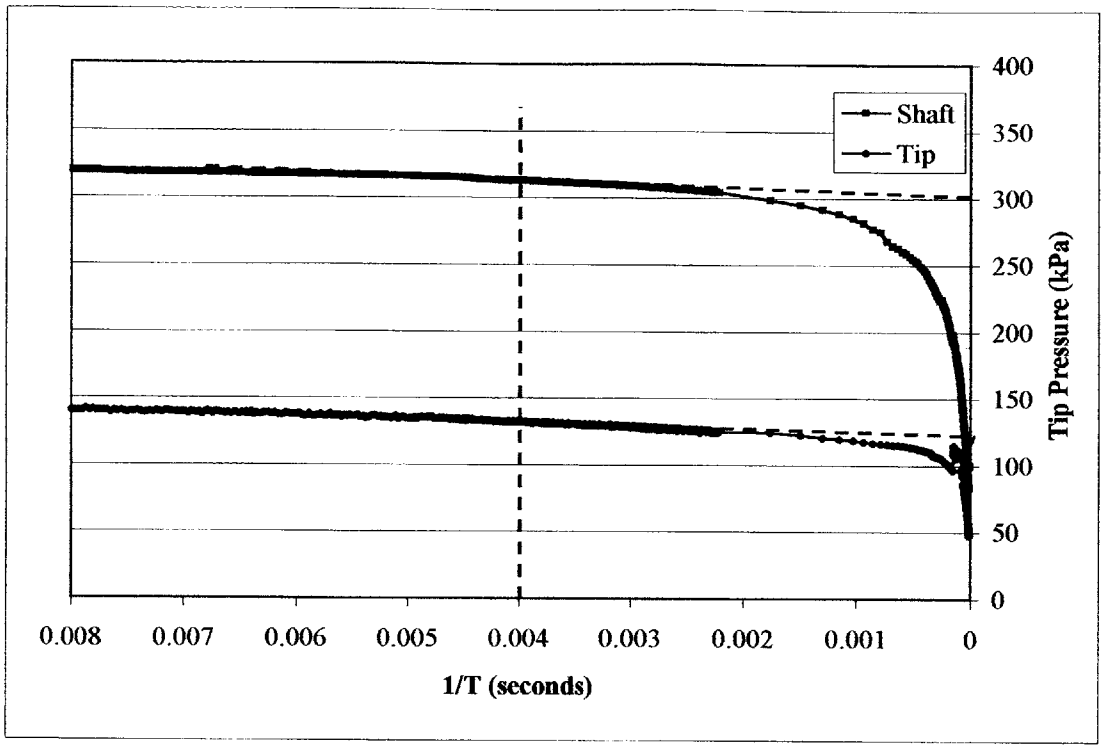

Figure 6.9 **1/t Method on TP2_P2 Dissipation Record with t = 250 sec**

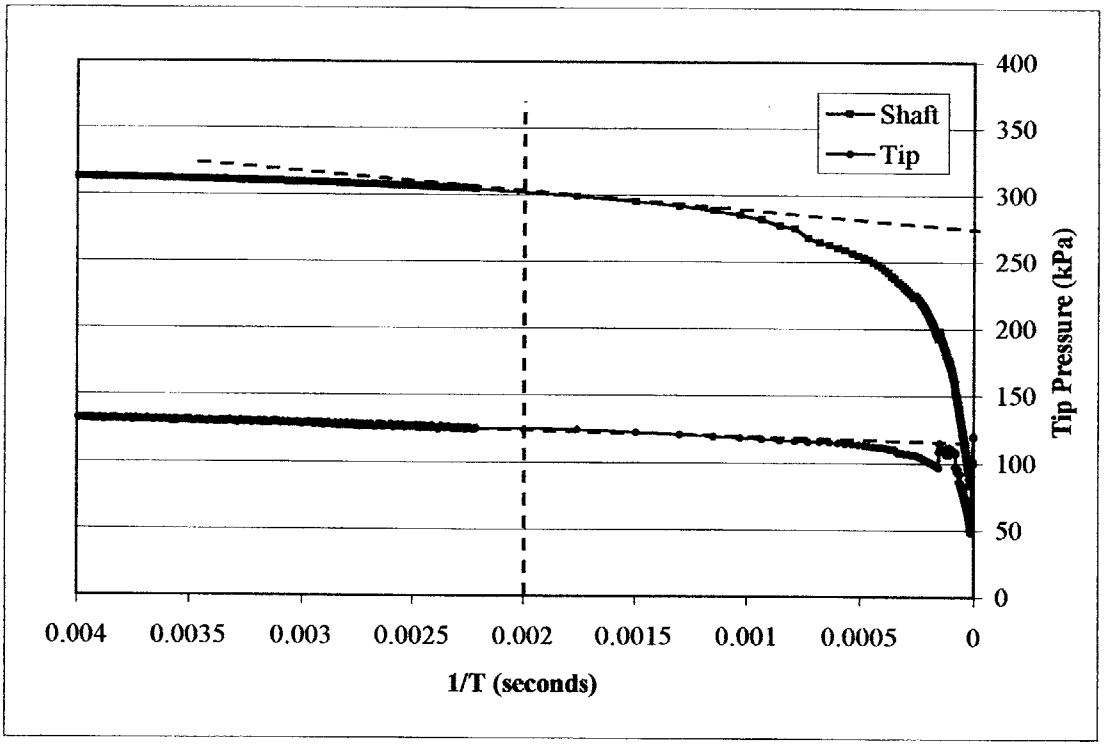

Figure 6.10 **1/t Method on TP2_P2 Dissipation Record with t = 500 sec**

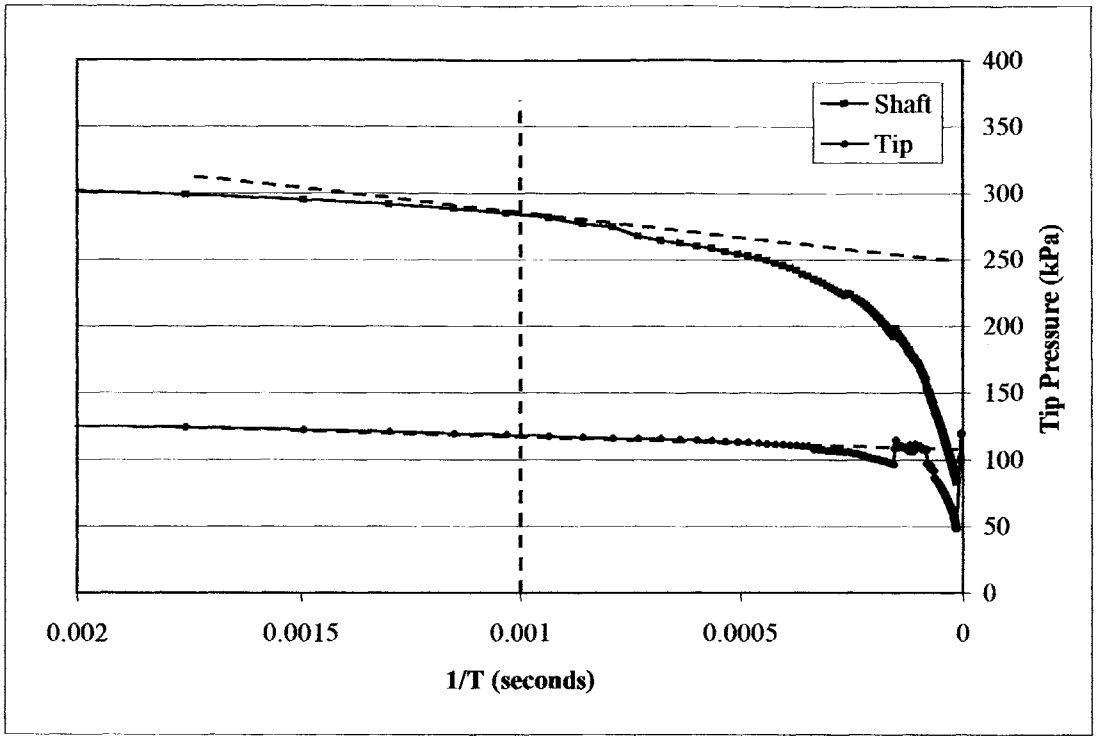

Figure 6.11 1/t Method on TP2_P2 Dissipation Record with t = 1000 sec

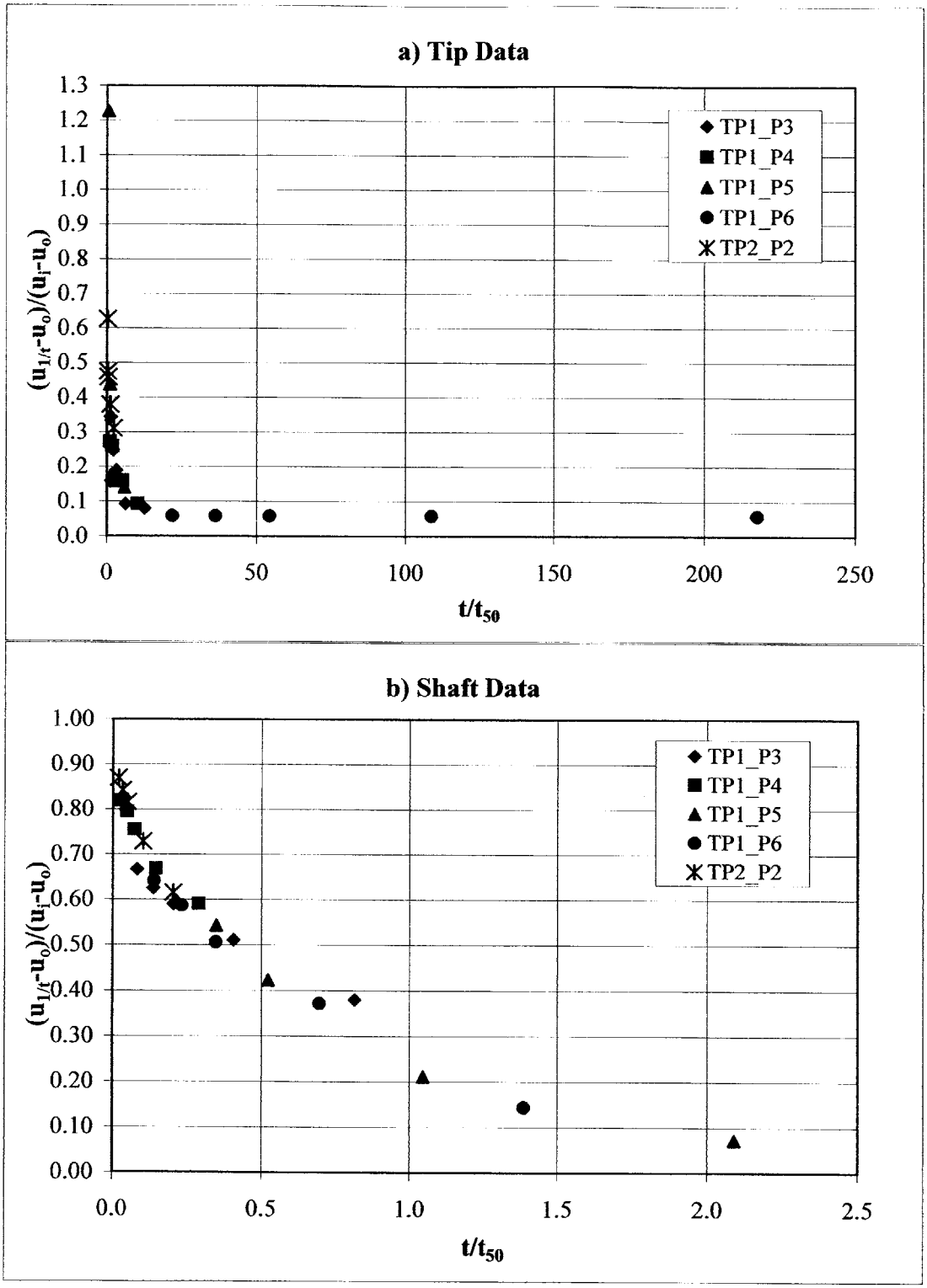

Figure 12 **Results from the 1/t Method for T2P Tip and Shaft Dissipation Data - Natural Scale**

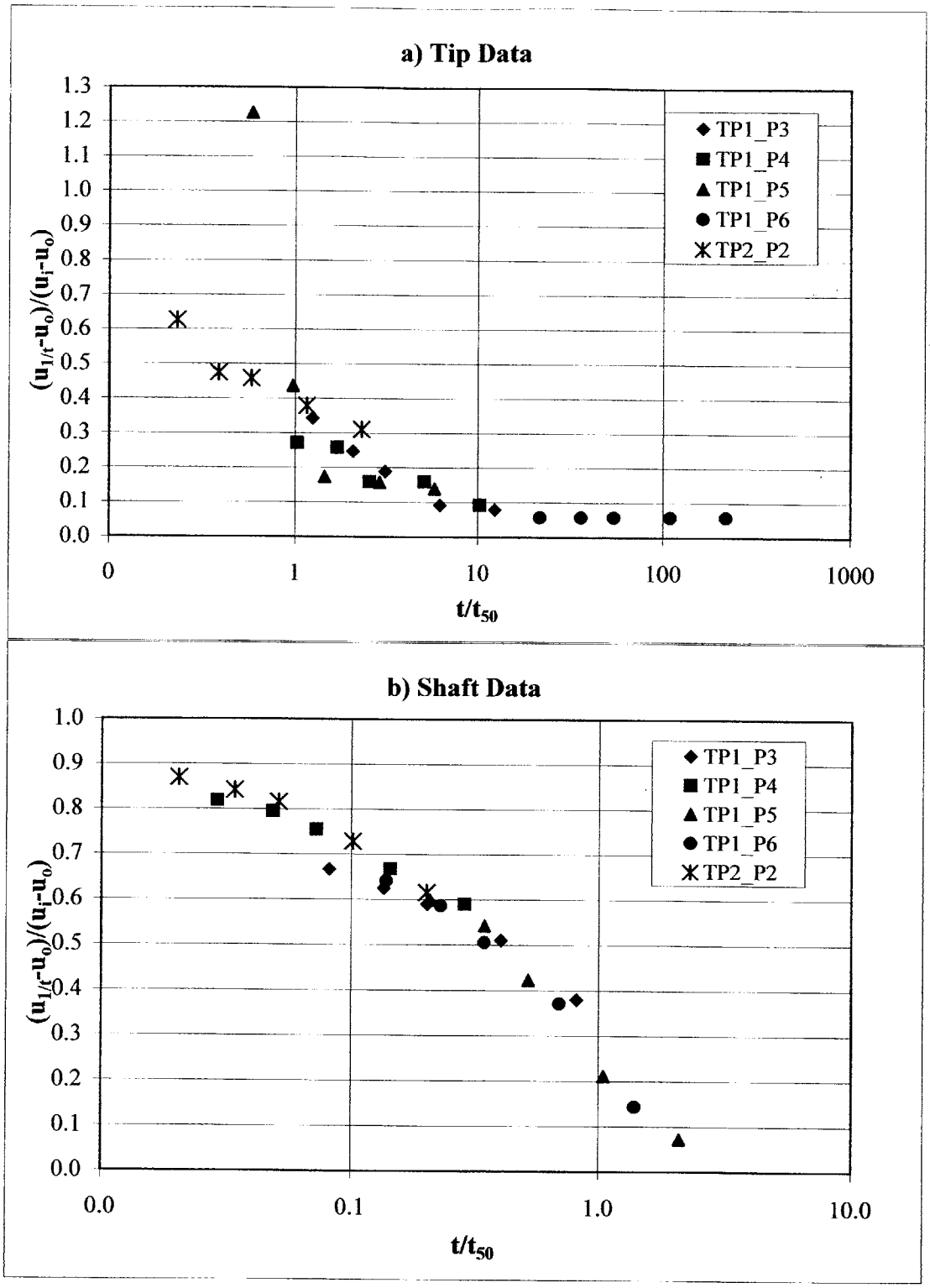

Figure 13 **Results from the 1/t Method for T2P Tip and Shaft Dissipation Data - Logarithmic Scale**

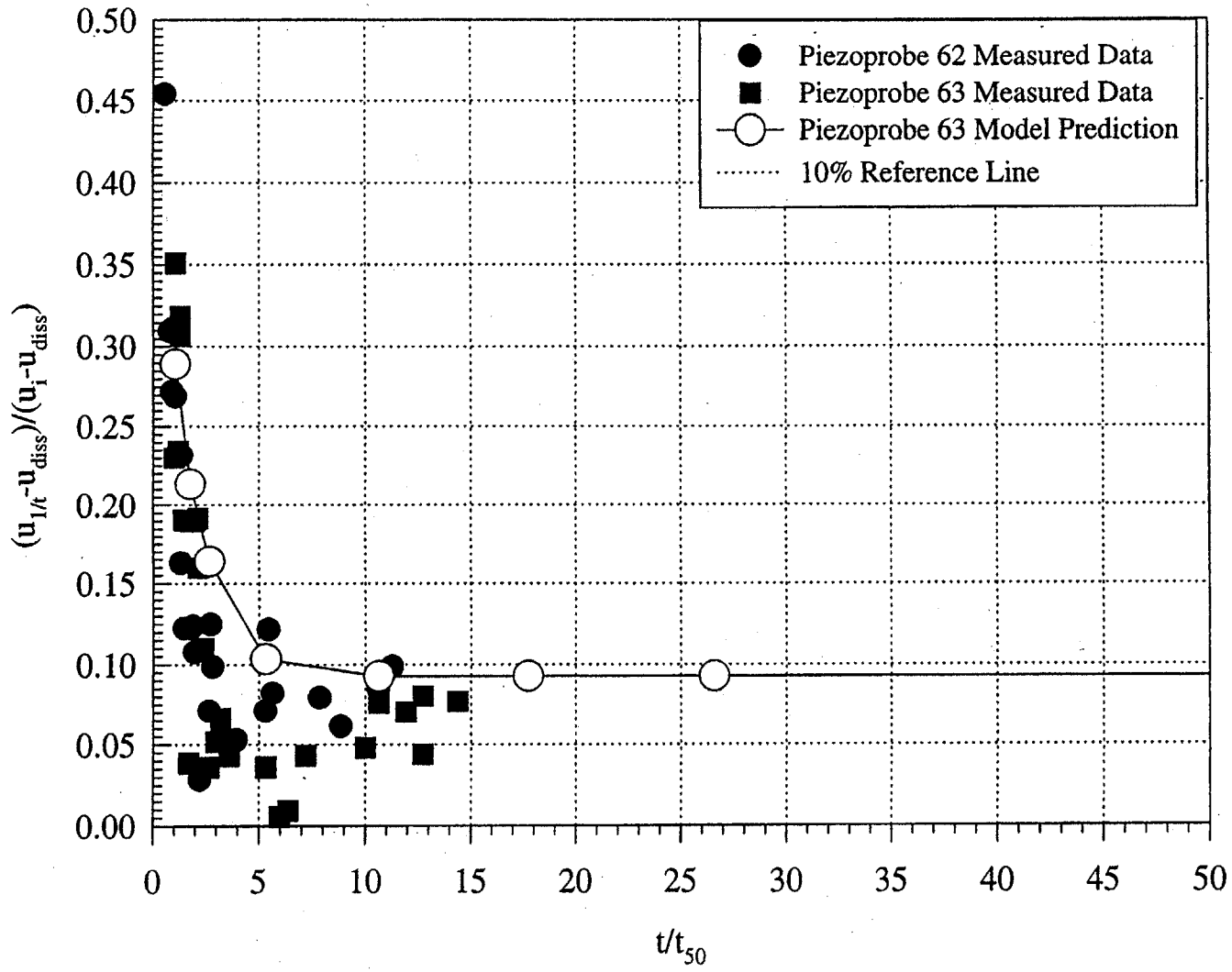

Figure 6.14 **Convergence of the Pore Pressure Predicted by the Inverse Time Extrapolation Method to the Dissipated Pore Pressure Value for the Piezoprobes (Varney, 1998)**

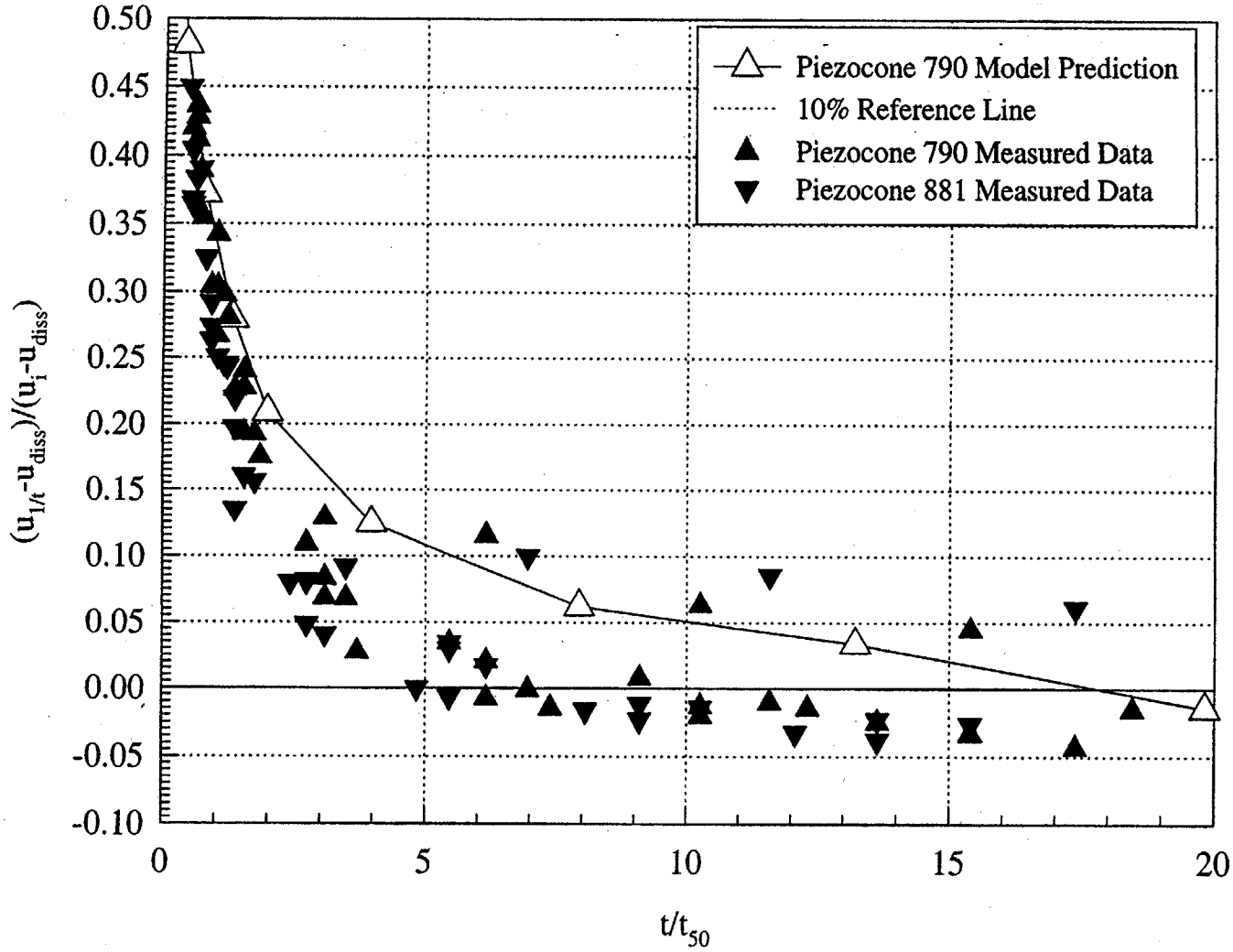

Figure 6.15 **Convergence of the Pore Pressure Predicted by the Inverse Time Extrapolation Method to the Dissipated Pore Pressure Value for the Piezocones (Varney, 1998)**

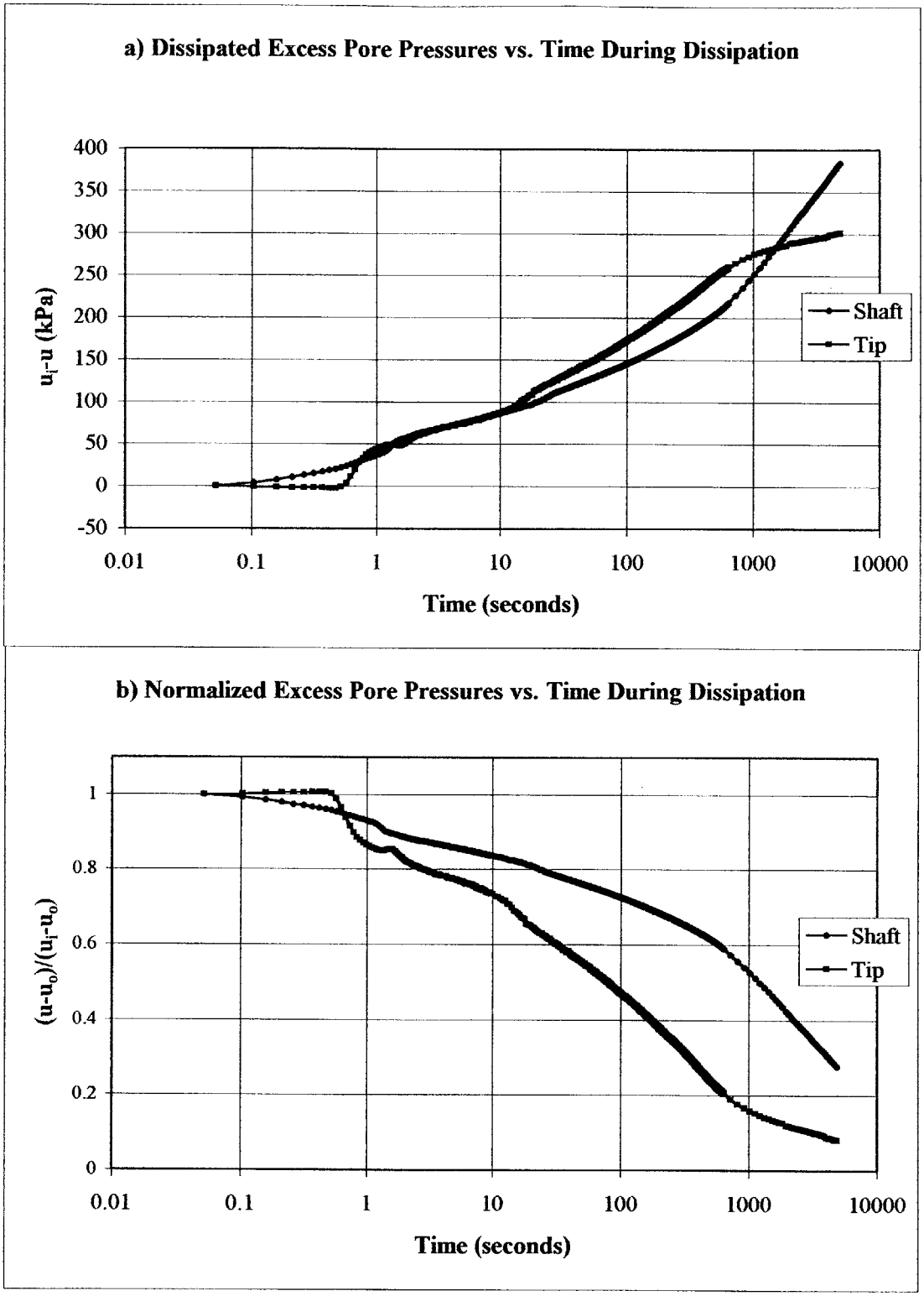

Figure 6.16 **Two-Point Matching Method - TP1_P3 Dissipation Data**

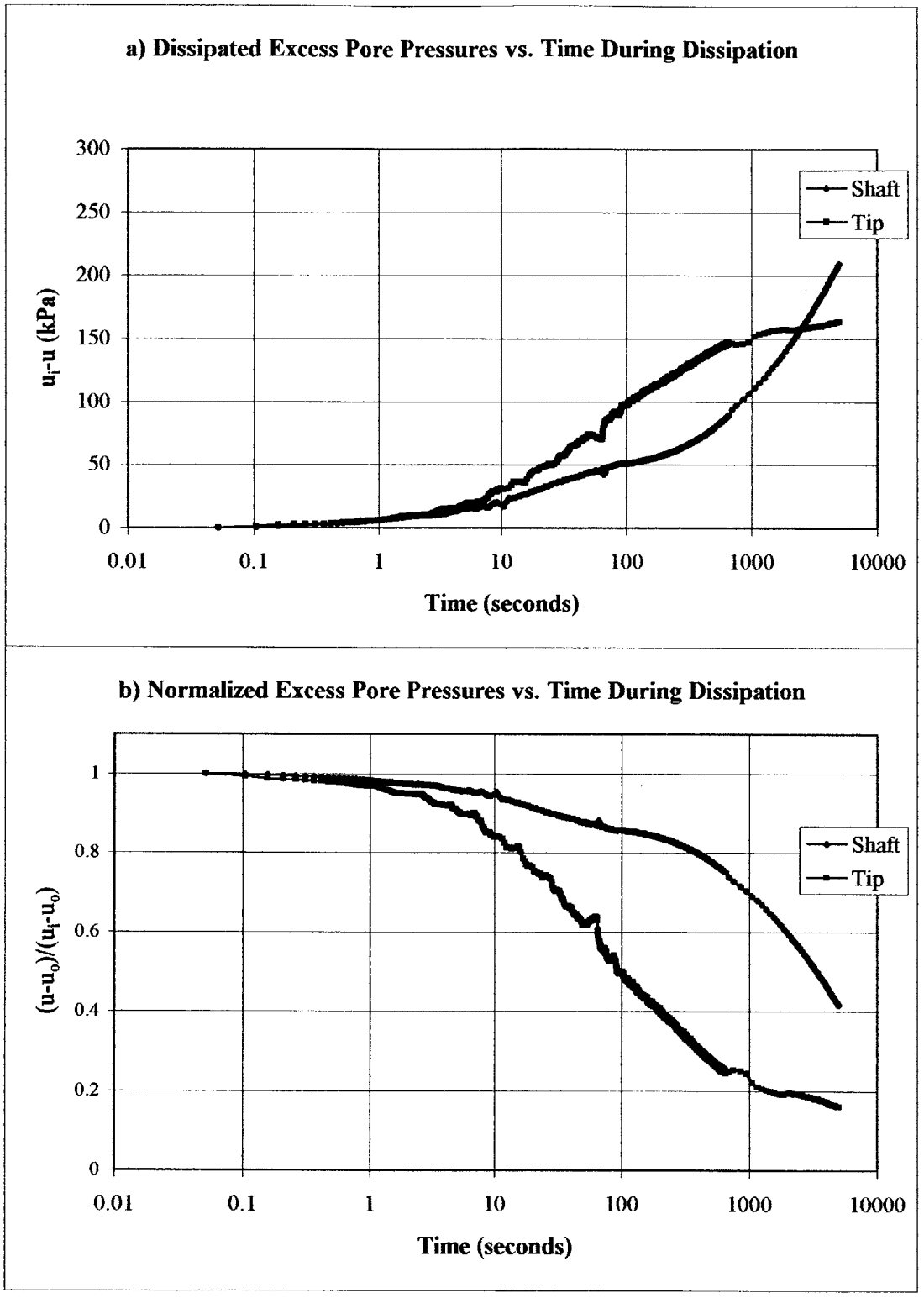

Figure 6.17 Two-Point Matching Method - TP1_P4 Data

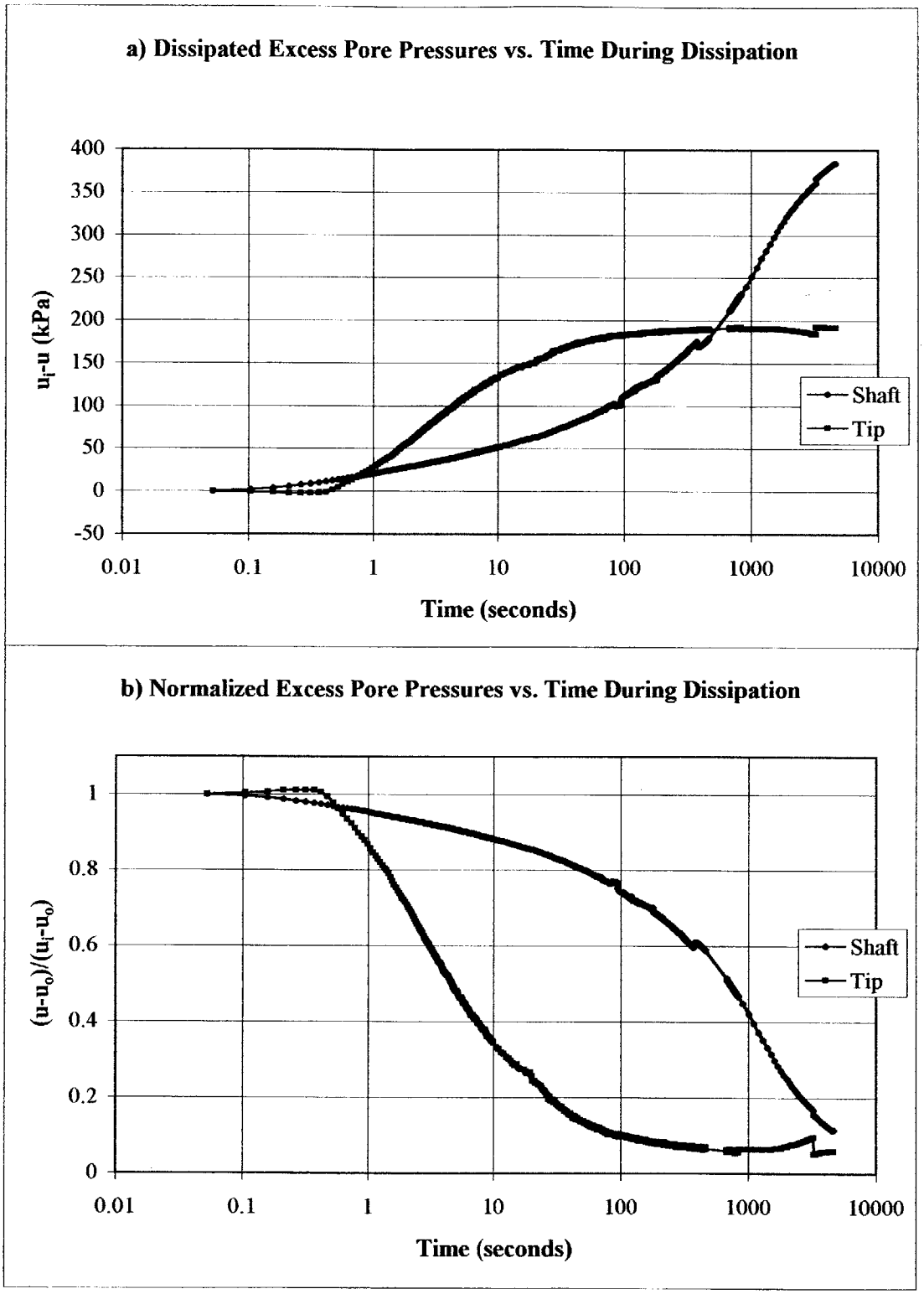

Figure 6.18 Two-Point Intersection Method - TP1_P6 Data

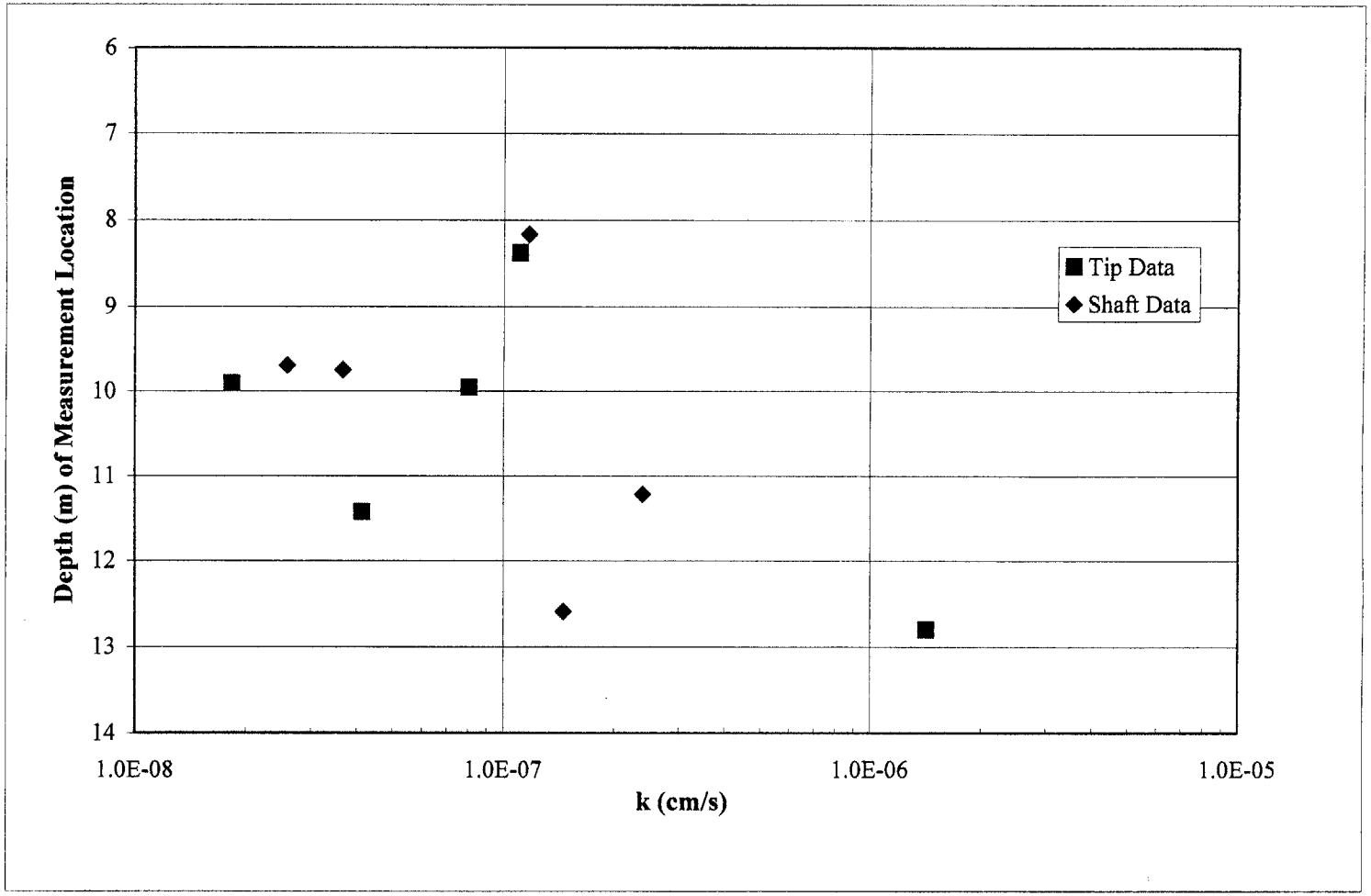

Figure 6.19 **Hydraulic Conductivity as Determined from the T_{50} Matching Method on T2P Dissipation Data**

7 SUMMARY, CONCLUSIONS, AND RECENT ADVANCEMENTS

This chapter summarizes and draws conclusions from the results of the 2004 T2P field program and describes the modifications made to the T2P in preparation for an upcoming sea deployment that will take place in June 2005.

7.1 Summary of Research

A new piezoprobe was designed and fabricated at MIT from January to December 2004. This tool, referred to as the T2P, is a penetration device that measures temperature at its tip and pore pressure at a point just above the tip and at a second location near the base of the probe shaft. The main purpose of the T2P is to reduce the time required to accurately estimate in-situ pore pressures (u_o) of marine sediments.

This thesis presents the results of a 2004 field program conducted at a site in Newbury, Massachusetts to collect both short and long-term dissipation records with the T2P prototype. The field test site in Newbury, Massachusetts was a convenient location for the field program due to its proximity to MIT and because it contains a 9 to 12 meter-thick deposit of soft BBC, close to the ground surface. Previous site investigations performed by the University of Massachusetts at Lowell have shown that the OCR of the deposit ranges from 4 to 7 at the top, decreases to 1 within the upper 7 meters, and then remains constant with depth. Laboratory testing of samples of the Newbury BBC indicate that the undrained shear strength approaches 100 kPa near the top of the deposit, and then ranges from 15 to 50 kPa below a depth of 5.5 meters (Paikowsky and Hart, 1998).

For the field program, two different probe tip geometries were used and pore pressure measurements were collected from two boreholes during eight penetrations, dissipations, and extractions of the T2P at various elevations throughout the clay deposit. All interpreted dissipations occurred in the normally consolidated portion of the Newbury BBC deposit and dissipation durations ranged from 0.7 to 19.7 hours. Temperature data were collected for the first penetration of the field program (TP1_P1); however, temperature measurements were not able to be collected during subsequent penetrations.

7.1.1 Field Test Data

While penetration-induced pore pressures measured at the T2P shaft are always larger than those collected at the tip, tip penetration pore pressures appear to be more sensitive to the existence of layering within the deposit than shaft pore pressures. The variations in pore pressure with depth measured by both transducers at the Newbury site indicate the presence of thin seams of silt or sand, generally ranging from 1 to 10 centimeters in thickness.

It was found that the tool must penetrate a disturbed zone at the base of each borehole before steady-state penetration pressures are reached. These shear zones are caused by the drilling process and have a minimum depth below the base of each borehole of roughly 2 times the borehole diameter. The depth of this zone below each borehole was found to increase if a constant level of vertical effective stress is not maintained on the base of the borehole during extraction of the drill bit by keeping the hole filled with drilling fluid.

Close inspection of the penetration and dissipation data indicated that relatively minor fluctuations of tool position at the end of penetration can have a significant impact on pore pressures around the tool. During several penetrations (TP1_P4, TP1_P5, and TP2_P2), sudden changes in tool position occurred during the last second of penetration, leading to abrupt drops in pore pressure around the probe. It was found that an upward shift in tool position at the end of penetration of as little as 0.4 cm was enough to cause sudden and significant reductions in pore pressure at both the tip and shaft pressure measurement locations. This is believed to reverse the shear stress on the shaft, hence changing the stress field around the probe. These pressure drops reflect broad changes in the stress field around the tool that are not accounted for in the theoretical model and may lead to variations in the shape of the dissipation data.

Examination of the dissipation records revealed that the detachment of the drill rods from the cross head during the later stages of dissipation did not have a significant effect on the shape of the dissipation curves.

The pore pressure extraction records indicate that pressures measured at the tip drop dramatically upon the start of extraction and typically rapidly become negative. In

contrast, shaft pressures generally drop more gradually during extraction than tip pressures. It was also found that when the tool was left in the ground overnight, pore pressures measured at the shaft during extraction became significantly more negative than shaft extraction pressures measured after tests having durations of one hour or less. Hence, there appears to be a correlation between shaft extraction pressures and the length of time the T2P remains embedded in the clay.

7.1.2 Data Interpretation

The T2P dissipation records are generally consistent with the model predictions described in Chapter 2. Dissipation at the tip initially proceeds more rapidly than at the shaft; however, tip pressures are subsequently affected by the pressure pulse induced by the larger-diameter shaft. Thus, tip pressure records generally exhibit a "brake point" at which the rate of dissipation significantly decreases. These brake points are predicted by the model and were seen in three (TP1_P3, TP1_P4, and TP1_P6) out of the five interpreted dissipation records that were collected using the modeled T2P tip geometry (the original geometry). The brake points became apparent at dissipated pore pressure ratios ranging from 18 to 25% and occurred from 31 to 828 seconds after the end of penetration.

The time required for 50% dissipation of excess pore pressures (t_{50}) was significantly smaller for tip measurements than for those collected at the shaft. Values of t_{50} measured at the tip varied from 4.6 to 431 seconds, with an average of 160 seconds. Shaft t_{50} values ranged from 480 to 4930 seconds for TP2_P2, with an average of 2160 seconds.

The monitoring periods were not of sufficient length to allow full dissipation to take place. It appears likely that final shaft pore pressure measurements collected during two of the dissipations (TP1_P5 and TP2_P2) approached the hydrostatic values. However, the data suggests that the dissipation measurement periods were too short to achieve hydrostatic conditions at the tip; thus, dissipation records recorded at the tip must be longer than 20 hours in order to reach the in-situ pore pressure. These findings are consistent with data collected by Varney (1998) at the Saugus site, which indicated that full dissipation requires a minimum of 28 hours for piezoprobes and piezocones in BBC.

The inverse time extrapolation and two-point matching methods were used to estimate in-situ pore pressures (u_o) from the T2P dissipation records. Both were found to overestimate the in-situ pressure when applied to partial dissipation records. The inverse time extrapolation method, when used with tip dissipation records, predicted u_o with an error less than 10% of the magnitude of penetration-induced excess pore pressure within an average monitoring time of 942 seconds. However, when this method was applied to dissipation records measured at the shaft, the average monitoring period required to predict u_o within the same level of error increased to 4328 seconds. Hence, it seems likely that inverse time extrapolation will predict in-situ pore pressures within a 10% error from T2P tip dissipation records in reasonable periods of time for routine use in sub-seafloor explorations. However, the measurement duration required for accurate estimation of u_o from shaft dissipation records appears to be too long to use routinely for marine investigations.

Intersection points occurred for three out of the five interpreted dissipation records that were collected using the modeled T2P tip geometry. When the intersection method was applied to these records (TP1_P3, TP1_P4, and TP1_P6), errors in the resulting estimates of u_o ranged from –3% to 11% of the magnitude of penetration-induced excess pore pressure, with an average error of 4%. The time from the start of each dissipation to the intersection point (t_p) ranged from 525 to 2769 seconds, with an average value of 1641 seconds. A comparison between the results from the two-point matching method and those from the inverse time extrapolation method indicated the intersection method consistently produces more accurate measurements of in-situ pore pressures from T2P dissipation data than does the inverse time extrapolation method at similar dissipation times.

The T50 matching method was used to estimate the soil hydraulic conductivity (k) from the tip and shaft dissipation records that were collected using the modeled tip geometry. The values of k calculated from the tip pressure measurements ranged from $1.8\text{x}10^{-8}$ to $1.4\text{x}10^{-6}$ cm/s, with an average value of $3.3\text{x}10^{-7}$ cm/sec. The values of k from the shaft dissipation records ranged from $2.6\text{x}10^{-8}$ to $2.4\text{x}10^{-7}$ cm/sec, with an average of $1.1\text{x}10^{-7}$ cm/sec. For the majority of the dissipations, the values of k

determined from tip measurements were relatively consistent with those calculated from shaft data. For those dissipations for which the values of k calculated from the tip data significantly differed from those estimated from the shaft records, it is suspected that the tip and shaft filters were located in layers with considerably different hydraulic conductivities during dissipation. Laboratory measurements of the hydraulic conductivity of normally consolidated BBC from the Saugus site were generally consistent with the values of k from the T50 matching method applied to the T2P dissipation data, thus supporting the validity of the T50 matching method when used on partial T2P dissipation records.

7.1.3 Recent T2P Modifications

Since the 2004 field test of the T2P prototype, significant modifications have been made to the upper section of the tool in preparation for an anticipated T2P sea deployment in June 2005. These modifications were jointly designed and fabricated by MIT and members of IODP at Texas A&M University. Individual drawings of the T2P sections designed after the 2004 field test are included in Appendix C.

7.1.3.1 Overview of Modifications

During the 2004 field test, the T2P prototype's electrical power source, data acquisition system, and microprocessor remained above-ground while the tool was beneath the surface. As described in Chapter 3, this arrangement was possible because the T2P received electrical power and communicated with the data acquisition system through a cable linking the tool to the surface equipment. However, during the sea deployment, it will not be feasible to electrically connect the tool to the ship at the ocean surface. Therefore, modifications have been made to provide the T2P with a self-contained data acquisition system, microprocessor, and power source. In addition, the range of the T2P's pore pressure transducers and mechanical capacity of its internal electrical connectors had to be increased to handle the water pressures that exist 1000 meters or more beneath the ocean surface. To prevent the stainless-on-stainless gauling that occurred during the 2004 field test, the external threads at the top and bottom of the transducer block were glass peened and copper plated. In addition to the original needle

design with a straight shaft, several needle shafts with a 1° taper were fabricated to provide additional strength. Finally, during the sea deployment, the tool will have to push open a heavy, steel "mud flap" at the base of the drill string before penetrating the sediment below. The mud flap is used to keep sediment from flooding the drill string. The T2P's thin needle shaft is not strong enough to withstand the force required to open the flap and would be significantly damaged in the process; therefore, a protective covering, referred to as the shroud, was designed and fabricated to protect the probe tip while exiting the drill string.

7.1.3.2 New Electrical Components and Power Source

As mentioned above, the pore pressure transducers used during the 2004 field test did not have adequate capacity for a sea deployment. These were replaced with Kulite XTM-190 pressure transducers, each with a 5,000 psi range. Each of the two cables containing the power, ground, and signal wires from the pressure transducers were soldered to a Fisher 5-pin cable receptacle. Two Fisher 5-pin cable plugs mechanically connect with these receptacles, and 26 AWG insulated wires electrically link the Fisher plugs to a high-pressure 12-pin Green, Tweed & Company electrical connector. The power and ground wires from the thermistor are soldered directly to this high-pressure connector, with a second, insulated solder connection halfway between the thermistor and high-pressure connector. This second soldered connection provides a point to easily detach the thermistor wires for disassembly of the tool.

The aforementioned Green, Tweed & Company electrical connector mechanically connects to a second and identical high-pressure connector, mounted at the base of the bulkhead carrier. The bulkead carrier, shown in Figure 7.1 and in Appendix C, has a steel housing containing a standard 25-pin plug at its upper end that is electronically wired to a Green, Tweed & Company high-pressure electrical connector at its lower end. Thus, when the two Green, Tweed & Company high-pressure electrical connectors are mechnically mated, the power, ground, and signal wires from the pressure transducers and the power and ground wires from the thermistor are electrically linked to the 25-pin plug at the top of the bulkhead carrier. This 25-pin plug connects directly with a 25-pin receptacle on the new data acquisition system.

The new data acquisition system is composed of a 16-bit A/D converter, designed by IODP, and a CF2 microprocessor manufactured by Persistor Instruments, Inc. The new data acquisition system has a 0 to 5 V range and can record data from up to three channels sequentially with a one second sampling rate. Custom amplifiers are used to increase the output of the transducers to the range of the A/D converter. The A/D converter and microprocessor are mounted on a single board, which, in turn, is supported by the electronics backbone (see Figure 7.1).

The entire system (A/D converter, microprocessor, and transducers) is powered by a single 6 V lithium battery, manufactured by Spectrum Batteries, Inc., that can provide 16 amp hours of electricity. The battery is mounted on the electronics backbone, next to the data acquisition system. One battery is expected to supply sufficient power for several days of operation.

7.1.3.3 Modified Housing Components

Drawings of the new T2P sections are included in Appendix C and an illustration of the modified and fully assembled sections is shown in Figure 7.1. At the bottom of the figure is the drive tube. The sections below the drive tube were not altered, except for the aforementioned peening and plating of the transducer block threads and the fabrication of several needle shafts with a 1° taper. The drive tube remained essentially unchanged from the tube used for the 2004 field test, except that the male threads at its upper end were changed to ACME threads and a 2.5 cm-long section of the tube, located 3.2 cm from its bottom end, now has a diameter of 3.8 cm. This 2.5 cm-long "upset" near the bottom of the tube is used to hold the shroud in place and will be discussed further below.

The split ring is inserted into the top end of the drive tube and then the drive tube nut is screwed onto the drive tube, thus holding the split ring in place. Finally, the pressure ring is bolted into place at the top of the drive tube nut. The split ring and pressure ring support a Green, Tweed & Company high pressure electrical connector, located within the drive tube nut. This arrangement is shown in Figure 7.1.

The drive tube nut is mechanically connected with the union by the coupling. This is accomplished by screwing the internal threads of the coupling onto the external threads of the union, thus locking the nut against the union. The union contains the

previously described bulkhead carrier, which provides the electrical connection between the lower Green, Tweed & Company connector and the data acquisition system's 25-pin receptacle, as is shown in Figure 7.1. The electronic adapter, mechanically connected to the electronics backbone and containing the 25-pin receptacle, slides into the union, completing the electrical and mechanical connection between the transducers, data acquisition system, and battery.

The electronics backbone is mounted within IODP's data acquisition housing (not shown), which screw onto the top threads of the union. The electronics backbone is protected from being damaged within the data acquisition housing by a cylindrical, plastic covering (not shown). The data acquisition housing is then screwed onto the colleted delivery system coupling (not shown), which attaches directly to IODP's colleted delivery system. Drawings of the data acquisition housing, colleted delivery system coupling, and colleted delivery system were not available and are not included in Appendix C.

As mentioned above, the shroud, shown in Figure 7.2, will be used to protect the T2P tip and needle shaft as it pushes past the mud flap and exits the drill string. An internal ledge within the shroud prevents it from moving downwards past the drive tube upset by an internal ledge within the shroud. The shroud is initially prevented from moving upwards along the drive tube by a system of 8 ball bearings and springs that rest below the 2.5 cm-long upset. A 70-pound axial force is required to release the set of springs and bearing, which is significantly greater than the force needed to open the mud flap. The shroud remains in this initial position as the tool passes through the mud flap, preventing the probe from being damaged, as shown by the illustration on the right side of Figure 7.3. Once the shroud comes in contact with sediment at the base of the borehole, the bearing capacity of the sediment overcomes the resistance provided by the set of ball bearings and springs, and the shroud retracts upwards relative to the probe tip. In this manner, the T2P is able to penetrate the soil while the shroud remains at the base of the borehole. The shroud in its retracted position is shown on the left side of Figure 7.3.

7.2 Conclusions

In general, the T2P proved to be a robust tool, simple in design and relatively easy to use. The use of the depth box and a fast sampling rate revealed significant new insights concerning the effects of tool movement on pore pressure penetration and dissipation measurements. Additionally, the 45-minute ultrasound filter saturation technique was an effective and convenient substitute for the 24-hour bell jar evacuation and saturation procedure, described in Chapter 4.

However, several equipment issues were identified during the field test that suggested the need to modify the design of the T2P prototype and support equipment. As previously mentioned, the T2P's needle shaft bent during the first penetration (TP1_P1) but was not damaged during subsequent penetrations. In fact, this is a common occurrence during offshore deployments of the FMMG tapered piezoprobe. Since the T2P will eventually be deployed in a variety of marine sediments, it is important that the operators of the probe have the option to readily exchange the existing needle shaft geometry with one with increased bending resistance.

During assembly of the prototype, the thermistor wires must first be threaded through the central conduit along the axis of the transducer block before the tip and needle shaft can be screwed onto the block. Then, if either of the two filters becomes de-saturated, the thermistor wires must be cut and then removed from this conduit. It would be more convenient to easily connect and disconnect the thermistor wires at the top of the thin tube containing the thermistor. This could be accomplished through the use of a small, reusable electrical connector at the top of this thin tube but this would most likely require using the tube as one of the electrical conductors.

As mentioned in Chapter 3, all T2P housing components are composed of stainless steel. It was found that stainless-on-stainless gauling occurred between the transducer block and drive tube and between the AW adapter and the spin collar. Hence, some sections of the T2P must be either copper plated or fabricated using alternative materials to prevent gauling from becoming an issue in the future. It was also discovered that using proper lubricant is essential.

During the field program, the replacement tip pore pressure transducer exhibited significant drift and instability while the shaft transducer proved to be more reliable. The replacement tip transducer is an old transducer found in the MIT lab that was used for several previous field programs. Since both transducers are manufactured by Kulite, the problems were probably associated with the particular transducer used for tip pressure measurements, and not with Kulite transducers in general. It is important that any additional transducers used for future field tests be checked for stability and drift before deployment.

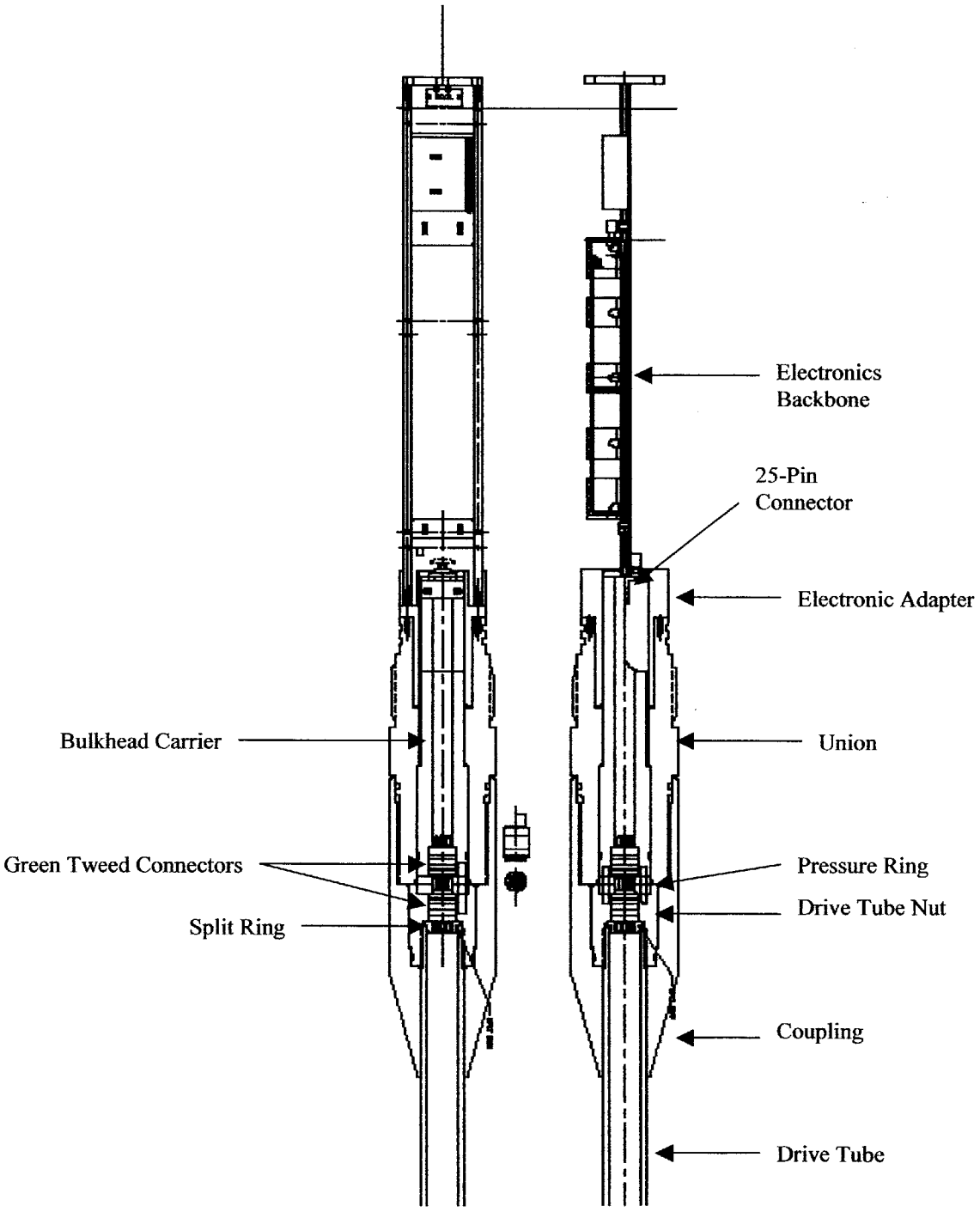

Figure 7.1 Modified Connection Between Drive Tube and New Data Acquisition System

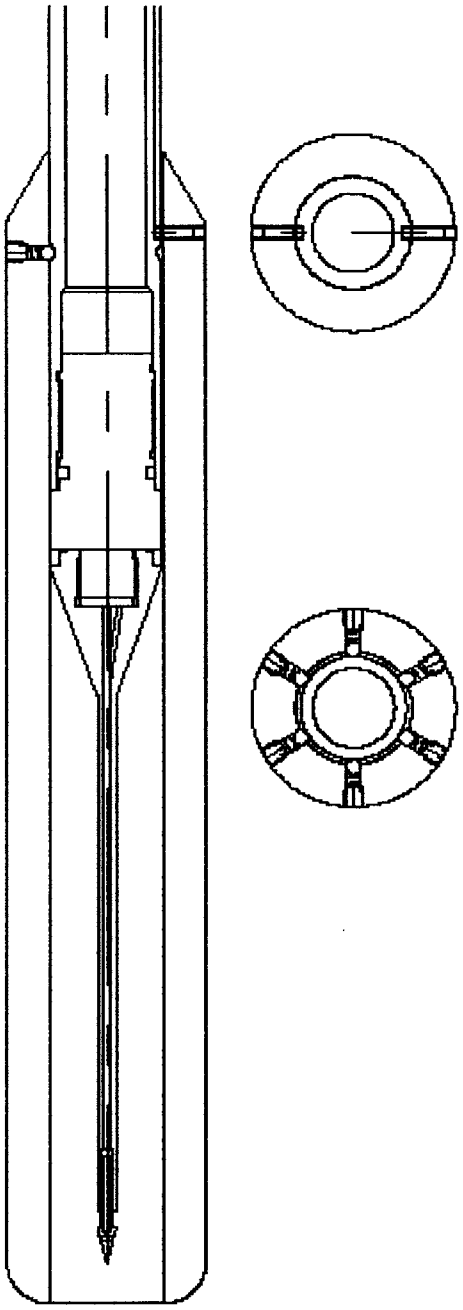

Figure 7.2 T2P Shroud

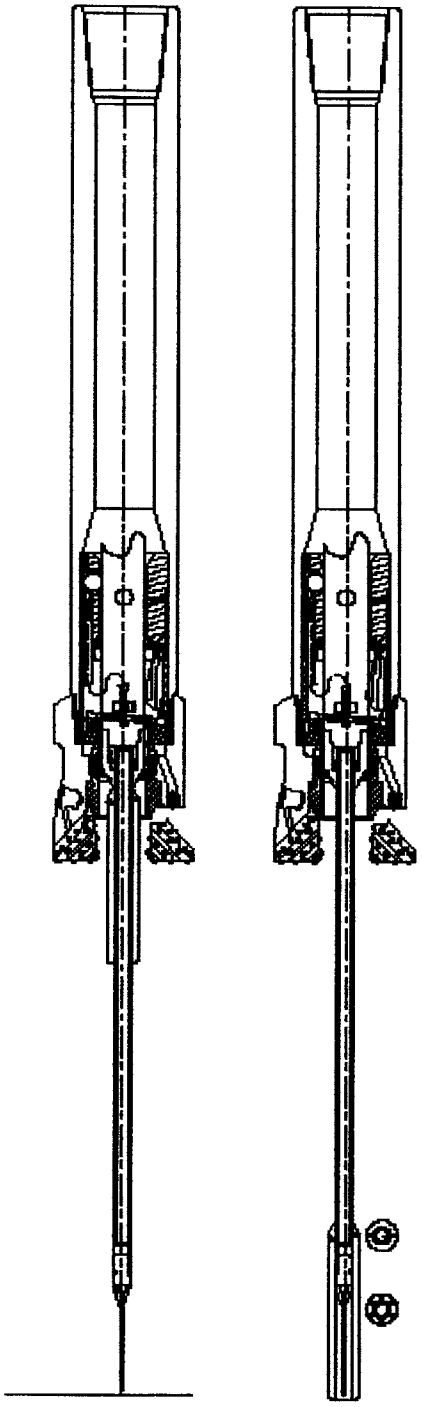

Figure 7.3 Operation of Shroud

REFERENCES

Aubeny, C.P. (1992) "Rational interpretation of in situ tests in cohesive soils," PhD Thesis, MIT, Cambridge, MA, pg. 433.

Aubeny, C.P., A.J. Whittle, and C.C. Ladd (2000) "Effects of disturbance on undrained strengths interpreted from pressuremeter tests," *ASCE Journal of Geotechnical and Geoenvironmental Engineering, 126* (12), 1133-1145.

Avallone, E.A., and Baumeister, T. (1996) "Marks' Standard Handbook for Mechanical Engineers, 10th Edition," McGraw-Hill, New York, NY, section 5-45.

Baligh, M.M. (1985) "Strain Path Method," *ASCE Journal of Geotechnical and Geoenvironmental Engineering, 111* (9), 1108-1136.

DeGroot, D.J. (2005) Personal communication.

de Ruiter, J., (1971) "Electric penetrometer for site investigation," *ASCE Journal of the Soil Mech. And Fdn. Engrg. Division*, Vol. 97, SM2, pp 457-472.

Dugan, B., and P.B. Flemings (2002) "Fluid flow and stability of the US continental slope offshore New Jersey from the Pleistocene to the present," *Geofluids, 2* (2), 137-146.

Flemings, P.B., B.E. Dugan, F.R. Rack, D. Schroeder, A. Trehu, J. Germaine, and O.L. Shipboard Scientific Party (2003) "Interpretation of Pore Pressure and Permeability at Hydrate Ridge with Piezoprobe and DVTP-P Penetrometers and Consolidation Experiments," in *American Geophysical Union.*

Germaine, J.T. (1982) "Evaluation of Self-Boring Pressuremeter Tests in Soft Cohesive Soils," SM Thesis, MIT, Cambridge, MA.

Jakubowski, J. (2004) "Use of the seismic CPTU for site characterization in soft clays," Masters of Science Thesis, University of Massachusetts Amherst, Amherst, MA.

Kvenvolden, K.A. (1993) "Gas hydrates-geological perspective and global change," *Reviews of Geophysics, 31*, 173-187.

Levadoux, J-N (1980) "Pore pressures in clays due to cone penetration," PhD Thesis, MIT, Cambridge, MA.

Levadoux, J-N., Baligh, M.M. (1980) "Pore pressures in clays due to cone penetration," Research Report R80-15, Order No. 666, Dept. of Civil Engineering, MIT, Cambridge, MA.

Norton, R.L. (2000) "Machine Design: an integrated approach," Prentice Hall, Upper Saddle Rive, N.J., section 14.2

Ostermeier, R.M., J.H. Pelletier, C.D. Winker, and J.W. Nicholson (2001) "Trends in Shallow Sediment Pore Pressures – Deepwater Gulf of Mexico," *Society of Petroleum Engineers, SPE/IADC 67772.*

Paikowsky, S.G. and L.J. Hart (1998) "Development and field testing of multiple deployment model pile (MDMP)," University of Massachusetts Lowell, Lowell, MA.

Rouse, H. (1959) "Advanced Mechanics of Fluids," Wiley & Sons, New York.

Schroeder, D. (2002) personal communication.

Timoshenko, S. (1961) "Theory of Elastic Stability," McGraw-Hill, New York, NY, chapter 4

Varney, A. (1998) "A performance comparison between a novel tapered piezoprobe and the piezocone in Boston Blue Clay," Masters Thesis, MIT, Cambridge, MA.

Weinstein, A. (1948) "On axially symmetric flows," *Quarterly of Applied Mathematics, 5(4)*, pg. 429-434.

Whittle, A.J. (1992) "Assessment of an effective stress analysis for predicting the performance of driven piles in clays," *Offshore Site Investigation and Foundation Behavior*, 607-643, Society for Underwater Technology, London.

Whittle, A.J., D.J. DeGroot, C.C. Ladd, and T.H. Seah (1994) "Model prediction of the anisotropic behavior of Boston Blue Clay," *ASCE Journal of Geotechnical and Geoenvironmental Engineering, 120* (1), 199-225.

Whittle, A.J., T. Sutabutr, J.T. Germaine, and A. Varney (1997) "Validation of Piezoprobe Dissipation Data and Application to Pile Design," MIT Report R97-03, Department of Civil and Environmental Engineering, Cambridge, MA.

Whittle, A.J., and T. Sutabutr (1999) "Prediction of pile set-up in clay," *Transportation Research Record, 1663*, 33-41.

Whittle, A.J., T. Sutabutr, J.T. Germaine, and A. Varney (2001) Prediction and interpretation of pore pressure dissipation for a tapered piezoprobe, *Geotechnique, 51* (7), 601-617.

APPENDIX A

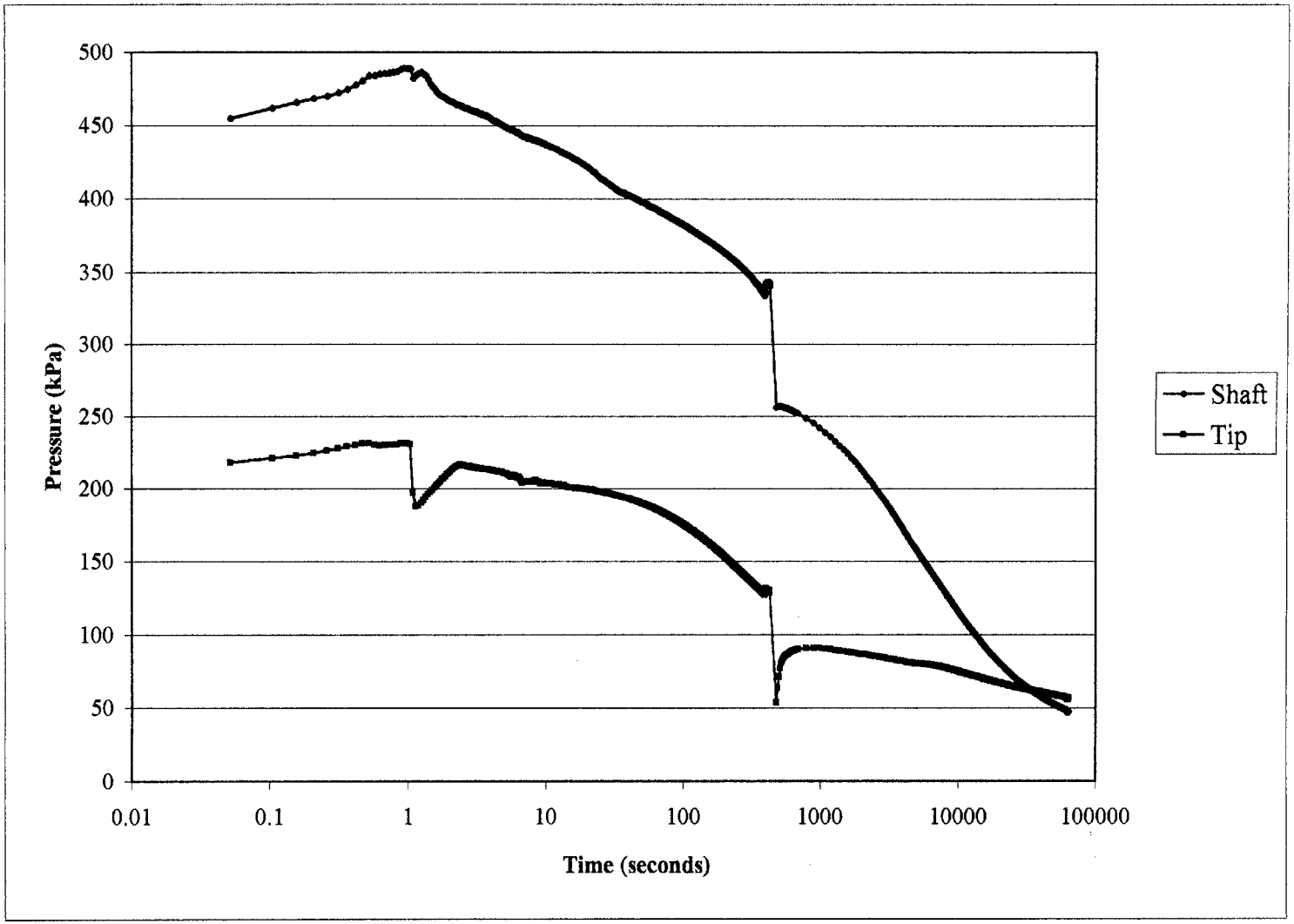

Measured Pore Pressure vs. Time During Dissipation TP1_P1

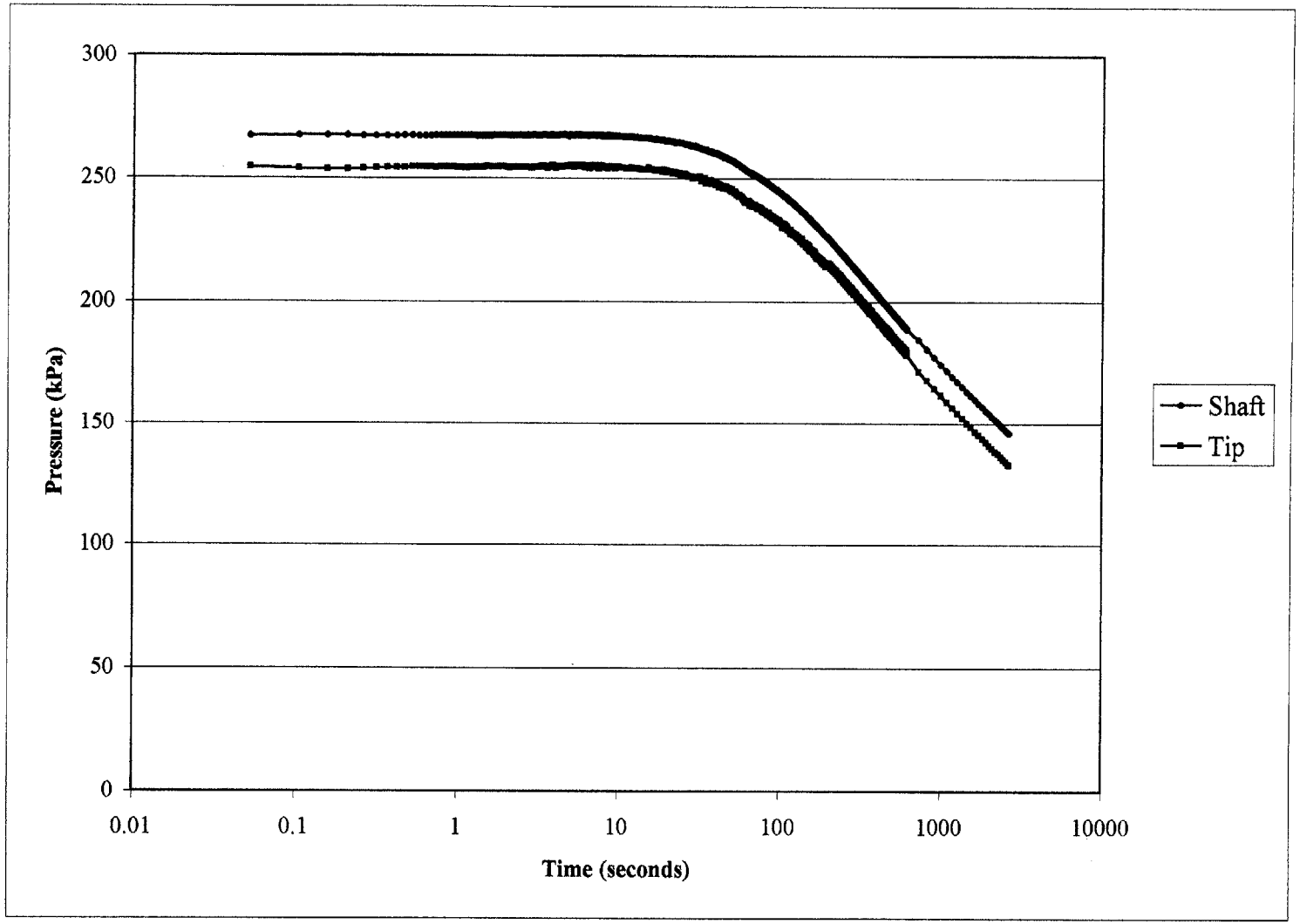

Measured Pore Pressure vs. Time During Dissipation TP1_P2

APPENDIX B

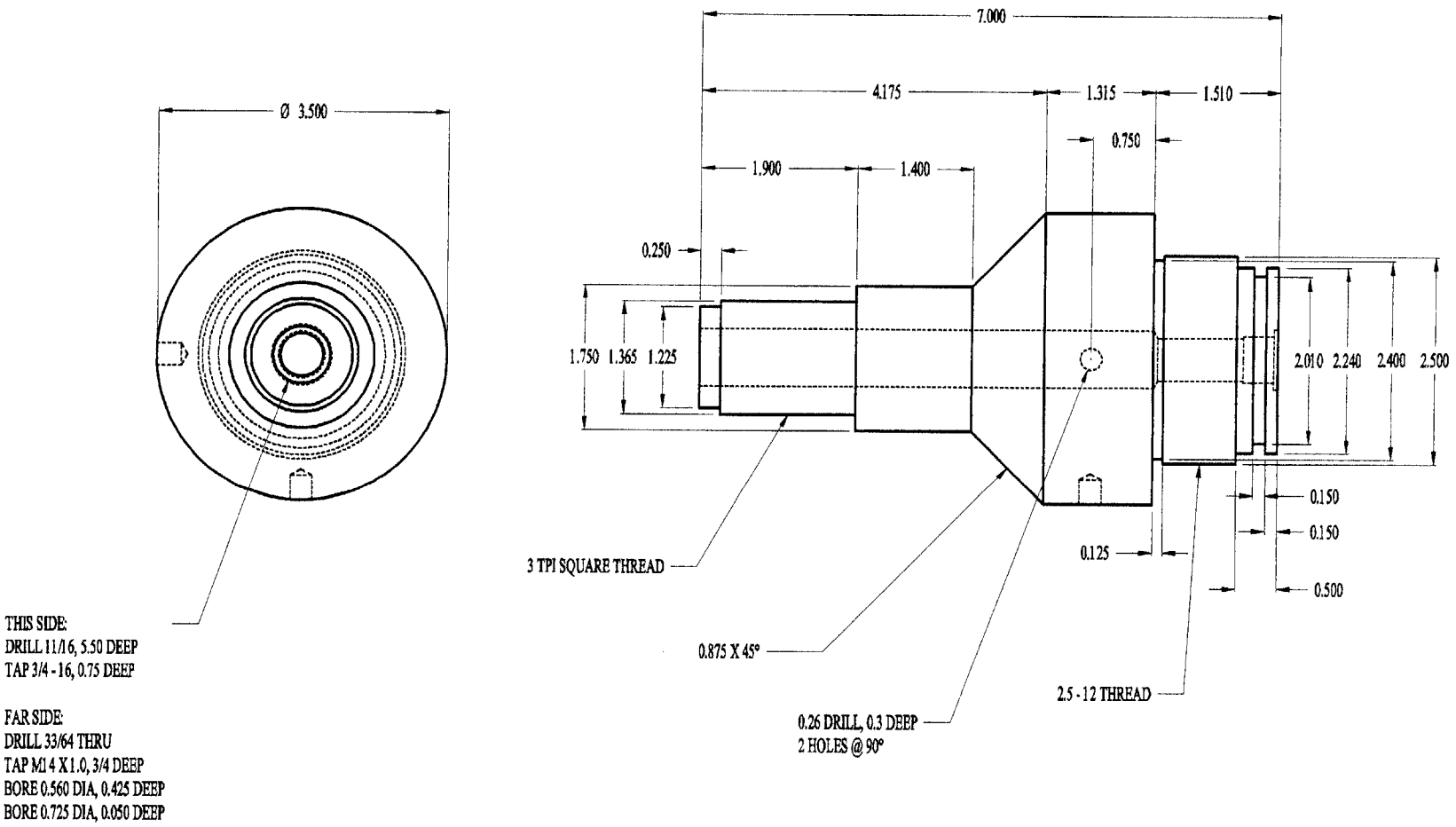
Ø 3.500
7.000
4.175
1.315
1.510
0.750
1.900
1.400
0.250
1.750
1.365
1.225
2.010
2.240
2.400
2.500
0.150
0.150
0.500
0.125
3 TPI SQUARE THREAD
0.875 X 45°
2.5 - 12 THREAD
0.26 DRILL, 0.3 DEEP
2 HOLES @ 90°
THIS SIDE:
DRILL 11/16, 5.50 DEEP
TAP 3/4 - 16, 0.75 DEEP
FAR SIDE:
DRILL 33/64 THRU
TAP M14 X 1.0, 3/4 DEEP
BORE 0.560 DIA, 0.425 DEEP
BORE 0.725 DIA, 0.050 DEEP

AW ADAPTER

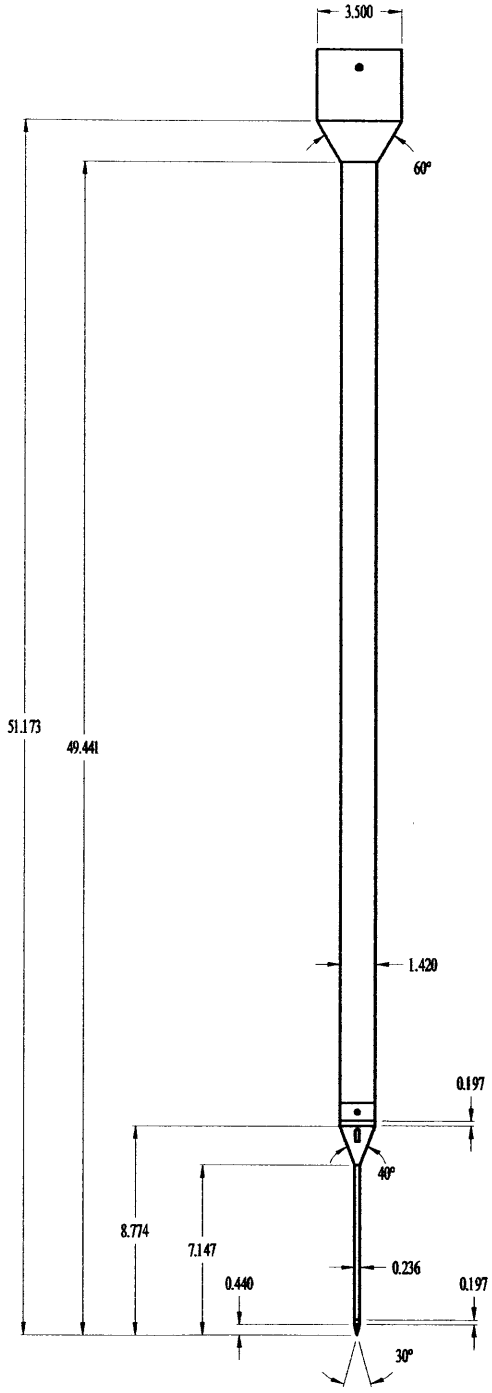

T2P OVERVIEW

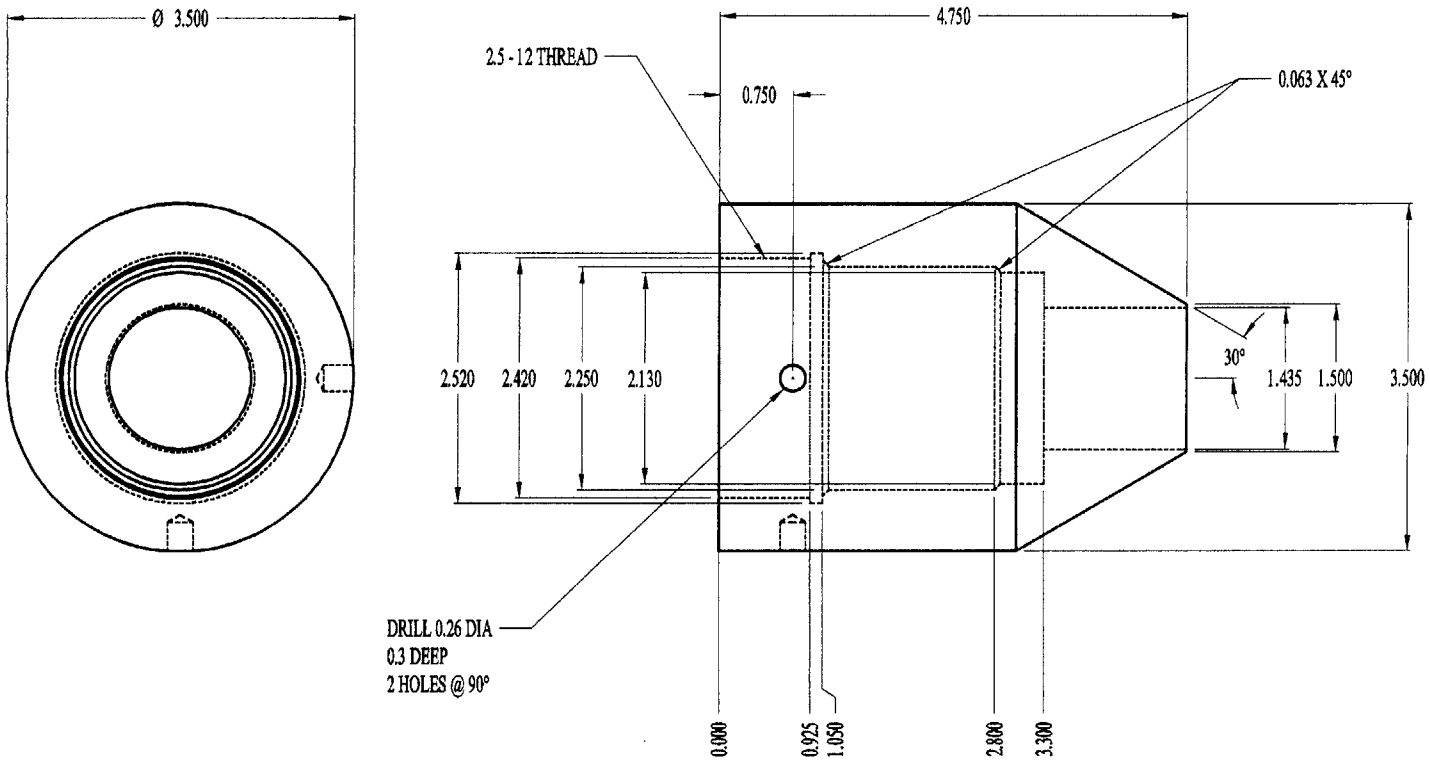
Ø 3.500
4.750
2.5 - 12 THREAD
0.750
0.063 X 45°
2.520
2.420
2.250
2.130
30°
1.435
1.500
3.500
DRILL 0.26 DIA
0.3 DEEP
2 HOLES @ 90°
0.000
0.925
1.050
2.800
3.300

COUPLING

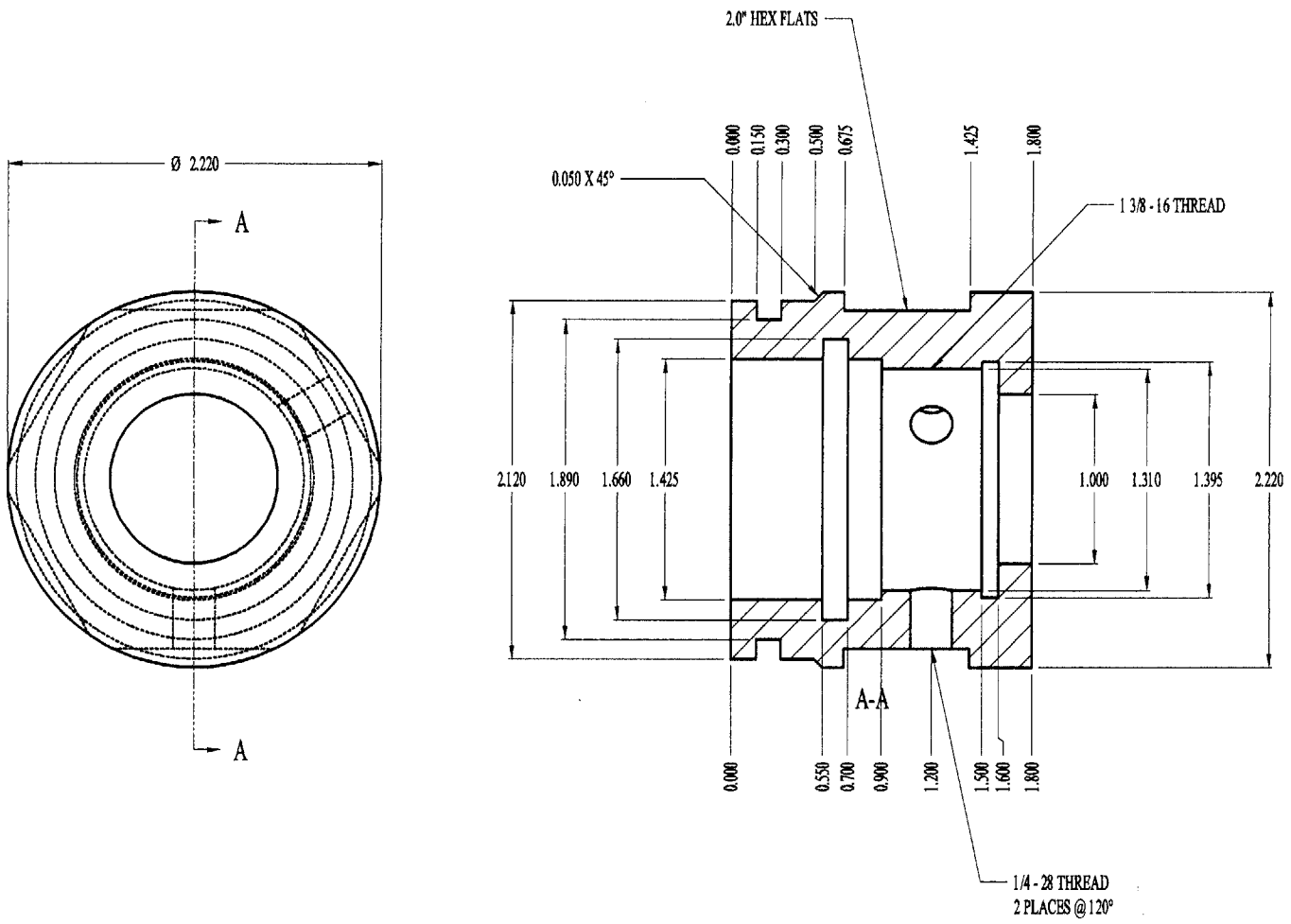

DRIVE TUBE NUT

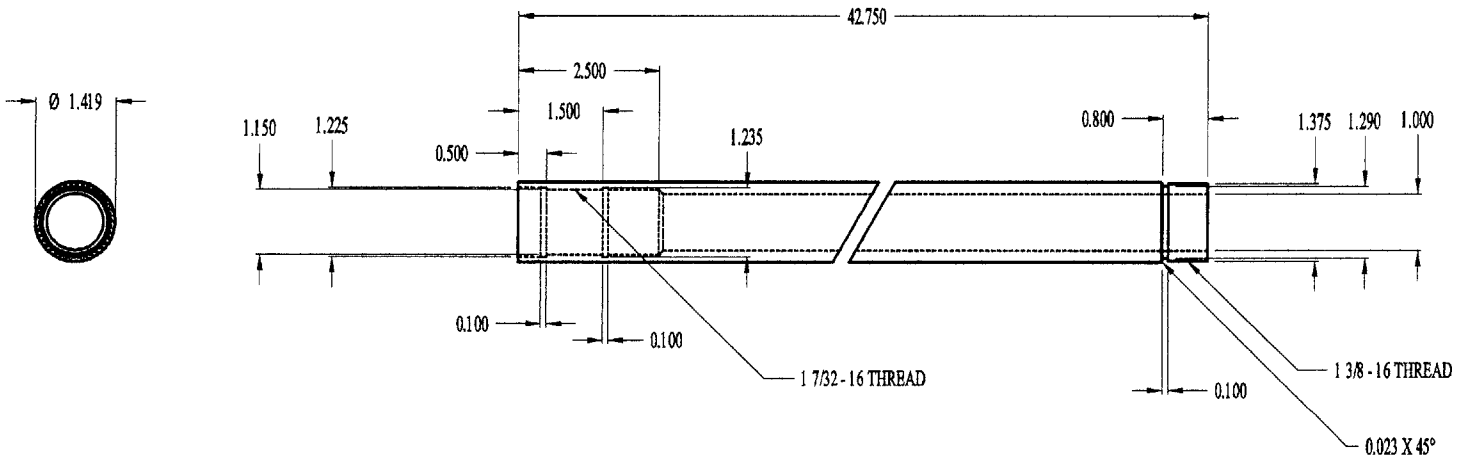
Ø 1.419
42.750
2.500
1.500
1.150
1.225
0.500
1.235
0.800
1.375
1.290
1.000
0.100
0.100
1 7/32 - 16 THREAD
0.100
1 3/8 - 16 THREAD
0.023 X 45°

DRIVE TUBE

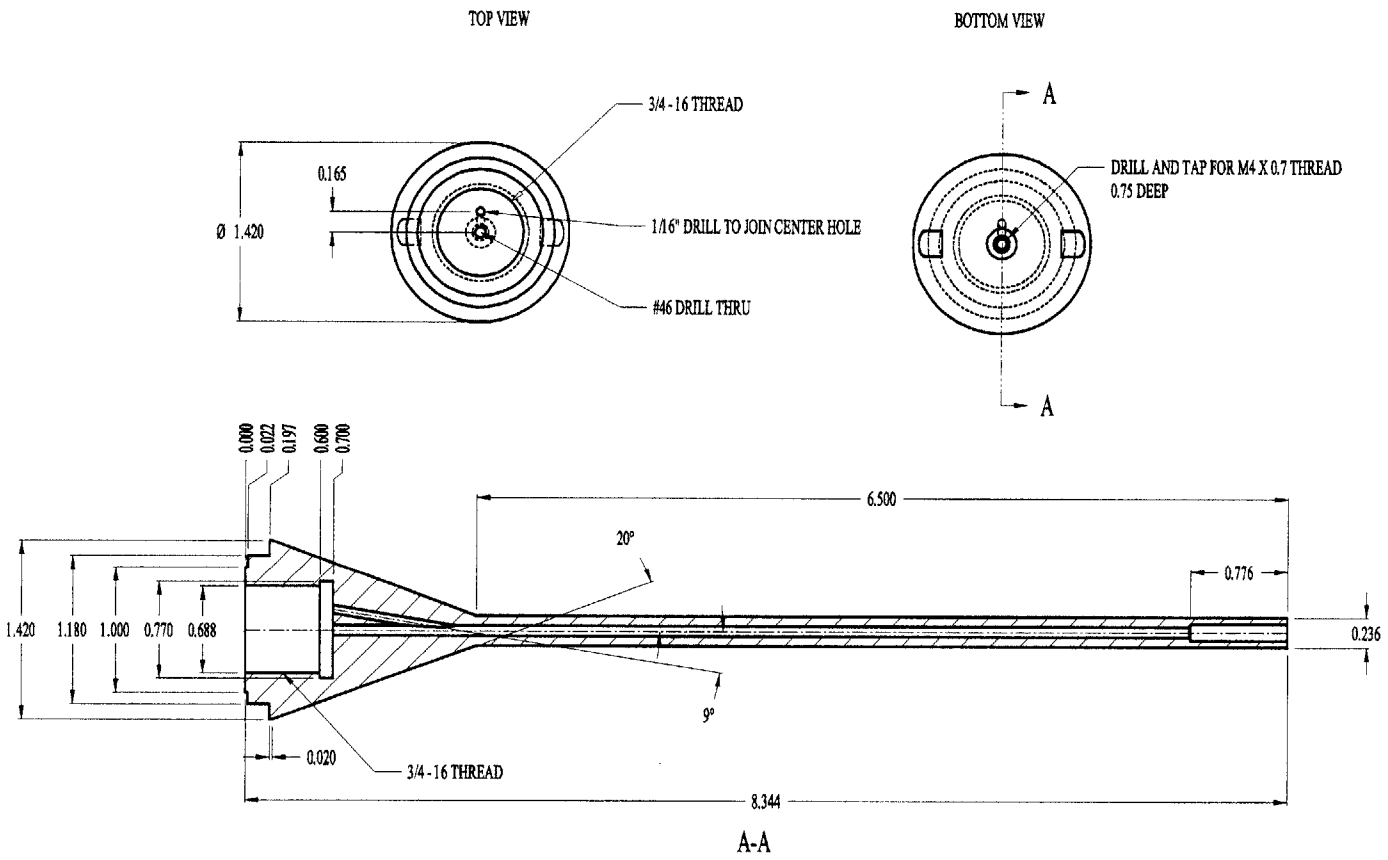
TOP VIEW
BOTTOM VIEW
3/4 - 16 THREAD
0.165
Ø 1.420
1/16" DRILL TO JOIN CENTER HOLE
#46 DRILL THRU
A
A
DRILL AND TAP FOR M4 X 0.7 THREAD
0.75 DEEP
0.000
0.022
0.197
0.600
0.700
6.500
20°
0.776
1.420
1.180
1.000
0.770
0.688
0.236
9°
0.020
3/4 - 16 THREAD
8.344
A-A

NEEDLE

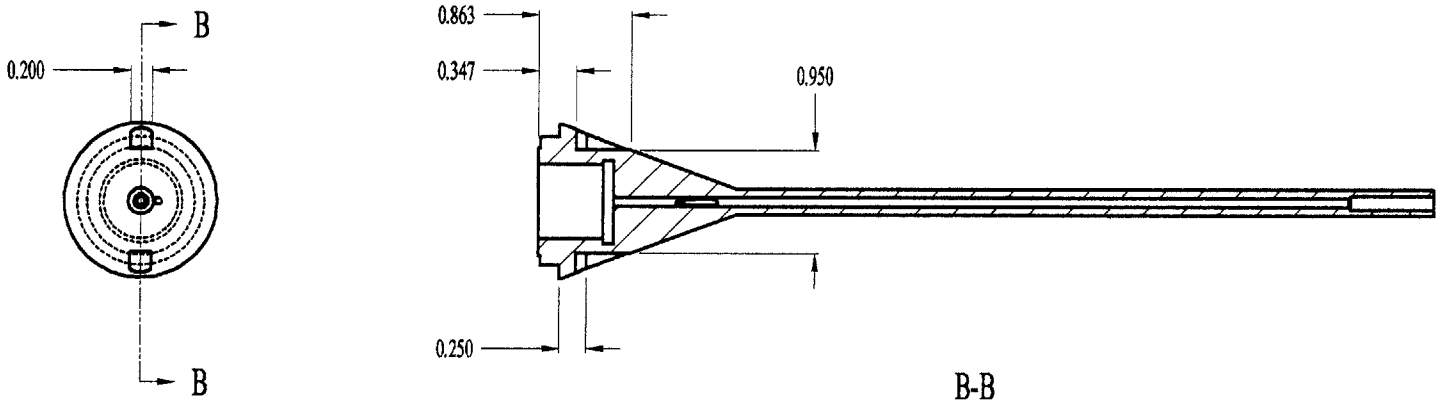

NEEDLE (VIEW #2)

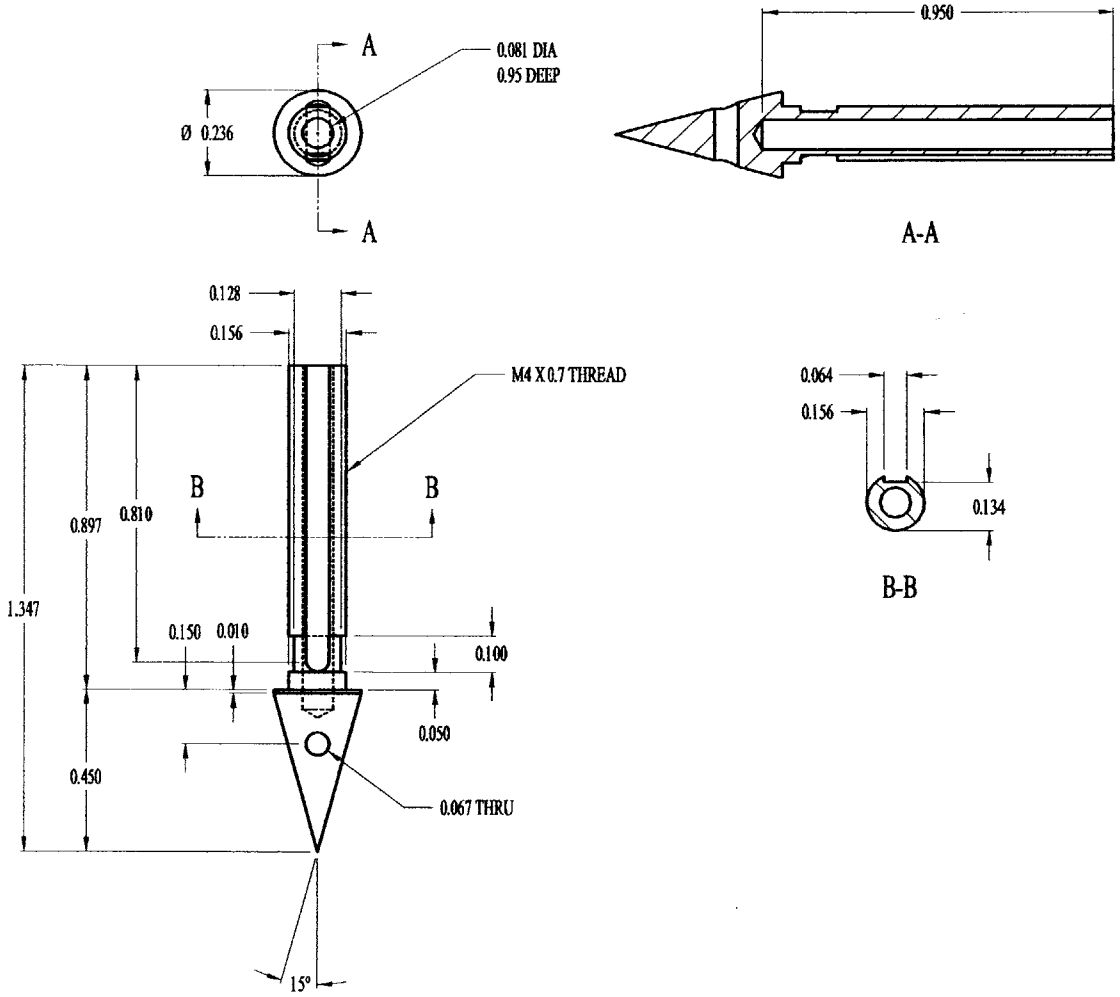
A
0.081 DIA
0.95 DEEP
Ø 0.236
A
0.950
A-A
0.128
0.156
M4 X 0.7 THREAD
B
B
0.897
0.810
1.347
0.150
0.010
0.100
0.050
0.450
0.067 THRU
15°
0.064
0.156
0.134
B-B

T2P Tip

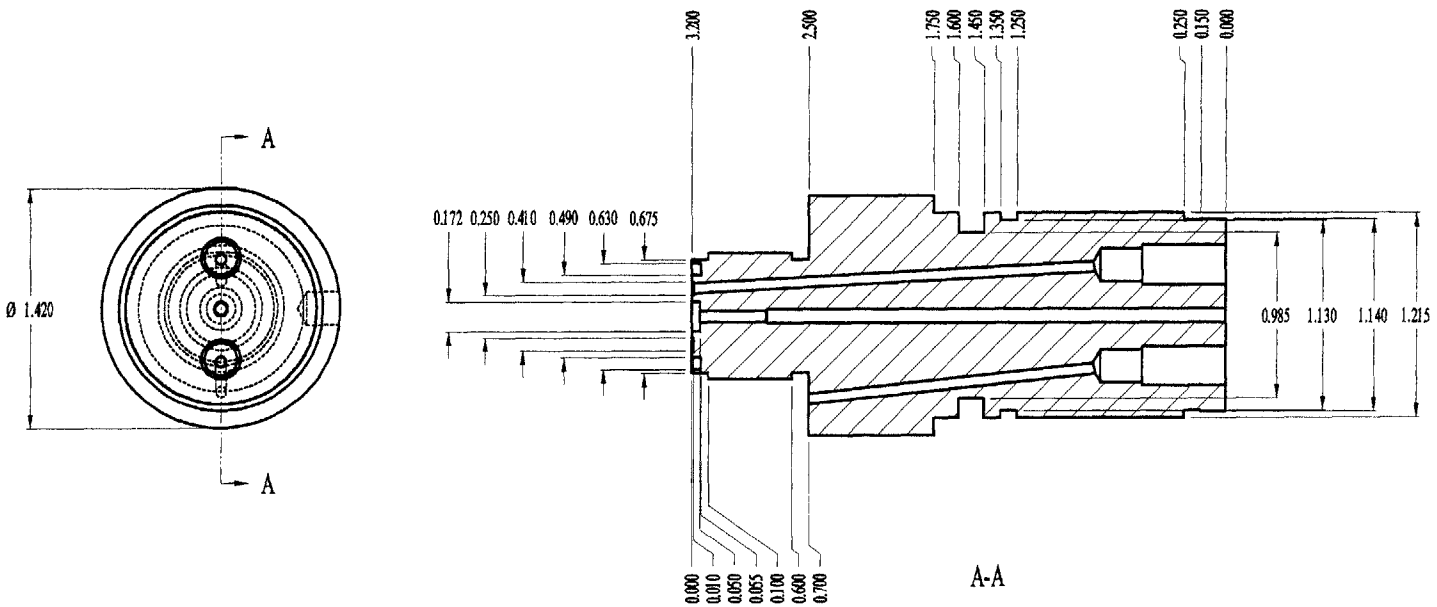

TRANSDUCER BLOCK

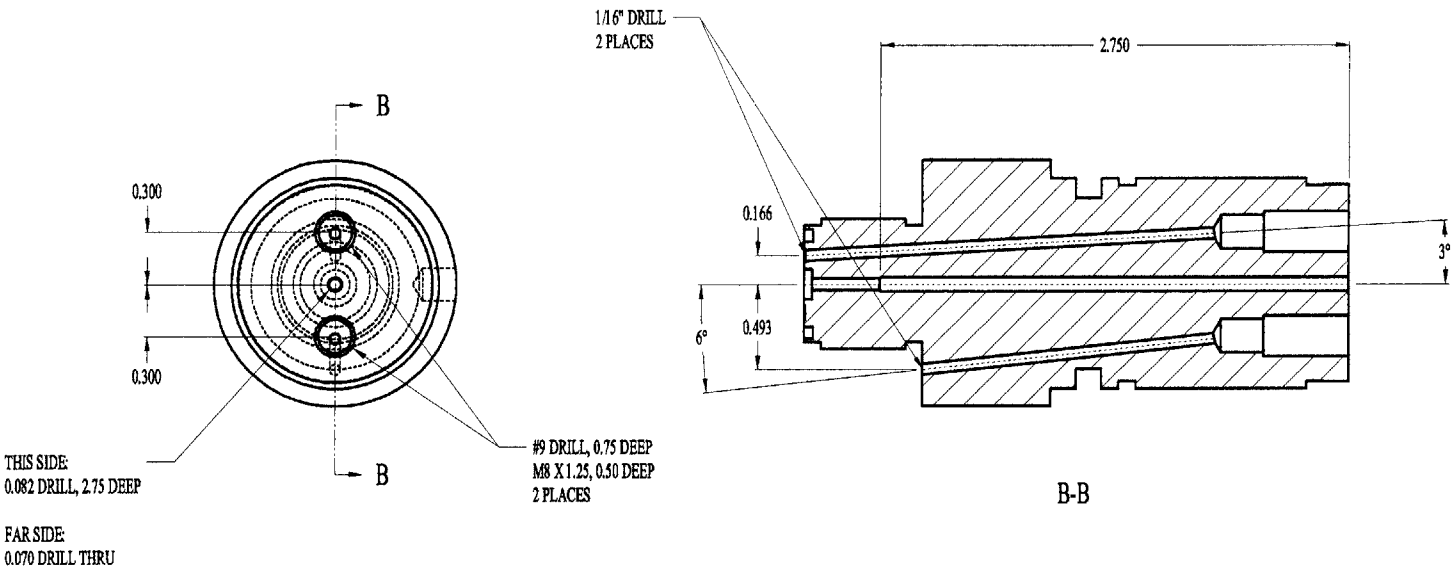

TRANSDUCER BLOCK (View #2)

APPENDIX C

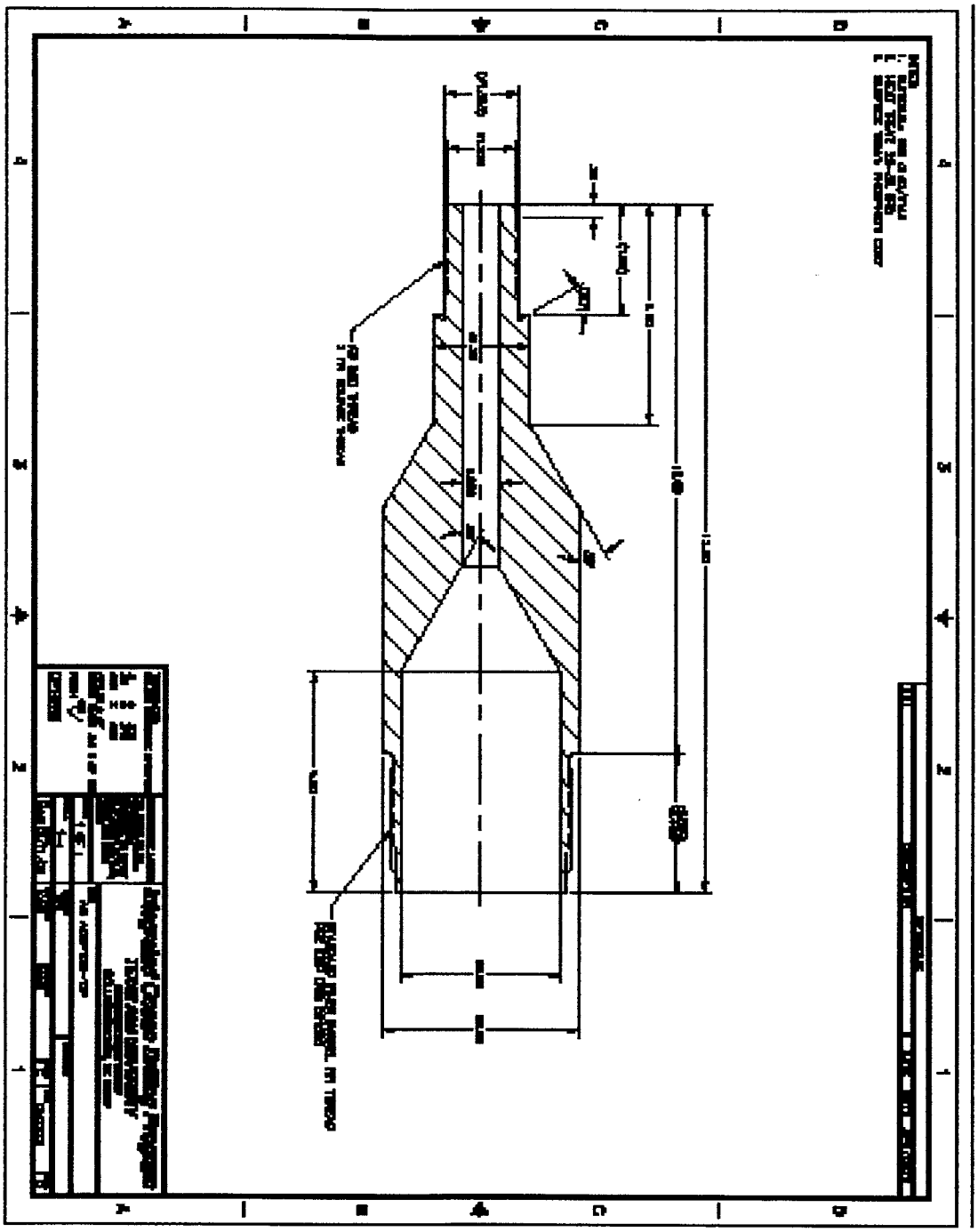

MODIFIED AW ADAPTER

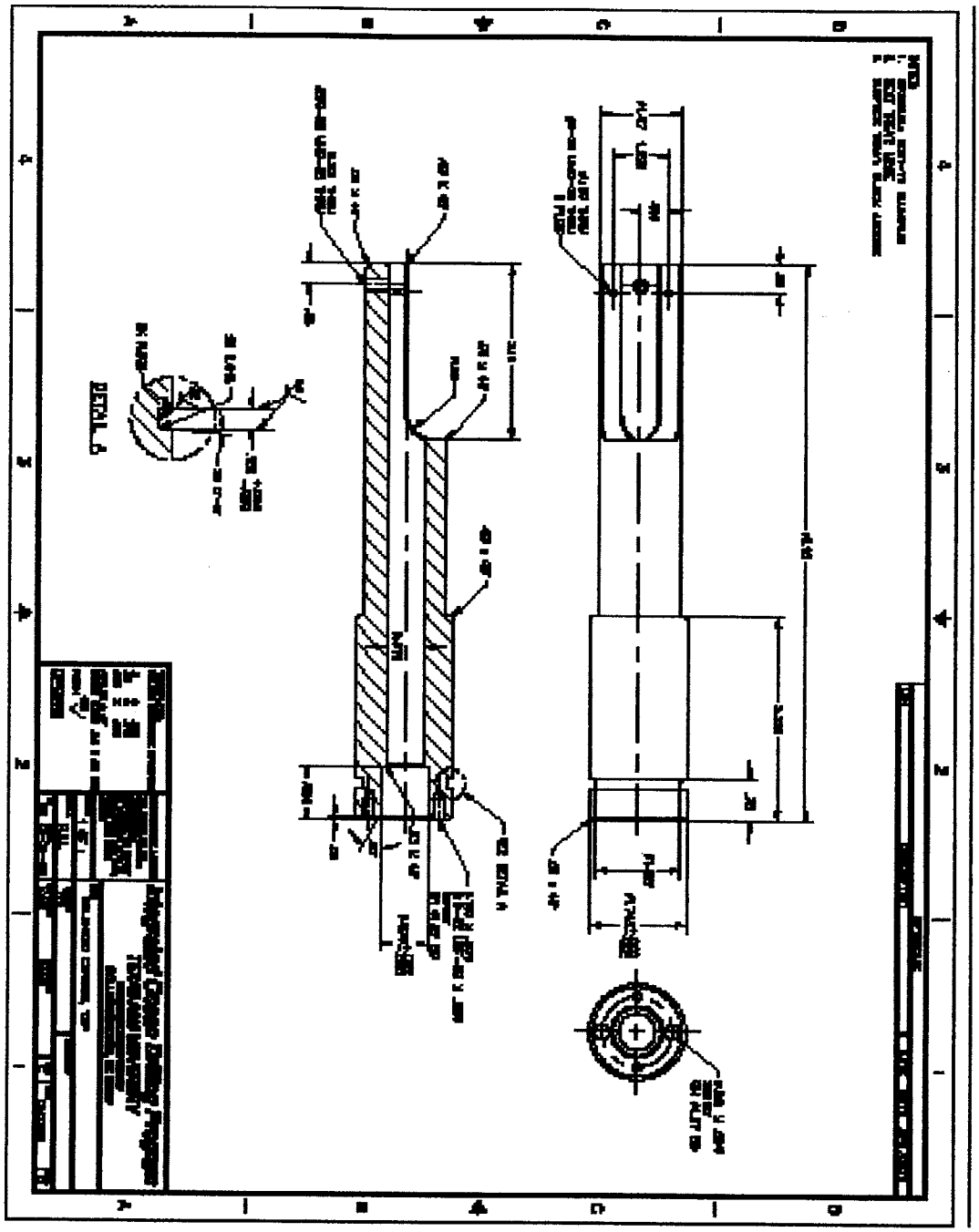

BULKHEAD CARRIER

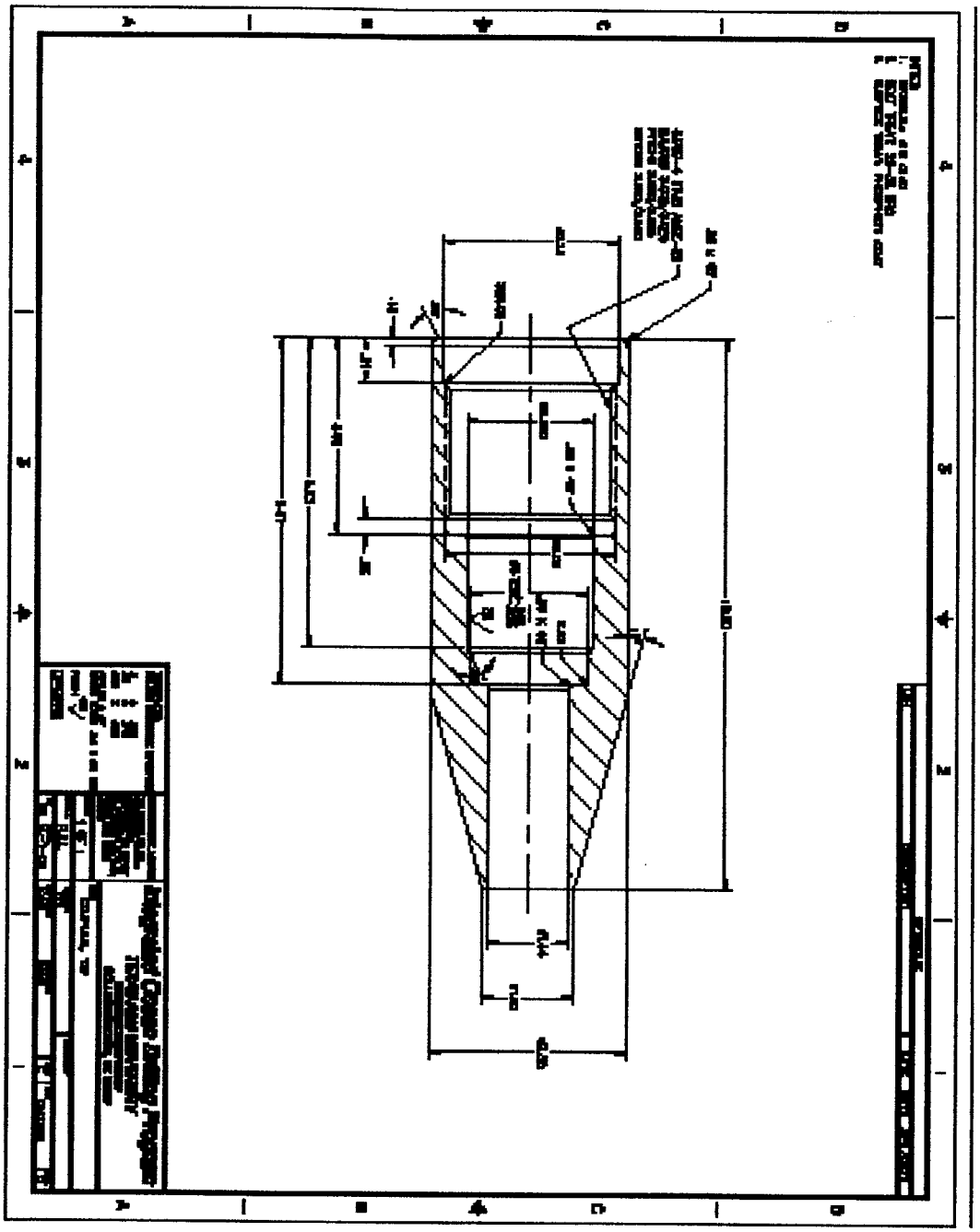

COUPLING

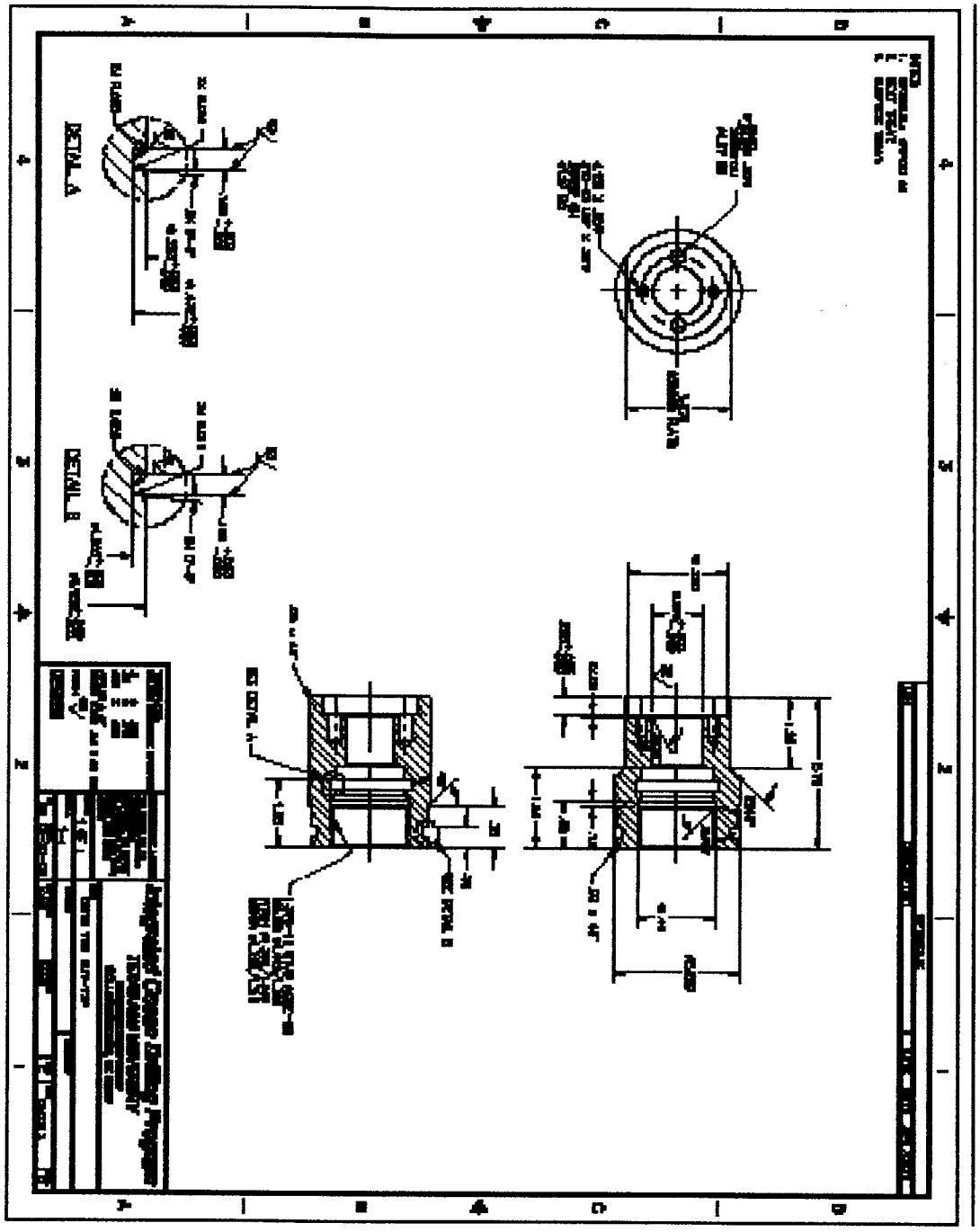

DRIVE TUBE NUT

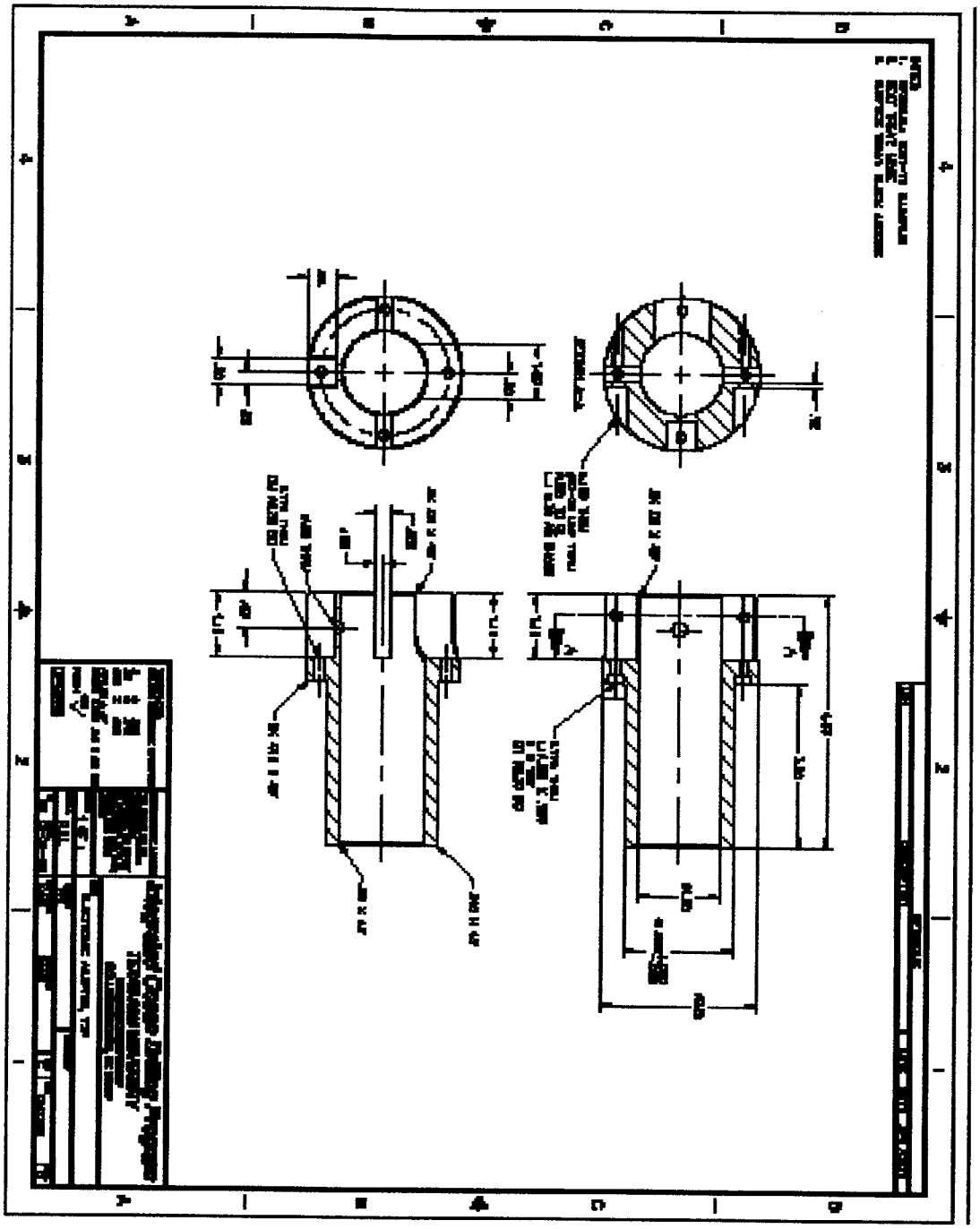

ELECTRONIC ADAPTER

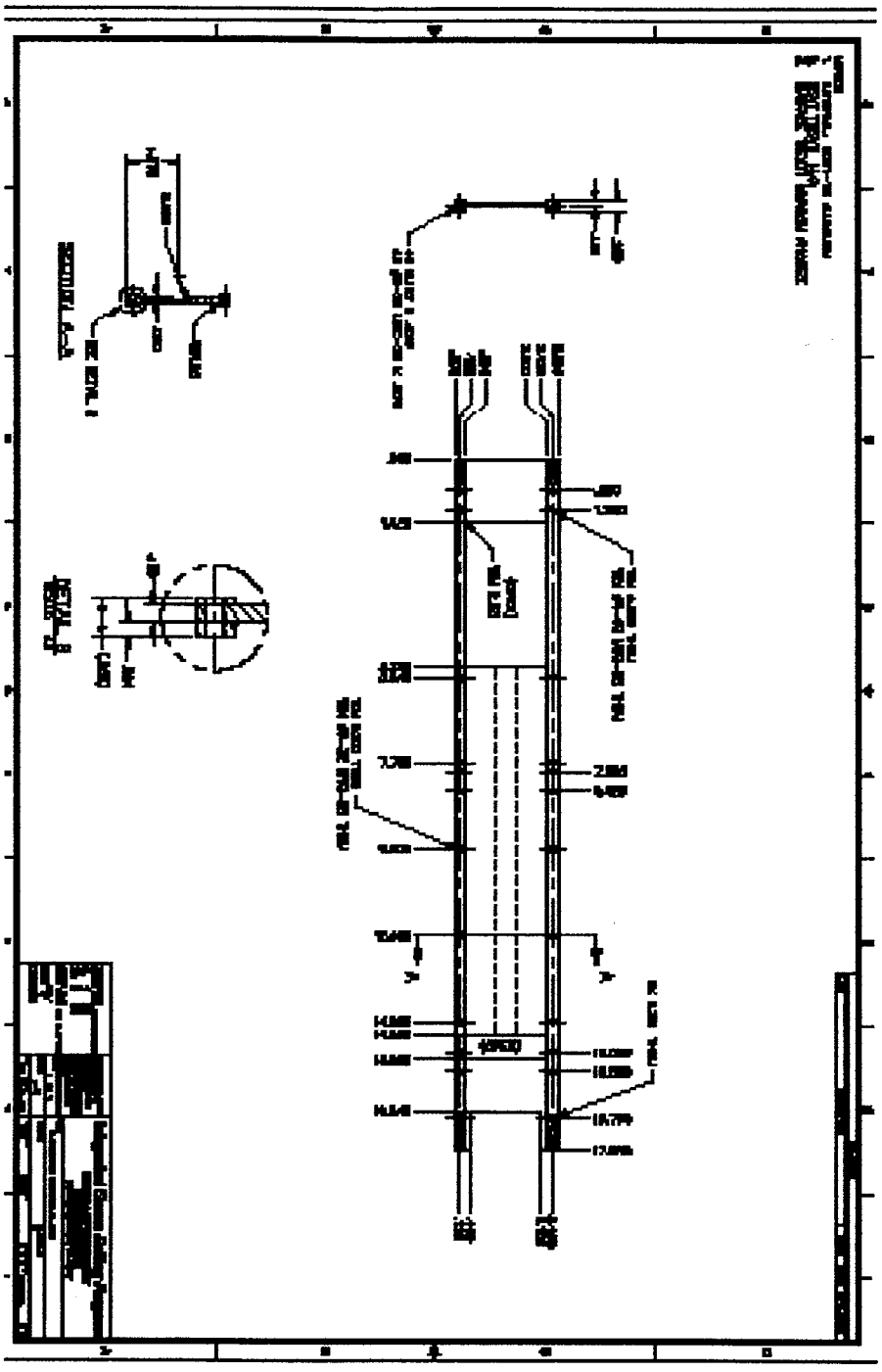

ELECTRONICS BACKBONE

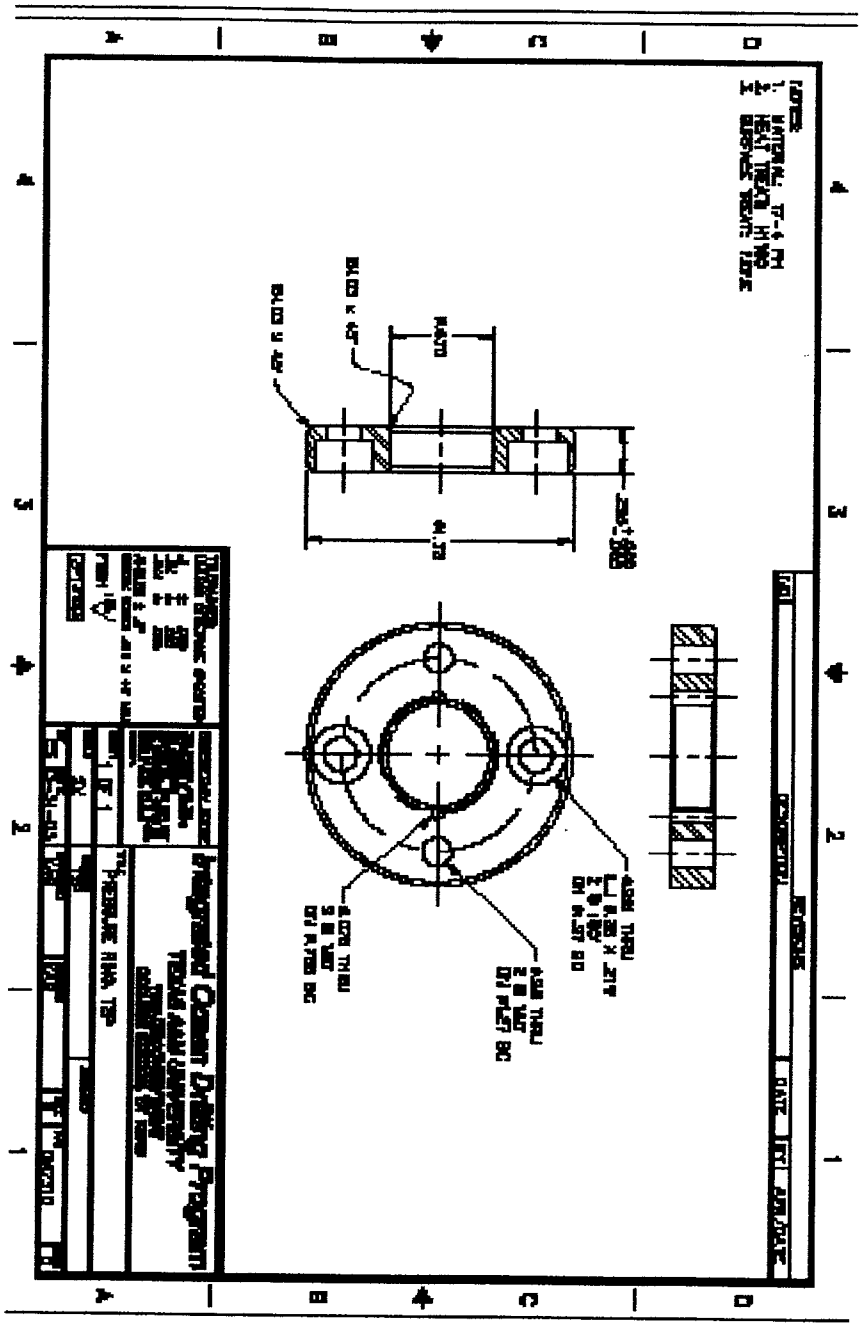

PRESSURE RING

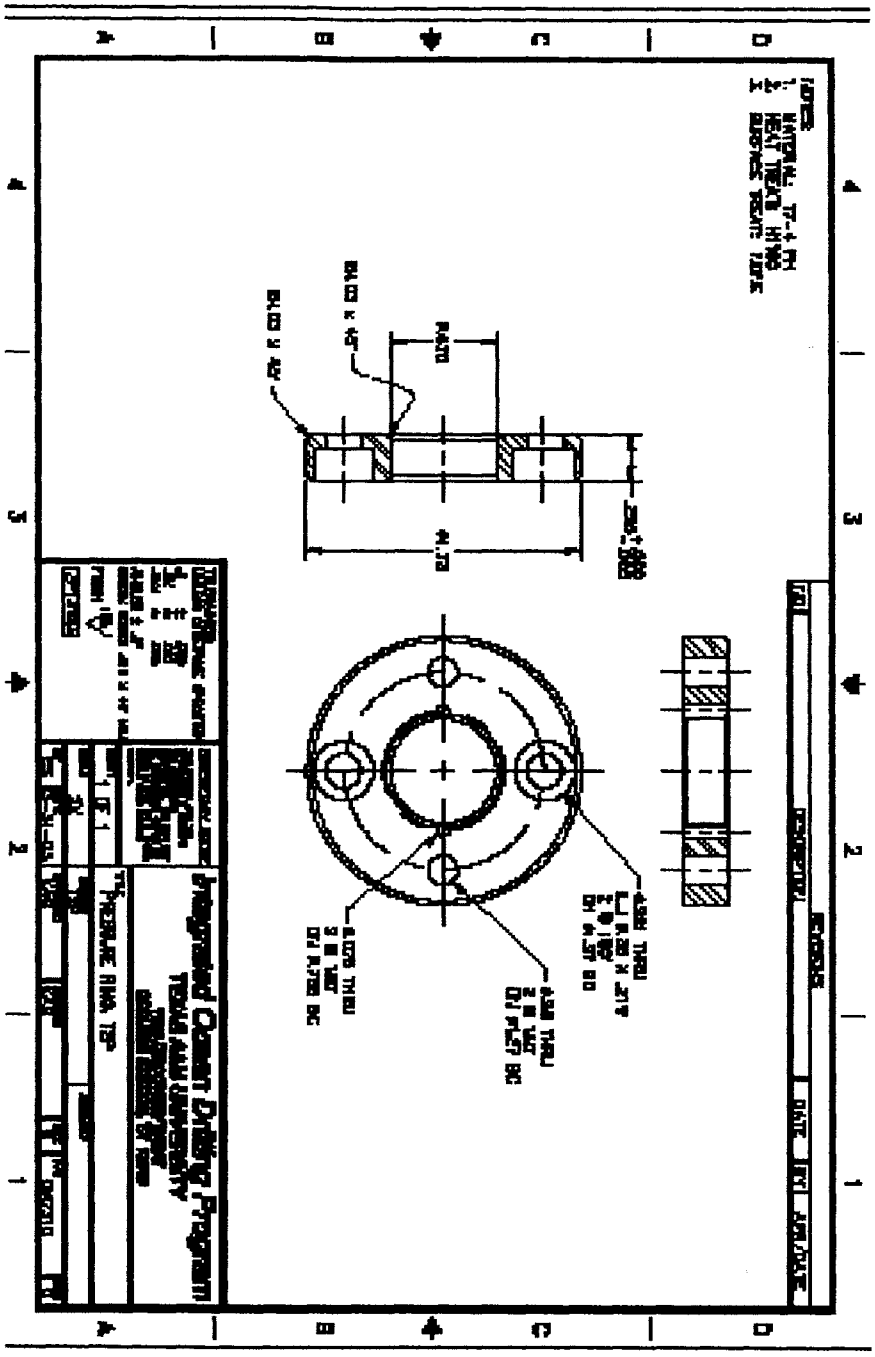

SPLIT RING

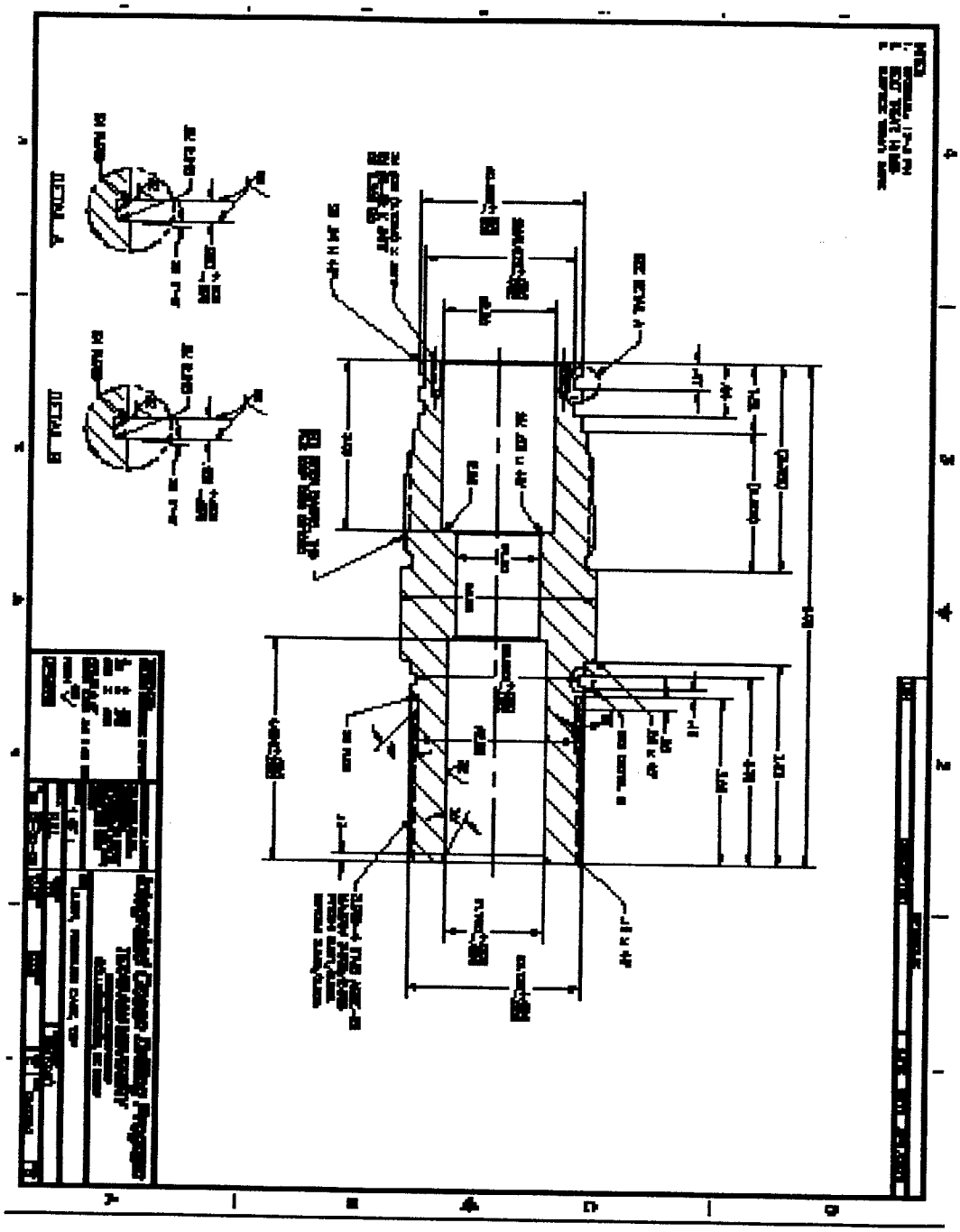

UNION